PAVEMENT SUBGRADE PERFORMANCE STUDY

Volume 1. Results from accelerated pavement testing of an A-2-4 subgrade soil at near optimum moisture content

by

Vincent Janoo[1]

Edel Cortez [1]

Robert Eaton[1]

Niclas Odermatt [2]

[1.] U.S. Army Cold Regions Research and Engineering Laboratory, 72 Lyme Road, Hanover, New Hampshire 03755, United States

[2.] Royal Institute of Technology, Highway Engineering, Brinellvägen 34, SE - 100 44, Stockholm, Sweden

CONTENTS

ILLUSTRATIONS

Figure

TABLES

Table

EXECUTIVE SUMMARY

This is the second of a series of reports on the subgrade failure criteria research study. The hypothesis for this study is that the failure criterion depends on the subgrade type and the in-situ moisture content. Many of the current mechanistic design procedures incorporate the results from AASHO Road Tests conducted in the late fifties. The criterion is based on one soil type (A-6), and most of all it was difficult to discern the effect of load and environment on the failure criterion. Our assertion is that the criterion is not applicable to other subgrades and possibly to areas other than where it was developed. Also, the criterion was inferred from surface distresses rather than from actual in-situ stress and/or strain measurements.

As part of the research program, four subgrade soils were selected for testing in the Frost Effects Research Facility (FERF). Each subgrade soil was to constructed at three moisture contents, with one at or near optimum density and moisture content. The test sections, consisting of 75 mm of asphalt concrete and 229 mm of crushed base over the test subgrade soil, were instrumented with stress, strain, moisture, and temperature sensors. The test sections were then subjected to accelerated loading under controlled environmental conditions.

This report presents the results from the accelerated pavement for one of the test subgrade soil. The subgrade, based on AASHTO soil classification system, was an A-2-4. It was constructed at near optimum density and moisture content of 1933 kg/m^3 and 9.5 % by weight, respectively. During construction, layer density, moisture content, and CBR were recorded. Accelerated pavement testing were conducted on four test windows in the test section. Each test window was approximately 6.0 m long and 1 m wide. Loading was applied unidirectionally at an average speed of 13 km/hr. The test section, barring any breakdowns, was subjected to about 700 load repetitions in an hour. Testing was conducted for 22 hours per day. The remaining 2 hours were used for maintenance. The load was varied in three of the test windows, ranging from 80 to 104 kN. The load was applied through dual truck tires, with the tire pressures averaging around 757 kPa.

Stress, strain, and surface rut measurements were taken periodically. Stress measurements were available in three of the four windows. All stress measurements were taken in the subgrade at approximately 150 mm from the top of the subgrade. In one of the

test windows, stress measurements were also taken at 450 mm from the top of the subgrade. Dynamic and permanent strains in the base and subgrade were measured in all four windows.

This report presents the measured response of the test section to accelerated loading. It was found that the current subgrade failure criterion for an A-2-4 subgrade soil is inadequate. The current criterion overestimates the limiting subgrade strain at a given load level by an approximate factor of two. It was also found that even with a 100% crushed base course, approximately 42–46% of the total deformation was in the base. It was also found that the vertical permanent strains were significant compared to the longitudinal and transverse strains. In the vertical direction the majority of the deformation occurred in the base and the top 300 mm of subgrade. However, there was a poor correlation between the vertical strain and load repetitions. Additional results from other test sections will be used to validate the findings from these tests.

PAVEMENT SUBGRADE PERFORMANCE STUDY

Volume 1. Results from accelerated pavement testing of an A-2-4 subgrade soil

by

Vincent Janoo, Edel Cortez, Robert Eaton, Niclas Odermatt

INTRODUCTION

As a result of the work by Dormon and Metcalf (1965) using data from the AASHO Road Tests, the current design criterion for pavements stipulates that the failure of the subgrade can be minimized by limiting the level of vertical compressive strain on top of the subgrade. However, it must be remembered that this limiting subgrade strain criterion was based exclusively on the A-6 soil at the AASHO Road Test. This failure criterion may not be applicable for other material types (gravel, sand, silt, or clay) nor for other moisture conditions. For example, the practical experience of pavement and geotechnical engineers indicates that a silt subgrade ruts more easily than gravel and that moisture conditions near saturation are more critical than when the subgrade is at or near optimum.

As part of an international study on pavement subgrade performance, several full-scale test sections were constructed in the Frost Effects Research Facility (FERF) at the U.S. Army Cold Regions Research and Engineering Laboratory (CRREL) in Hanover, New Hampshire. The test sections were constructed from different subgrade soils at different moisture contents. A detailed overview of the project can be found in Janoo et al. (1999).

The test sections consisted of a 76-mm asphalt concrete (AC) layer, a 229-mm crushed gravel base, and 3 m of test subgrade soil. They were instrumented with stress cells, strain

gages, and moisture and temperature sensors. The test sections were subjected to accelerated loading using the Heavy Vehicle Simulator (HVS). Surface rut depth measurements were taken periodically during the accelerated load tests. For this study, failure was considered to be a surface rut depth of 12.5 mm. At the same time, subsurface stress and strain measurements were taken. The testing was conducted at around 20°C. The results from the first full-scale accelerated load test section with a silty gravel subgrade soil constructed at near-optimum moisture content and density are presented in this report.

MATERIAL PROPERTIES

The subgrade soil for this test section was obtained from a local quarry in West Lebanon, New Hampshire, USA. An initial analysis of the soil indicated that the material was a non-plastic A-1-b material (Fig. 1). The soil was blended with some A-4 soil to change the gradation to an A-2-4 and to increase the plasticity of the soil (Fig. 1).

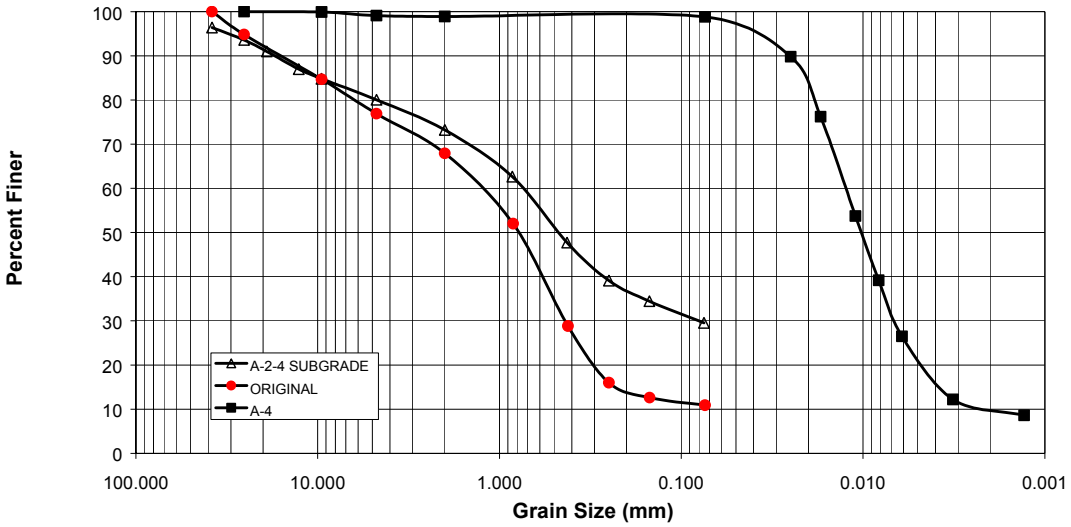

Figure 1. Gradation of original and blending soil to create the A-2-4 subgrade.

The blending was done at the pit, and approximately 1500 m^3 of the blended material was delivered to CRREL and stockpiled (Fig. 2). Routine classification tests conducted on the stockpiled material included optimum moisture, maximum density, gradation and hydrometer analyses, specific gravity, and liquid and plastic limits. Standard AASHTO test procedures were used. Additional details on the soil characterization can be found in Janoo et al. (1999).

Figure 2. Stockpiled A-2-4 test soil at CRREL

Additional routine tests were conducted on the subgrade soil in the test section. The results presented here are from six random samples from the test section. The average grain size distribution of the subgrade soil is shown in Figure 3. The soil has approximately 30% passing the 0.074-mm sieve. The average liquid limit (LL) and plasticity index (PI) of the soil were 30% and 2.1, respectively. The average specific gravity was 2.72. According to the

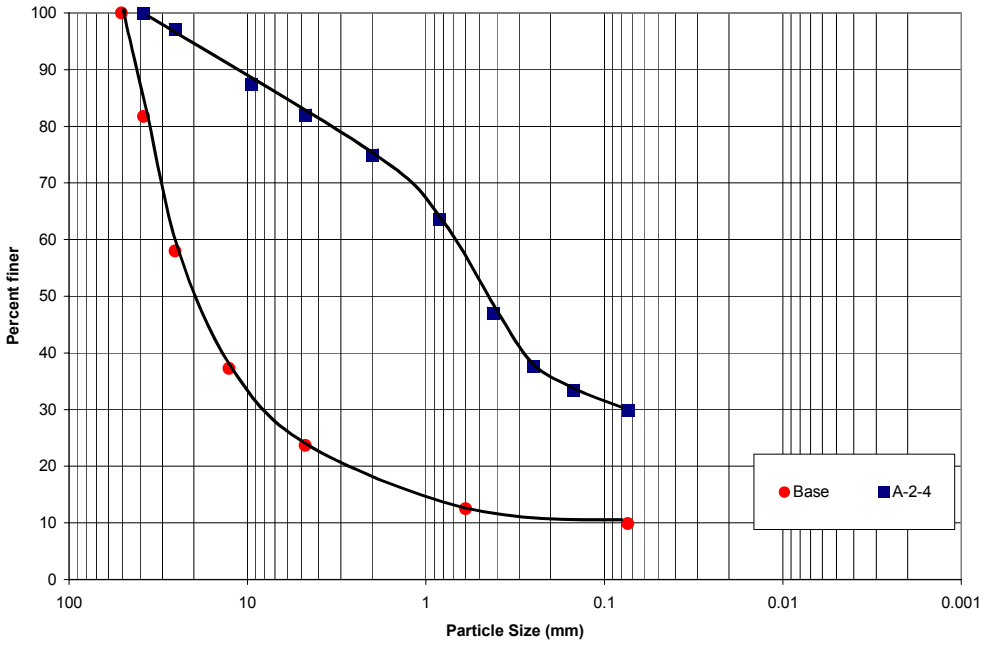

Figure 3. Grain size distribution of the subgrade material, the A-2-4 soil.

American Association of Highway and Transportation Officials (AASHTO) soil classification system, the subgrade soil was characterized as an A-2-4. According to the Unified Soil Classification System (USCS), the subgrade soil was classified as silty sand (SM).

Two sets of optimum moisture content and maximum density tests were conducted on the subgrade material in the test section using the AASHTO test procedure, *The Moisture-Density Relations of Soils Using a 5.5 lb (2.5 kg) Rammer and a 12 in. (305 mm) Drop* (T 99-90). The results from these tests are shown in Figure 4. The average optimum density and moisture content were 1934 kg/cm^3 and 10%, respectively. The results from the classification tests are summarized in Table 1.

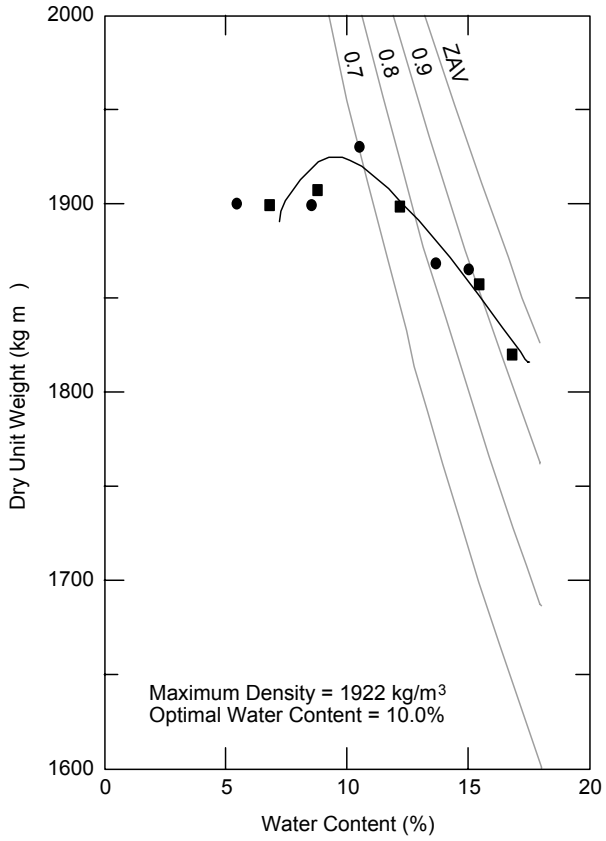

Figure 4. Moisture density relationship for A-2-4 subgrade soil.

The base course was crushed gravel (No 304 NH State DOT base course specification) and was classified as an A-1-a or GP-GM using the AASHTO or ASTM classification systems, respectively. This material was also stockpiled at CRREL. The gradation of the base course as shown in Figure 1 is the average of several tests conducted on the stockpiled material. The optimum moisture content of the base course was 3.3%. The asphalt layers met

the standard NH AC 20 base and surface course mix requirements. No tests were conducted on the asphalt mixture.

Table 1. Summary of classification test on 701 subgrade soil.

AASHTO	A-2-4
USCS	SM
Spec. Gravity	2.72
LL (%)	30
PI	2.1
Optimum moisture content (%)	10.0
Maximum Density (kg/m^3)	1934
% pass. #10	71.8

DESCRIPTION OF THE TEST SECTION

The test section was constructed in the Frost Effects Research Facility (FERF). A detailed description of the FERF can be found in Janoo et al. (1999). The overall facility is 56 m long by 31 m wide and can accommodate up to 12 test sections at one time. The 701 test section was constructed on the north side of the building, as shown in Figure 5. The available area for the test section was 42 m long by 6.4 m wide and 3.7 m deep.

Of the 42 m, approximately 19.5 m was sloped. The actual length used for testing was approximately 23 m long (Fig. 6). There were the six test windows within the test area for conducting accelerated load tests. Each test window was 7.8 m long, of which the

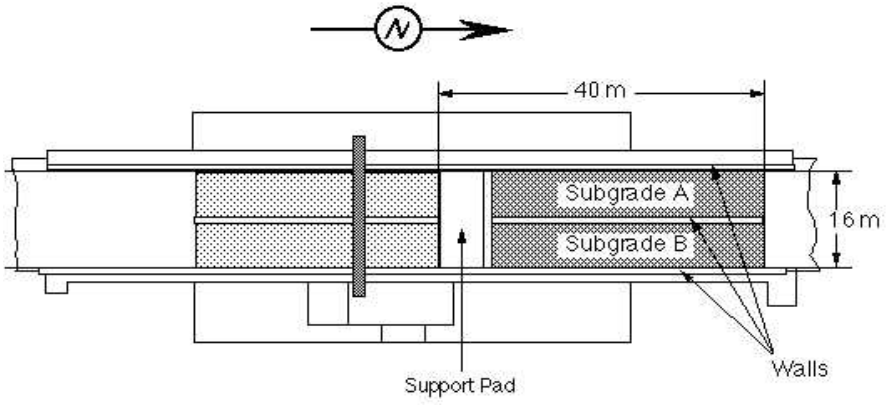

Figure 5. Test section area in the FERF.

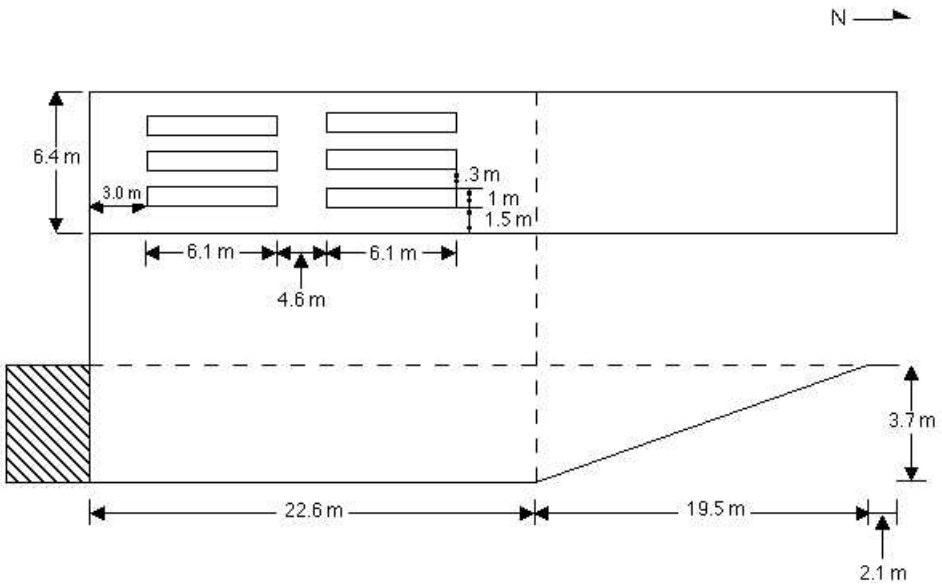

Figure 6. Location of test section in the FERF.

beginning and the end 0.9 m were used as acceleration and deceleration areas for the wheel. The area between these two areas (6 m long) was where the constant velocity tests were conducted. The width of each of the test window was 0.9 m. The center-to-center distance between the test windows was 1.2 m.

The thicknesses of the test section layers were based on theoretical multi-layered analysis (Hildebrand and Irwin 1994) and from results from Danish Road Institute (DRI) test sections using the Road Testing Machine (RTM) (Janoo et al. 1999). In the FERF the test section cross section was 76 mm of asphalt concrete and 229 mm of crushed base over 3048 mm of test subgrade soil (Fig. 7).

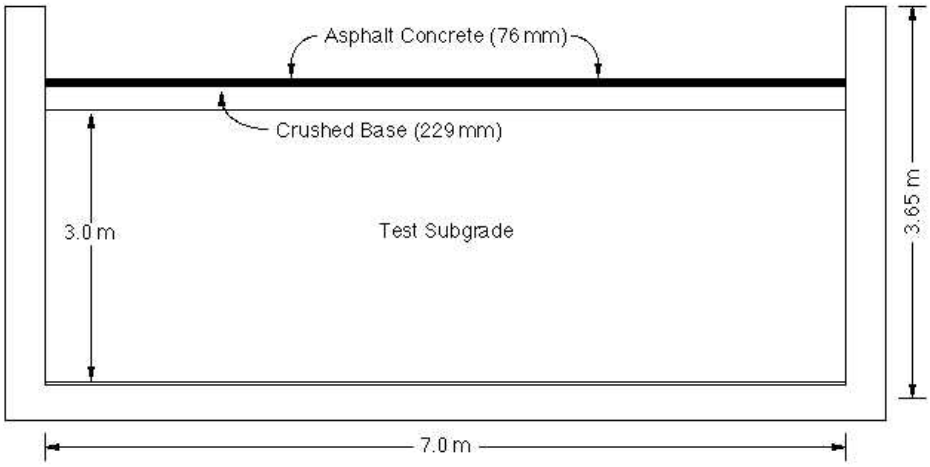

Figure 7. Cross section of test section.

CONSTRUCTION OF THE TEST SECTION

The specifications required that the subgrade be constructed in lifts and that each lift be compacted at moisture contents within ± 2% of the optimum and to a density between 95 and 100% of the maximum dry density obtained from the Standard AASHTO T99 test procedure. The bottom 1.88 m of the subgrade in the test section was constructed in 300-mm lifts, while the remaining 1.2 m of the subgrade was constructed at a nominal lift thickness of 150 mm.

Construction of the test section was delayed due the delay in the delivery of the Heavy Vehicle Simulator (HVS). However, because the analysis by Hildebrand and Irwin (1994) showed that below 1.5 m from the pavement surface the effect of the wheel load was minimal, a decision was made to build the test section in two phases. In phase 1 the bottom 2.1 m was constructed, beginning on September 26, 1995, and completed on September 28, 1995. Seven lifts were constructed in phase 1. The seventh lift was constructed as a cover for the test section and was covered with a tarp to minimize moisture loss. Because of delays in the delivery of the HVS, the construction of the second phase of the test section did not begin until mid-October 1996. The construction in phase 2 involved removing the top existing 300 mm of subgrade, reworking the material, and reconstructing in two 150-mm layers.

During the stockpiling process, some blended oil was placed directly on top of the concrete floor in the test basin (Fig. 8). This material was mixed and placed into the first 300-mm lift. The remaining lifts were constructed from the stockpiled material. The construction sequence was as follows. First, a bucket loader was used to bring the stockpiled material to the top of the test basin. A bulldozer was used to move and mix the subgrade into the test basin and level it to the proper grade (Fig. 9). For this soil, from random sampling of the stockpiled material, the moisture content was around 10%. The soil was placed at its in-situ water content. During the construction process, stones larger than 50 mm were removed manually. Once the grade was reached, the layer was compacted using a 9000-kg steel-wheel roller (Fig. 10). Compaction started at one end of the longitudinal wall and moved in approximately 0.3-m increments towards the other longitudinal wall. The compaction was done in the non-vibratory mode so as not to disturb any instrumentation in the layers below. The area approximately 0.3 m long from the south supporting pad was compacted using a hand compactor since the steel-wheel compactor could not reach this area.

Figure 8. Placement of first lift in 701 test section.

Figure 9. Grading of subgrade layer.

Figure 10. Compaction of subgrade soil.

Construction Control

As part of construction control, once the compaction was completed, a series of tests were conducted on the compacted layer. These measurements were made on every 300-mm lift. The tests included determination of moisture, density, CBR, layer thickness, and surface deflection. The primary properties used for construction control were the moisture content and dry density of the lifts. Additional details on construction control of the subgrade soil can be found in Janoo et al. (1999).

Moisture and density measurements were taken using the Troxler nuclear gage at the locations shown in Figure 11. The moisture and density determinations were made in a volume of soil using the direct approach. The probe from the Troxler penetrated into 150 mm of soil. On each lift, 30 measurements of moisture and densities were made. A total of 300 moisture and density measurements were made during the construction of the subgrade.

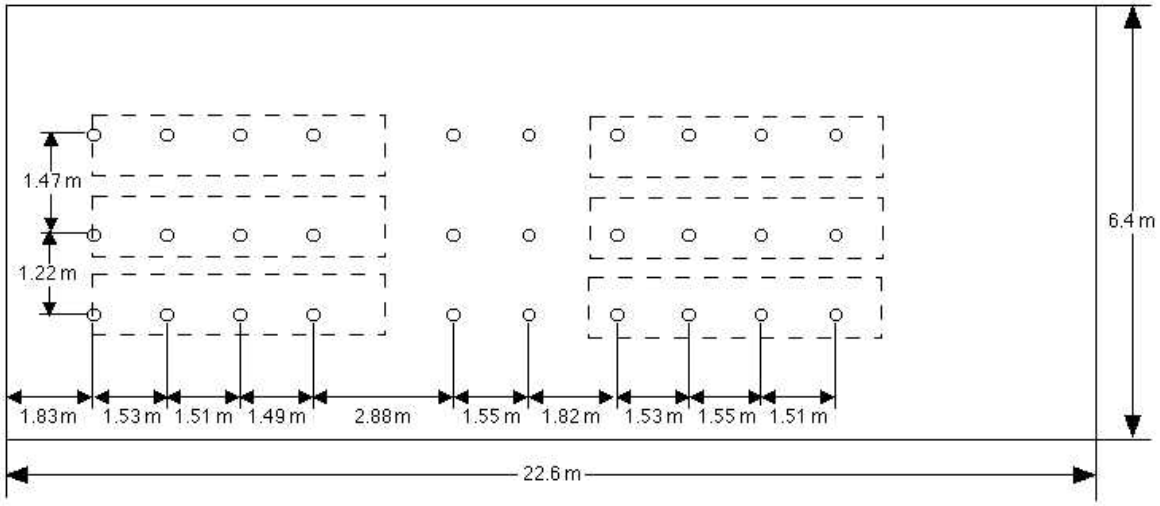

Figure 11. Location of moisture and density measurements on test section 701.

Dry Densities

The mean density of the subgrade is 1901 kg/m^3, with a coefficient of variation (COV) of 3%. A histogram and cumulative frequency plot of the relative compaction is presented in Figure 12, which shows that 12% of the data was below the minimum 95% relative compaction and 69% of the compaction is at or below the maximum density. An additional 21% of the measurements are below 102%.

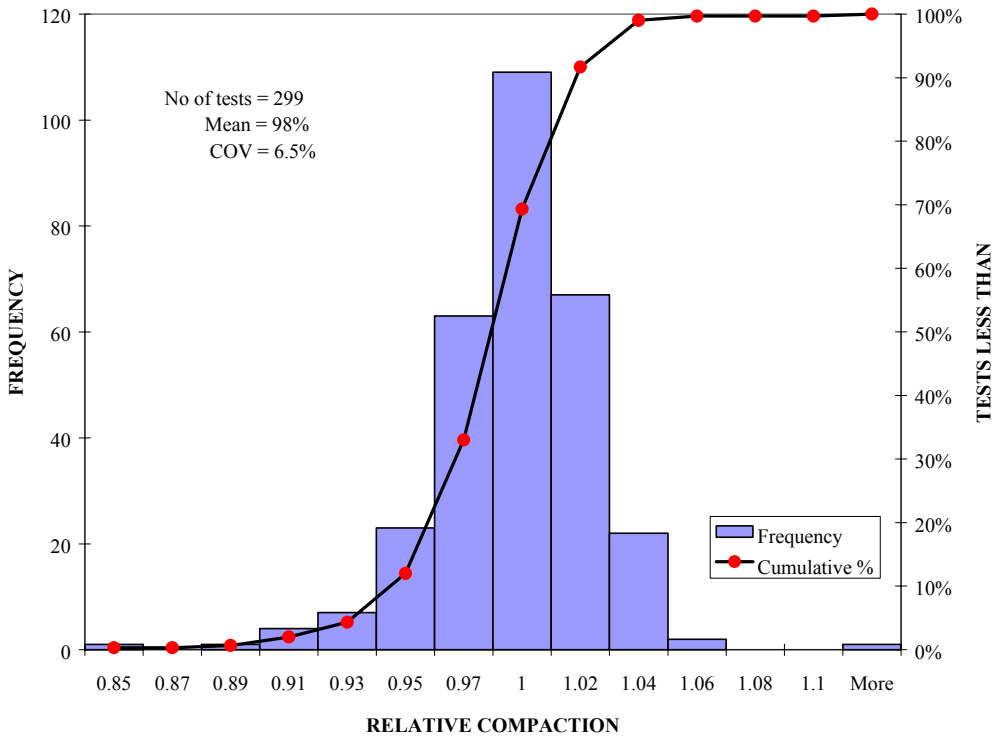

Figure 12. Constructed relative densities of the 701 subgrade.

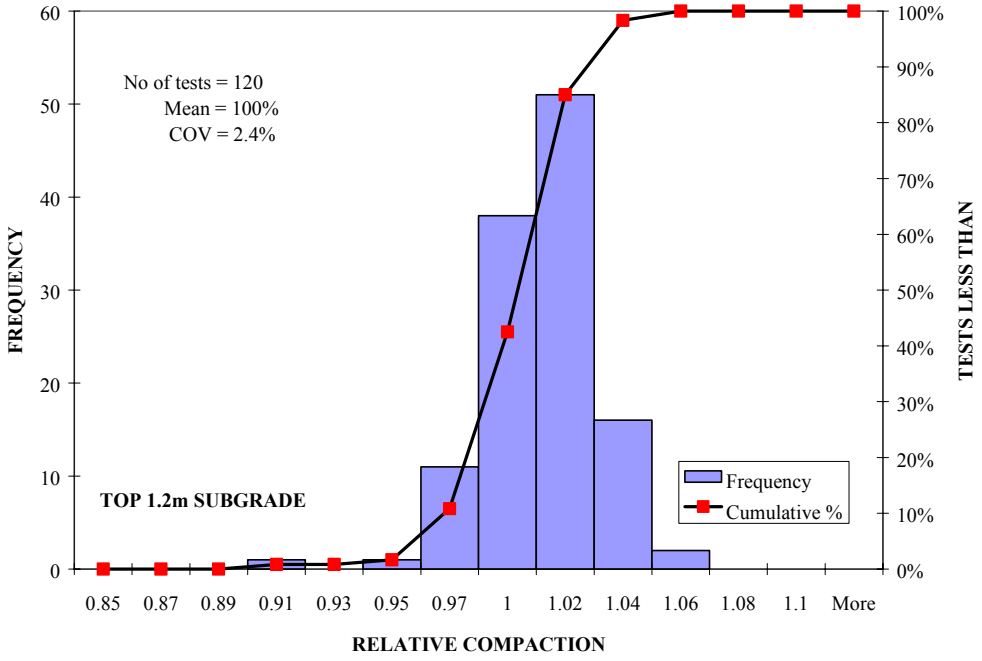

Figure 13. Constructed relative densities of the top 1.2 m of subgrade.

A similar histogram and cumulative frequency plot for the relative compaction of the upper 1.2 m of subgrade soil is shown in Figure 13. The mean dry density of the upper 1.2 m of subgrade is 1933 kg/m^3, with a COV of 2.4%. Approximately 2% of the measurements indicated that relative compaction of the upper 1.2 m of subgrade was less than 95%. Approximately 83% of data indicated that the relative compaction of the upper 1.2 m of subgrade was between 95 and 102% of the laboratory maximum density.

The results of the measurements are tabulated in Appendix A, Table A-1. Also shown in the table are the densities measured on top of the base course. On top of the base course, density measurements were taken using the backscatter method. The mean density of the base course was 2068 kg/m^3, with a COV of approximately 6%.

Moisture Content

The mean moisture content of the test subgrade soil was 9.0%, with a COV of 13.6%. The distribution of the moisture contents in the subgrade is shown in Figure 14. Approximately 79% of the data are within the ± 2% specification. Another distribution of the moisture content in the upper 1.2 m is shown in Figure 15. The mean moisture content of the upper 1.2 m of subgrade was 9.5%, with a COV of 6.1%. With respect to the target moisture content of 10%, approximately 79% of the data were within the ± 2% specification. The measured moisture contents of the subgrade and base course are presented in Table A-2.

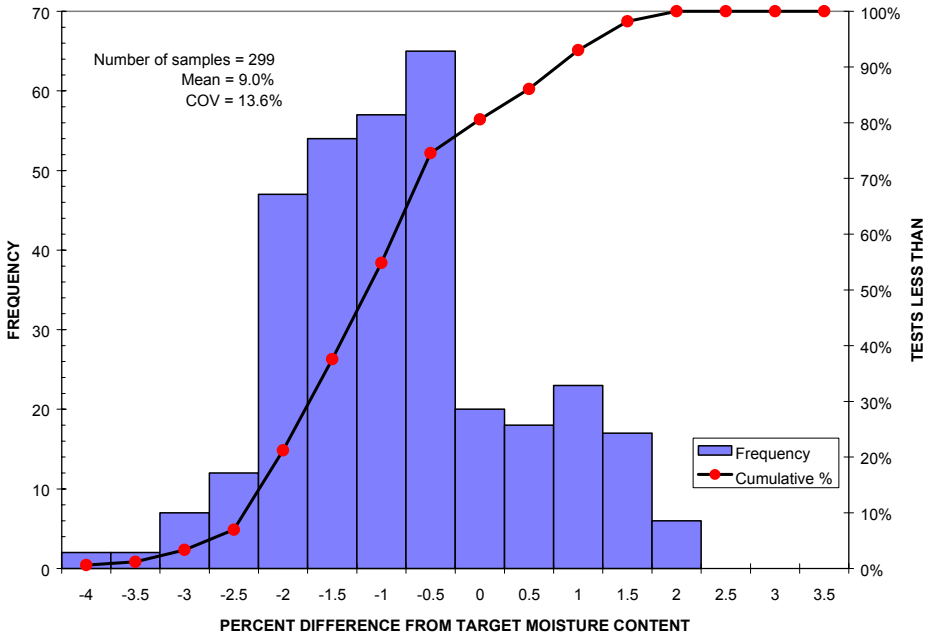

Figure 14. Distribution of moisture content in the subgrade.

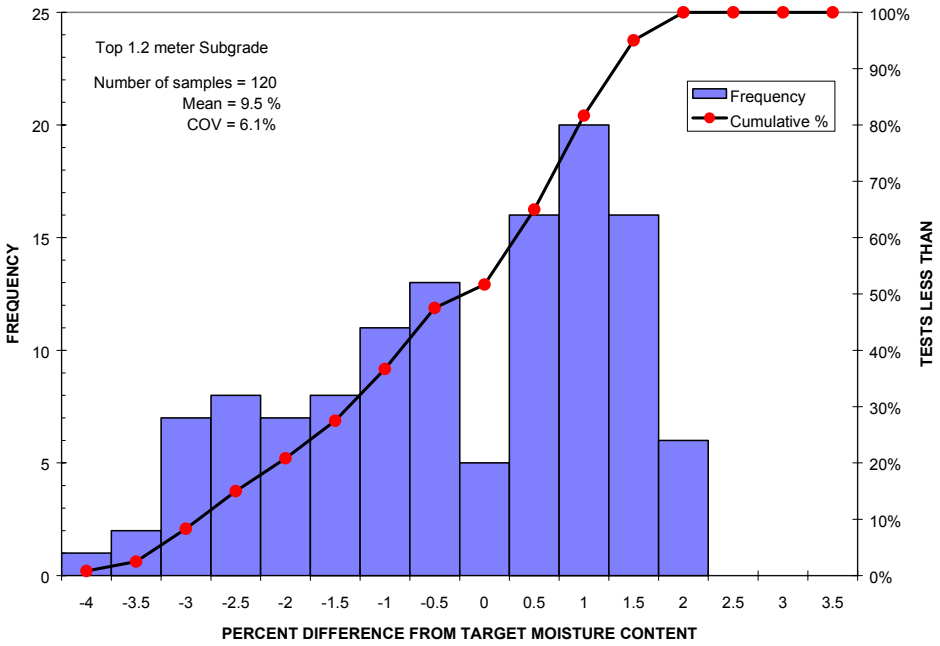

Figure 15. Distribution of moisture content in the upper 1.2 m of subgrade.

Table A-2 indicates that the top 300 mm of soil from phase 1 had dried slightly since the end of phase 1 construction. When the layer was reworked, no water was added. Ignoring the moisture content of layer T4, the mean moisture content in the upper subgrade layers is 10.3%, with a COV of 9.9%. The distribution of the moisture content in the upper 0.9 m is shown in Figure 16. Approximately 98% of the data are within the ± 2% specification.

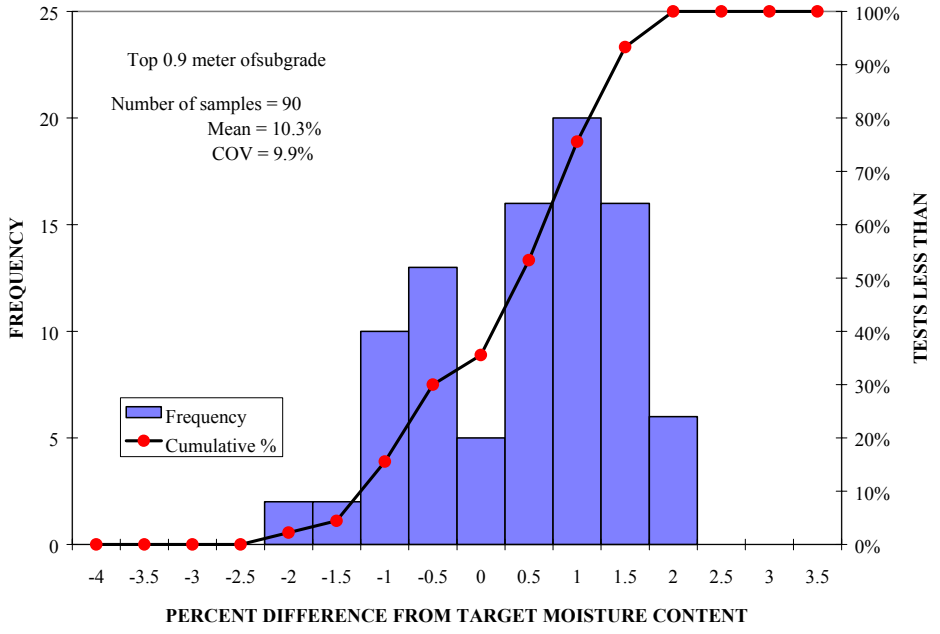

Figure 16. Distribution of moisture content in the upper 0.9 m of subgrade.

California Bearing Ratio (CBR)

Layer CBR data were obtained from the Clegg hammer and dynamic cone penetrometer (DCP). Details on the Clegg hammer and DCP can be found in Janoo et al. (1999). Locations where the CBR tests using the Clegg hammer were measured are shown in Figure 17. A total of 48 measurements were made with the Clegg hammer tests on every 300-mm lift. The Clegg hammer test is a fast, nondestructive test and provides a good indicator of lift uniformity. The Clegg hammer is essentially a modified AASHTO compaction hammer fitted with a piezoelectric accelerometer and is commonly used in Canada, Australia, and Europe for compaction control of subgrade, subbase, and base courses. The deceleration is converted to the Clegg impact value (CIV), and the CBR of the layer is determined using the relationship $CBR\ (\%) = 0.07 \times (CIV^2)$.

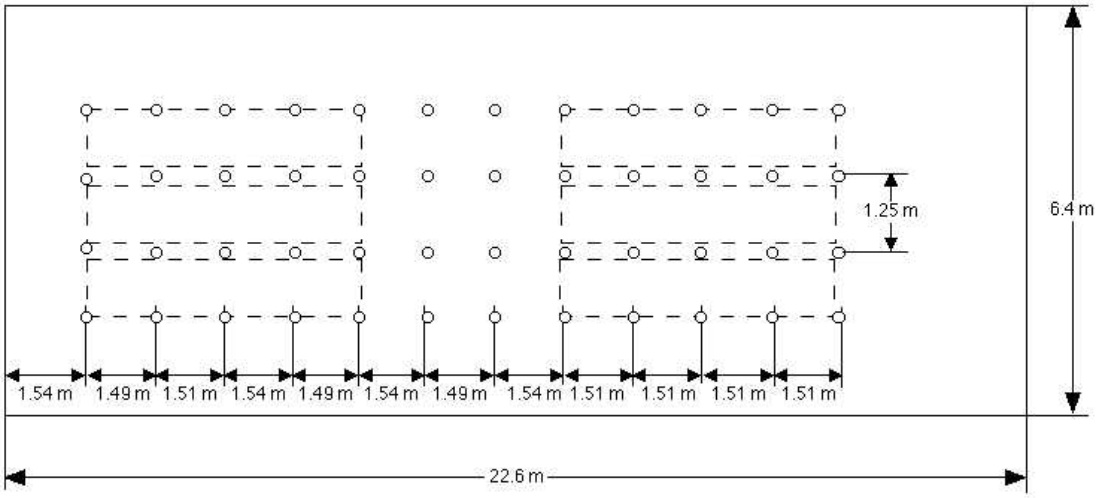

Figure 17. Location of CBR measurement points using the Clegg hammer.

During the construction of the bottom subgrade layers in phase 1, due to miscommunications, CBR measurements were only made in the middle two rows. A total of 24 measurements were made on each layer. During phase 2 construction of the upper 1.2 m of subgrade, CBR measurements were made at all locations. The results of 351 measurements made during the construction of the subgrade are presented in Table A-3. A distribution of the CBR in the subgrade is shown in Figure 18. The mean CBR was 14%, with a COV of 40%.

A similar distribution of the CBR for the upper 1.2 m of subgrade is shown in Figure 19. The mean CBR of the upper 1.2 m subgrade was 16%, with a COV of 50%. A review of

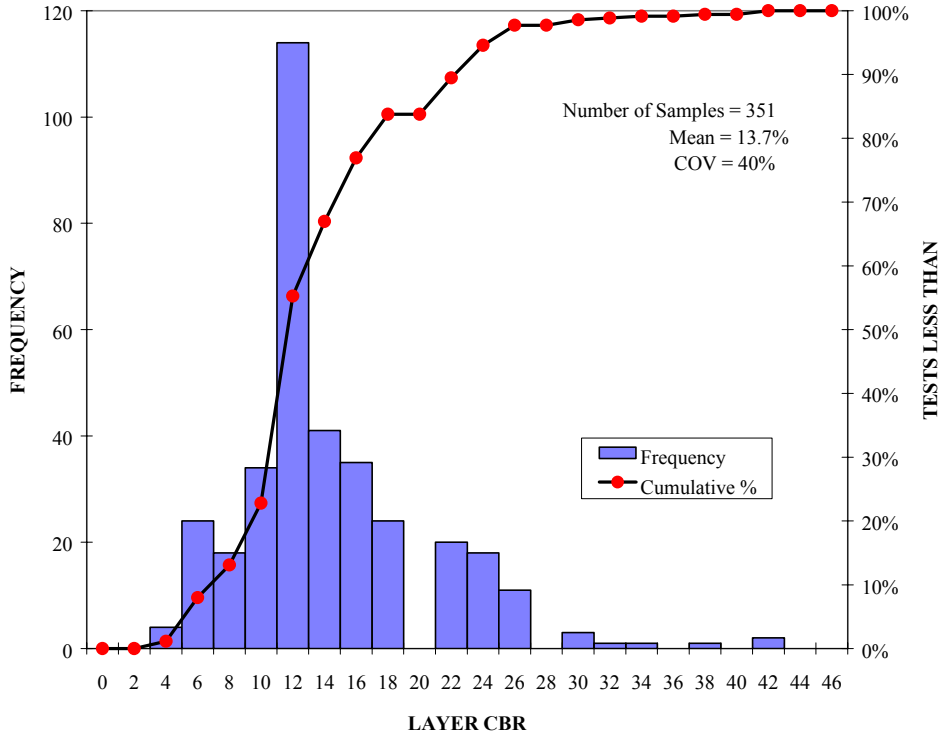

Figure 18. Distribution of CBR in the subgrade.

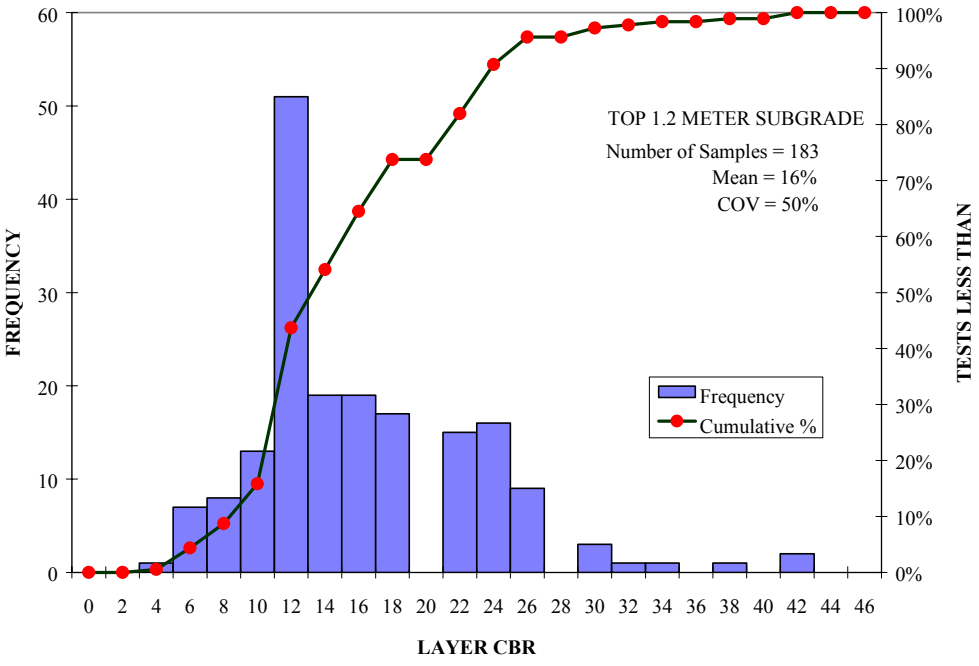

Figure 19. Distribution of CBR in the upper 1.2 m of subgrade.

Table A-3 indicates that many of the lower CBR values were close to the south wall (1, 2, 13, 14, 25, 26, 37, and 38, Fig. 18). These were in the areas where it was difficult to compact the soil with the roller and it was done manually.

The CBR of the subgrade was also determined from the dynamic cone penetrometer (DCP). The DCP tests consisted of raising a 4.5-kg hammer to a height of 584 mm and then dropping it onto an anvil attached to the DCP rod. The force on the anvil drives the cone into the soil, and the number of blows required to drive the cone to a depth of 25-mm increments is noted. The DCP index, which is the amount of penetration per blow, was converted to CBR using relationships developed by the Corps of Engineers (Webster et al. 1992). A total of 24 measurements per lift were conducted, as shown in Figure 20. A distribution of the CBR results from the DCP tests are shown in Figure 21. The results are also tabulated in Table A-4.

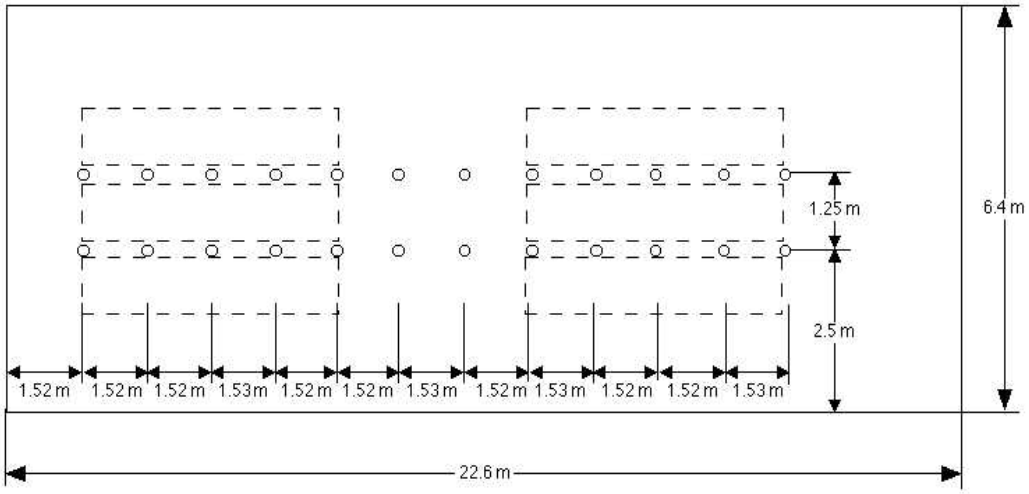

Figure 20. Location of dynamic cone penetrometer (DCP) test points.

The mean CBR of the subgrade was 13, with a COV of 56%. This is similar to that obtained from the Clegg hammer. A similar distribution for the upper 1.2 m of subgrade is shown in Figure 22. The mean CBR of the upper subgrade was 12, with a COV of 56%.

The high coefficient of variation with the CBR data may be due to stones in the subgrade material. Even though attempts were made to remove stones larger than 50 mm, when the test section was removed at the end of testing, we found the subgrade to contain a significant number of stones (Fig 23).

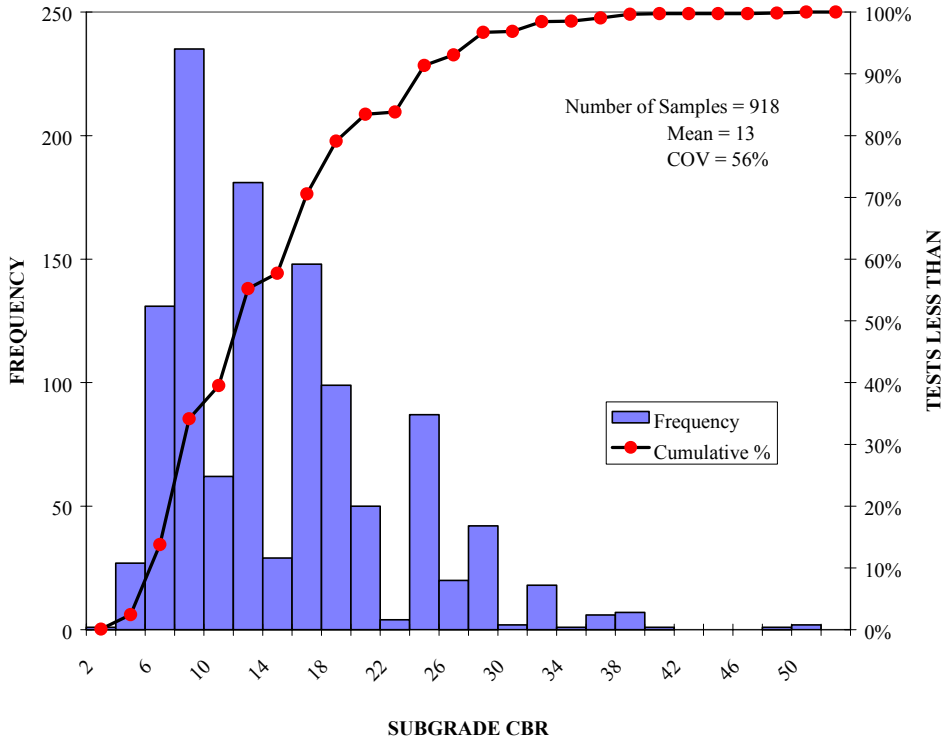

Figure 21. Distribution of subgrade CBR from the DCP tests.

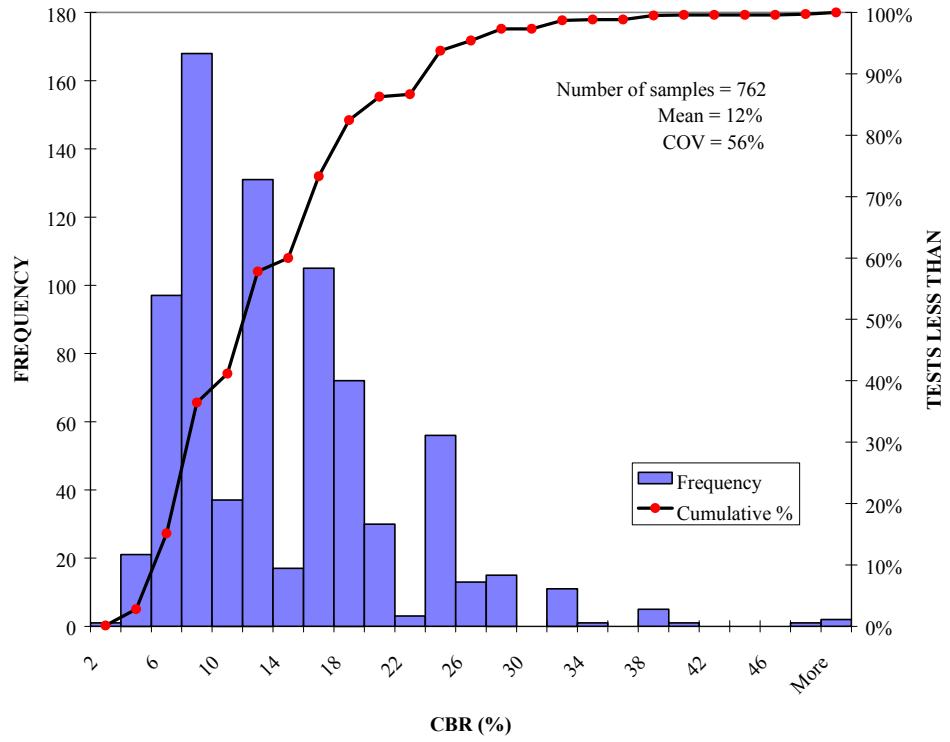

Figure 22. Distribution of subgrade CBR in the upper 1.2 m from the DCP tests.

Figure 23. Stones in 701 found during the removal process.

Elevation Measurements

Elevation measurements were taken for every 300-mm lift. Below 1.2 m from the surface the bottom six lifts were constructed at nominal thicknesses of 300 mm. The top 1.2 m of subgrade was constructed in 150-mm lifts. Lift thicknesses measured during the construction of the test section are presented in Table A-5. The distribution of layer thickness during the construction of the subgrade is shown in Figure 24. The mean layer thickness of the subgrade was 304 mm, with a COV of 15%. The mean lift thickness of the base layer was 267 mm, with a COV of 7%. The mean thickness of the asphalt concrete layer was 84 mm, with a COV of 14%.

Deflection Testing

Although not used as part of construction control, as the test section was constructed, falling weight deflection (FWD) measurements were taken at locations close to where the DCP tests were conducted. A total of 24 measurements were taken on each 300-mm lift in the subgrade and on top of the base and the asphalt concrete layer. Prior to construction of the test sections, FWD measurements were also taken on the concrete slab beneath the subgrade. The tests were done using the SHRP protocol. The geophone sensors were located at 0, 203, 300, 600, 900, 1200, and 1800 mm from the center of the loading plate. The plate diameters used

on the subgrade and on the AC layer were 457 and 300 mm, respectively Additionally FWD tests were conducted after completion of the accelerated load tests.

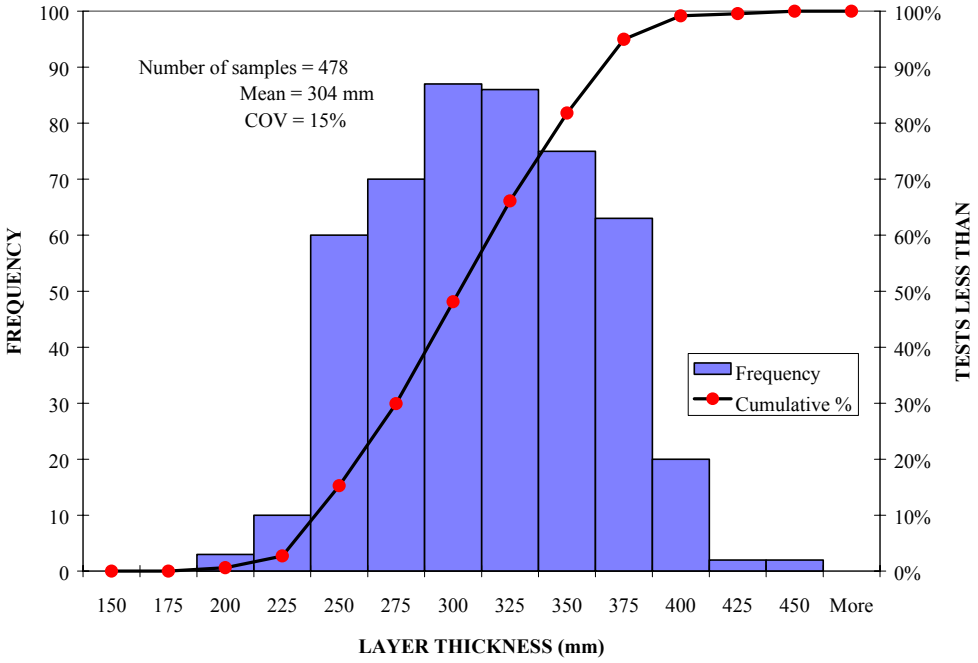

Figure 24. Distribution of layer thickness measured during subgrade construction.

Instrumentation

Instrumentation for measuring stress, strain, temperature, and moisture content were installed in the pavement structure during construction of the test section. The locations of the gages are shown in Figures 25. In Figure 25a, a plan view of the location of all the gages is presented. In Figures 25b–e, the locations of the moisture, stress cells and strain and temperature gages as a function of depth are shown. A brief description of the gages is presented here. Detail descriptions can be found in Janoo et al. (1999).

Strain measurements

Strain measurements were made with the Ɛmu system (Fig. 26). The system consisted of one sending coil and three receiving coils [longitudinal (x), transverse (y), and vertical (z)], the Ɛmu signal conditioner, and a computer data acquisition system. Details of the system can be found in the users manual by Dawson (1994).

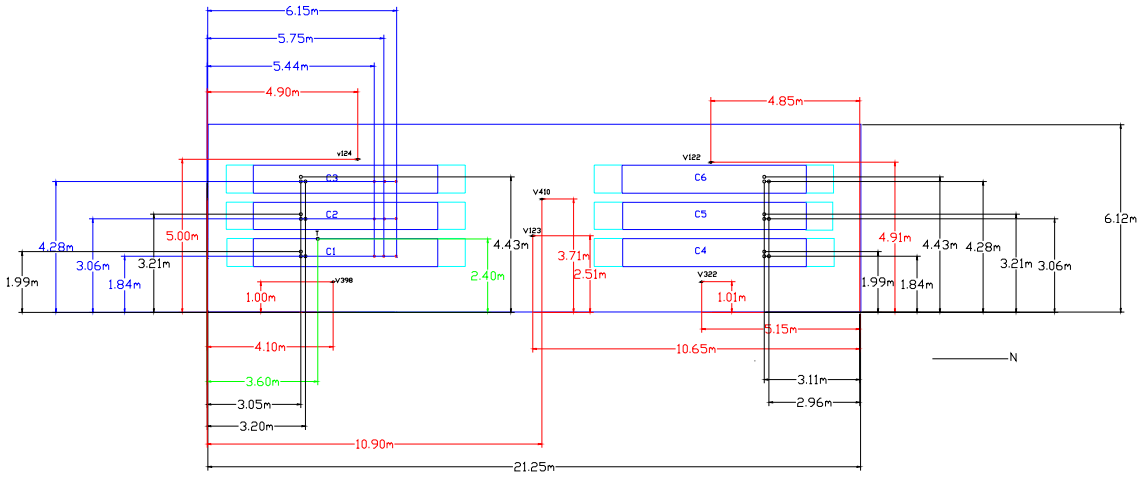

Figure 25a. Plan view showing the locations of various instrumentation in test section.

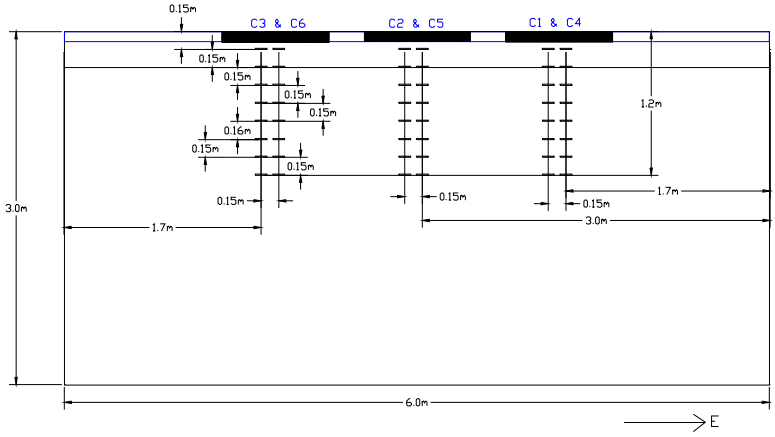

Figure 25b. Locations of εmu coil gages in the test section.

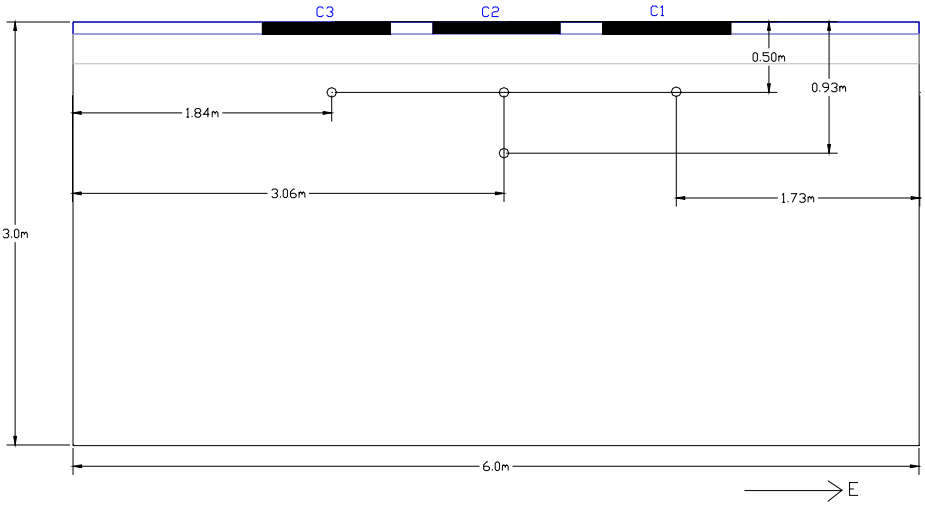

Figure 25c. Locations of stress gages in the test section.

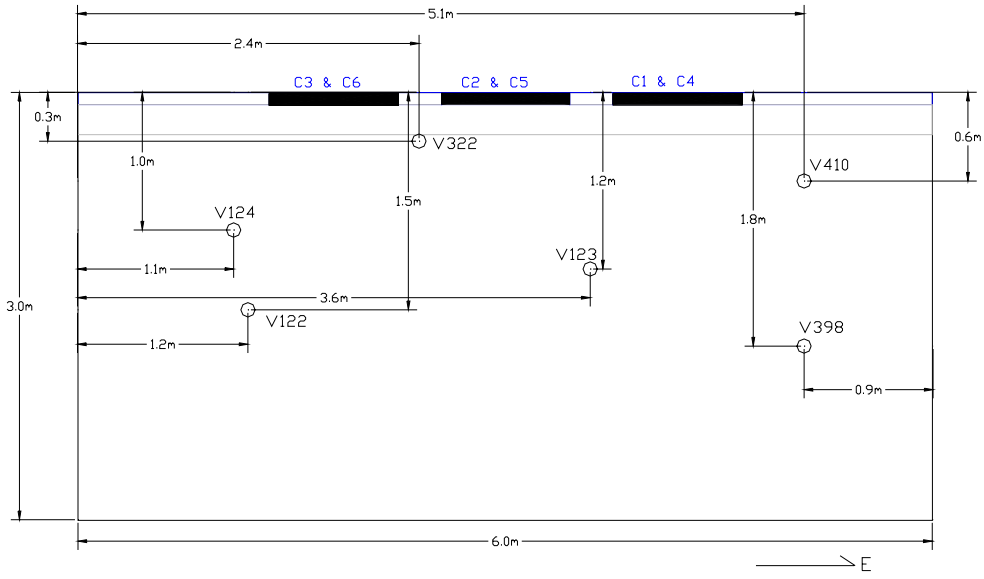

Figure 25d. Locations of moisture gages in the test section.

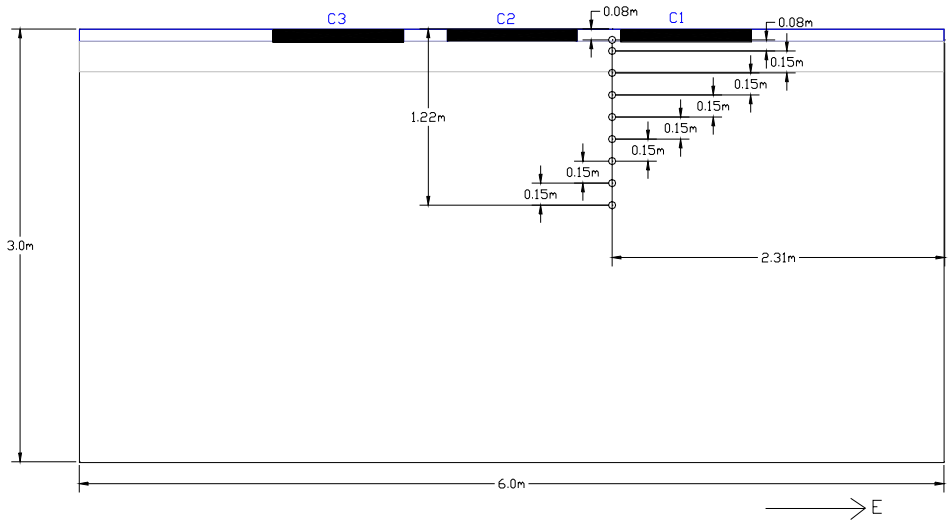

Figure 25e. Locations of temperature sensors in the test section.

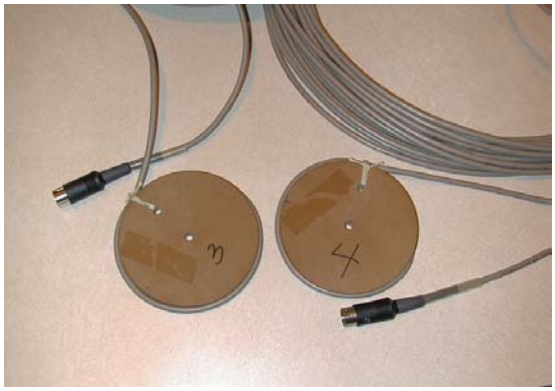

Figure 26. εmu coils for measuring strain.

The principle behind the system is that when an alternating current is passed through a coil of wire, an alternating magnetic field is generated. Another coil placed within this field will have an alternating current induced in it. The magnitude of the induced current is proportional to the magnitude of the exciting current and the distance between the transmitting and receiving cells.

Sets of 100-mm-diameter coil sensors were installed in each test window in the base course and subgrade. They measure the displacements in the vertical direction (designated as the z direction) and in two perpendicular horizontal directions (the x and y directions), as shown in Figure 27. The z-direction coils are coaxial, while the x- and y-direction coils are coplanar. The x direction is parallel to the wheel travel, and the y direction is perpendicular to it. The coils are installed at eight depths in columnar stacks, starting at 150 mm below the pavement surface and extending to 1.2 m at a nominal center-to-center spacing of 150 mm. A loose coil was used on the asphalt surface to measure the permanent deformation in the upper layer of asphalt and base. The ID and location of the coils in each window are presented in Tables B-1, Appendix B.

Figure 27. Ɛmu coil placement in the test section.

The horizontal locations are based from a datum located 0.3 m in the y direction from the northeast corner of the test section (Fig. 25a). The column identified as “Layer” in Table B-1 represents the material between the vertical coil pairs, as illustrated in Figure 28.

To relate the output voltage to the coil spacing in engineering units (millimeters), the following power equation gave a good fit:

$$V = a\,D^{n}$$

where D = static distance between the transmit and receive coils

V = demodulated (d.c.) "static" voltage from the coils

a and n = regression constants for a pair of coils.

Details on the calibration process can be found in Janoo (1999). The coefficients a and n for each coil pair are presented in Table B-2.

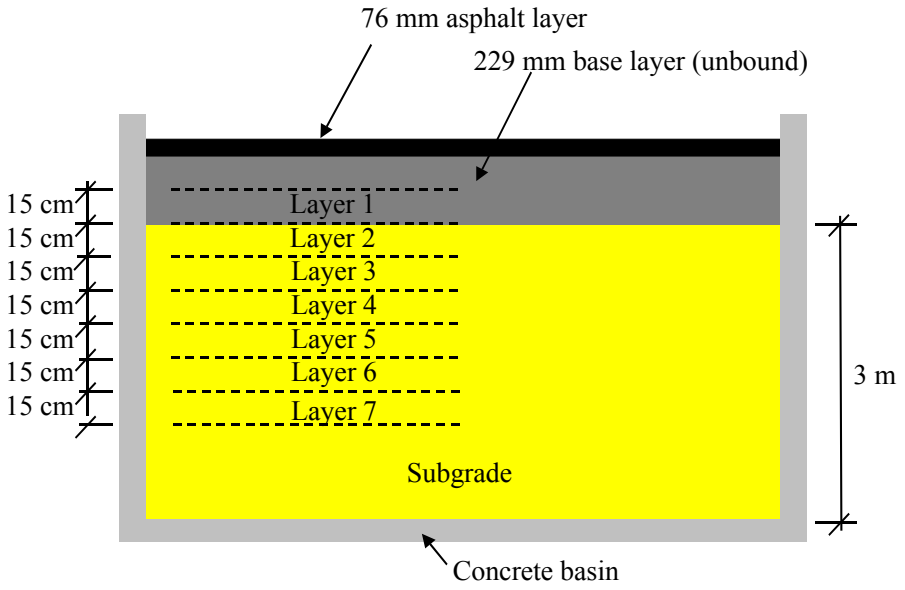

Figure 28. Illustration of the layers in the test section.

Once the grade of the lift was achieved, the surface where the coils were to be placed was raked smooth and leveled. To assure that the coil was aligned coaxially with the coil immediately below, the next lower coil was excited and the static response from the upper coil was measured. The coils were aligned when a maximum output from the coil pair was achieved. The coil was pressed down on the surface, checked with a carpenter's level, and shimmed with soil, if necessary, to assure that it was level. The thickness of the underlying compacted lift of soil was then measured. A thickness of approximately 150 mm was desired. If the lift was too thick, a small amount of trimming was done in the area where the coil was placed. If the lift was too thin, a small amount of shimming with soil was done. After the coil was properly aligned and leveled, it was covered with about 5 cm of soil, which was lightly

tamped. The coaxial cable leading to the coil was routed in a small trench, with a strain-relieving loop in the cable. The alignment dowels, visible in Figure 27, were then removed, and a 150-mm lift of compacted subgrade soil or base course was constructed using normal construction procedures.

Stress measurements

Vertical, longitudinal, and transverse stress measurements were made with the Dynatest soil pressure cells. They were used to measure the dynamic stresses due to the moving wheel load on the surface of the test windows. Details of the stress cell and calibration procedure can be found in Janoo et al. (1999).

Stress cells with a range of 10–200 kPa were used to measure the horizontal stresses, while stress cells with a range of 100–800 kPa were used to measure the vertical stresses (Fig. 29). The longitudinal-direction stress cell had its sensing elements facing the direction of wheel travel, while the transverse-direction stress cell had its sensing element facing the transverse direction of wheel travel. Due to delays in delivery of the cells, only windows 701C1, 701C2, and 701 C3 were instrumented with stress cells.

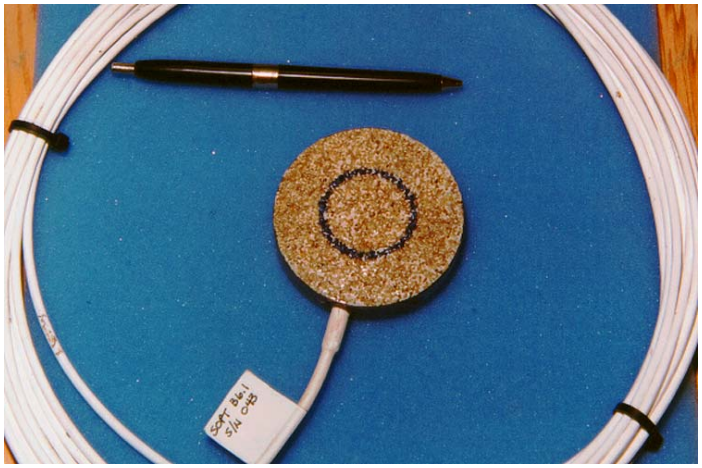

Figure 29. Dynatest soil pressure cell.

The locations of the soil pressure cells are shown in Figure 25c and tabulated with the respective calibration coefficients in Table B-3. The longitudinal (x) and transverse distances in Table 10 are based from a datum located 0.3 m in the y direction from the northeast corner of the test section (Fig. 25). The depth is from the surface of pavement surface. The calibration between stress and voltage is given below:

$$\sigma(kPa) = \frac{(1000 \times V)}{(V_{ex} \times Gain \times GF \times 10^{-5})}$$

where σ = measured stress

V = measured voltage

V_{ex} = excitation voltage = 10 V

GF = gain factor (Table B-3, Appendix B)

$Gain$ = 500 × A/D card gain.

The A/D card gain was set at 2 for 701C1 and 8 for 701C2 and 701C3.

Moisture measurements

Soil moisture was measured with Vitel soil moisture probes (Fig. 30). Details on the probe can be found in Janoo et al. (1999). Basically the probe is used to measure the dielectric constant of the soil at a high frequency of 50 MHz. The measured dielectric constant is divided into its two components (capacitive and conductive). The capacitive component depends on the volumetric moisture content of the soil. Through the use of appropriate calibration curves, the dielectric constant measurement can be related to soil moisture. The accuracy of the volumetric moisture content is ±2% using the calibration equations provided by the manufacturer. The accuracy is increased to ±0.5% if calibrations are conducted with the test soil. The reproducibility of the measurements is ±0.3%. The reliability of the data deteriorates below –10°C.

Figure 30. Vitel Hydra moisture probe.

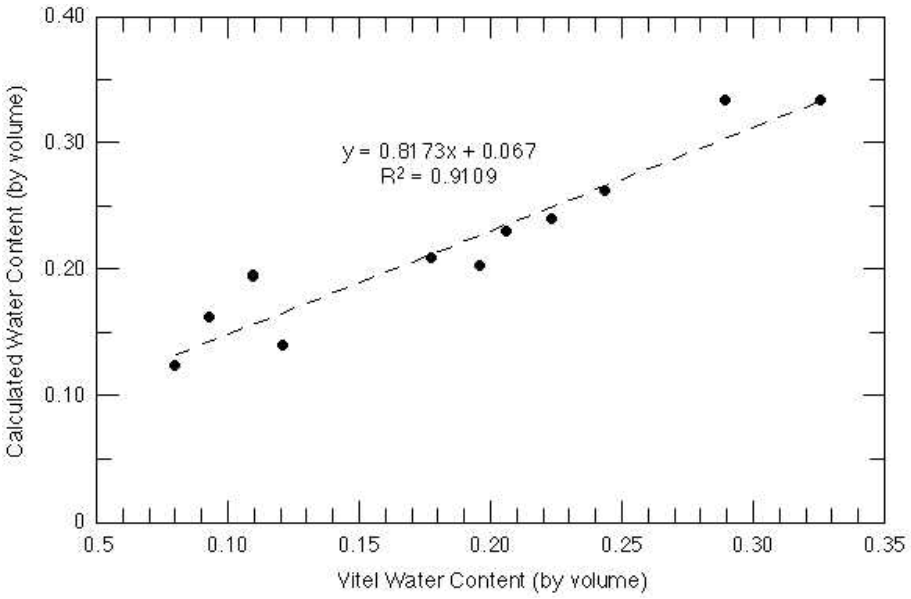

Figure 31. Vitel moisture probe calibration results for the A-2-4 soil.

The Vitel moisture probes were calibrated for the test subgrade soil (Fig. 31). The sand calibration equation in the Vitel software was used to convert the dielectric constant to volumetric moisture content. Details on the calibration of the probes can be found in Janoo et al. (1999). The following linear equation was used to determine the volumetric water content in the A-2-4 test subgrade soil in test section 701:

$$\omega_{vol} = 0.8173 \times (Vitel) + 0.067 \quad R^2 = 0.91$$

where ω_{vol} is the calibrated volumetric moisture content and *Vitel* is the volumetric moisture content measured from Vitel Hydra probe.

Six sensors were installed in each test window in test section 701. The longitudinal (x) and transverse distances are based from a datum located 0.3 m in the y direction from the northeast corner of the test section (Fig. 25). The depth is from the surface of the pavement. The locations in the x-y plane are shown in Figure 25a, and the elevation view is shown in Figure 25d. The locations are also tabulated in Table B-4. Details of the installation procedure can be found in Janoo et al. (1999). Moisture measurements were taken on a hourly basis from the end of construction of the test sections to the end of all the testing of 701.

Temperature measurements

Air, surface, and subsurface temperatures were taken using thermocouple sensors. The thermocouples have an accuracy of ±0.5°C. Since thermocouples require a reference if a single junction is used and they can also pick up electrical noise, the datalogger system used had reference junctions for the thermocouples.

In this test section we tried to install a thermocouple string at the end of phase 1 construction (i.e. in the bottom 1.8 m of subgrade), but we had difficulty drilling into the subgrade soil. Single thermocouples were installed in the top 1.2 m of subgrade and in the base. The locations of the thermocouples are shown in Figure 25a and e. In addition the locations are tabulated in Table B-4. Single thermocouples were also used for measuring the air and asphalt concrete surface temperatures.

Testing Program

Test windows 701C1, 701C2, 701C3, and 701C4 were subjected to accelerated pavement testing. Windows 701C5 and 701C6 were not tested because of delays in the testing of the other four windows and because of the time available for construction of 703 prior to the onset of winter.

Prior to the accelerated load tests, FWD measurements were taken on the surface of the AC layer using the same locations as during the construction phase (Fig. 21). Initial transverse profiles were measured using the 3-m-long laser profilometer (Fig. 32). The laser located 45 cm from the ground surface measured the surface profile at approximately 9-mm intervals. In addition to the profilometer measurements, level surveys were made during every test to determine whether the reference points (i.e. where the three feet of the profilometer were located during the surface profile measurements) moved. The results from the level surveys indicated that the points were stationary throughout the test. Twenty-four transverse cross-section measurements spaced 0.3 m apart were made in each window (Fig. 33). Measurements taken at locations 1, 2, 23, and 24 (acceleration and deceleration zones) and are not presented here. Surface profile measurements were made after 500, 1,000, 2,500, 5,000, 10,000, 25,000, 50,000, 100,000, 200,000, 500,000, 1,000,000, etc. load repetitions. The rut depth was defined as the distance in the vertical direction from a point located 30 cm outside the actual test window at each side to the bottom of the rut, as shown in Figure 34. Testing was terminated when a surface rut depth of 12.5 mm was reached or exceeded.

Figure 32. The laser profilometer.

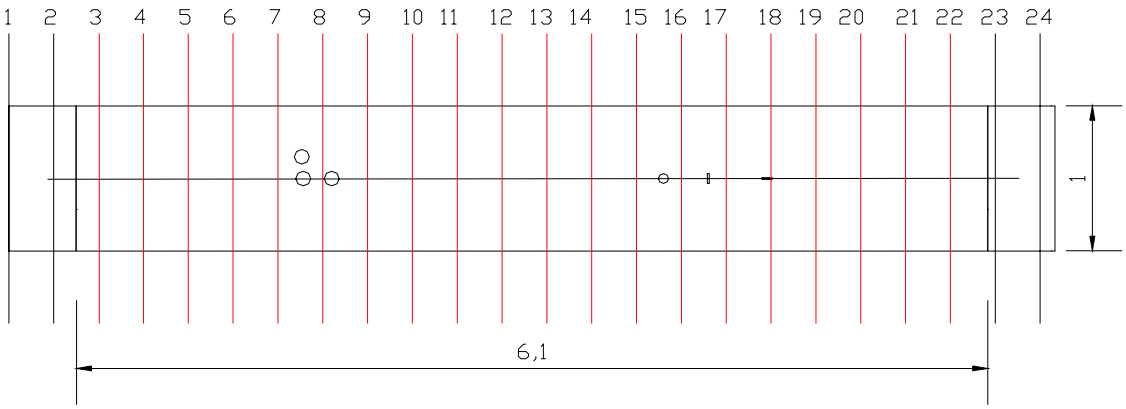

Figure 33. Locations for profile measurements in test section 701.

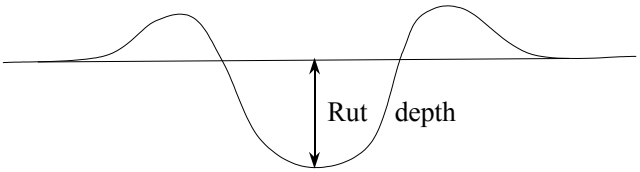

Figure 34. Definition of rut depth.

Subsurface stresses, strains, and permanent displacements were also measured in the vertical and in two perpendicular horizontal directions after 0, 500, 1,000, 2,500, 5,000, 10,000, 25,000, 50,000, 100,000, 200,000, 500,000, 1,000,000, etc. load repetitions. Dynamic stress and strain measurements in the test windows were taken when the wheel was in the positions shown in Figure 35. Measurements were taken at these three locations because one of the dual tires was either on top or very close to the sensors as the wheel traversed the test section. It was decided, at least for this window, to measure the stresses and strains at the three locations identified in Figure 35 and determine if there were any significant differences.

At the end of the dynamic stress-strain measurements, permanent deformation measurements were taken using the εmu coils. A loose coil gage on the surface was used to measure the permanent deformation between the surface and the first coil in the base course. The locations in Figure 35a, b and c were identified as Position 1, Position 2 and Position 3, respectively.

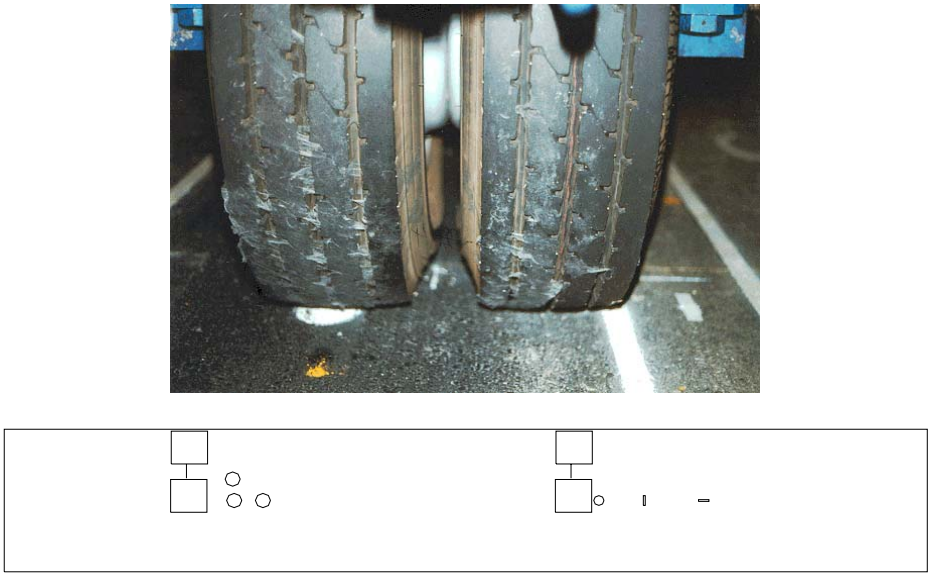

Figure 35a. Location of test wheels over coil and stress cells for Position 1 measurements.

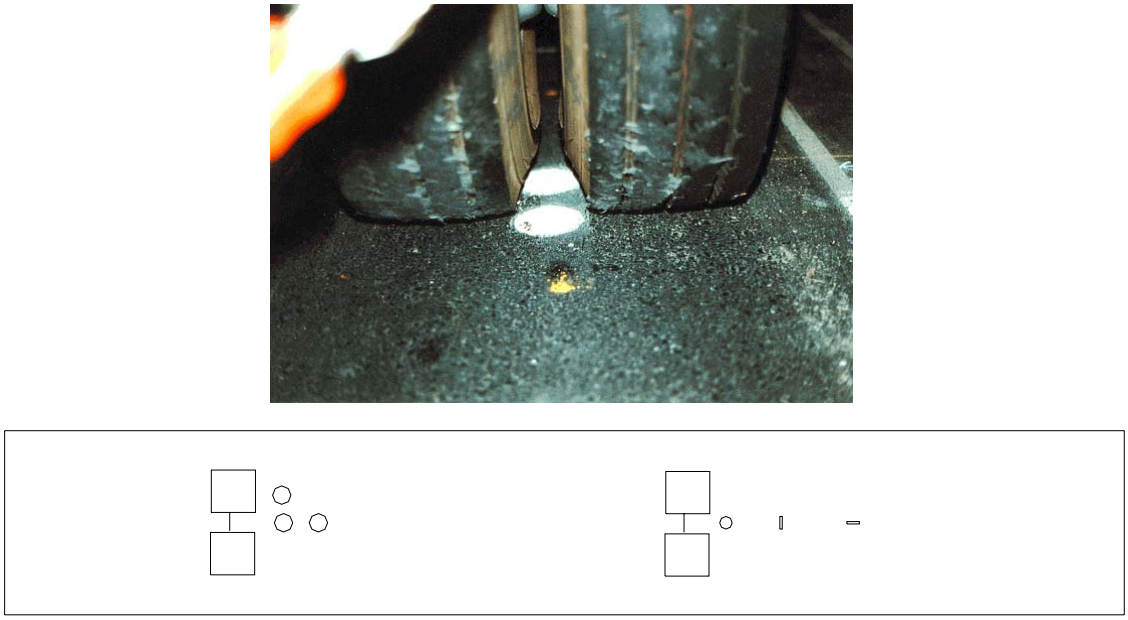

Figure 35b. Location of test wheels over coil and stress cells for Position 2 measurements.

Figure 35c. Location of test wheels over coil and stress cells for Position 3 measurements.

Accelerated Loading of the Test Section

The test windows were loaded using the Mark IV Heavy Vehicle Simulator (HVS), accelerated loading system (Fig. 36). The tire pressure was set between 690 and 757 kPa, and the tests were conducted in the unidirectional mode at 13 km/hour. At 13 km/hour the average number of load repetitions was 700 per hour. The tests were conducted for approximately 22 hours per day, seven days a week. The load was wandered over the test window in 50-mm increments. Additional details on the HVS can be found in Janoo et al. (1999). The dimensions of the test tires are shown in Figure 37.

Figure 36. The Heavy Vehicle Simulator (HVS), Mark IV.

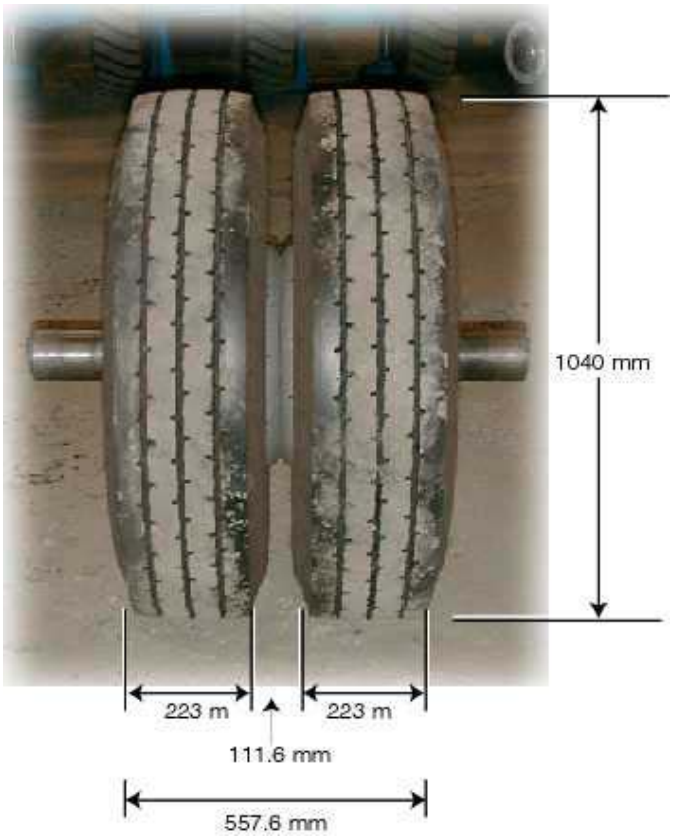

Figure 37. Dimensions of the test tire

RESULTS

Temperature and Moisture

Temperature Measurements

The mean daily temperatures of the test sections and the air above during the test period are presented in Figure 38. Only small temperature gradients were registered in the test section. The air temperature fluctuated somewhat more, as expected. For the purpose of these experiments, the temperature variations recorded at large are not significant. These temperatures were measured with thermocouples.

Temperature data were also obtained from thermistors built into the Vitel Hydra moisture probes. The temperatures recorded with these thermistors were consistent with those recorded by the thermocouples, as shown in Figure 39.

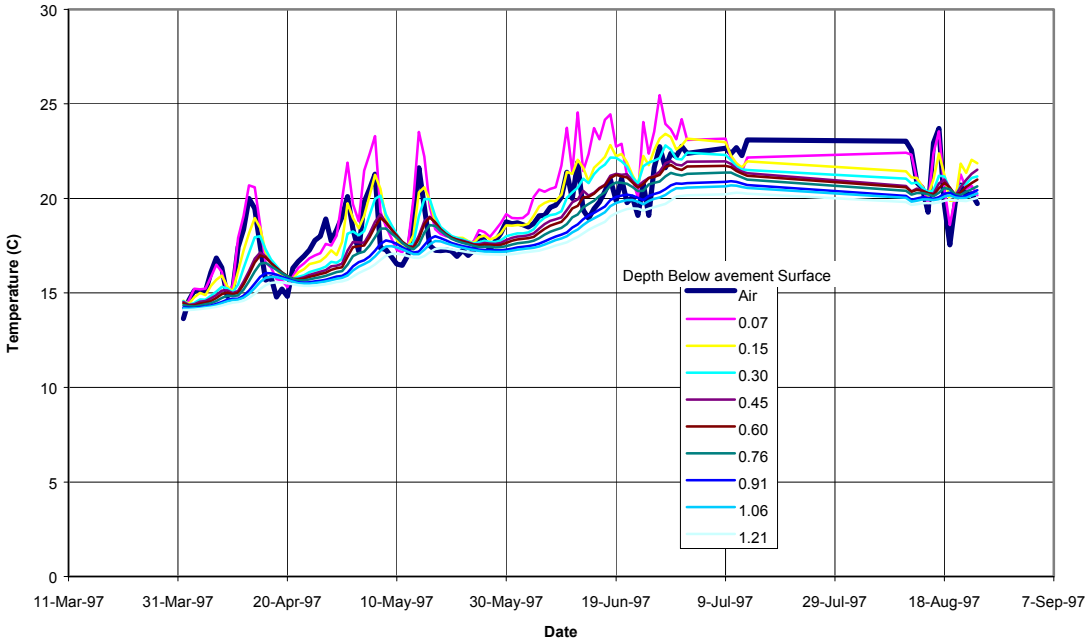

Figure 38. Mean daily temperatures during the test period.

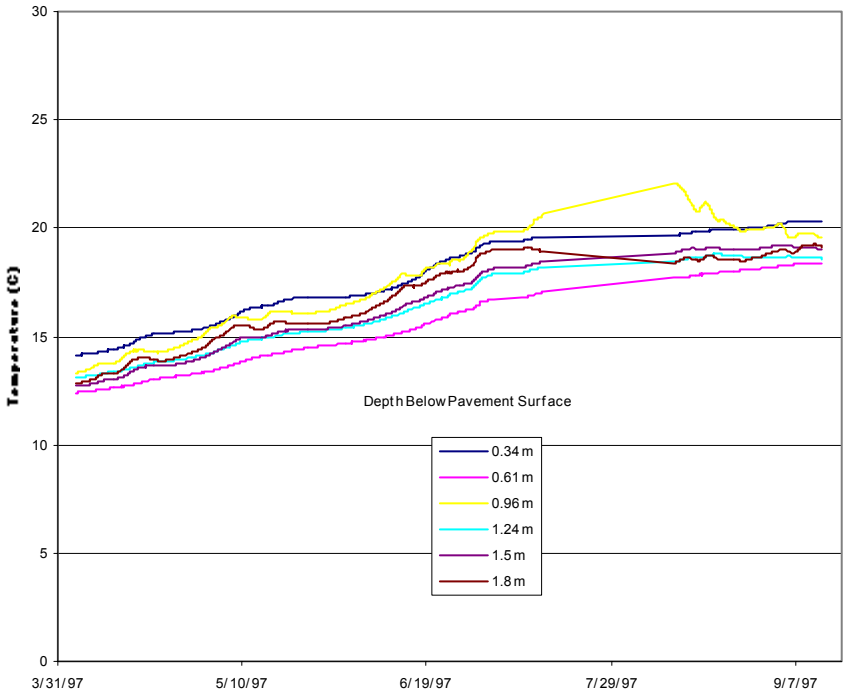

Figure 39. Temperature regime as measured by thermistors built into the Vitel Hydra probes.

Figure 40 shows a profile of the average temperatures within the test section along with a range that indicates the extreme temperature values registered during the test period.

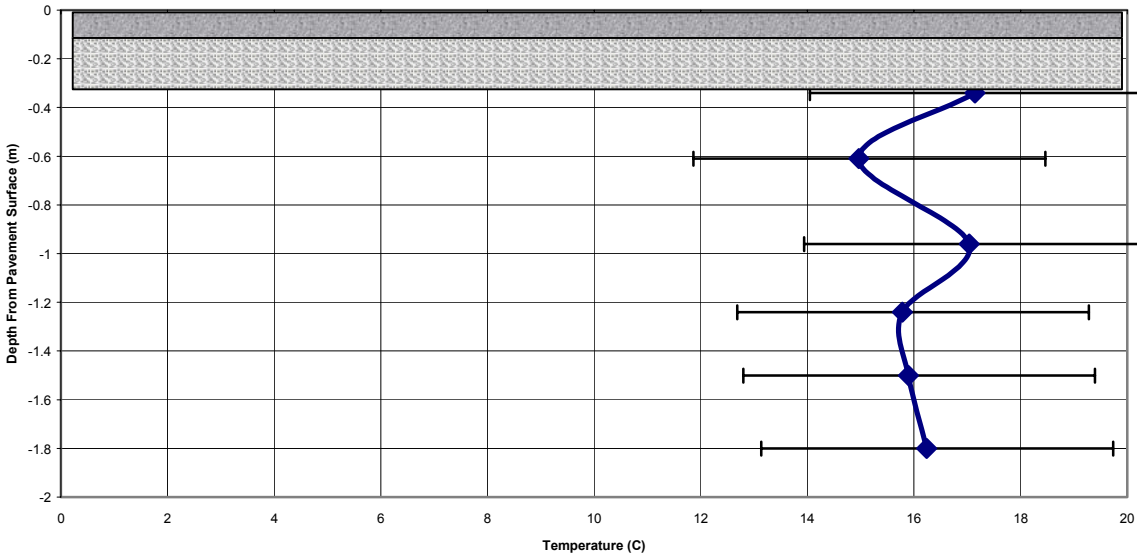

Figure 40. Subgrade temperature profile displaying average and range.

Moisture Measurements

Moisture content is a critical parameter that affects important mechanical properties of subgrade soils. Moistures variations during the test period were relatively small, as shown in Figure 41. Moisture content was monitored with the Vitel Hydra probes. As explained earlier, these probes measure moisture content indirectly. They measure the capacitive component of a high-frequency electrical signal to determine the soil's dielectric constant. The volumetric moisture content is then determined from the apparent dielectric constant. The corrected volumetric moisture contents were then converted to the gravimetric moisture content using established weight-volume relationships. The dry density of the subgrade soil used in the conversion process was 1922 kg/m^3.

Figure 42 shows a profile of moisture content with average values, as well as the range of measured values during the test period. The variation of the moisture data was relatively narrow. The moisture content ranged between 8% near the top of the subgrade to approximately 13% at the lower depths. In the top 1.22 m of subgrade, the moisture content ranged between 8 and 11%, with a mean around 10%.

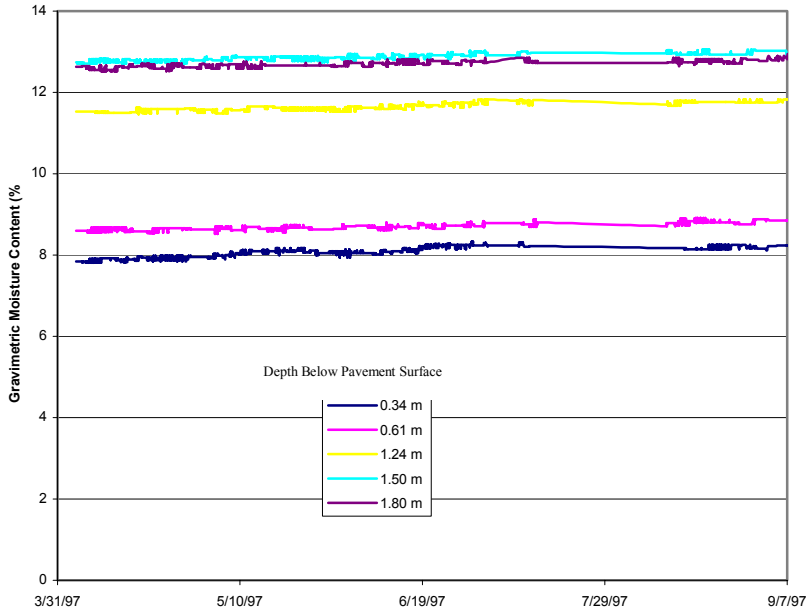

Figure 41. Subgrade moisture regime at various depths during the test period.

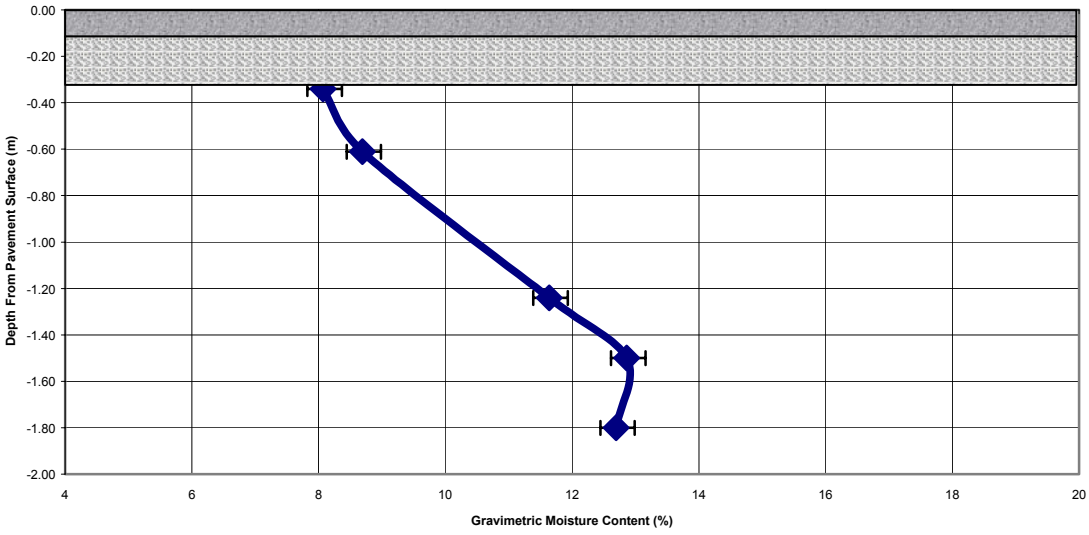

Figure 42. Profile of moisture content with average values during the test period.

Results from Test Window 701C1

Testing of window 701C1 began on April 10, 1997, and ended on July 1, 1997. This was the first time the HVS was used in the FERF, and during the tests there were several breakdowns. The longest period of breakdown (15 days) was at the end of 52,800 passes,

when there was a catastrophic failure of the wheel carriage. Once the carriage was repaired, a series of tests were conducted to determine if there was any rebound of the pavement structure during the breakdown period. Zhang et al. (1998) found from their program of testing a pavement section for 8 hours a day that there was a decrease in the dynamic strains prior to resumption of loading the following morning. At the end of the test, a series of tests were conducted to determine the effect of speed on the dynamic stress and strain in the pavement structure.

The test load was 80kN, with a COV of 0.9%, and the tire pressure was 690kPa was 6.7%. The tire pressure gages failed between May 4 and June 5, 1997.

Dynamic Stress

Stress measurements were made at a single depth of 508 mm from the surface in 701C1, which was approximately 203 mm from the top of the subgrade. Typical stress responses at the three positions are shown in Figure 43. Negative values indicate compressive stress. Review of the stress data from the remaining test windows and other test sections indicates that the stress measurements were taken with a 40-kN load instead of the test load of 80 kN. The maximum stresses occurred when the sensors are directly under both the wheels, i.e. at position 2. The longitudinal and transverse stresses were insignificant (ranging around 5 kPa). The results from the stress measurements are tabulated in Table C-1, Appendix C.

The changes of the vertical stress (position 2) as a function of load repetition are shown in Figure 44. With the vertical stress it appears that up to approximately 10,000 passes, there is no significant increase in the stress as a function of load repetition. After 10,000 passes, the stress increases with increasing repetition.

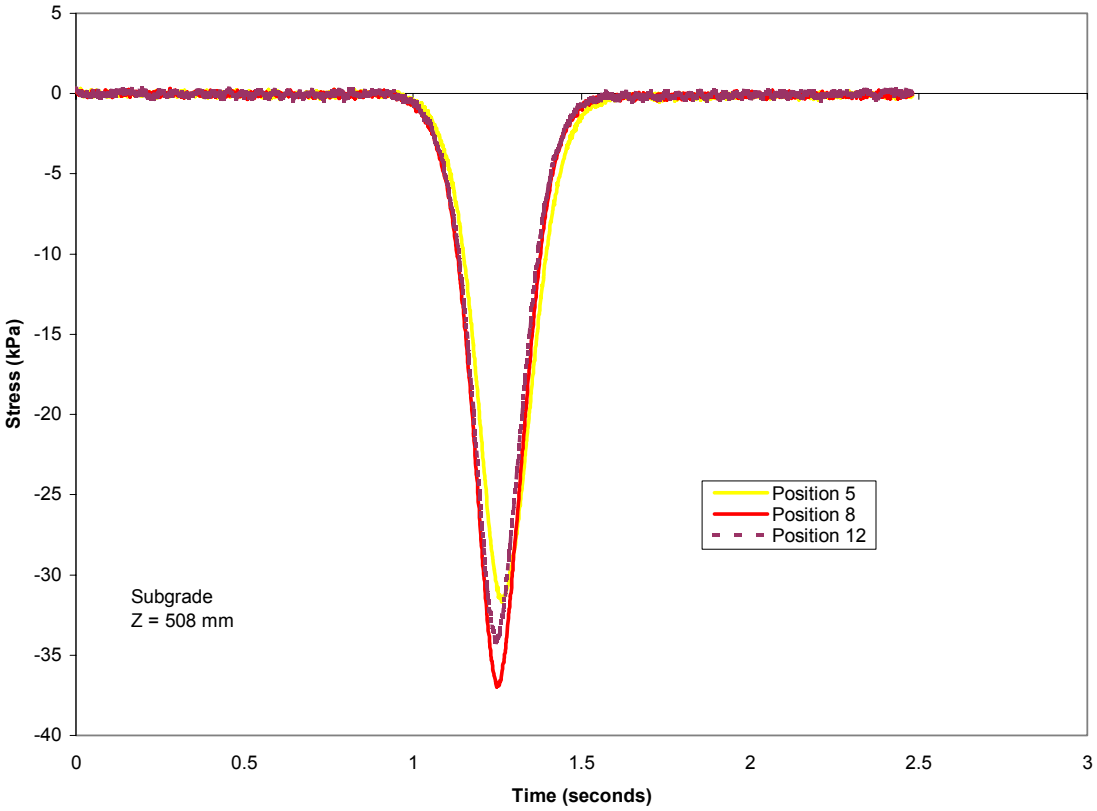

Figure 43. Typical vertical stress response in the subgrade after 20,000 repetitions.

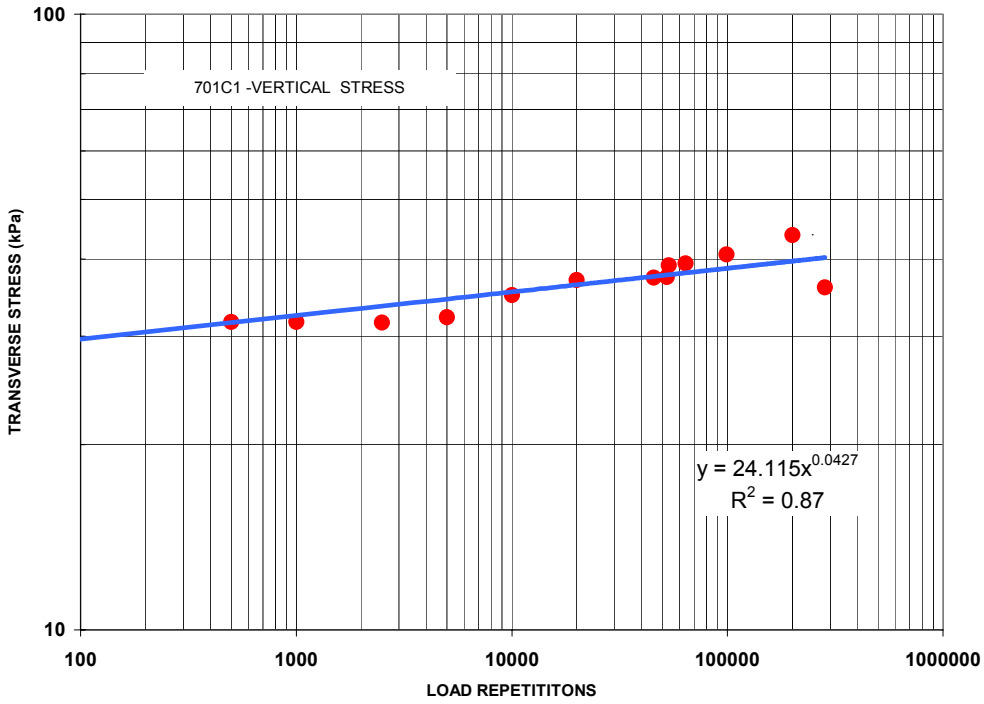

Figure 44. Change in vertical stress as a function of load repetition.

Dynamic Strain

Vertical, longitudinal, and transverse dynamic strains were measured as a function of load repetitions at the three wheel locations. Typical strain responses in the subgrade at the three wheel positions are presented in Figure 45. Generally the vertical strain is compressive, while the longitudinal and transverse strains are expansive. However, the longitudinal strain is compressive as the wheel approaches the sensors and becomes expansive as the wheel is on top of the sensor. As the wheel leaves the sensor, the strain drops and becomes compressive before returning to zero. It was also found that in general the maximum strains occur when the wheel was in position 2.

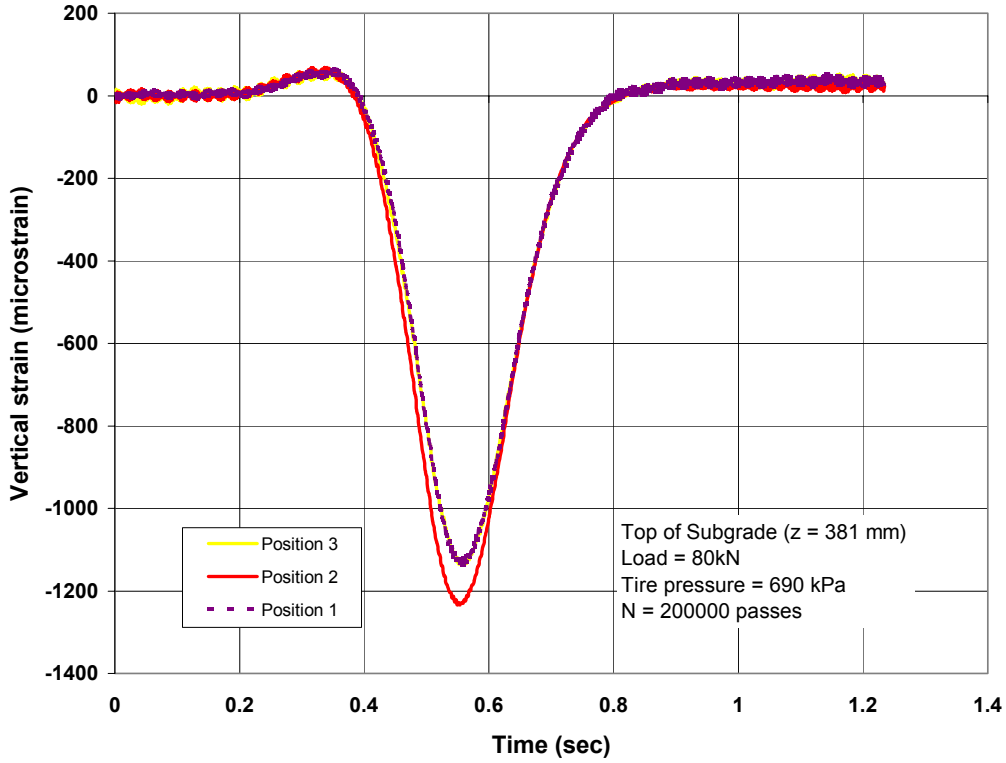

Figure 45a. Typical vertical strains at the three wheel positions.

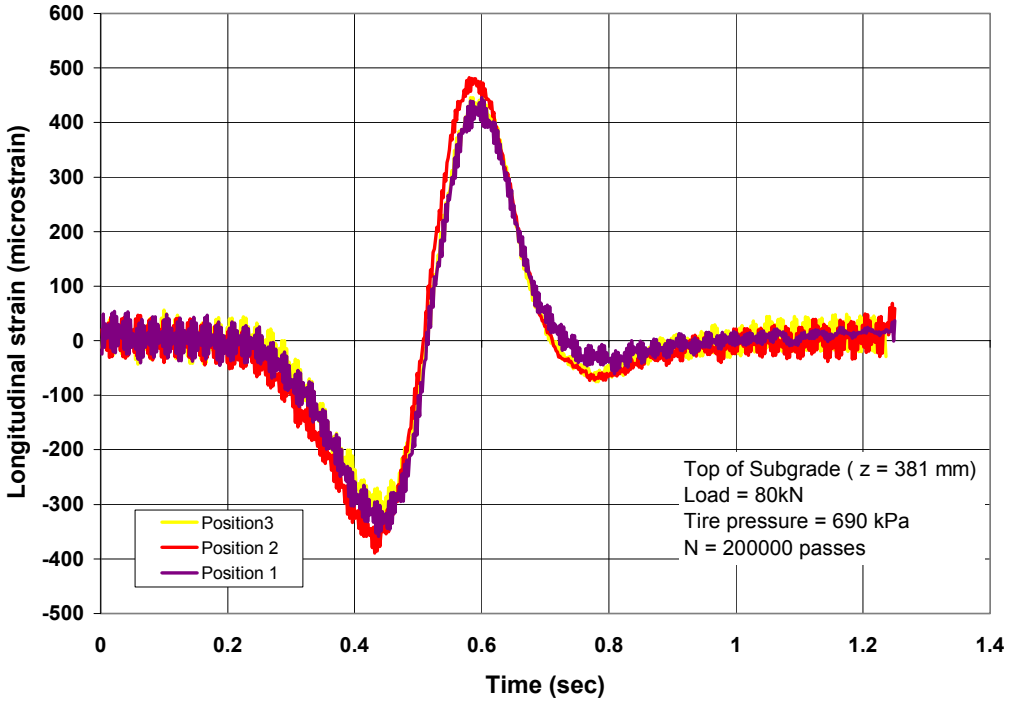

Figure 45b. Typical longitudinal strains at the three wheel positions.

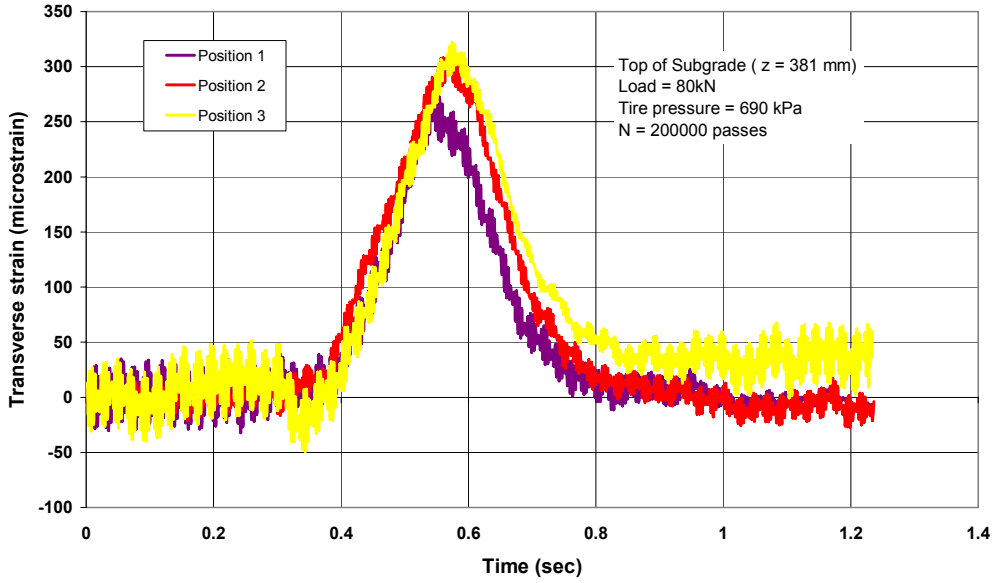

Figure 45c. Typical transverse strains at the three wheel positions.

A comparison of the vertical, longitudinal, and transverse strains (position 2) at various depths in the subgrade is shown in Figure 46. Several typical observations were made:

- The maximum vertical strain is about 2.5–3 times the maximum longitudinal strain.
- The maximum vertical strain is about 2.5–4 times the maximum transverse strain. The factor decreases with depth.

- The response of the longitudinal and transverse strains are similar at depths of 840 mm and greater from the surface of the AC layer.
- At the top of the subgrade the initial compressive strain is about 80% of the maximum strain (expansive). This drops to about 30% at 150 mm from the top of the subgrade and below.

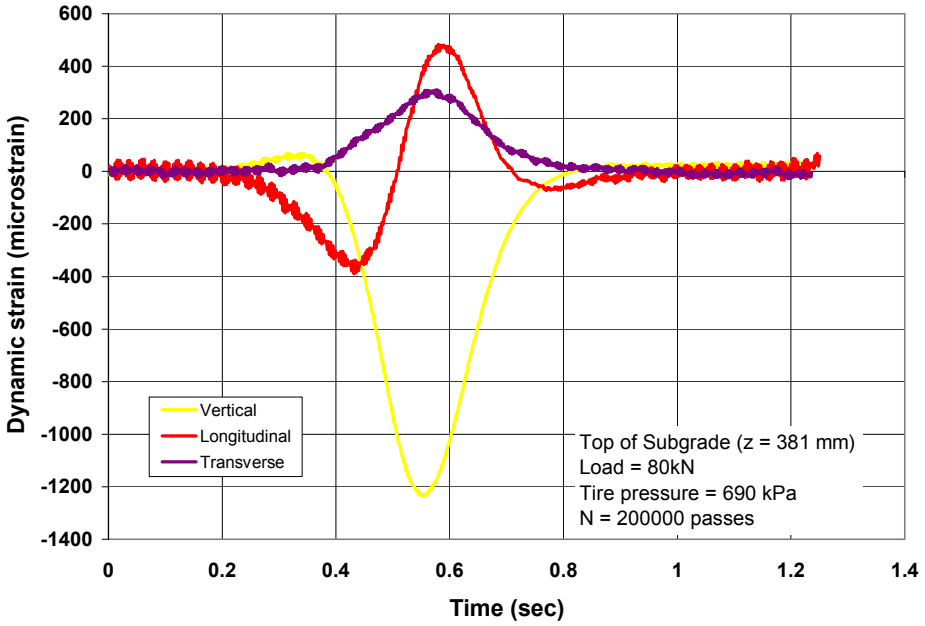

Figure 46a. Strain response as a function of depth (z = 381 mm from the surface).

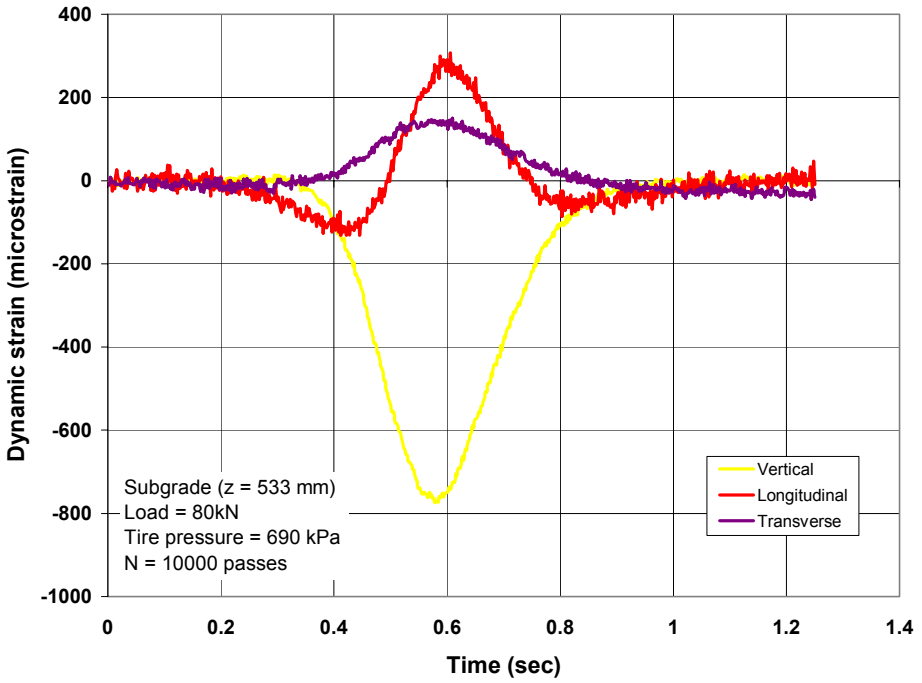

Figure 46b. Strain response as a function of depth (z = 533 mm from the surface).

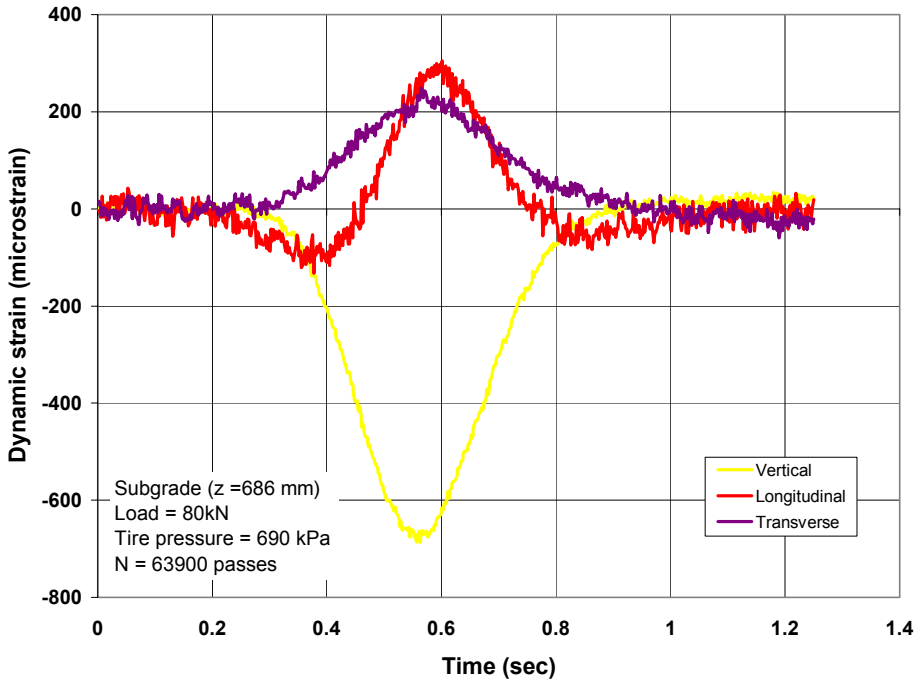

Figure 46c. Strain response as a function of depth (z = 686 mm from the surface).

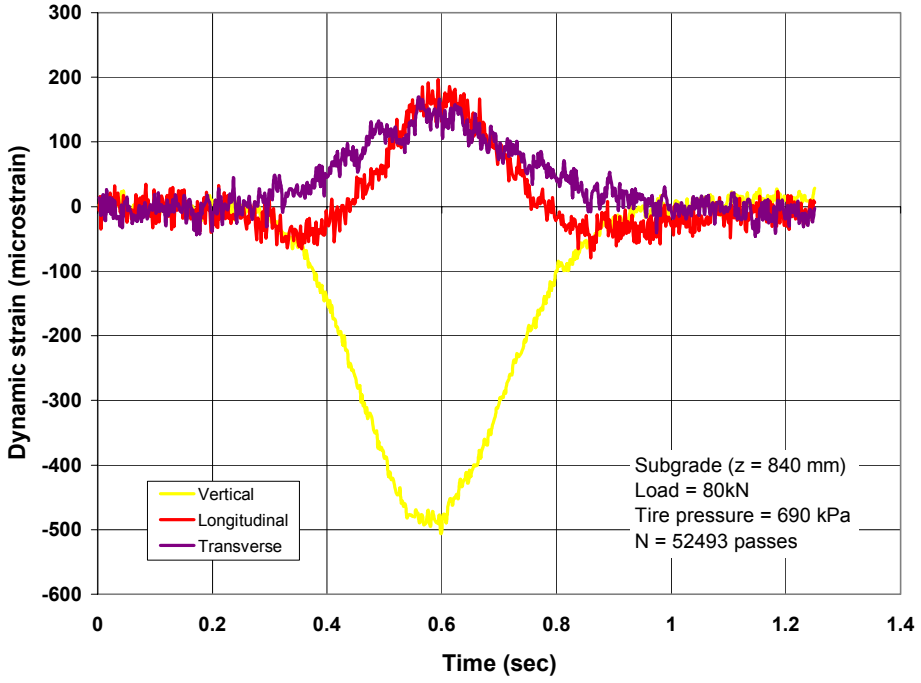

Figure 46d. Strain response as a function of depth (z = 840 mm from the surface).

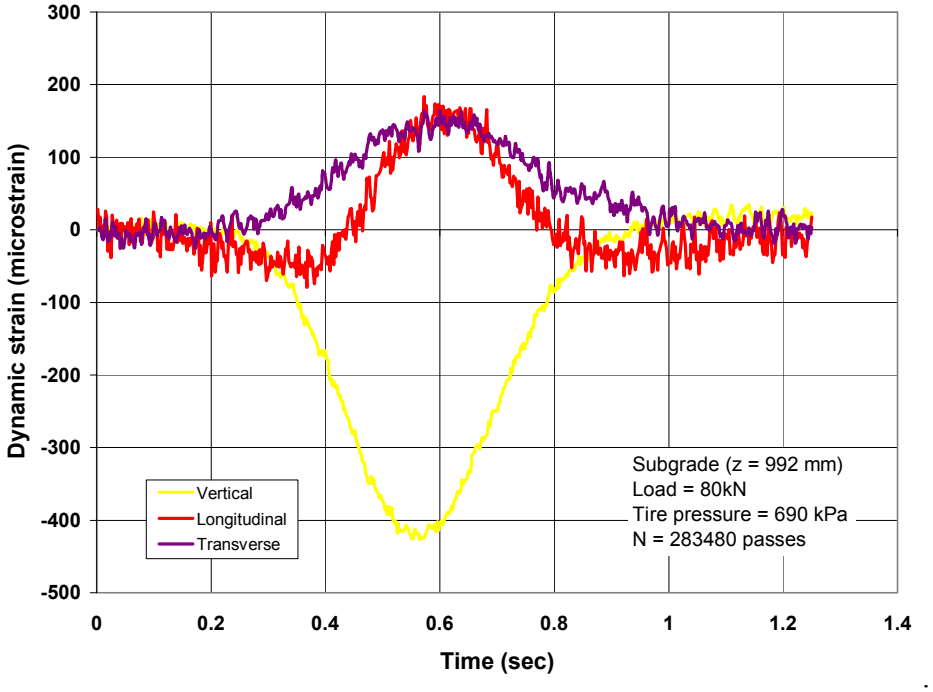

Figure 46e. Strain response as a function of depth (z = 992 mm from the surface).

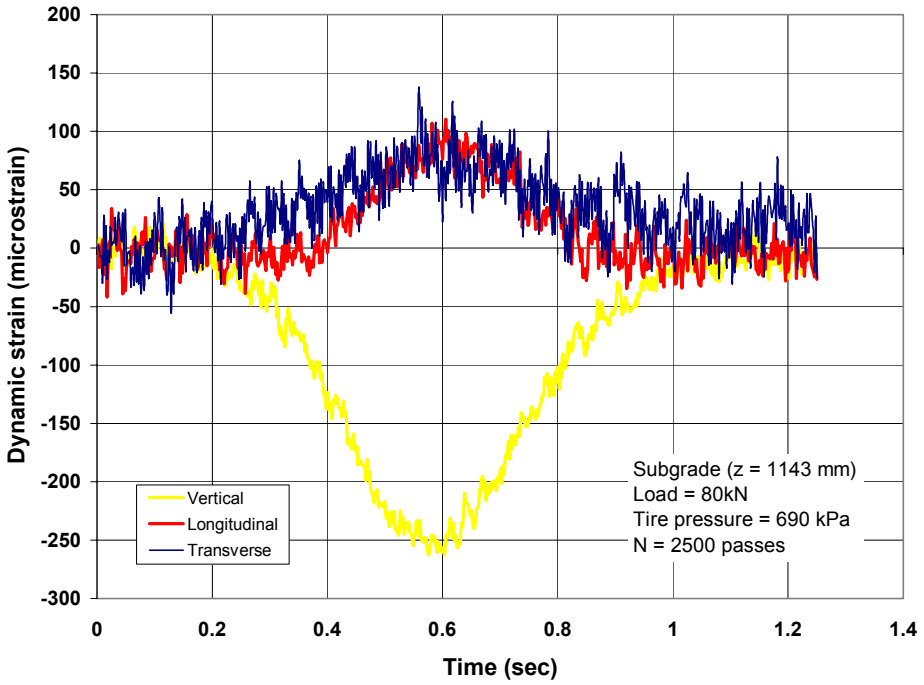

Figure 46f. Strain response as a function of depth (z = 1067 mm from the surface).

The maximum strains in Tables C-2 to C-4 were obtained after the data were smoothed using a 10-point averaging scheme. The vertical strains are an average between the coil pairs, and the depths presented in the Table C-2 are the midpoints between the coil pairs. In the longitudinal and transverse strains, the depths in Table C-4 are the actual locations of the coil gages. Therefore, the longitudinal and transverse strains were measured slightly above the vertical strains. The difference is about 75 mm. Three sets of measurements are reported for the longitudinal strain, initial compressive strain, maximum expansive strain, and compression strain during unloading (Fig. C-1).

The development of the peak vertical, longitudinal, and transverse strains as a function of load repetitions at the different depths are presented in Figures 47–49. With the longitudinal strains, the peak strain was defined as the peak-to-peak distance between the first compressive strain A (Fig. C-1) and the peak extension strain B. We felt that near the surface, the peak compressive strain was as large as the extension strain and therefore had an impact on the overall subgrade response in the longitudinal direction.

With respect to the vertical dynamic strains in the subgrade, there was a rapid increase in strain in the first 2500 repetitions, after which there was a more gradual increase with increasing load repetitions (Fig. 47). The response of the peak longitudinal strain is shown in Figure 48. The longitudinal strain continues to increase with increasing load repetition. The rate of increase of the longitudinal strain is much greater than the vertical dynamic strain, especially in the upper subgrade layers. The peak transverse strain as a function of depth increases with increasing load repetitions (Fig. 49). The data from z = 1067 mm is not shown either in Table C-4 or in Figure 49 because in most cases the output was too noisy to clearly define the peak strain. The results shown in Figure 49 indicate that the peak transverse strains are approximately the same from the top of the subgrade to a depth of 610 mm from the AC surface. Below 610 mm there is some difference in the strain as a function of depth. Another observation made from the transverse strain results is that the strains are constant for approximately the first 5000 load repetitions.

The dynamic strain data was fitted with a power curve $y = Ax^n$ and replotted in log-log space (Fig. 50–52).

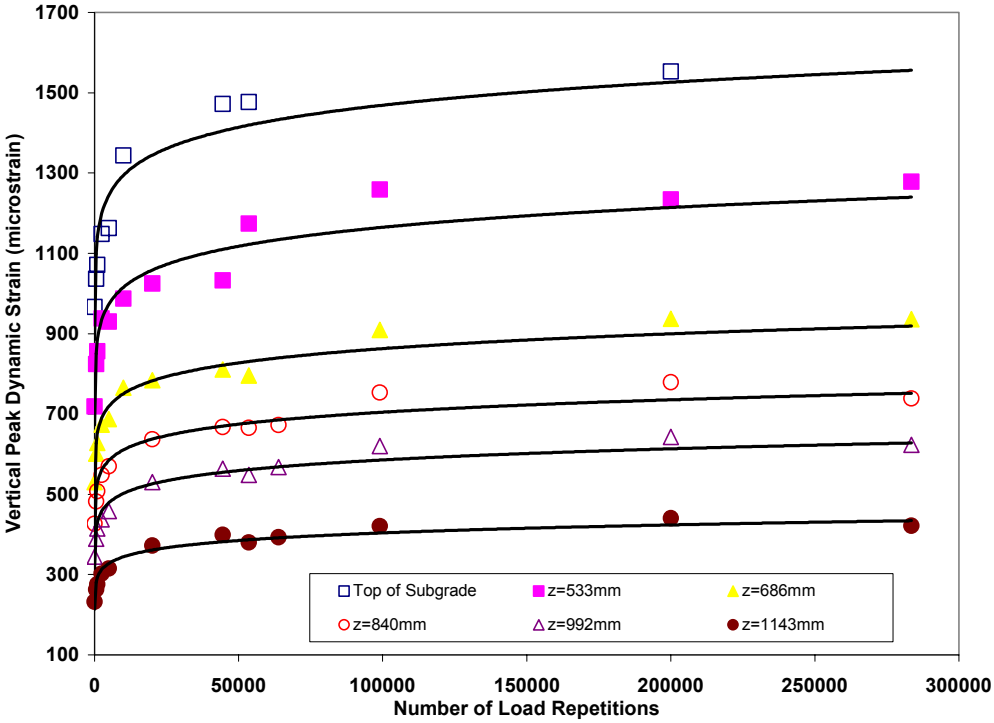

Figure 47. Vertical strains as a function of depth and load repetition (701C1).

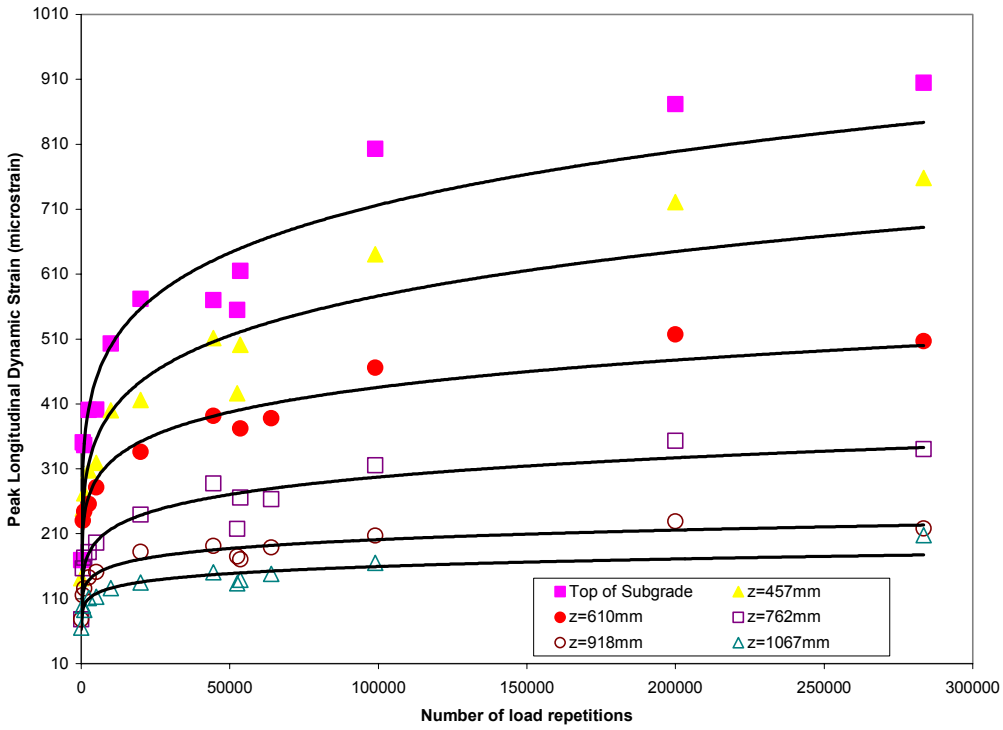

Figure 48. Longitudinal strains as a function of depth and load repetition (701C1).

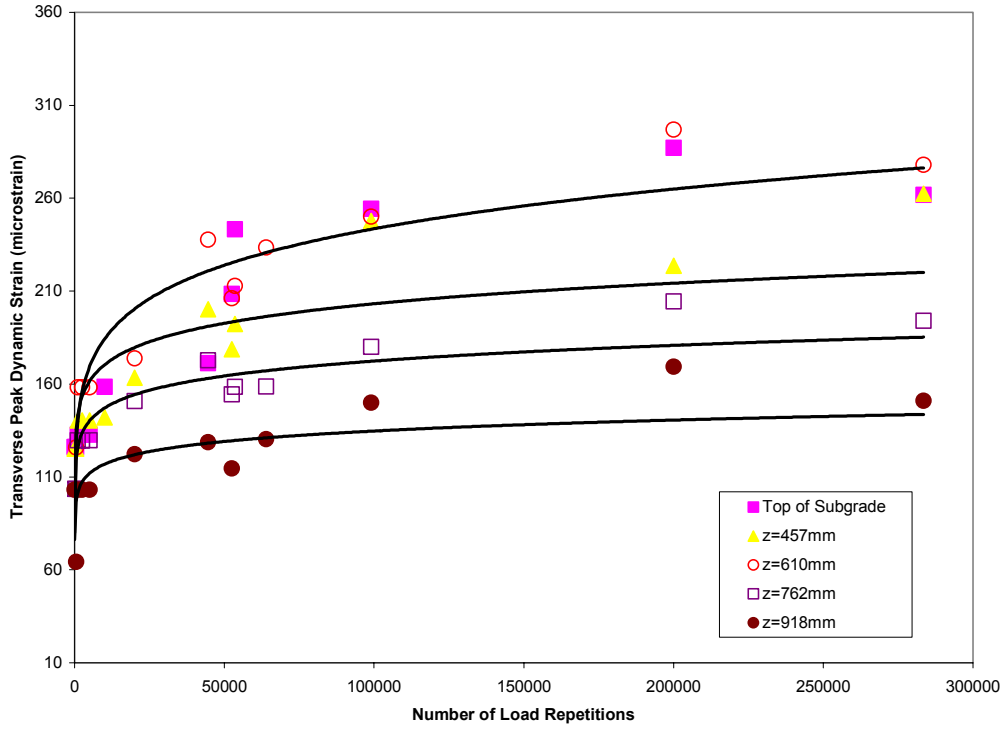

Figure 49. Transverse strains as a function of depth and load repetition.

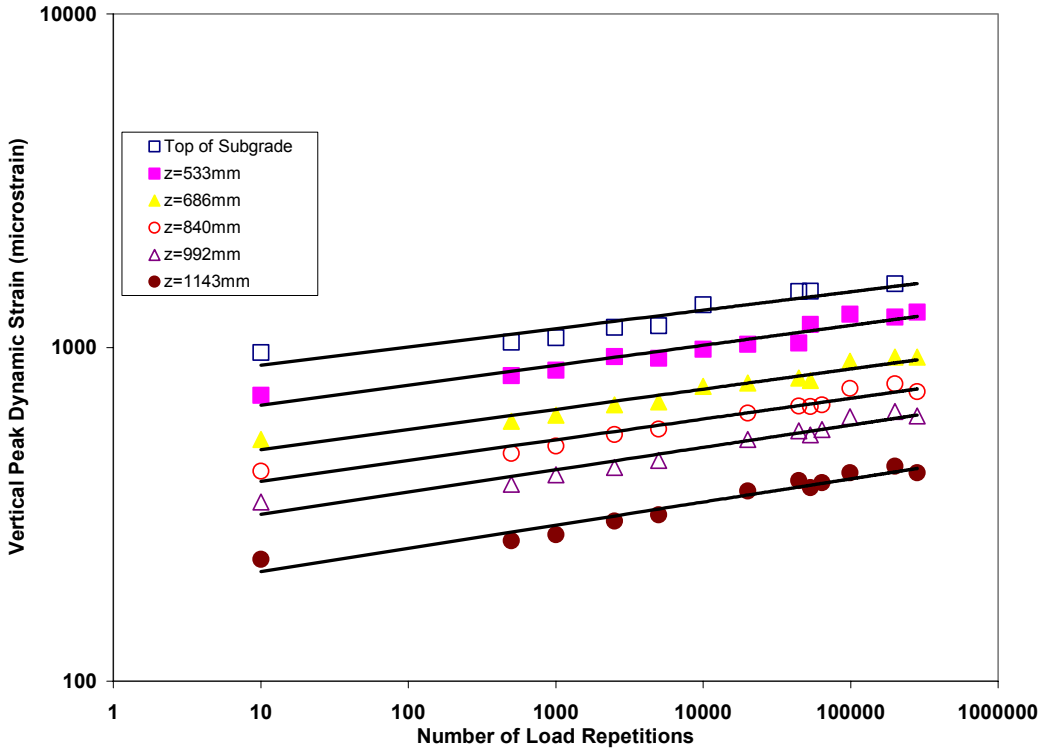

Figure 50. Change in vertical dynamic strain as a function of load repetition.

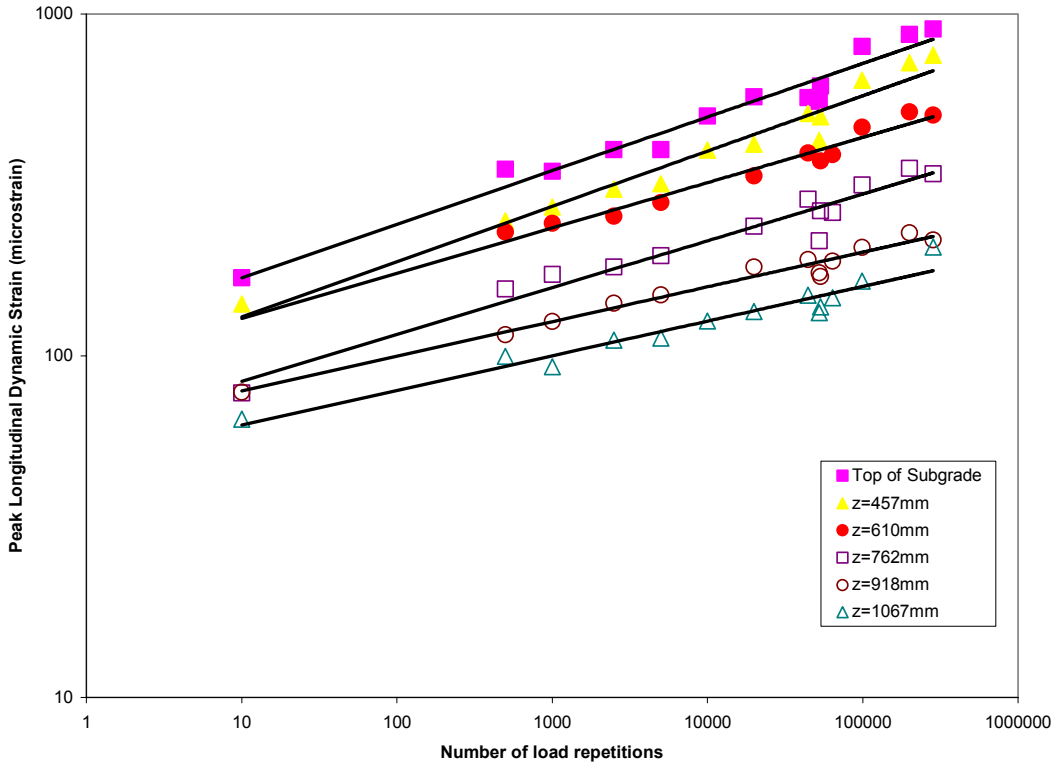

Figure 51. Change in peak longitudinal dynamic strain as a function of load repetition.

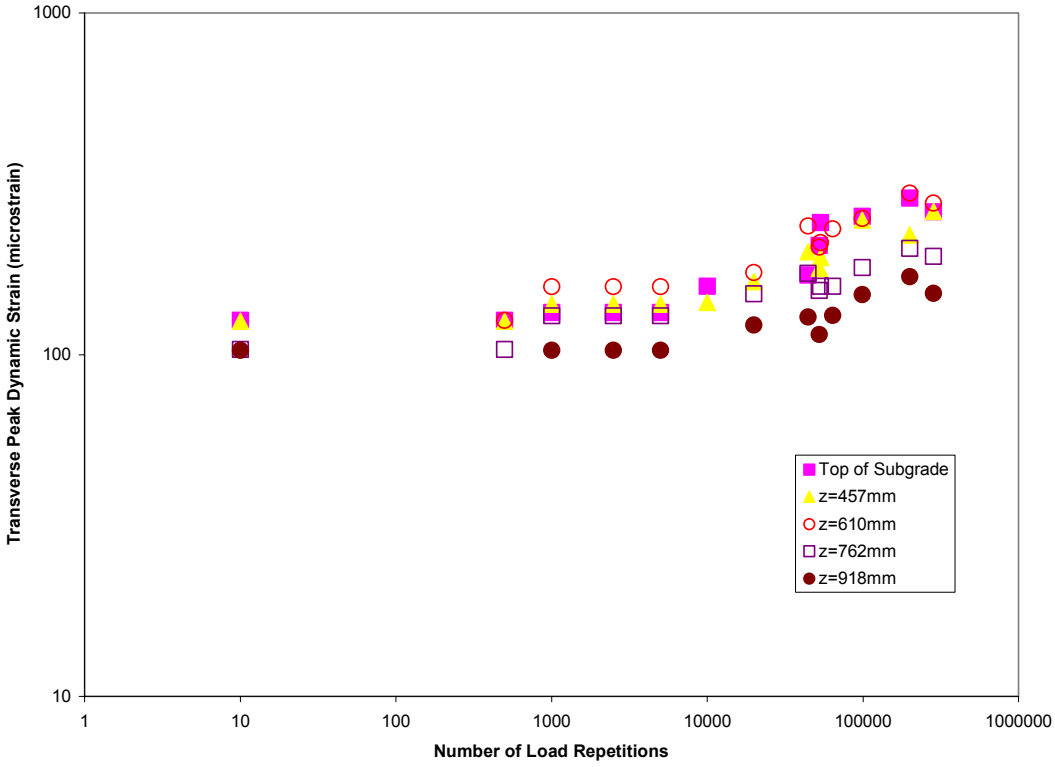

Figure 52. Change in peak transverse dynamic strain as a function of load repetition.

The coefficients *A* and *n* for the vertical, longitudinal, and transverse strains are presented in Table 2. The mean of the exponent *n* for the vertical strain is 0.605, with a COV of 8.5%. The means for the longitudinal and transverse strains are 0.1318 and 0.081, respectively. The COVs are 19.7 and 34.3%, respectively.

Table 2. Coefficients for power law curves applied to dynamic strain data.

Vertical				*Longitudinal*				*Transverse*		
Depth (mm)	*A*	*n*	R^2	*Depth (mm)*	*A*	*n*	R^2	*A*	*n*	R^2
381	778.21	0.0529	0.87	305	117.76	0.1568	0.96	76.68	0.0918	0.72
533	591.28	0.0577	0.90	457	89.57	0.1617	0.96	84.14	0.0765	0.73
686	429.65	0.0605	0.95	610	94.67	0.1326	0.96	60.36	0.1212	0.91
840	347.72	0.0599	0.90	762	61.45	0.1369	0.95	77.93	0.069	0.86
992	273.91	0.0647	0.91	918	62.46	0.1015	0.97	79.38	0.0465	0.6
1143	183.31	0.0674	0.92	1067	49.57	0.1015	0.94			

Generally the exponent *n* for the longitudinal and transverse strain decreases with increasing depth of subgrade, whereas *n* increases with depth for the vertical strain. Over the 1.22-m range of subgrade, a linear model for *n* as a function of depth (from top of subgrade) appears to be possible:

Vertical: $n = 2E-5+0.0526d$, $R^2 = 0.94$

Longitudinal: $n = -8E-5+0.164d$, $R^2 = 0.87$

Transverse: $n = -6E-5+0.090d$, $R^2 = 0.90$.

The changes in the vertical and longitudinal strains as a function of depth at different representative load repetitions are shown in Figures 53 and 54. The mean change in dynamic vertical strain from the beginning of the test to failure was about 78%, with a COV of approximately 4% at all depths of measurements. Power curves tend to model the variation of the strain with depth at all load levels. For the longitudinal strains, it was found that in the top 150 mm of the subgrade, the mean change in the strain from the beginning to the end of the test was about 430%. At the remaining depths of measurement, it was approximately 190%. For the transverse strains, it appears that the strains remain fairly constant to a depth of approximately 300 mm. The transverse strains decrease with depth (Fig. 55). There is an 80–100% increase in the dynamic transverse strain from the beginning to the end of the test, except at the depth of 918 mm, where it appears to be about 50%.

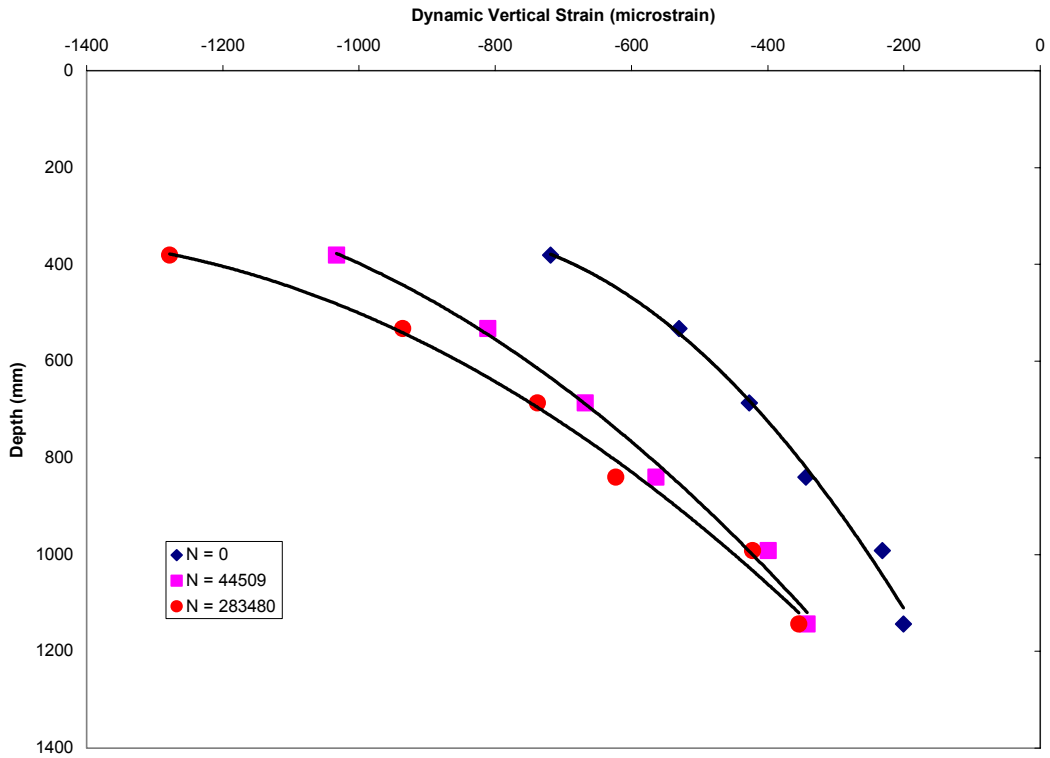

Figure 53. Vertical strain as a function of depth (701C1).

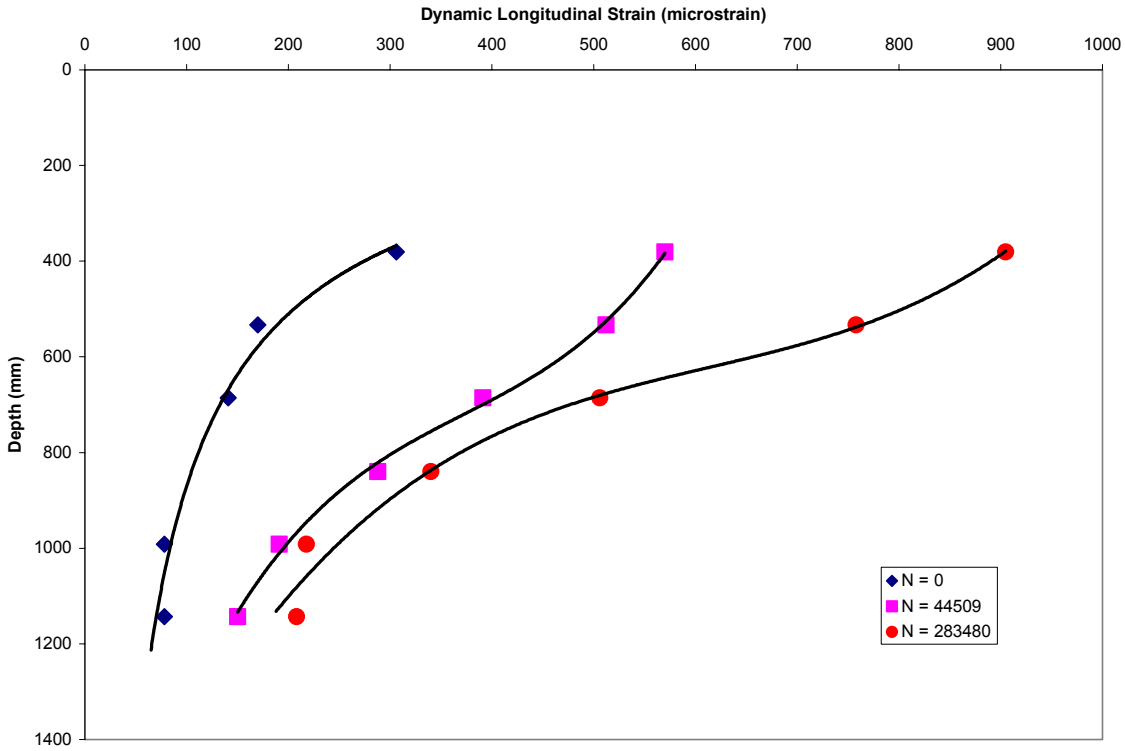

Figure 54. Longitudinal strain as a function of depth (701C1).

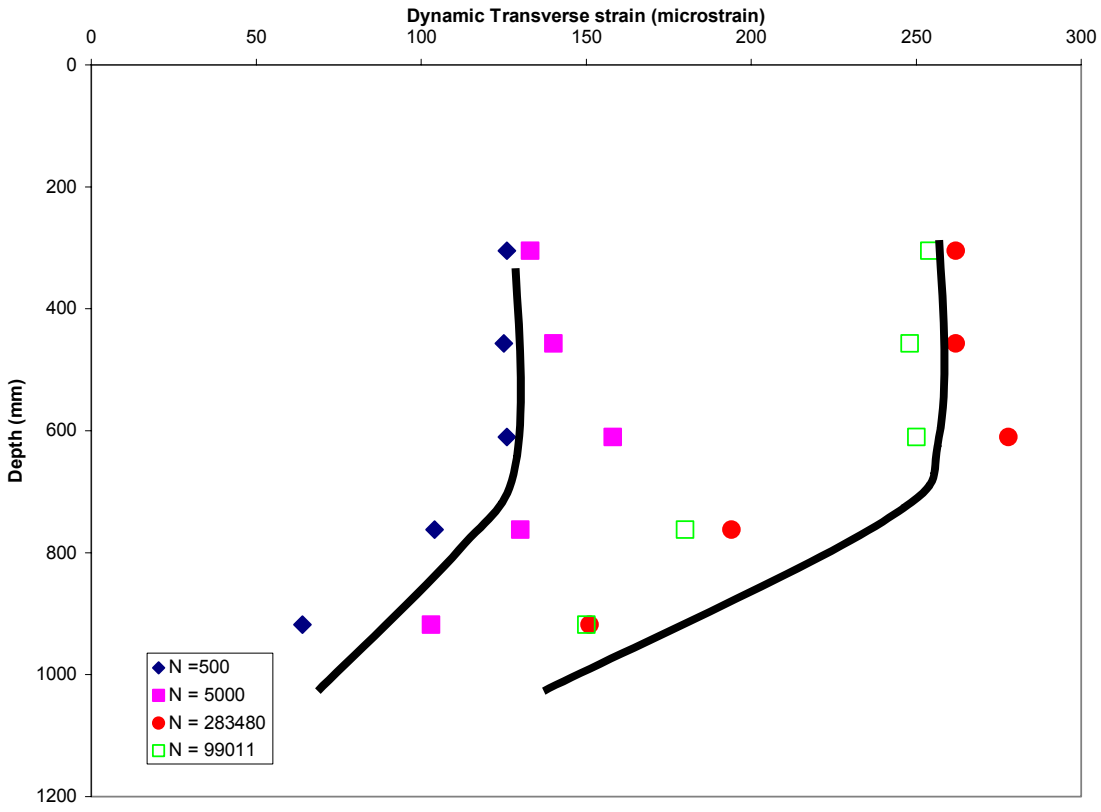

Figure 55. Transverse strain as a function of depth (701C1).

Permanent Strain

The permanent deformations in the base and subgrade were obtained from static measurements between the εmu coils. A second source for the permanent deformations was from the dynamic measurements. During dynamic strain measurement the coils were triggered about 0.6 seconds before the wheel reached the top of the coils (Fig. 46), and it was assumed that the first 100 data points in the dynamic response measurements were unaffected by the wheel and that the mean distance between the coils represented the permanent deformation between the coils. In this way, permanent deformation data were collected from the three loading positions. The mean of the three deformations are presented in Table C-5a in Appendix C. The deformations calculated from the static measurements are presented in Table C-5b. Generally the permanent deformations measured from the dynamic and static tests agree relatively well, as seen in Figure 56. The relationship tends to breakdown at greater depths (>992 mm) in the subgrade.

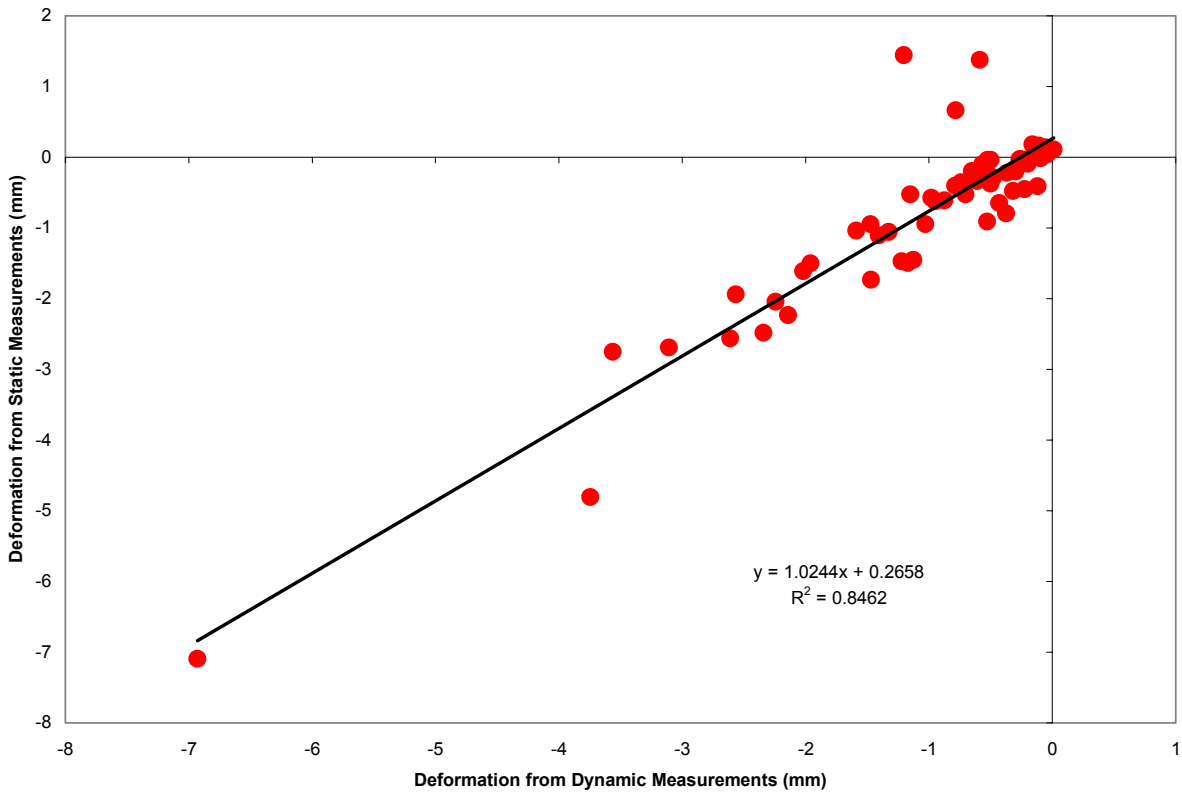

Figure 56. Relationship between dynamic and static measured permanent deformation.

One issue with coil gages is that none of the coils are anchored in the ground, so a fixed point of reference is missing. However, the data in Table C-5 show that the deformations of the coil gages at a mean depth of 1143 mm are less than 1mm (static measurements) and can be considered to be fixed.

The deformations were converted to strains and are tabulated in Tables C-6a and b. The development of the vertical permanent strain in the subgrade as a function of depth and load repetitions is shown in Figure 57, which shows a combination of data from the permanent strain measurements shown in Table C-6a and b. There appear to be four trends. The largest permanent strains were in the bottom part of the base layer. The top of the base and the top of the subgrade appear to follow one trend. The permanent strain between 533 and 686 mm appears to be the same. The same can be said for the strains between 840 and 1143 mm.

Power curves were fitted to the data (Fig. 58); the coefficients for the power curve fit are presented in Table 3. The exponents for the rate of permanent strain increase in the subgrade ranges between 0.46 and 0.54.

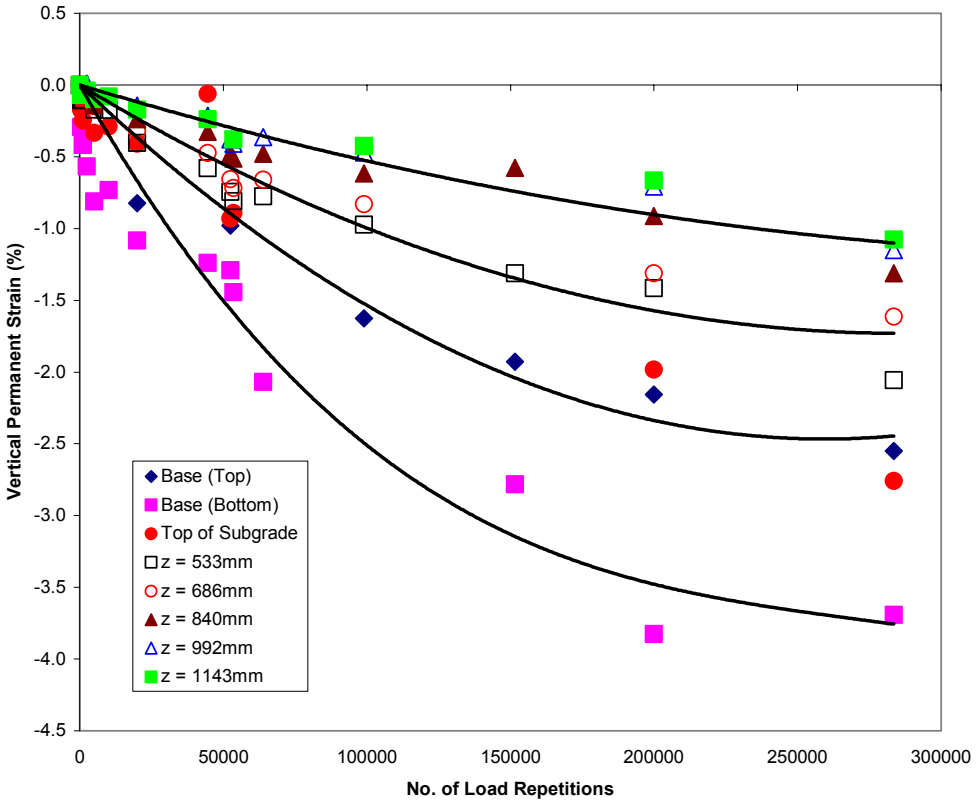

Figure 57. Progression of vertical permanent strain as a function of load repetition.

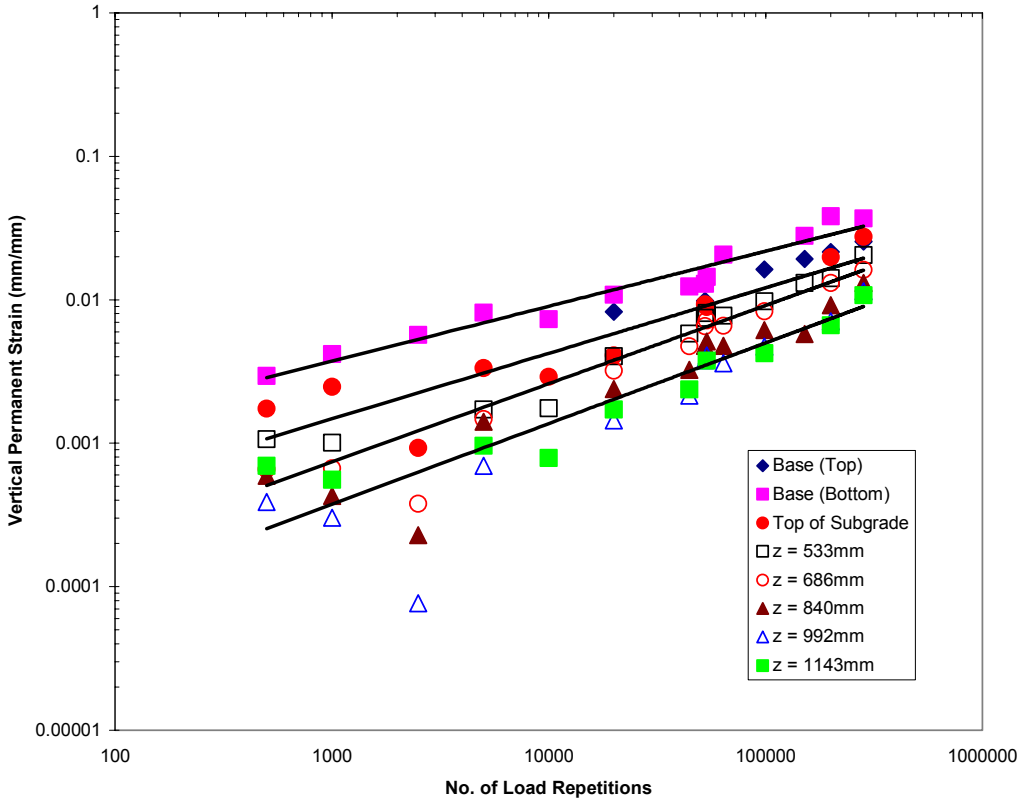

Figure 58. Log-log representation of change in vertical strain as a function of load repetition.

Table 3. Coefficients for power law curves applied to permanent strain data.

Mid layer depth (mm)	*A*	*n*	R^2
381	6E-05	0.4566	0.84
533	2E-05	0.5454	0.92
686	2E-05	0.5454	0.92
840	8E-06	0.5622	0.83
992	8E-06	0.5622	0.83
1143	8E-06	0.5622	0.83

With respect to the permanent deformations in the longitudinal and transverse directions, the results are tabulated in Table C-7 and C-8. The maximum longitudinal and transverse strain deformations occurred at the top of the subgrade (Fig. 59 and 60). However, the magnitude of the deformations were 1 mm or less. In terms of strains, the maximums are about 1% or less.

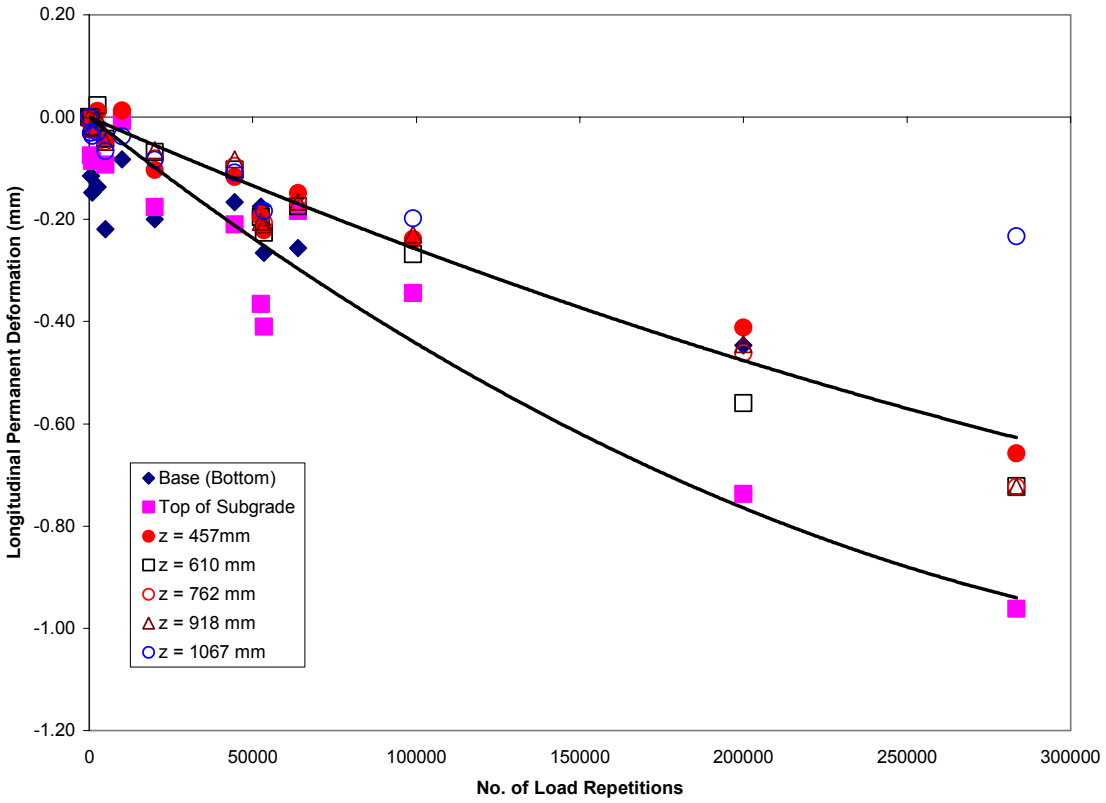

Figure 59. Permanent longitudinal deformation as a function of load repetition.

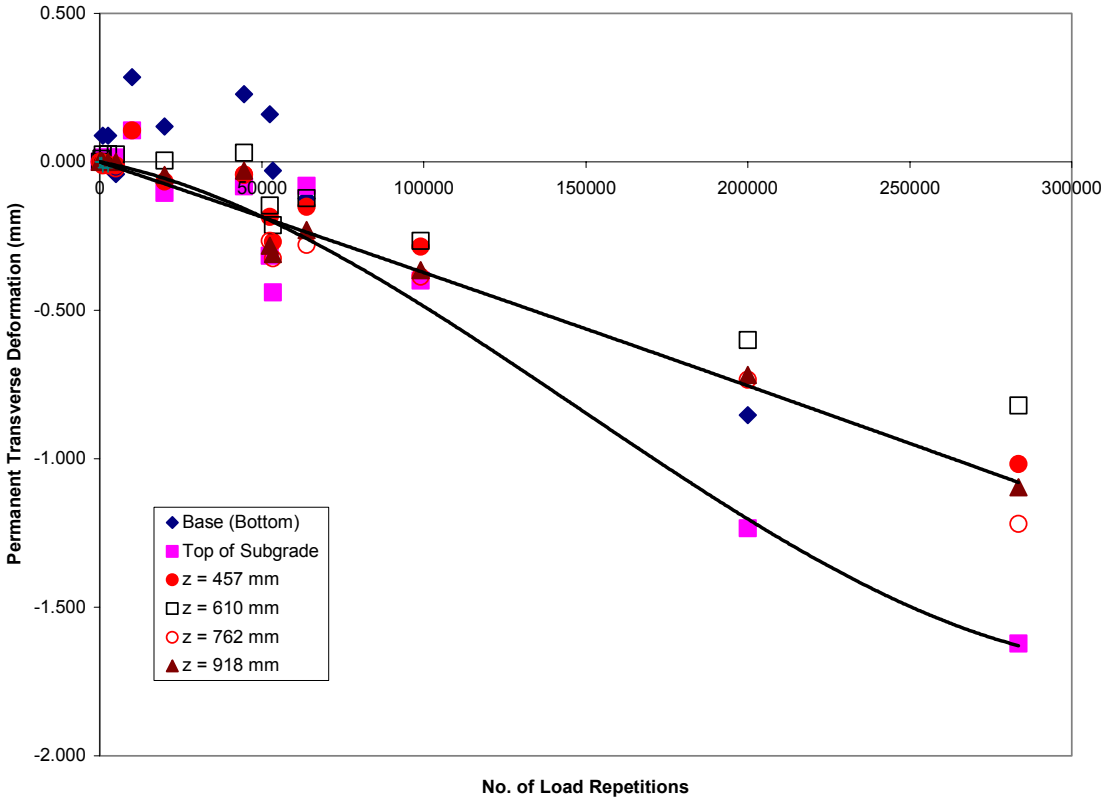

Figure 60. Permanent transverse deformation as a function of load repetition.

Surface Profile Measurements

Twenty-four surface profile measurements were made periodically to determine the surface deformation as a function of load repetition. Of the 24 measurements, the first two (1, 2) and last two (23, 24) measurements were taken in the acceleration and deceleration areas (Fig. 34). The measurements at these locations are not reported. The coil gages for measuring dynamic and permanent deformation are in the vicinity of locations 7, 8 and 9 (Fig. 34). A typical set of surface deformations as a function load repetitions is shown in Figure 61. A ten-point running average was applied to the data shown in Figure 61. The maximum rut depth was extracted from the data after the ten-point averaging was done. The maximum rut depths across the test section as a function of load repetitions is presented in Table C-9.

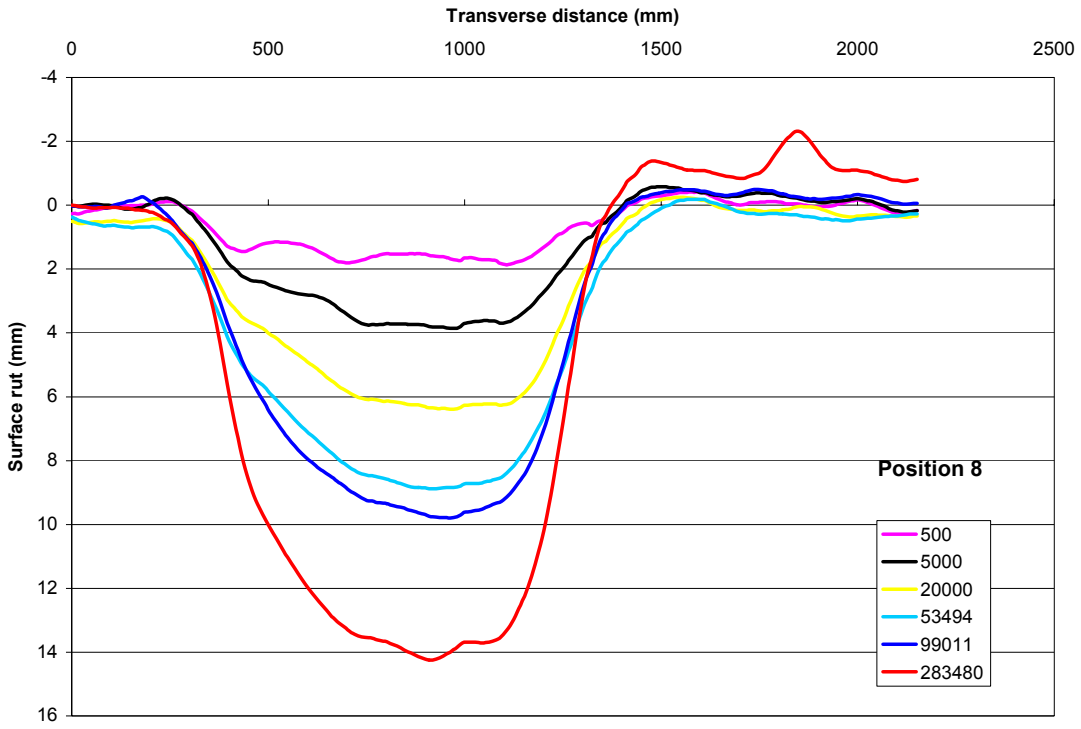

Figure 61. Typical rut depth response as a function of load passes.

The variation in rut depth ranged from 23% to 30% in the longitudinal direction, with most of the variation at locations 3–6 (Fig. 62). This can be explained by the way the load was applied to the test section. After each load application, the wheel was raised from the pavement surface and returned to the start position. At this position the wheel was literally dropped onto the acceleration zone surface. The average rut depth in this zone was 5–7 mm higher than at other locations. This high impact loading was corrected after approximately 50,000 passes. Another potential reason for the high surface ruts is the lower densities (Table A-3) measured near these locations, which happen to be close to the south wall.

The surface rut development from the profilometer (Fig. 63) can be modeled by

$$R = 0.30N^{0.3095} \qquad R^2 = 0.99.$$

A comparison of the total rut depth measured from the profilometer and strain coil gages is shown in Figure 63. Data from the coil gages were summed through the depths. However, the data were sporadic since surface measurements were not taken at all load measurements. As seen in Figure 63, the summations from the dynamic measurements are closer to the surface rut measurements than the summations from the static measurements. The greatest difference from the dynamic measurements is approximately 3 mm.

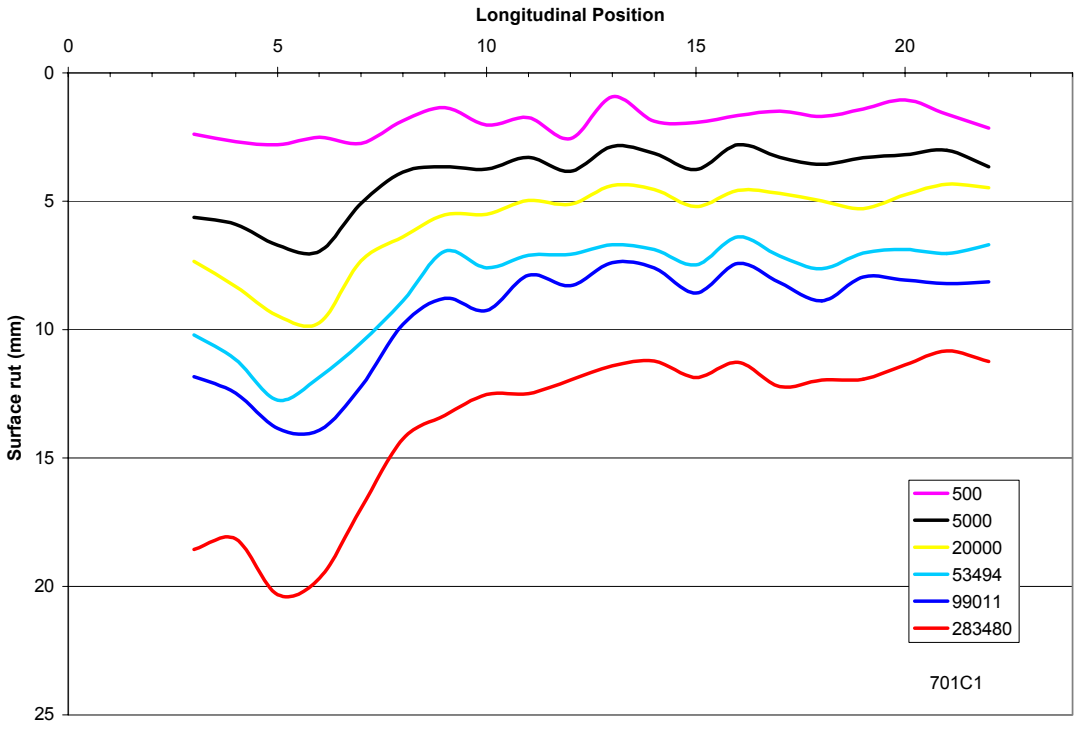

Figure 62. Longitudinal surface rutting as a function of load repetition.

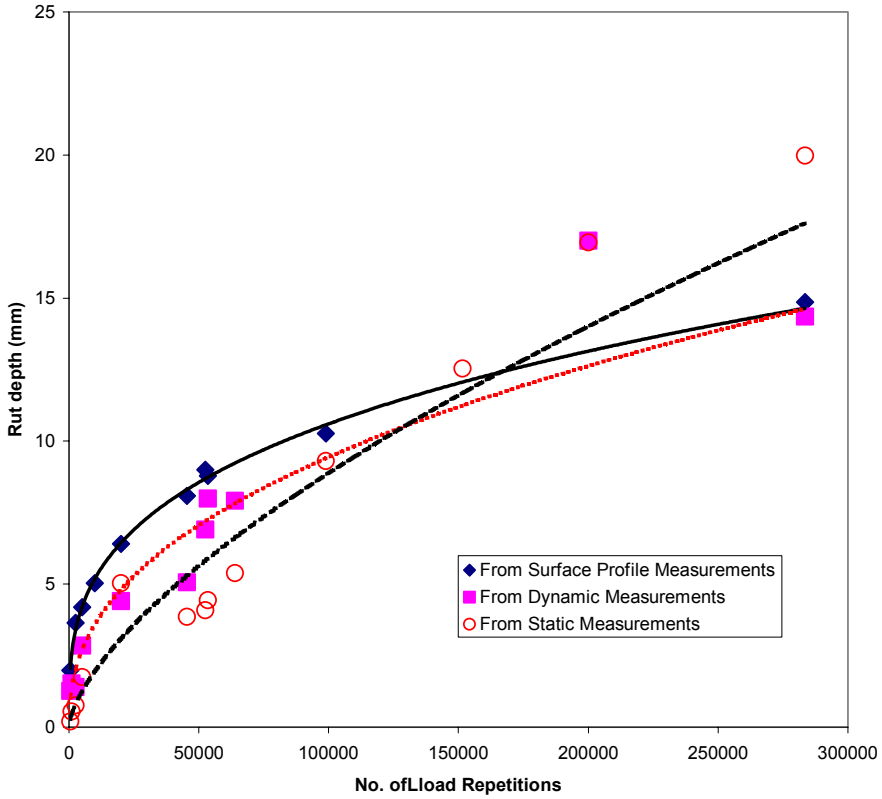

Figure 63. Comparison of total pavement deformation between profilometer and coil gage systems.

Results from Test Window 701C2

Testing of window 701C2 began on August 20, 1997, and ended on September 2, 1997. The test window was subjected to a test load was 89kN, with a COV of 1.1%, and the tire pressures in the dual wheels were 748 (COV = 5.7%) and 763k Pa (COV = 1%), respectively. As before with 701C1, during the accelerated loading phase, stress and strain responses were measured periodically. At the end of the strain and stress measurements, twenty-four surface profile measurements were made as discussed previously.

Dynamic Stress

Stress measurements in the vertical, longitudinal, and transverse directions were made at two depths of 500 and 929 mm from the AC surface in the subgrade. Typical stress responses in the vertical direction are shown in Figure 64. Negative values indicate compressive stress. The maximum vertical stress occurred when the sensors were directly under both the wheels, i.e., at position 2. The measured vertical stresses as a function of load repetition are presented in Table D-1, Appendix D. As seen in Figure 65, there was no significant change in the vertical dynamic stress as a function of load repetition. At 500 mm deep (approximately 195 mm into the subgrade) the measured stress was approximately 160 kPa. This is about 21% of the mean applied stress (755 kPa) on the surface. At 929 mm deep the stress dropped to about 8% of the applied stress on the surface.

Typical stress measurements in the longitudinal direction are presented in Figures 66 and 67. The drop in pressure as the wheel traverses over the sensor (z = 500 mm) could be explained by the thickness of the pressure gage. As the wheel approaches the pressure cell, the stress increases. However, when the wheel crosses the thickness of the pressure cell, the stress drops and then starts to pick up again after the load has traversed the thickness of the pressure cell. Later, as the load departs from the cell, the stress decreases again to zero. The thickness of the pressure cell has also an effect on the response at 929 mm; however, it is minimal (Fig. 67). It can be surmised that the decrease in longitudinal stress when the wheel is on top of the pressure cell is artificial and that the response is more of the typical V-shaped response seen in the vertical direction. The effect of the cell thickness appears to decrease with depth.

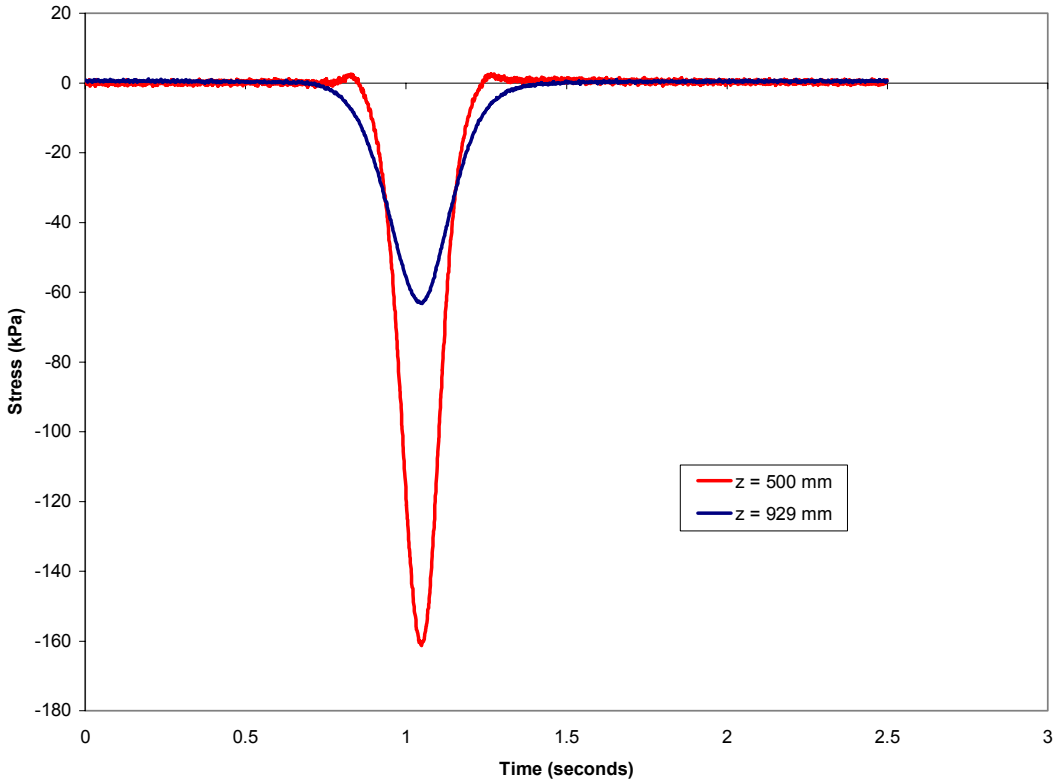

Figure 64. Typical vertical stress response in the subgrade after 27,260 repetitions.

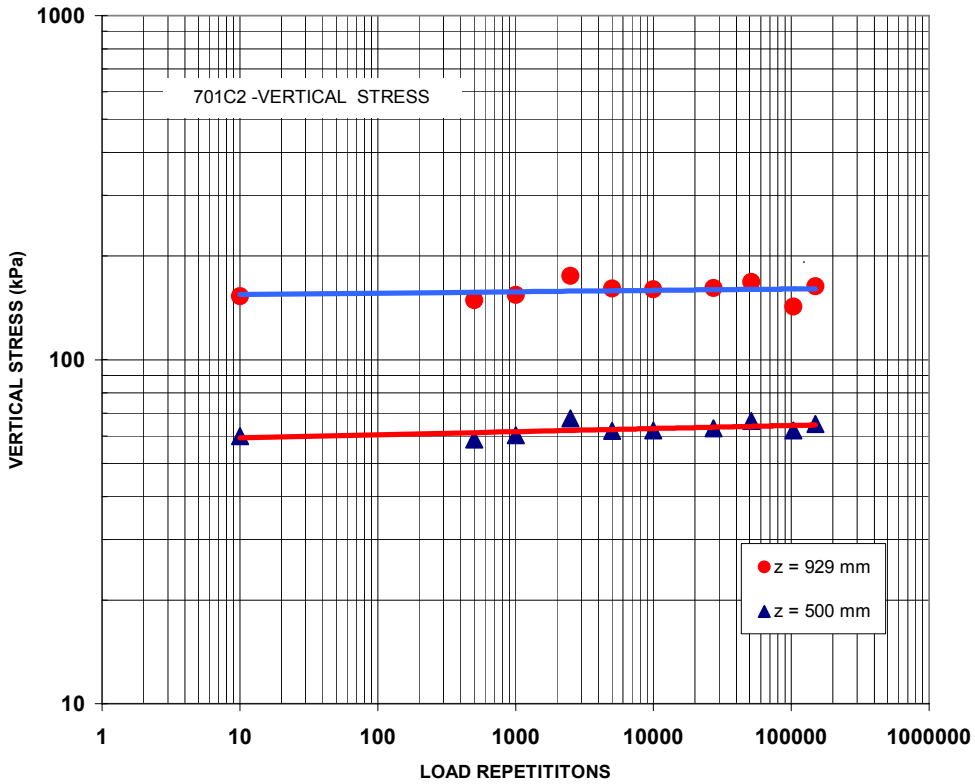

Figure 65. Vertical stress (Position 2) response as a function of load repetition.

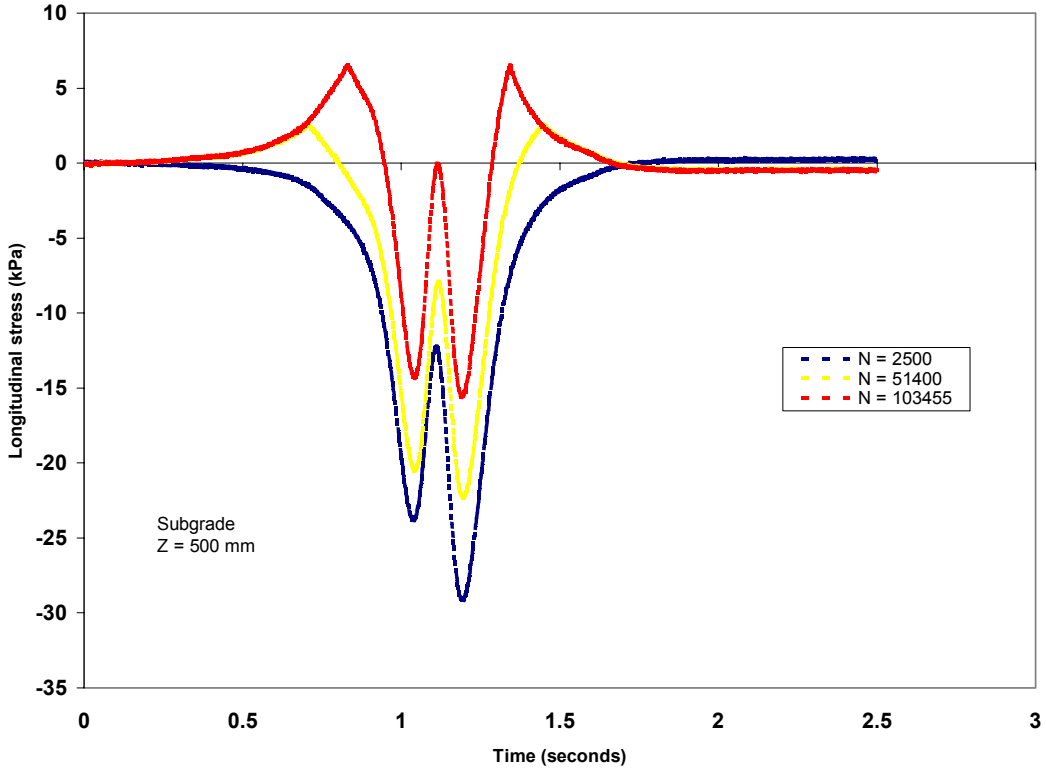

Figure 66. Typical longitudinal stress response in the subgrade (z = 500mm).

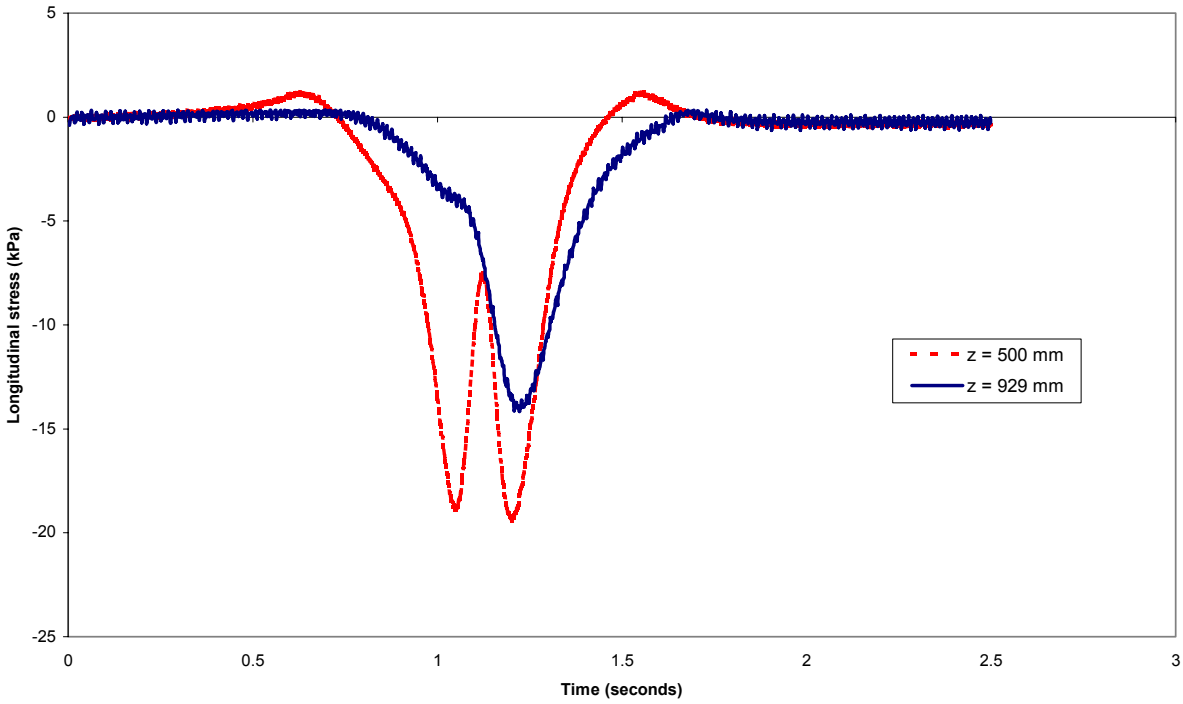

Figure 67. Typical longitudinal stress response in the subgrade.

The maximum longitudinal stress was compressive and initially was not affected by load repetitions. However, after 10,000 passes the longitudinal stress started to decrease. Significant decrease in the stress started to show up after 27,000 load repetitions, suggesting failure of the subgrade at this depth (Fig. 68). This is also about the time we started seeing a "tensile" stress response as the load approached and left the pressure cell. The measured longitudinal stresses as a function of load repetition are also tabulated in Table D-2.

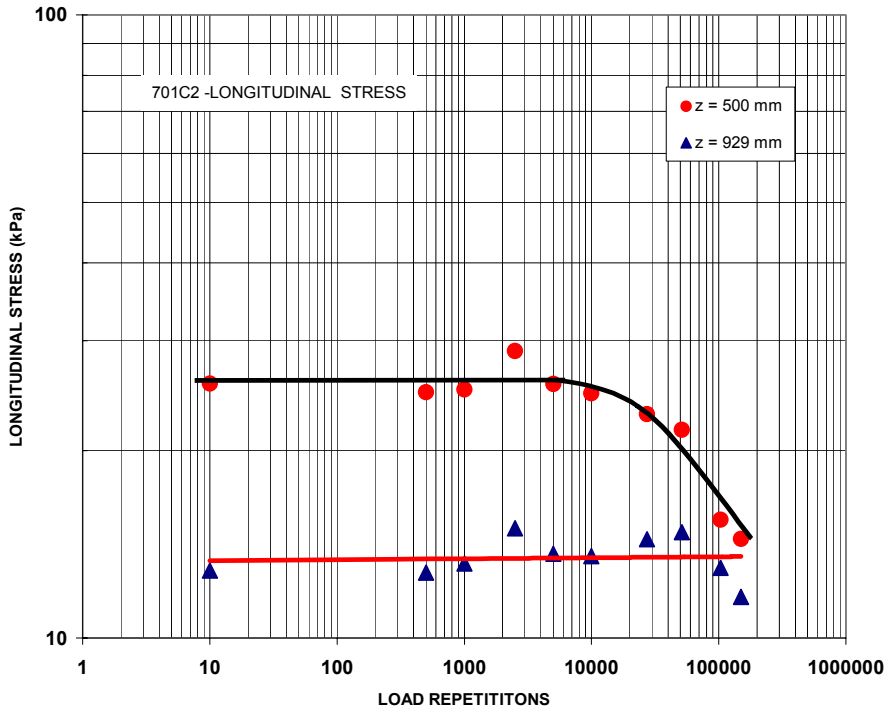

Figure 68. Change in longitudinal stress (Position 2) as a function of load repetition.

Based on the response of the longitudinal stress at 929 mm, it is proposed that the maximum stress is higher than the measured stress at z = 500 mm, as shown by the dashed line in Figure 69. The "corrected" longitudinal stress is shown in Figure 70.

Transverse stresses were also measured at both depths (500 and 929 mm) in the subgrade. The results are tabulated in Table D-3. Typical responses are shown in Figure 71. At 929 mm the measurements were negligible, and we believe that it was more noise than actual response. The response indicated maximum compressive stresses in the vicinity of 6 kPa. However, at 500 mm deep the maximum average measured transverse stress was 36 kPa, and it was fairly constant as a function of load repetition (Fig. 72).

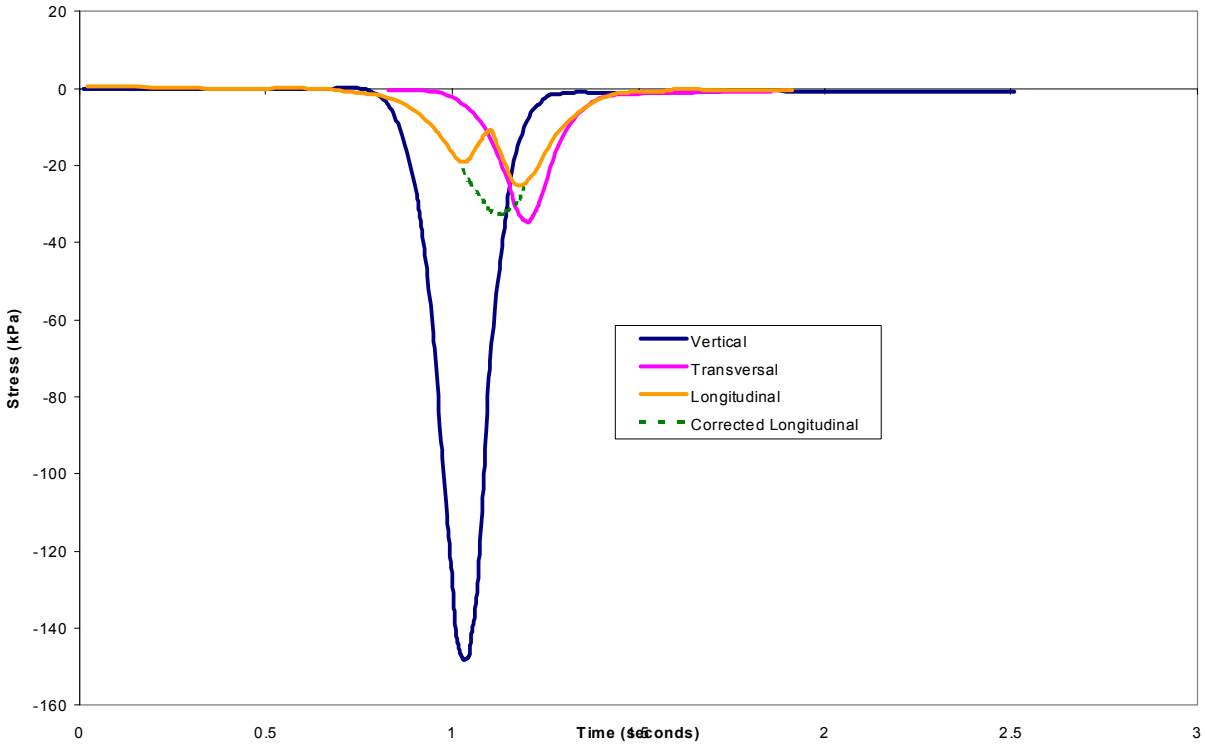

Figure 69. Stress response after 500 load repetitions (z = 500 mm, N = 500, Load = 89kN).

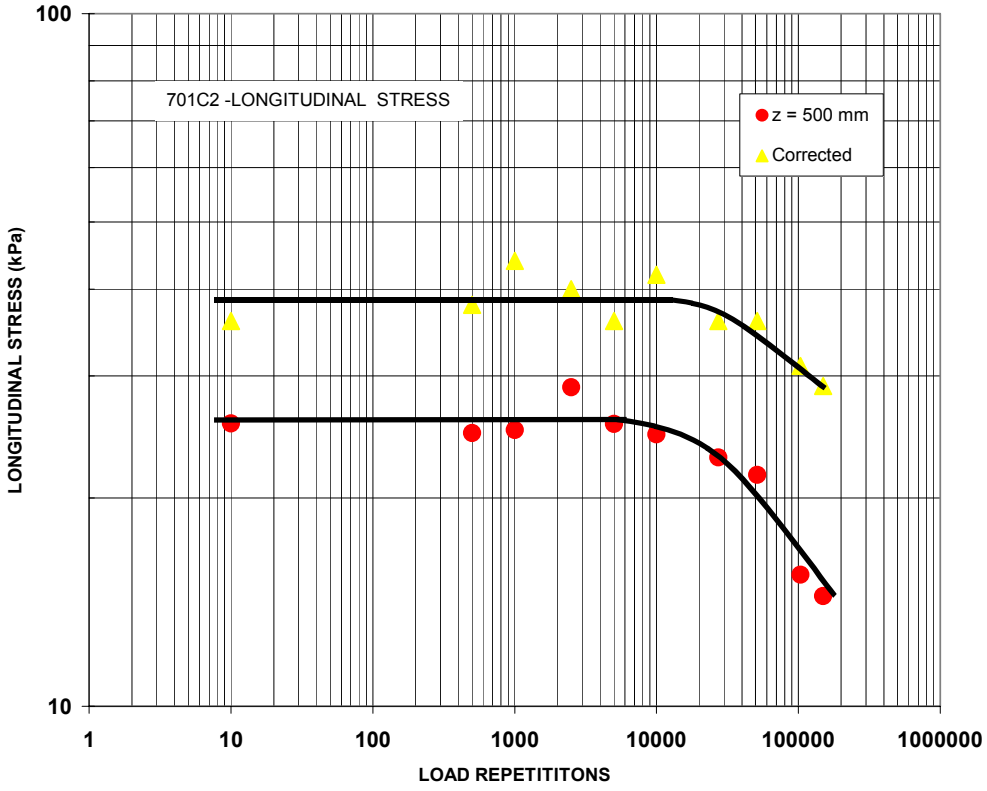

Figure 70. “Corrected” vs. measured longitudinal stress as a function of load repetition.

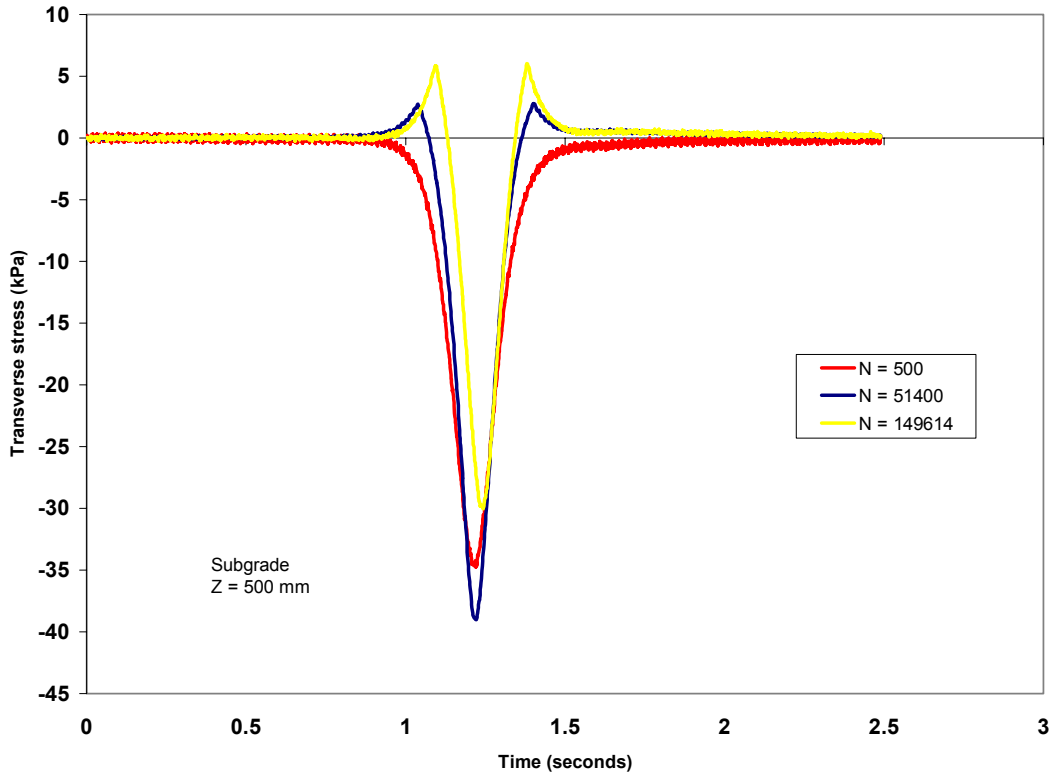

Figure 71. Typical transverse stress response in the subgrade (z = 500 mm).

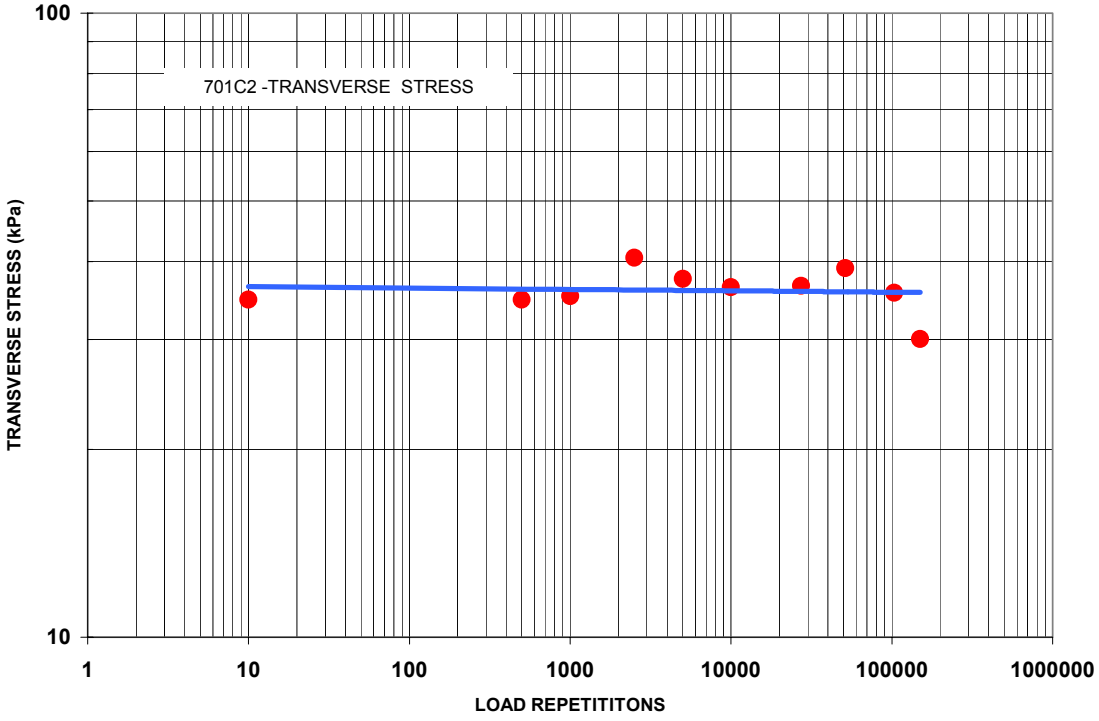

Figure 72. Change in transverse stress as a function of load repetition.

Dynamic Strain

Vertical, longitudinal, and transverse dynamic strains were measured as a function of load repetitions at the three wheel locations similar to that in 701C1. The results are presented in Tables D-4, D-5, and D-6, Appendix D. The vertical strain response from the εmu coils was well defined, and it was compressive at all depths. The longitudinal strain response was similar to that seen in 701 C1, i.e., the strain was compressive as the wheel approached the sensors and became expansive as the wheel was on top of the sensor. As it left the sensor, the strain dropped and became compressive before returning to zero. The second compression was significantly lower than the first. However, it was found that the magnitudes of the first compressive strain and the expansive strain can be close to equal. The quality of the longitudinal strain degraded with depth. At a depth of 1143 mm the quality of the signal was so poor that it was discarded from further analysis. At depths of 840 mm and deeper the longitudinal strain measurement at position 3 was noisy. However, the shape of the output was similar to the other two positions. The measurements at location 1 and 2 were good enough that peak strain measurements could be made from the output.

The transverse strain measurements were good at positions 1 and 2, but it was quite noisy at position 3. We had some problems with the transverse strain measurements at 0, 500, and 1000 load repetitions. It stabilized after 27,260 load repetitions. It was also found that the maximum strains in the vertical and longitudinal directions occurred when the wheel was in position 2.

Comparisons of the vertical, longitudinal, and transverse strains at various load repetitions (position 2) are shown in Figures 73–75. We found that in most cases the magnitudes of the expansive longitudinal and transverse strains were close to one another. The difference was in the shape of the response curve. This difference probably has a significant effect on the performance of the pavement structure.

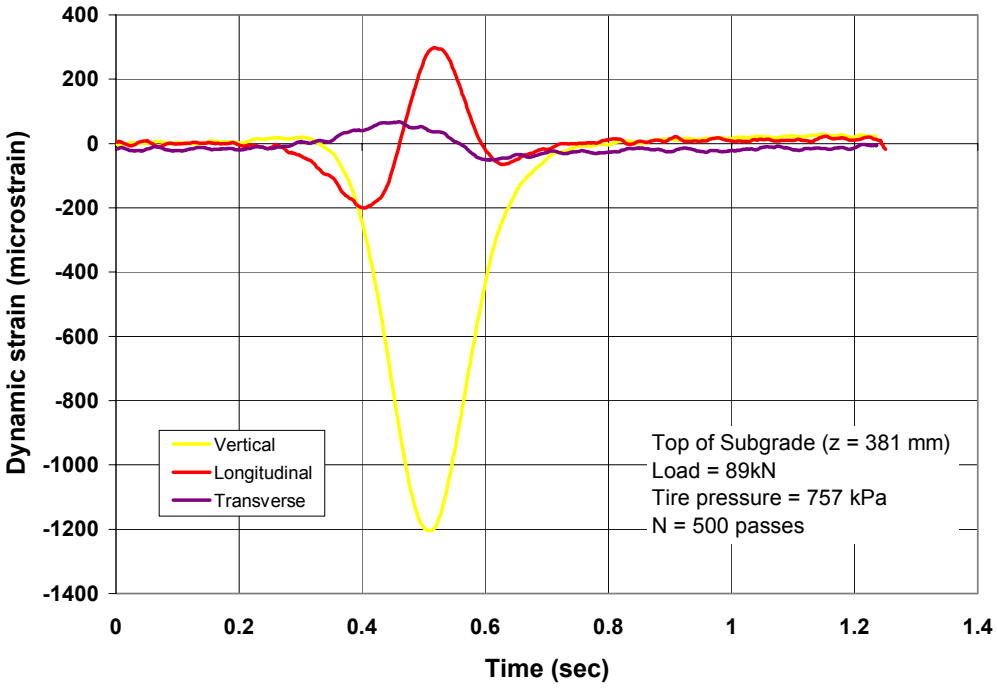

Figure 73. Strain response as a function of depth (z = 381 mm from the surface).

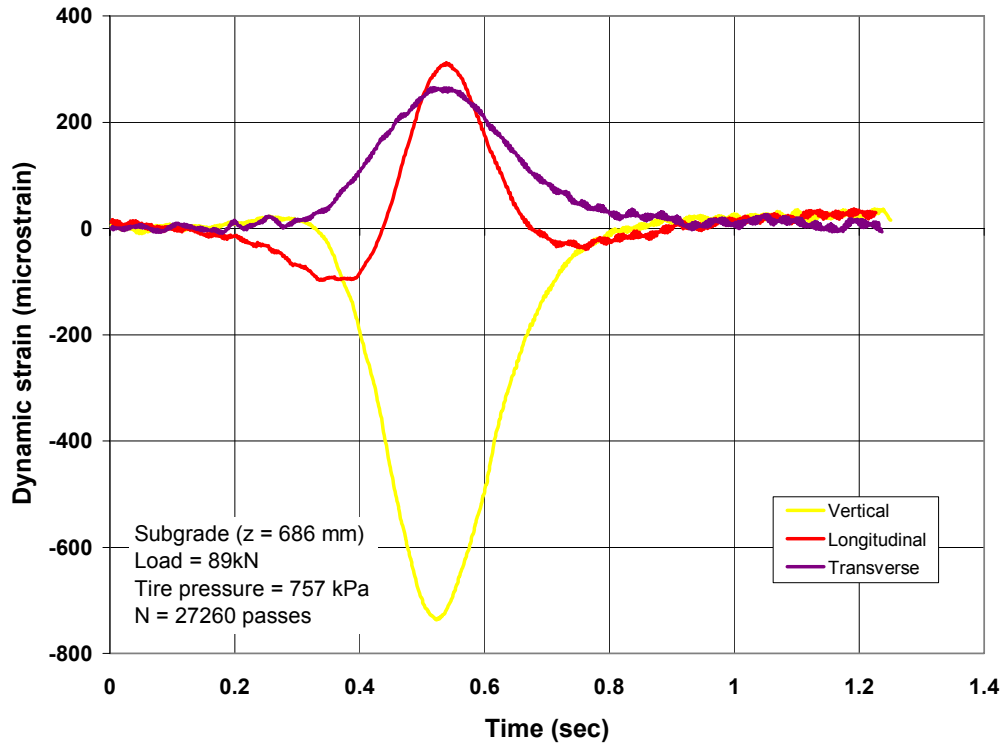

Figure 74. Strain response as a function of depth (z = 686 mm from the surface).

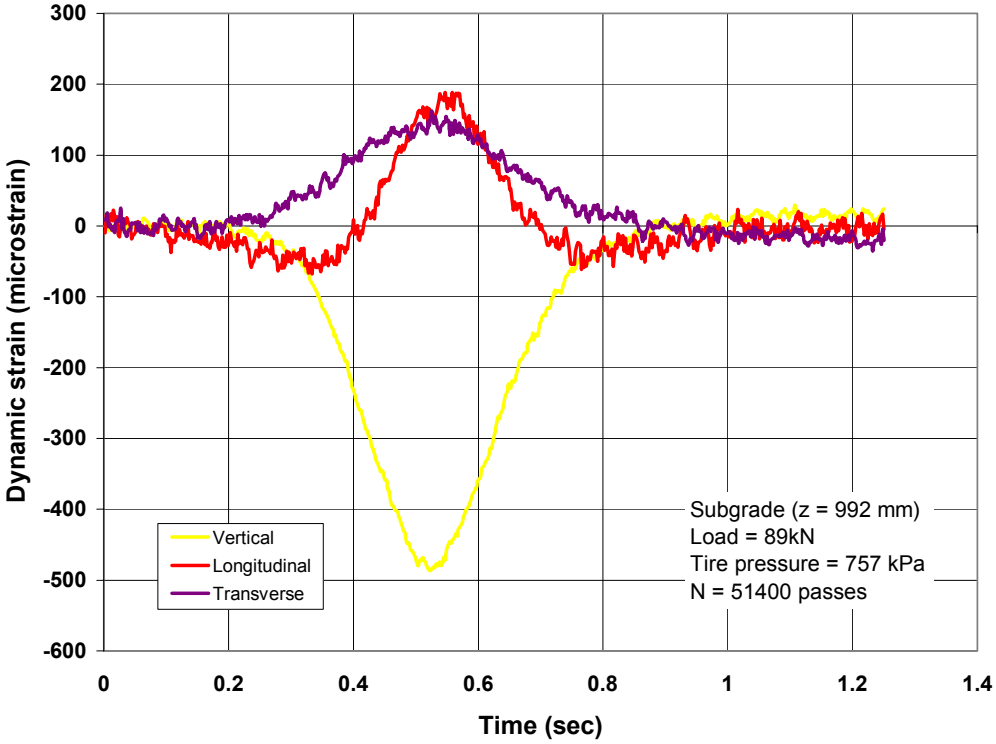

Figure 75. Strain response as a function of depth (z = 992 mm from the surface).

The maximum strains in Table D-5 were obtained after the data were smoothed using a ten-point averaging scheme. As before, the vertical strains are an average between the coil pairs, and the depths presented in the table are the midpoints between the coil pairs. The vertical strains increased with load repetitions at all positions (Fig. 76). There is a rapid increase in strain to about 10,000 load repetitions, after which the increment in strain significantly reduced. The data in Figure 76 were replotted in log-log space (Fig. 77) and fitted with a power curve. The coefficients for the power curves are presented in Table 4.

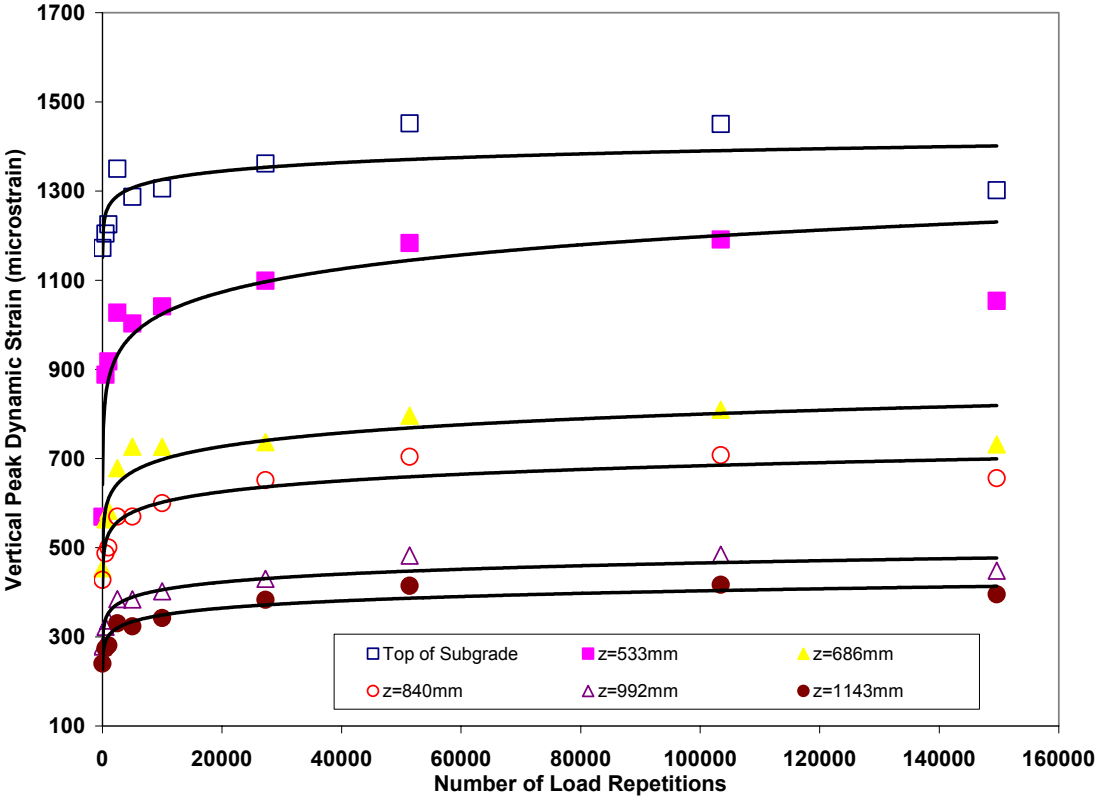

Figure 76. Development of dynamic vertical strain as a function of load repetition.

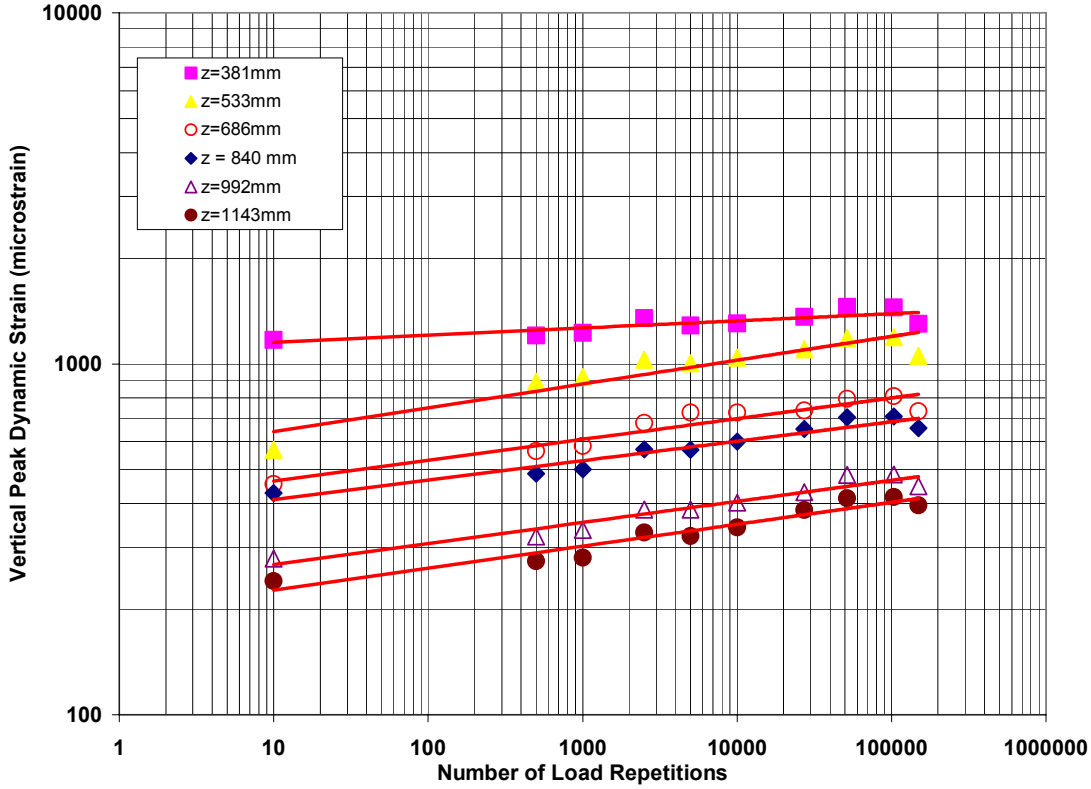

Figure 77. Dynamic vertical subgrade strain as a function of load repetitions .

As seen by the coefficient *n* in Table 4, the exponent for the power curve of the vertical strain in the subgrade is approximately 0.06, with the exception of the top of the subgrade, where the gradient is 0.02.

Table 4. Coefficients for power law curves applied to dynamic strain data.

Depth (mm)	*A*	*n*	R^2
381	1098	0.020	0.67
533	549	0.068	0.86
686	405	0.060	0.90
840	361	0.055	0.93
992	233	0.060	0.94
1143	196	0.063	0.92

As done previously, the longitudinal strains reported in Table D-5 are the absolute peak-to-peak distances between the first compressive strain (A in Table D-5) and the peak extension strain (B in Table D-5). Three sets of measurements are reported for the longitudinal strain. The depths in Table D-5 are the actual locations of the coil gages. The progression of the longitudinal strains as a function of load repetitions are shown in Figure 78. Clearly, in this case the longitudinal strains are significantly higher at the top of the subgrade. The absolute magnitude of the peak A and B longitudinal strains from position 2 were used to determine the rate of strain development as a function of load repetitions (Fig. 79). The coefficients *A* and *n* for describing the power curve in Figure 79 are presented in Table 5. The coefficient *n* is around 0.09–0.1, with the exception of the subgrade at 918 mm. This is different from 701C1, as the average *n* value was around 0.13. Again, the lower increase in longitudinal strain as a function of load repetition may be due to the high load used in the test. It is possible that significant damage had occurred earlier on and that any increase in load repetition produced minor additional damage to the subgrade.

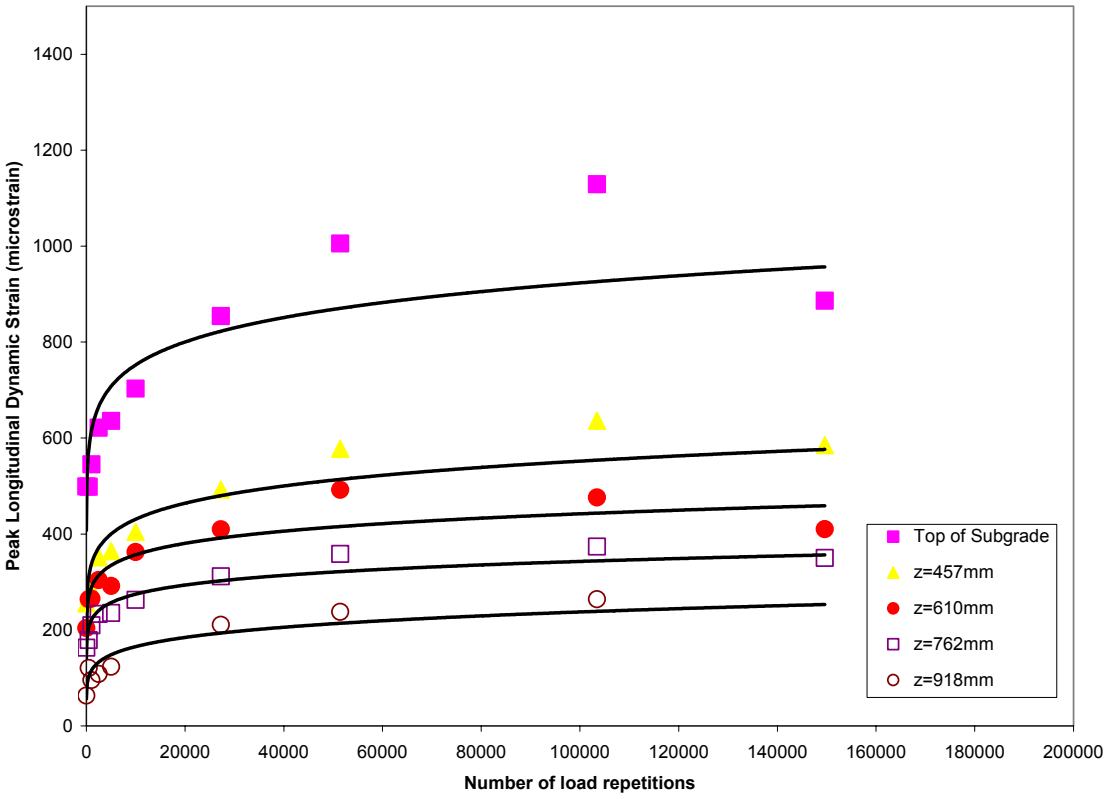

Figure 78. Change in peak longitudinal dynamic strain as a function of load repetition.

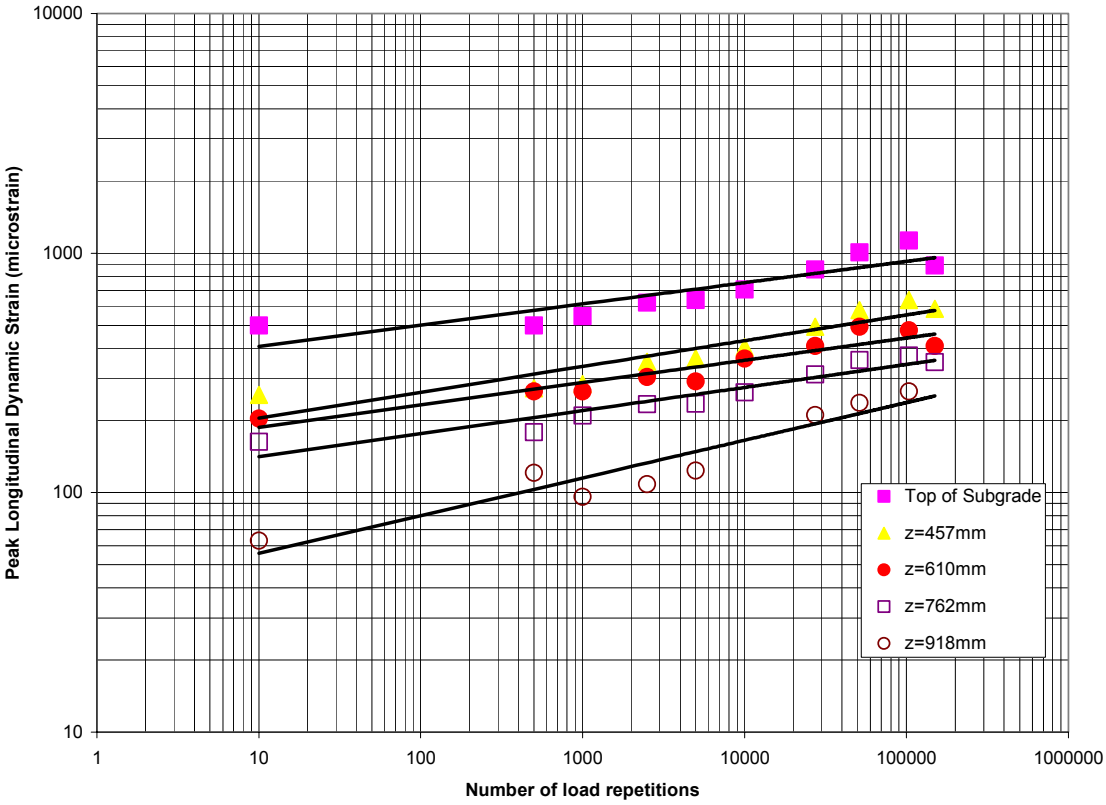

Figure 79. Change in longitudinal strain as a function of depth and load repetition.

Table 5. Coefficients for power law curves applied to dynamic longitudinal strain data.

Depth (mm)	*A*	*n*	R^2
305	332	0.089	0.79
457	160	0.108	0.86
610	151	0.093	0.89
762	113	0.096	0.91
918	39	0.157	0.90
1067	-	-	-

The peak transverse strains as a function of load repetitions are tabulated in Table D-6. As mentioned earlier, the measurements at position 3 were extremely noisy and therefore are not reported. Generally the transverse strains increased with load repetition. In this test the largest transverse strains occurred at a depth of 610 mm; this was also seen in 701C1. The higher strain values occurred when the wheel was in position 1; this was also seen in 701C1. This is to be expected as the transverse coil gages are closer to position 1. In the upper layers this difference is small (2–3%). At the lower depths the difference is about 10%.

The change in transverse strain as a function of load repetitions is shown in Figure 80. Data from the top of the subgrade are not shown in Figure 80, because they were insufficient to develop a clear conclusion. With the existing data, the trend is significantly different from the others. Power curves were used to fit the data, and the appropriate coefficients are presented in Table 6. The coefficient *n* ranges between 0.06 and 0.09. The poor R^2 values can be attributed to the small transverse strains measurements.

Table 6. Coefficients for power law curves applied to dynamic transverse strain data.

Depth (mm)	*A*	*n*	R^2
305	332	0.089	0.79
457	71	0.086	0.57
610	132	0.067	0.75
762	71	0.081	0.87
918	68	0.062	0.82
1067	-	-	-

The progression of the transverse strain as a function of depth and load repetitions is shown in Figure 81. The variation of the transverse strain with depth is actually small, approximately 100 microstrains. The exception is at a depth of 610, where the strains are about 50% higher. Another exception to the data is that there is a significant increase in strain as a function of load repetition, as seen in Figure 81.

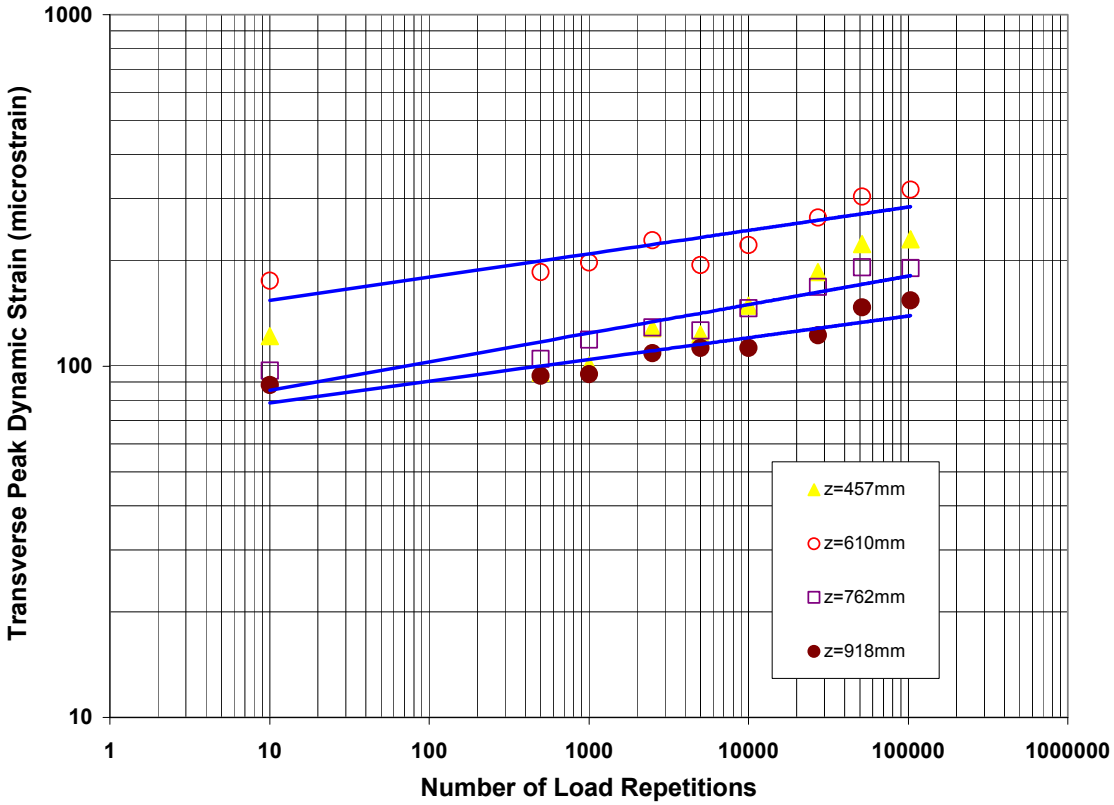

Figure 80. Change in transverse strain as a function of load repetition.

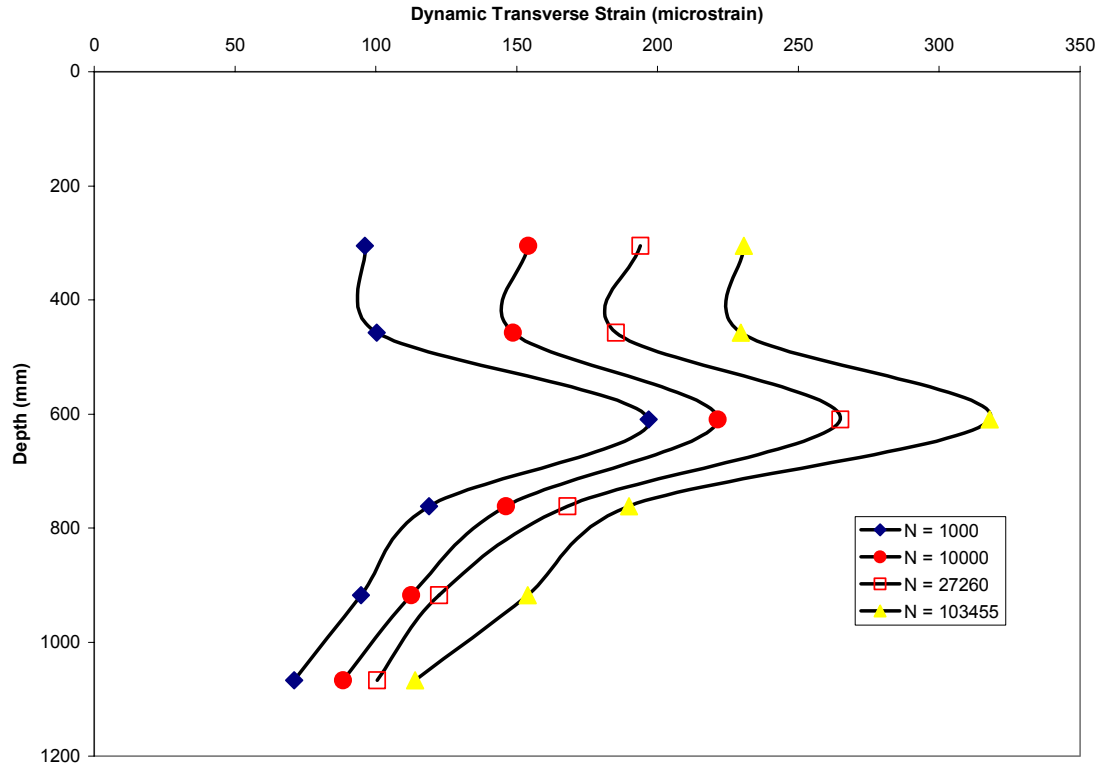

Figure 81. Progression of dynamic transverse strains as a function of depth and load repetition.

Permanent Strain

Permanent deformations were obtained from static measurements between the εmu coils and are presented in Table D-7. The surface measurements were taken between a coil gage placed on the AC surface and the coil gage in the base course layer. The distance between the two coil pairs was 182 mm. These coil pairs were not calibrated, and the calibration curve was assumed to be similar to the coil pairs in the base course. The error was considered to be minimal, as we were looking for changes in distances between the coil pairs and not the magnitude of the separation.

Generally it was found that the vertical deformations measured were compressive and increased with increasing load repetitions (Fig.82). It was also found that most of the permanent deformation occurred in the base course layer and on top of the subgrade. Relative to the base and the top of the subgrade, very little deformation occurred in the other layers.

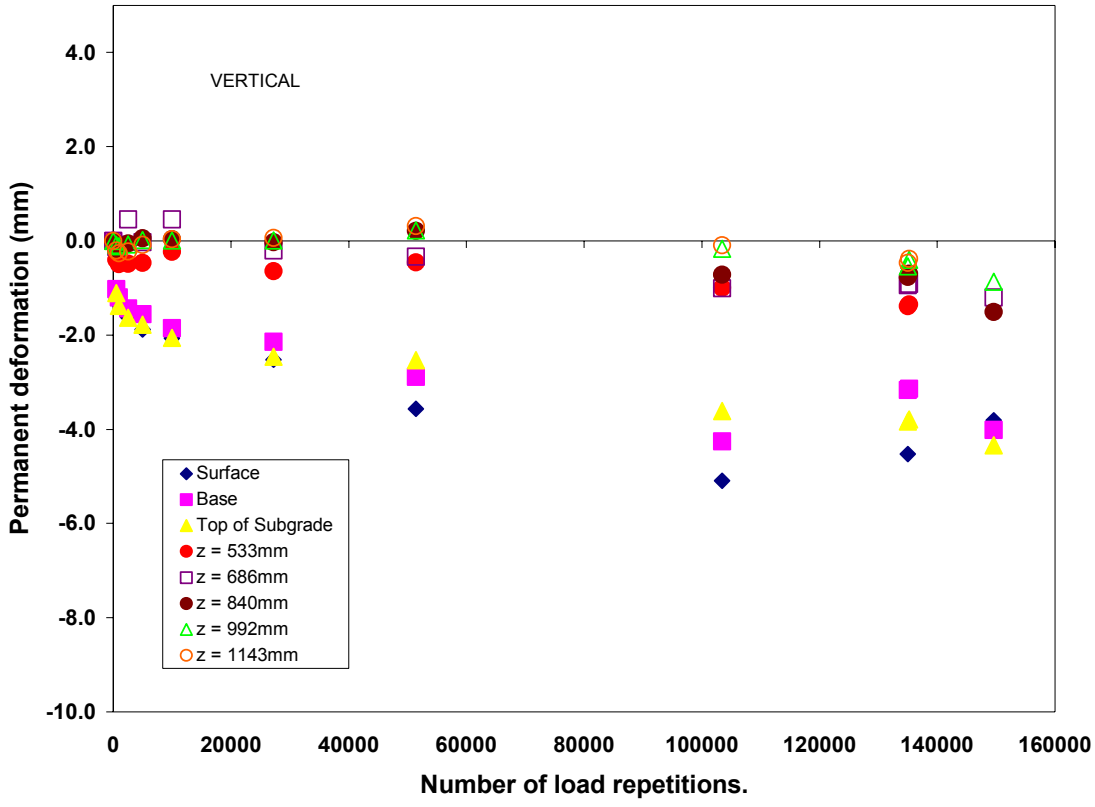

Figure 82. Development of vertical permanent deformation as a function of load repetition.

The measured longitudinal deformations in the base and in the upper subgrade were small. However, at the lower depth in the subgrade there were some small extensional deformations

in the early phase of loading. After 27,260 load repetitions, the deformation returned to its near-original state or became compressive (Fig. 83). With respect to the deformation in the transverse direction (Fig. 84), generally the deformation was extensional in the subgrade. However, the largest deformation in the subgrade was around 1 mm and occurred on top of the subgrade.

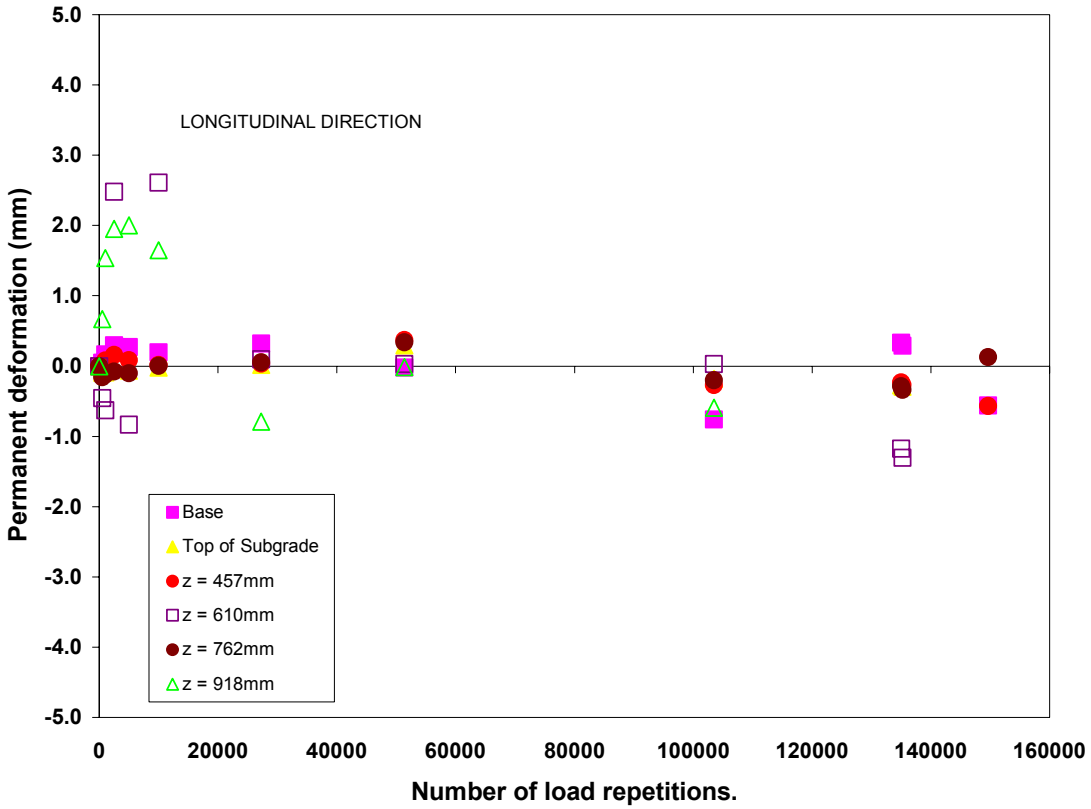

Figure 84. Development of longitudinal permanent deformation as a function of load repetition.

It was found that approximately 8 mm of the vertical permanent deformation occurred in the subgrade. Another 4.5 mm occurred in the base layer. It was also seen that the deformation of the subgrade occurred in three stages (Fig. 85). First there was the deformation due to compaction of the layer. This occurred until load repetition 10,000. The deformation remained fairly constant to load repetition 51,400. After that there was another increase in deformation until failure. In the longitudinal direction the overall deformation of the subgrade started in extension. After 25,00 load repetitions the deformation changed to compressive, and at failure it became extensive again. The maximum extensive deformation was approximately 3 mm. The maximum compressive strain was approximately 1 mm. Generally the overall deformation of the subgrade in the transverse direction was very small.

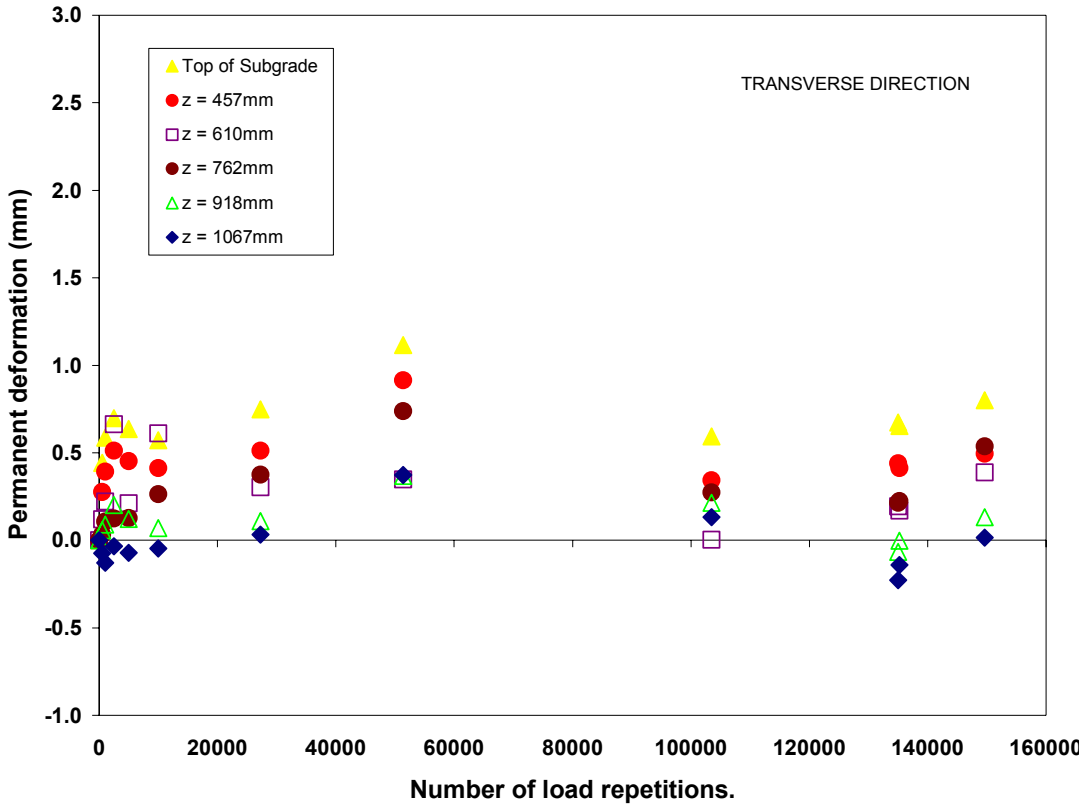

Figure 84. Development of transverse permanent deformation as a function of load repetition.

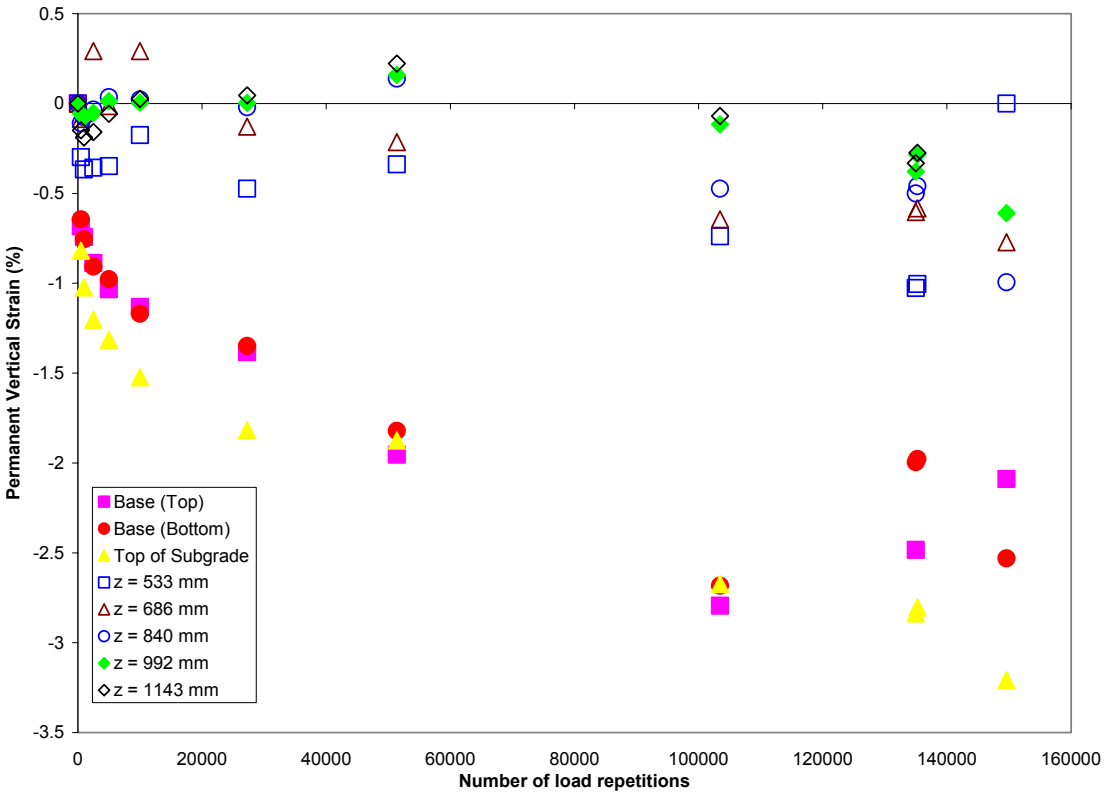

Figure 85. Vertical strain in the base and subgrade as a function of load repetition.

The respective permanent strains in the base and subgrade as a function of load repetitions and depth are presented in Table D-8. The maximum strains in the vertical direction is about 2–3%. In the longitudinal and transverse directions, the strain is less then 1%. The progression of the vertical strain as a function of load repetition is shown in Figure 86. There are basically two trends, as seen with the vertical deformation (Fig. 82).

The development of vertical permanent strain in the subgrade as a function of depth and load repetitions is shown in Figure 86. It is interesting to see the subgrade at depths below 800 mm goes into extension during part of the loading and becomes compressive at failure.

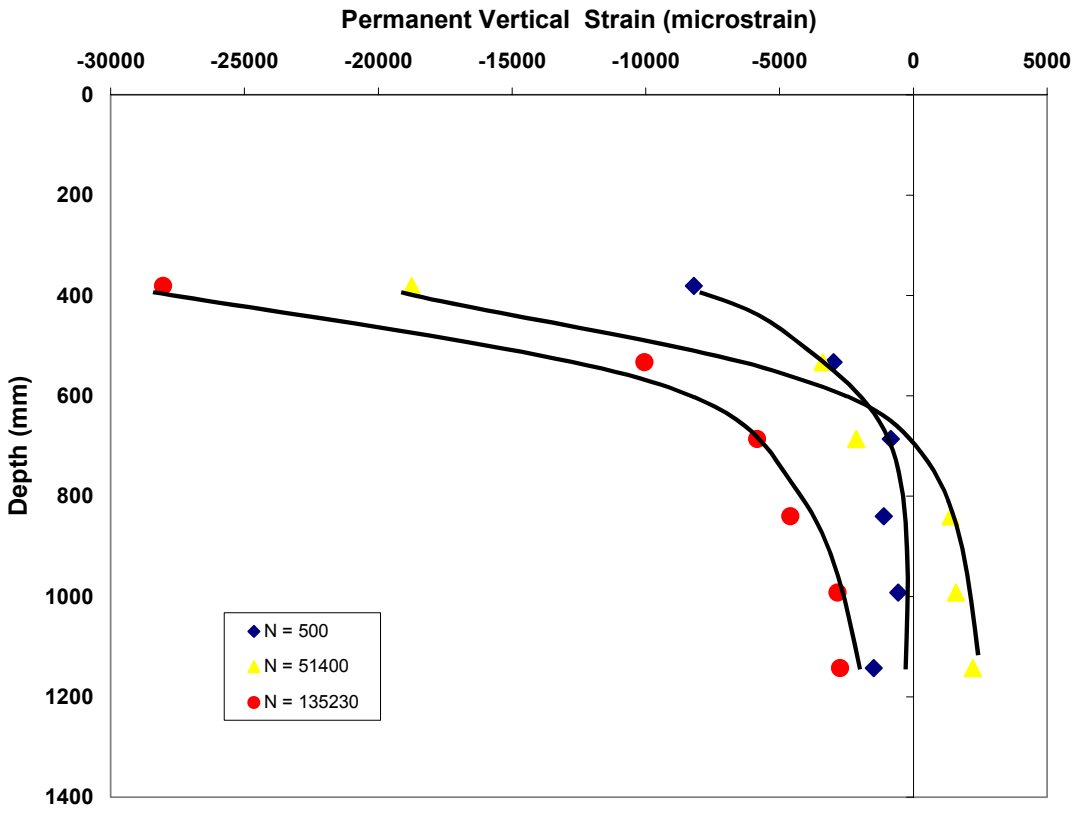

Figure 86. Progression of vertical permanent strain as a function of load repetition.

Surface Profile Measurements

Twenty-four surface profile measurements were made periodically to determine the surface deformation as a function of load repetition. Of the 24 measurements, the first two (1, 2) and last two (23, 24) measurements were taken in the acceleration and deceleration areas (Fig. 34). The measurements at these locations are not reported. Locations 7, 8, and 9 are in the vicinity of the εmu coils (Fig. 34). A typical set of surface deformation as a function load

repetition is shown in Figure 87. A ten-point running average was applied to the data shown in Figure 87, and the maximum rut depth was extracted from the averaged data. The maximum rut depths across the test section as a function of load repetition is presented in Table D-9.

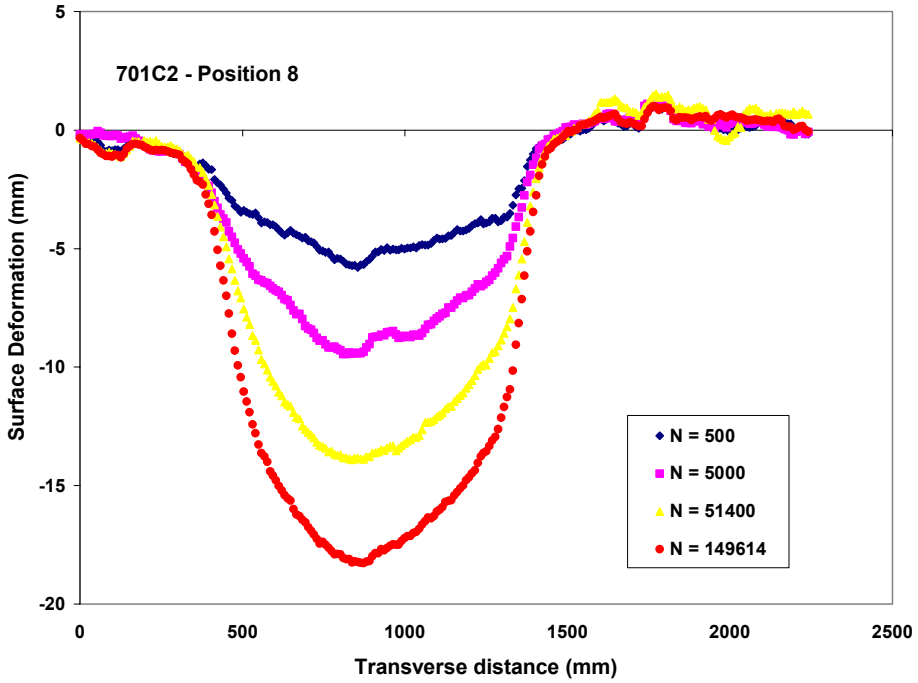

Figure 87. Typical rut depth response as a function of load passes, Position 8.

The variation of surface deformation or rut depth in the longitudinal direction as a function of several levels of road repetition is shown in Figure 88. Again, as in 701C1, we see larger rut depths near the south wall. The longitudinal rut depth is fairly constant after position 8. All our measurement systems are placed at position 8 and after. After we finished the tests in this section, we moved the instrumentation to locations where we expected the rut formation to be more uniform.

A comparison of the total rut depths measured from the profilometer and strain coil gages are shown in Figure 89. Data from the dynamic measurements are not shown in Figure 89, as there were errors in the measurements. There was about a 3-mm difference between the deformation measured at the surface using the profilometer and that determined from the permanent deformation from the coil gages. However, near and at failure, the difference is less than 1 mm.

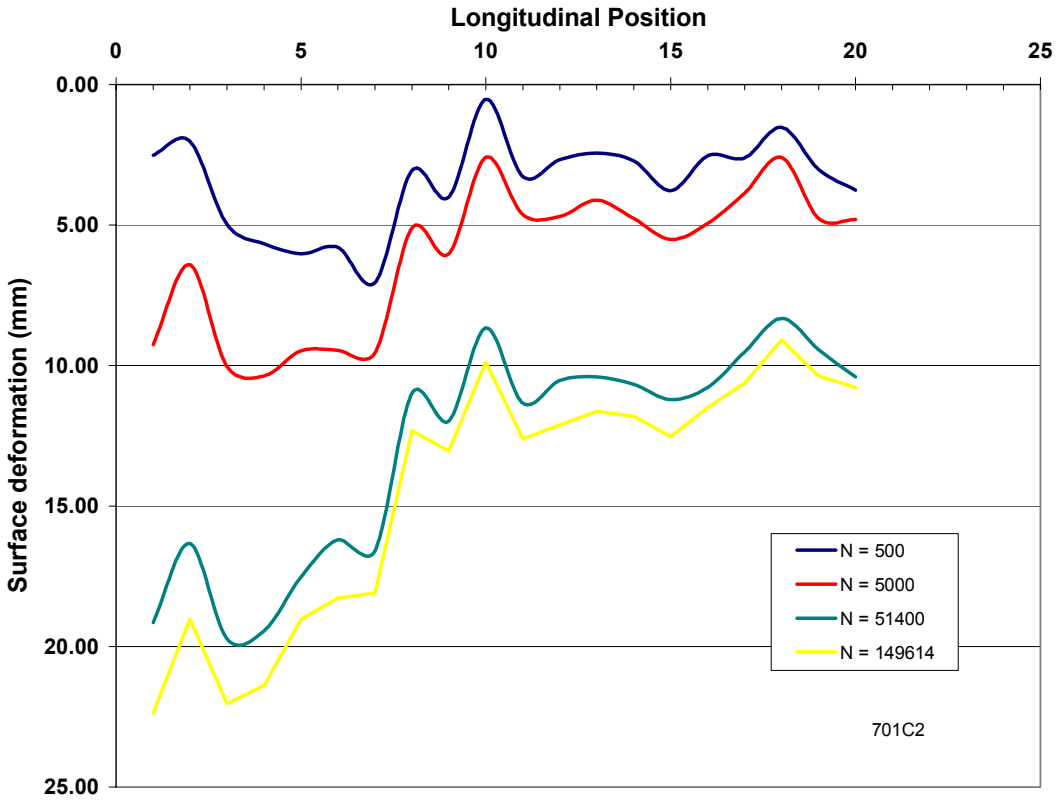

Figure 88. Longitudinal surface rutting as a function of load repetition.

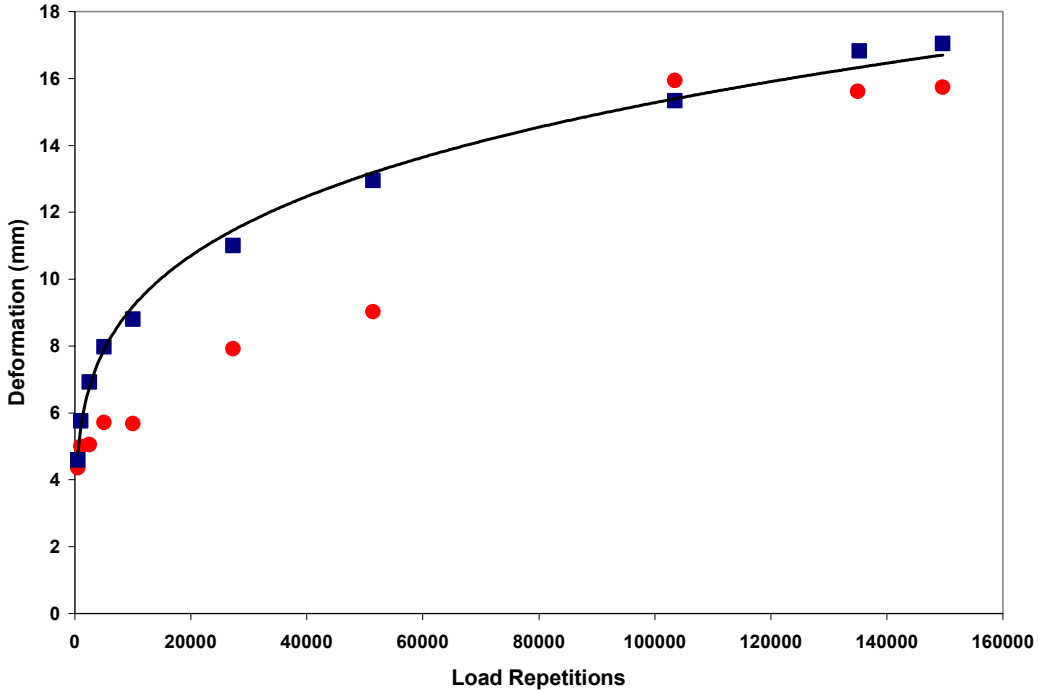

Figure 89. Comparison of total pavement deformation between profilometer and coil gage systems.

Results from Test Window 701C3

Testing of window 701C3 began on September 4, 1997, and ended on September 10, 1997. The test window was subjected to a test load was 103.5 kN, with a COV of 1.9%, and the tire pressures in the dual wheels were 751 kPa (COV = 1.0%) and 764 kPa (COV = 0.9%), respectively. The average tire pressure was 758 kPA (COV = 1.25%).

Dynamic Stress

Dynamic stresses measurements were made in the vertical, longitudinal, and transverse directions at a depth of 508 mm from the AC surface in the subgrade in the test window. There were significant problems with the measurements. First, it was discovered that the wrong stress sensors were read prior to 500 passes. Second, no initial measurements were made prior to trafficking. The second error was not as serious as the first, since we found from previous test windows that the change in stresses from 0 to 500 passes is negligible. A more serious problem was discovered with the results of the vertical stress when measurements were taken at positions 2 and 3. For nearly all the measurements (except for those at 30,000 and 40,000 passes), the amplifier gains for the vertical stress measurements were set at a maximum, so the output signals were saturated at 10 V. This error was not discovered until near the end of the tests (i.e. after 30,000 passes). Stress measurements taken at 30,000 passes are presented in Figure 90. As with the previous test windows, negative values indicate compressive stress. The average maximum vertical stress at a depth of 500 mm (approximately 195 mm into the subgrade) was 315 kPa, and it occurred when the sensors were directly under both the wheels, i.e., at position 2. This is about 42% of the applied stress (758 kPa) on the surface. This clearly shows the effect of the load in addition to tire pressure on the stress in the subgrade. In 701C2 the tire pressure was similar, but the load was 89 kN versus 103.5 kN in 701C3. The stress in the subgrade was 21% and 42% of the applied tire pressure.

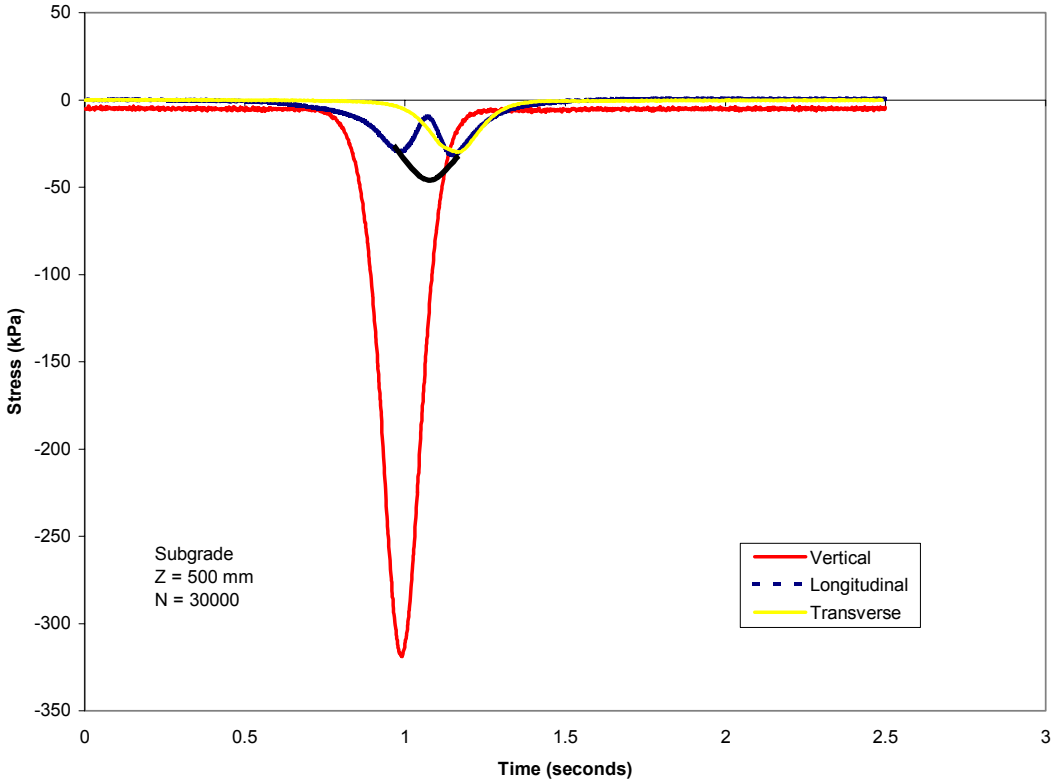

Figure 90. Typical stress responses in the subgrade after 30,000 repetitions.

The longitudinal stress response curves were similar to those seen in 701C2 (Fig. 69). Again, a correction was applied to the response curve to account for the effect of the sensor wall thickness, as discussed in 701C2. It was also found that the responses of the longitudinal stress at positions 1 and 2 were very similar. In general, the peak longitudinal stresses ranged between 40 and 50 kPa, and over the range of load repetition, we found that there was a small increase of approximately 10 kPa from the beginning to the end of testing (Fig. 91). The stresses in Figure 91 are those corrected for the sensor wall thickness, as discussed in 701C2.

The transverse stresses measured in the subgrade were also compressive. Again, we found that the maximum transverse stress measurements occurred when the wheel was in position 3. This was similar to the results obtained from 701C2. The response curves from the transverse stress measurements were similar to those obtained in 701C2 (Fig. 71). The peak transverse stress was approximately 30 kPa, and it stayed fairly constant throughout the test (Fig. 92).

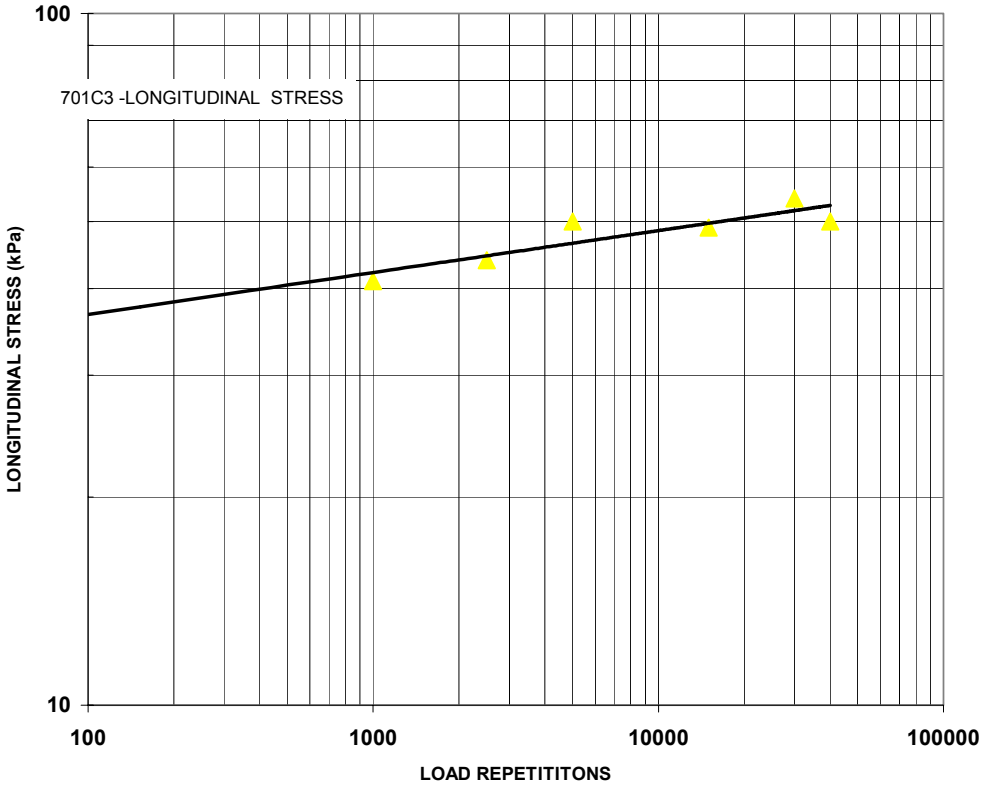

Figure 91. Longitudinal stress response (Position 2) as a function of load repetition.

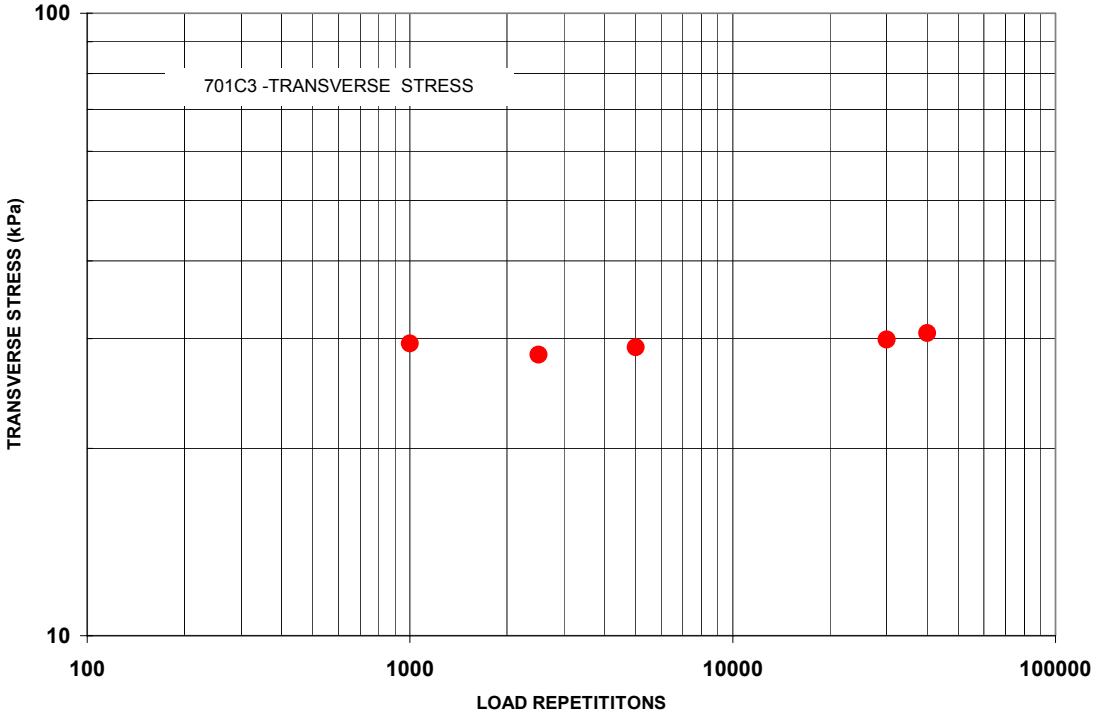

Figure 92. Transverse stress response (Position 3) as a function of load repetition.

Dynamic Strain

Vertical, longitudinal, and transverse dynamic strains were measured as a function of load repetitions at the three wheel locations similar to those in the other test windows. The results are presented in Appendix E. There was a problem with the measurements in the vertical direction at the upper depths in the subgrade. A summary of the maximum strain as a function of depth and load repetition is presented in Table E-4. Generally the strains decreased with depth and increased with load repetition.

Most of the vertical strain measurements on top of the subgrade failed during testing. Similarly, because of a coil failure, we were unable to obtain any strain measurements at a depth of 686 mm. The change in the dynamic vertical strain as a function of load repetition and depth are shown in Figure 93. The available data for the top of the subgrade, shown in Figure 93, appear to be clustered with the data from z = 533 mm. A power curve trend line is added to the data, and an assumed power curve having an average exponent of the other layer data is presented in Figure 93 for the limited top of the subgrade strains. This is not a bad

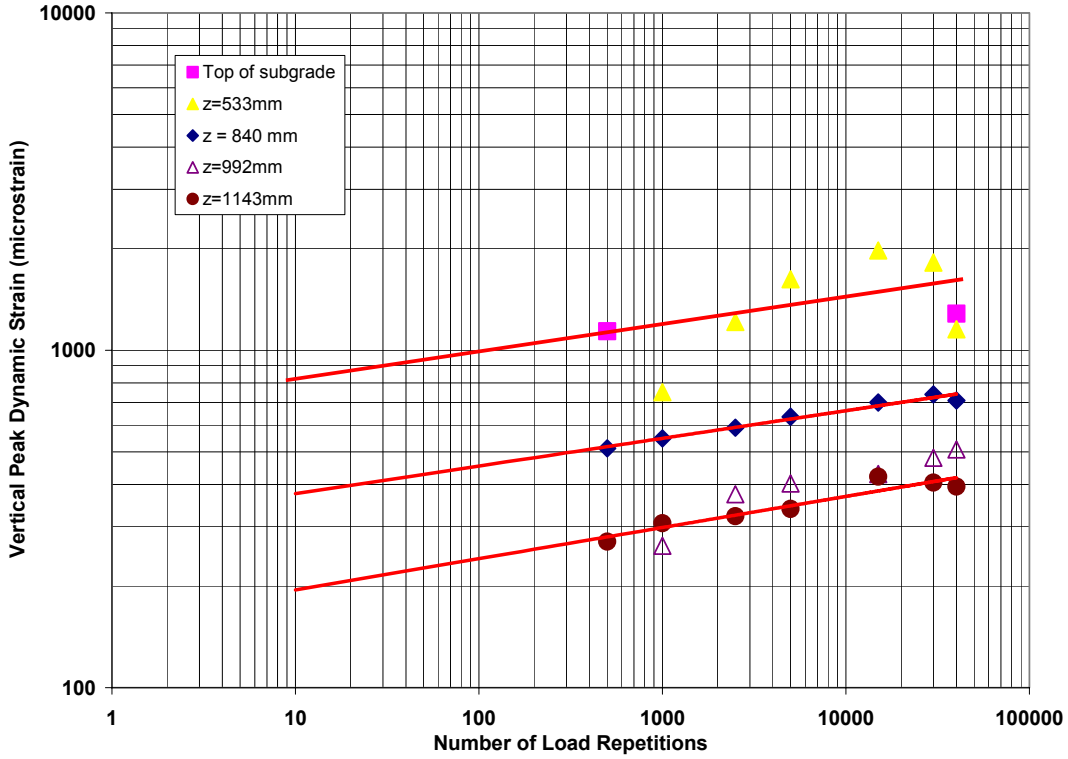

Figure 93. Development of dynamic vertical strain as a function of load repetition and depth, Position 2.

assumption, as it was seen in previous windows that the curves are nearly parallel to one another. It was also noted that the vertical strain decreased at the end of the test (i.e. at 40,000 load repetitions). This may be due to further compaction of the subgrade layer.

Also noted was that the maximum strains occurred at position 2, i.e., when the strain gages were between the dual tires. The following exponents were calculated after fitting the data with a power curve. The subgrade at depths of 992 and 1143 mm were fitted with a single power curve with the following coefficients (152, 0.092, $R^2 = 0.90$). The subgrade at a depth of 533 mm was fitted with the following coefficients (311, 0.082, $R^2 = 0.97$). The first number within the parentheses is the intercept and the second number is the exponent. The exponent for the top of the subgrade and the subgrade at 533 mm is assumed to be around 0.87.

The measurements of the longitudinal strains were better than the vertical strains. However, we were unable to measure the longitudinal strains at a depth of 686 mm. We also found the measurements at z = 553 mm to be extremely noisy and had to apply averaging techniques to the data to remove the extraneous noise in the measurements. The results of the measurements are presented in Table E-5. We also found that the longitudinal strains at position 3 were quite noisy; at times they tended to mask out the other results from positions 1 and 2. At the top of the subgrade, the strains were extremely high and mostly compressive. This was not seen in the other test windows, and with the problems with the vertical strains, we decided not to use the results in future analysis. In addition, as done with previous longitudinal strain measurements, the sums of the peak values are presented as a function of load repetition and depth in Figure 94. The coefficients for the power curve fit to the available data in Figure 94 are presented in Table 7. If an estimate was made for the top of the subgrade, the exponent will be between 0.123 and 0.153.

Table 7. Coefficients for power law curves applied to longitudinal strain development.

Depth (mm)	*A*	*n*	R^2
305			
457	168	0.14	0.99
610			
762	97	0.123	0.97
918	52	0.153	0.94
1067	-	-	-

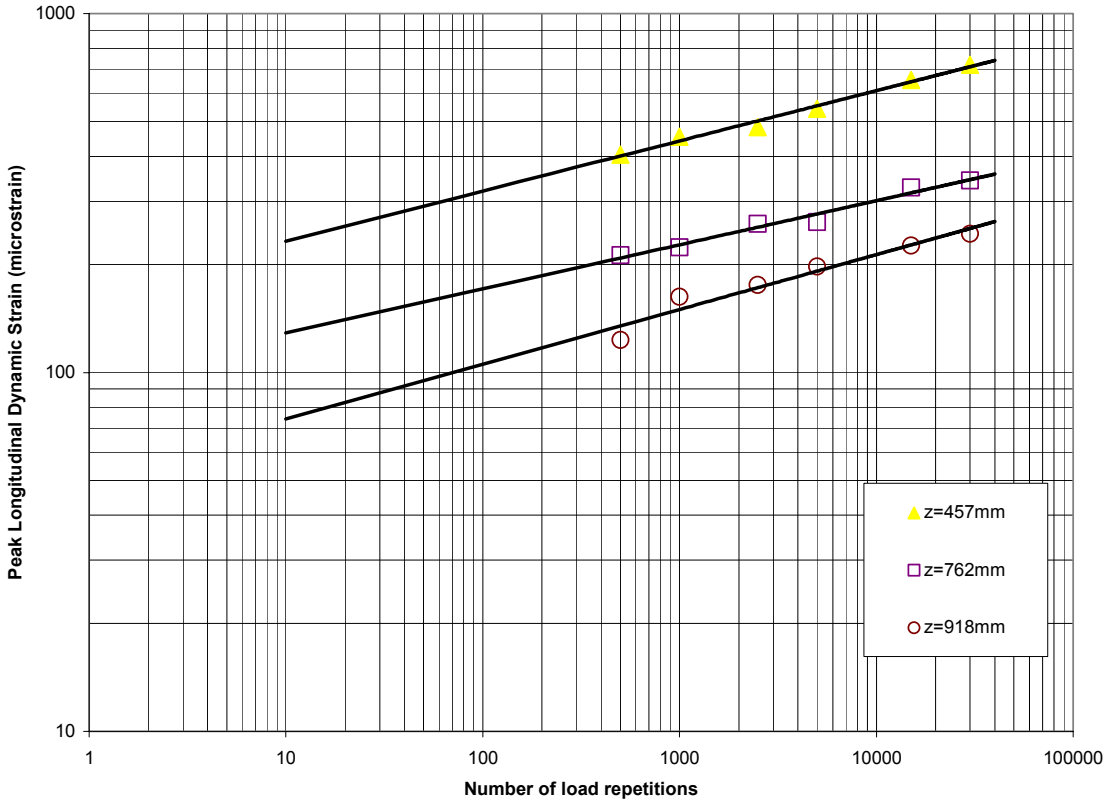

Figure 94. Change in longitudinal strain as a function of load repetition and depth, position 2.

The maximum transverse strains as a function of load repetition and depth are presented in Table E-6. The problems with the vertical and longitudinal strain measurements at the top of the subgrade and at a depth of 610 mm were also seen in the transverse direction. The coefficients for the power curve fits to the transverse data in Figure 95 are presented in Table 8.

Table 8. Coefficients for power law curves applied to transverse strain development.

Depth (mm)	*A*	*n*	R^2
305			
457	130	0.14	0.80
610			
762	86	0.106	0.97
918	38	0.148	0.94
1067			

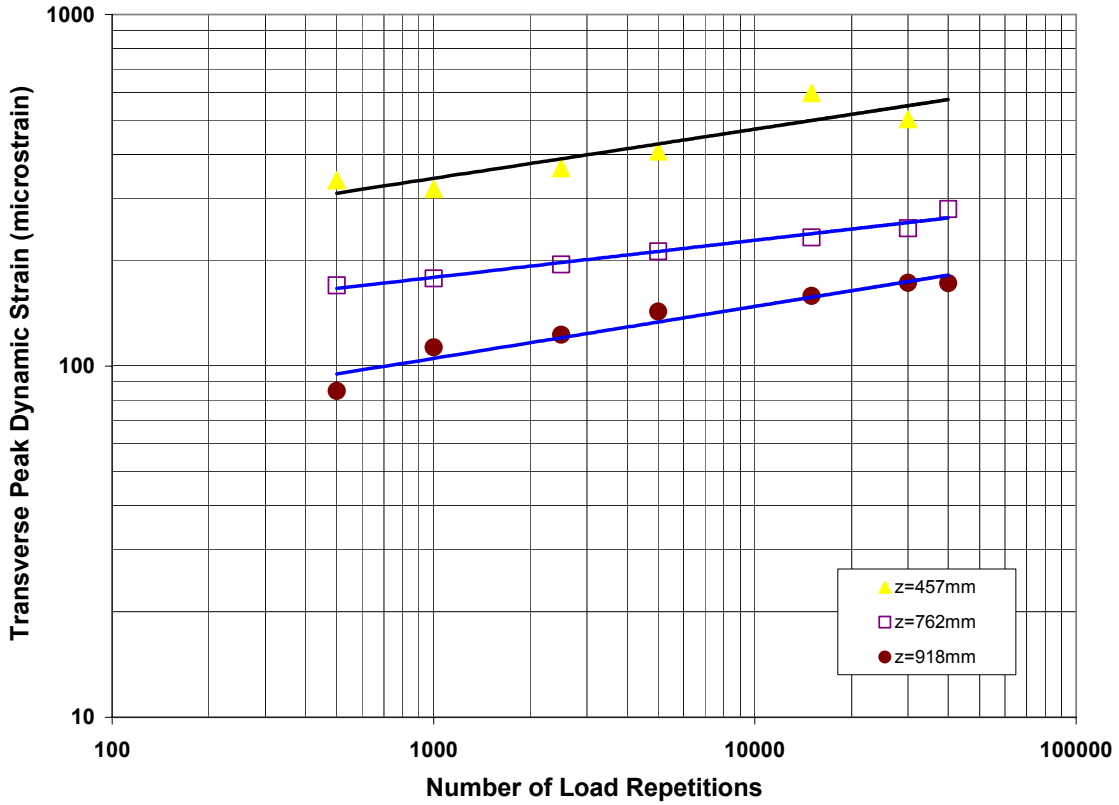

Figure 95. Development of the transverse strain as a function of load repetition and depth, position 2.

Permanent Strain

Permanent deformations were obtained from static measurements between the εmu coils and are presented in Table E-6. The surface measurements were taken between a coil gage placed on the AC surface and the coil gage in the base course layer. The distance between the two coil pairs was 182 mm. These coil pairs were not calibrated, and the calibration curve was assumed to be similar to the coil pairs in the base course. The error was considered to be minimal, as we were looking for changes in distances between the coil pairs and not the magnitude of the separation.

Again, the data from several of the depths were unavailable due to gage failure. However, with the limited data, it can be seen that generally the vertical and longitudinal deformations were compressive and that they increased with increasing load repetitions. The transverse strains were mostly in extension.

Surface Profile Measurements

The maximum rut depths across the test section as a function of load repetition are presented in Table E-7. The variation of surface deformation or rut depth in the longitudinal direction as a function of several levels of road repetition is shown in Figure 96. Again, as in the other test windows, we see larger rut depths near the south wall. The longitudinal rut depth is fairly constant after position 7. All our measurement systems are placed at position 8 and after.

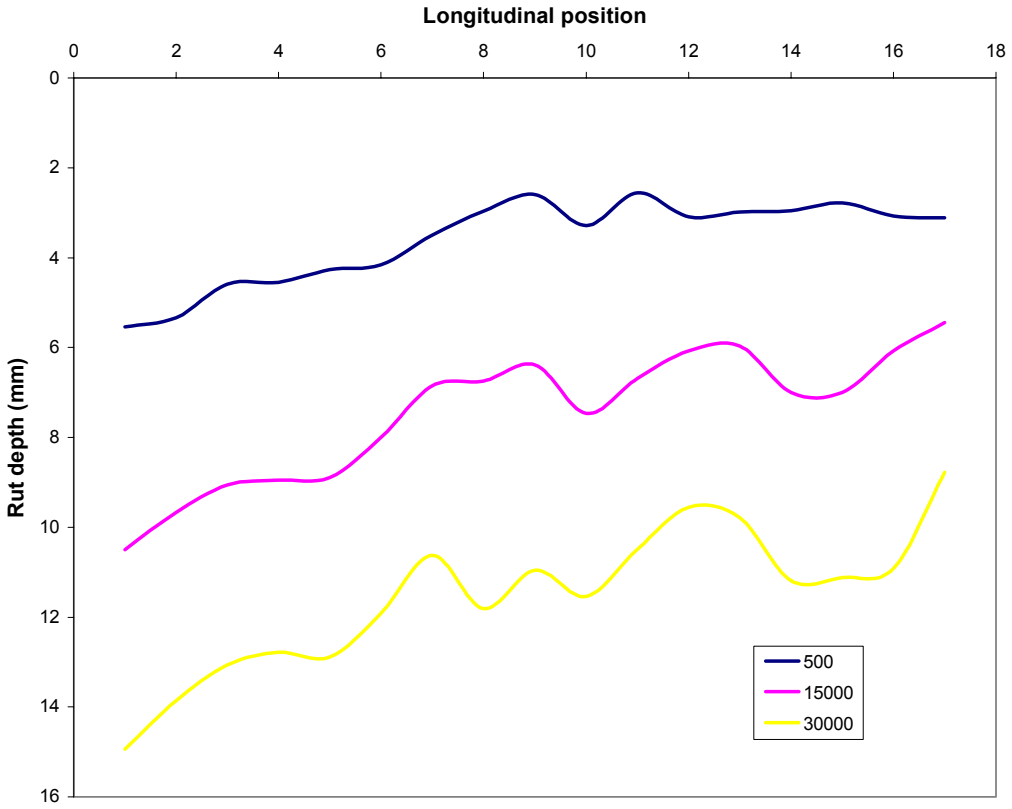

Figure 96. Longitudinal surface rutting as a function of load repetition.

We did not compare the measured rut depths from the surface profilometer with the calculated rut depth from the coil gages due to limited data from the gages in this test window.

Results from Test Window 701C4

Testing of window 701C4 began on July 9, 1997, and ended on August 11, 1997. The test load was 89 kN, with a COV of 1.7%, and the mean tire pressure of the dual wheels was 748 kPa, with a COV 3.5%. The speed of the test wheel was 13 km/hr. Problems with the HVS

after 55,000 repetitions prompted us to drop the speed to 10 km/hr for the remainder of the tests. It should be noted that 701C4 was the second window to be tested, and we were still having problems with the HVS. Also, this was one of the test windows that did not have any stress cells because of delays in delivery of the stress cells. Therefore, during the accelerated loading phase, only strain responses were measured periodically.

Dynamic Strain

As with the other windows, vertical, longitudinal, and transverse dynamic strains in the base and subgrade were measured as a function of load repetitions at three wheel locations. The results are presented in Appendix F. The responses in the three directions were similar to those seen in the other windows. The vertical strain response from the εmu coils was well defined and was compressive at all depths. The longitudinal strain response was compressive as the wheel approached the sensors and became expansive as the wheel was on top of the sensor. As the wheel left the sensor, the strain dropped and became compressive before returning to zero. With increasing depth, the second compression was lower than the first. At a depth of 1143 mm, the sensor output when the wheel was at position 2 was so poor that it is not reported or used in the analysis. The transverse strain measurements were reasonably good at all positions and depths. The peak transverse strains near the surface were higher when the wheels were at the edge (position 1 and 3). With increasing depth, the peak strains at all wheel positions tended to equalize. There was some drifting in the longitudinal and transverse strains in the base and at the top of the subgrade, and corrections were applied to remove the effect of drifting.

The change in the vertical strain at various depths in the subgrade as a function of load repetitions is shown in Figure 97. There is a rapid development of strain in the initial loading phase (up to approximately 20,000 load repetitions), followed by more of a gradual increase. Power law curves were applied to the strain response (position 2) (Fig. 98); the coefficients for the power curves are presented in Table 9. As seen by the coefficient *n* in Table 9, the gradient of the vertical strain in the subgrade is approximately 0.06–007, except for the top of the subgrade, where the gradient is 0.04. The gradient of 0.06 is similar to that found from the results from 701C1 and 701C2.

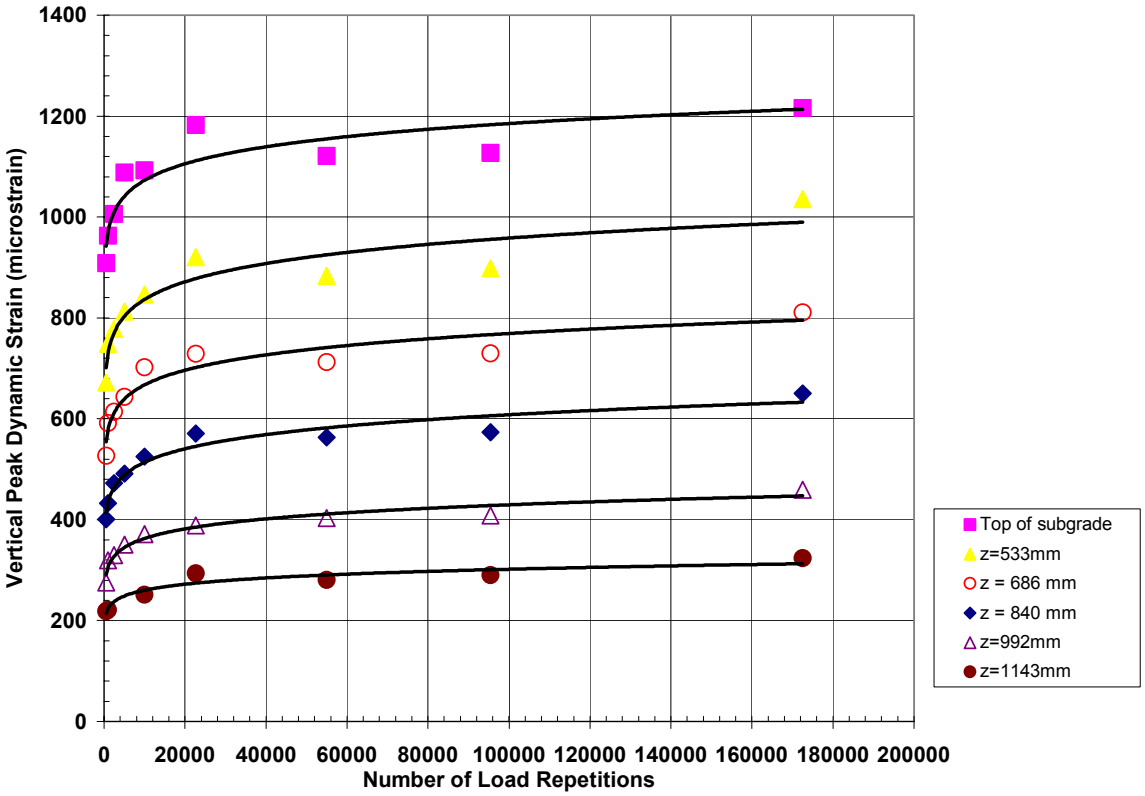

Figure 97. Development of the dynamic vertical strain as a function of load repetition.

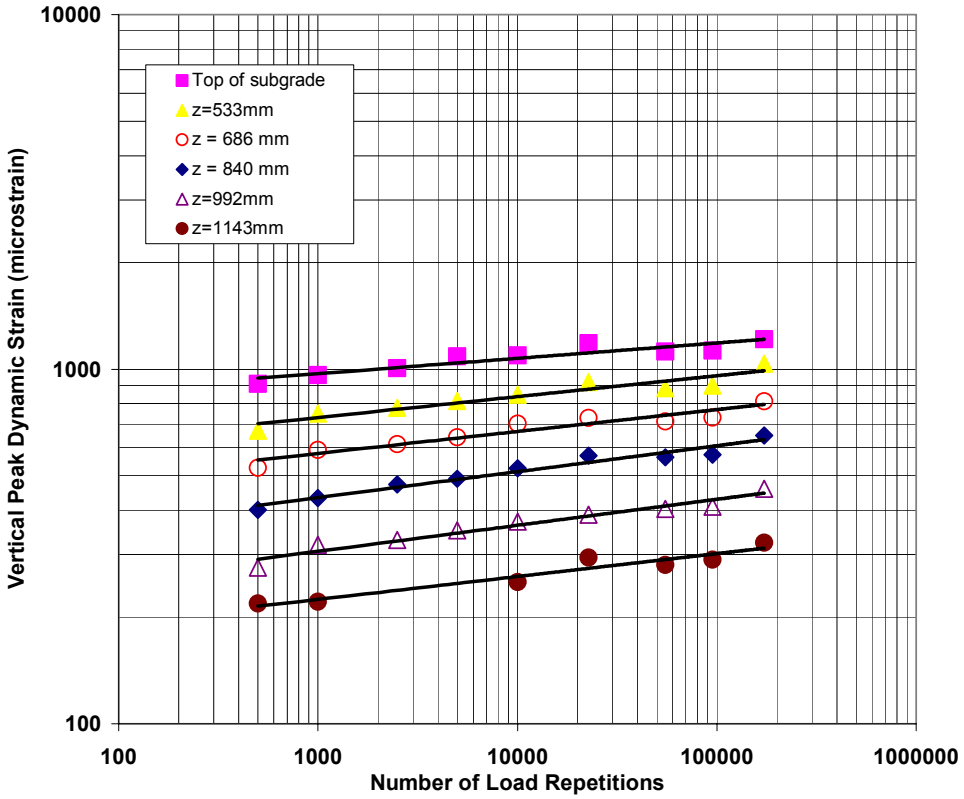

Figure 98. Dynamic vertical strain as a function of load repetition (701C4).

Table 9. Coefficients for power law curves applied to dynamic strain development.

Depth (mm)	*A*	*n*	R^2
381	720	0.0433	0.85
533	486	0.0590	0.90
686	378	0.0618	0.92
840	262	0.0732	0.96
992	185	0.0733	0.95
1143	144	0.0645	0.92

The development of the dynamic vertical strain with depth and as a function of load repetition is shown in Figure 99. This is similar to that seen in the other test windows. There is about a four- to five-fold decrease in strain from the top of the subgrade and the measurement taken at a depth of 1143 mm. The difference in depth is 610 mm.

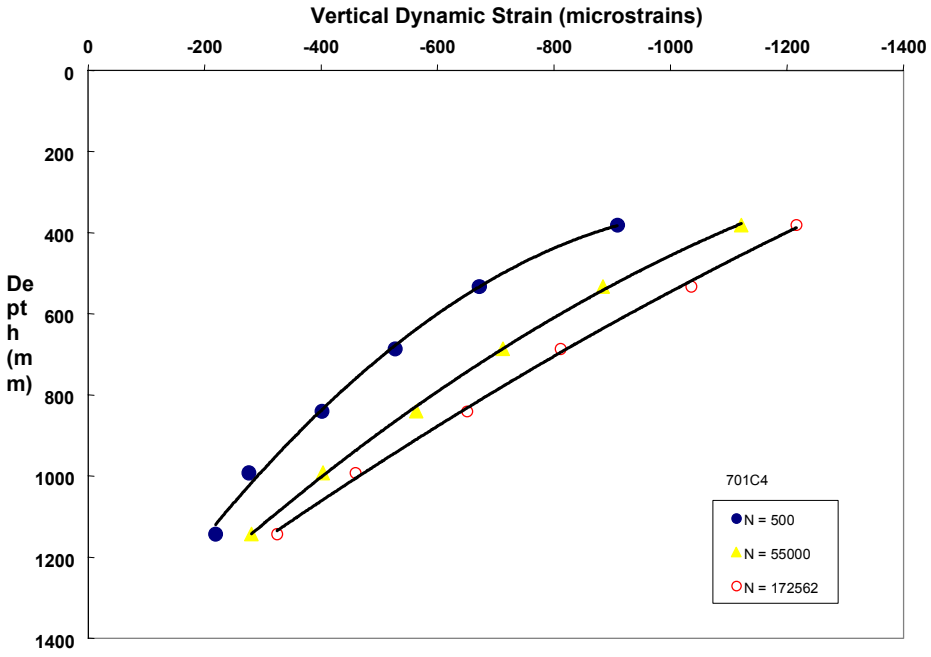

Figure 99. Progression of vertical dynamic strain as a function of depth and load repetition.

As done with the other test windows, the longitudinal strains reported in Table E-2 are the peaks of the first compressive strain, the peak extension strain, and the peak of the second compressive strain. The second compressive strain is usually lower in the subgrade, so it was not used in the summation process. As in the other test windows, the largest strains occurred when the wheel was in position 2. The absolute values of the magnitude between peaks A and B of the longitudinal strains from position 2 were used to determine the strain as a function of

load repetition (Fig. 100). There was a rapid increase up to about 20,000 load repetitions, after which the rate became more gradual. The peak strain curve in Figure 100 was fitted with a power curve (Fig. 101), and the coefficients for the power curve are presented in Table 10.

The exponent for longitudinal strain in the subgrade ranged between 0.11 and 0.14. This is within the range reported for 701C1 and 701C2.

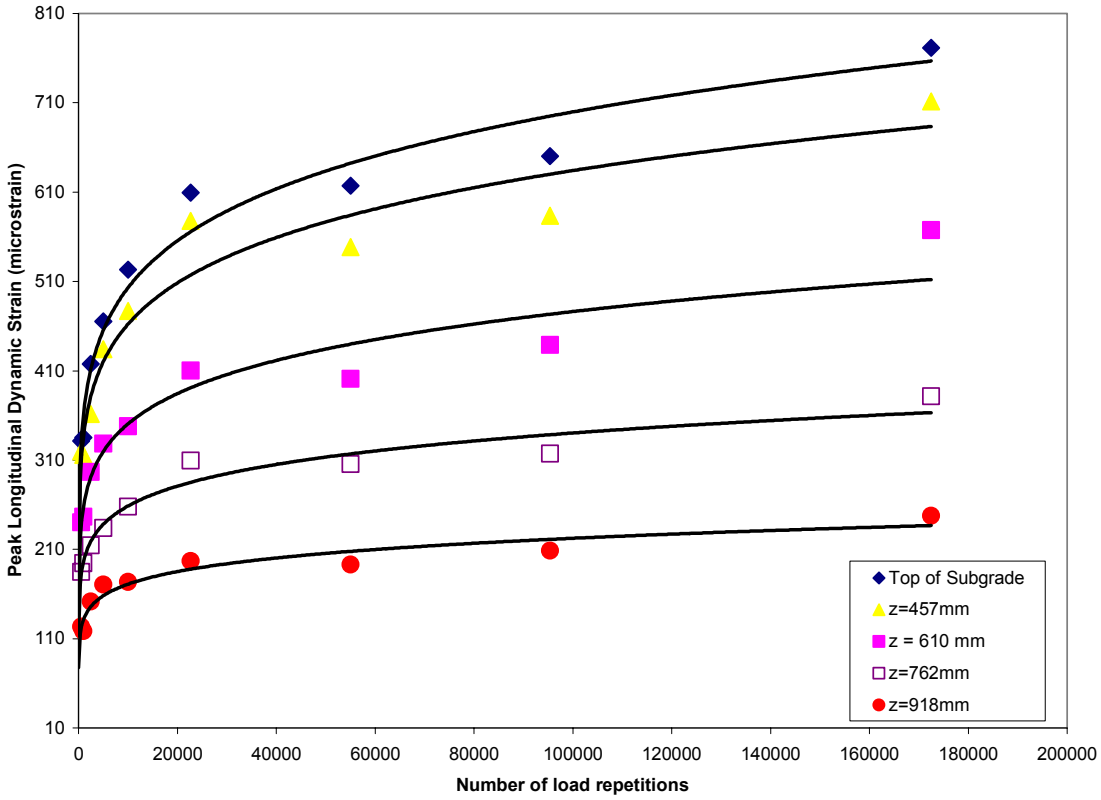

Figure 100. Development of longitudinal strain as a function of load repetition.

Table 10. Power-law coefficients for dynamic longitudinal strain development.

Depth (mm)	*A*	*n*	R^2
305	134	0.1435	0.97
457	130	0.1374	0.95
610	103	0.1332	0.95
762	86	0.1193	0.97
918	60	0.1140	0.93
1067			

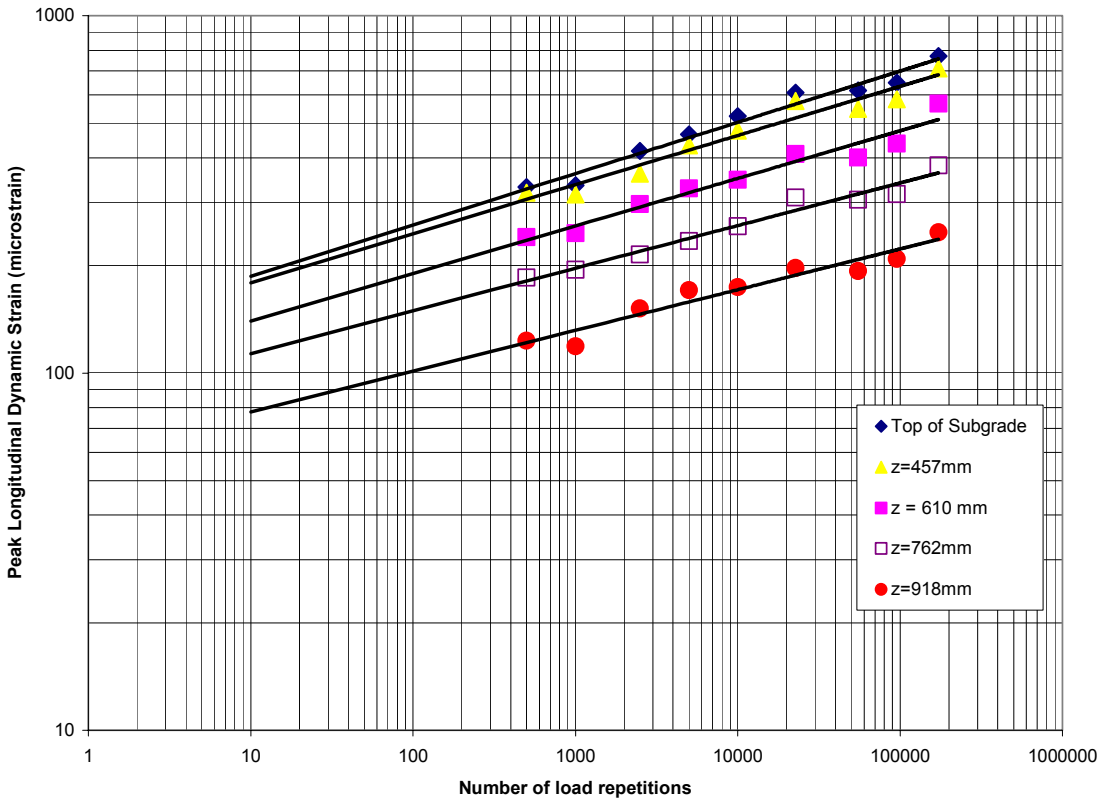

Figure 101. Change in peak longitudinal dynamic strain as a function of load repetition.

The peak transverse strains as a function of load repetitions are tabulated in Table F-3. Generally the transverse strains increased with load repetition. In this test the largest transverse strains occurred at a depth of 610 mm. This was also seen in the other test windows. However, in the subgrade the transverse strains ranged between 100 and 200 microstrains. The highest strains occurred in the base. In the base and subgrade the higher strain values generally occurred when the wheel was in position 1. At other depths they were fairly close to one another.

The change in transverse strain as a function of load repetitions is shown in Figure 102. The response is similar to the vertical and longitudinal strains. Power curves were used to fit the data (Fig. 103), and the appropriate coefficients are presented in Table 11.

The progression of the transverse strain as a function of depth and load repetitions is shown in Figure 104. Again, as with the other test sections, there was an increase in transverse strain at a depth of approximately 800 mm.

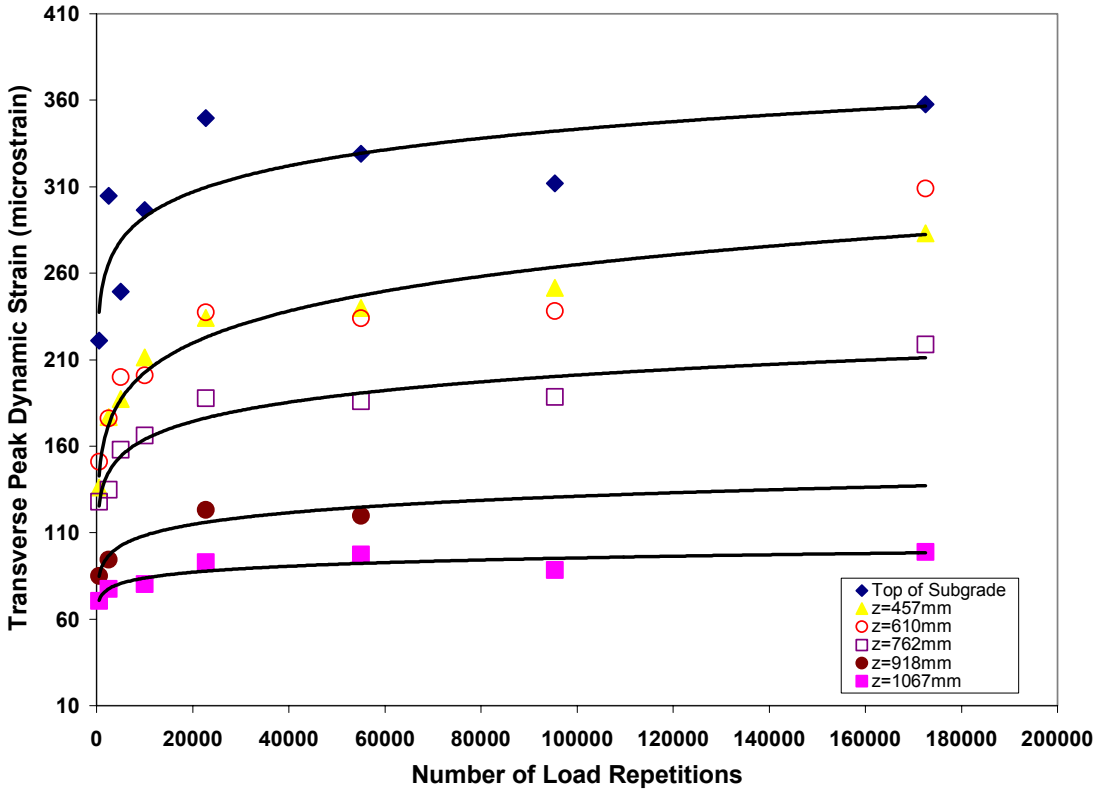

Figure 102. Change in transverse strains with load repetition in the subgrade (701C4).

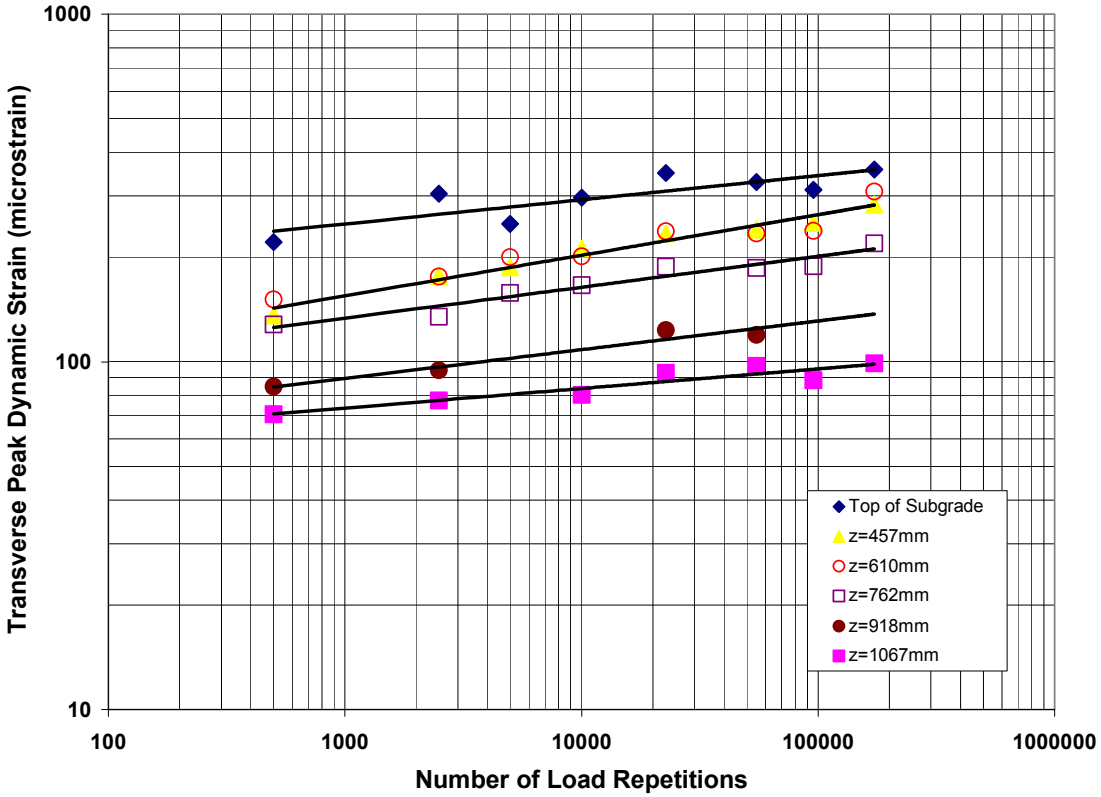

Figure 103. Change in transverse strain as a function of load repetition.

Table 11. Coefficients for power law curves applied dynamic transverse strain development.

Depth (mm)	*A*	*n*	R^2
305	154	0.0696	0.69
457	69	0.1167	0.97
610	78	0.1056	0.92
762	72	0.0890	0.93
918	51	0.0826	0.94
1067	63	0.0363	0.80

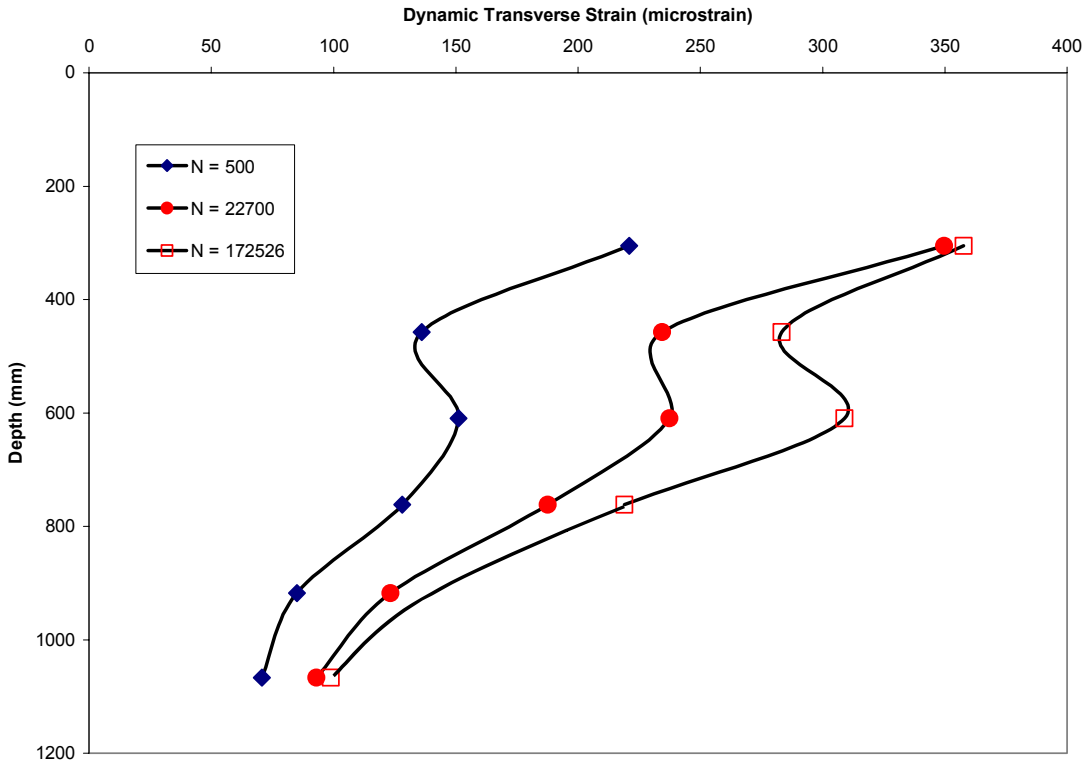

Figure 104. Progression of dynamic transverse strains as a function of depth and load repetition.

Permanent Strain

Permanent deformations were obtained from static measurements between the εmu coils and are presented in Table F-4. The vertical deformations were generally compressive and increased with increasing load repetition (Fig. 105). Most of the permanent deformation occurred in the base course layer and in the top 200 mm of the subgrade.

In the longitudinal direction, there was significant deformation in the base, and the deformation was compressive. In the subgrade the deformation was extensional, with most

occurring in the top of the subgrade (Fig. 106). With respect to the deformation in the transverse direction, the strain in the base was the largest and was compressive. At the top of the subgrade and to a depth of approximately 300 mm, the strain was extensive. Below, at a depth of 762 mm from the surface, the subgrade strains were compressive. Overall, the deformation in the transverse strains was small.

The development of vertical permanent strain in the subgrade as a function of depth and load repetitions is shown in Figure 107. As can be seen, the strains at all depths started in extension and became compressive with load repetitions (Fig. 108). It was also observed that the largest permanent strain occurs at a depth of 457 mm. This is about 150 mm below the top of the subgrade.

A summary of the total permanent vertical, longitudinal, and transverse deformation of the subgrade as a function of load repetition is shown in Figure 109. In general, the vertical deformation was approximately 14 mm (compressive), and the longitudinal and transverse deformations reached about 2 mm (extension) at the end of testing.

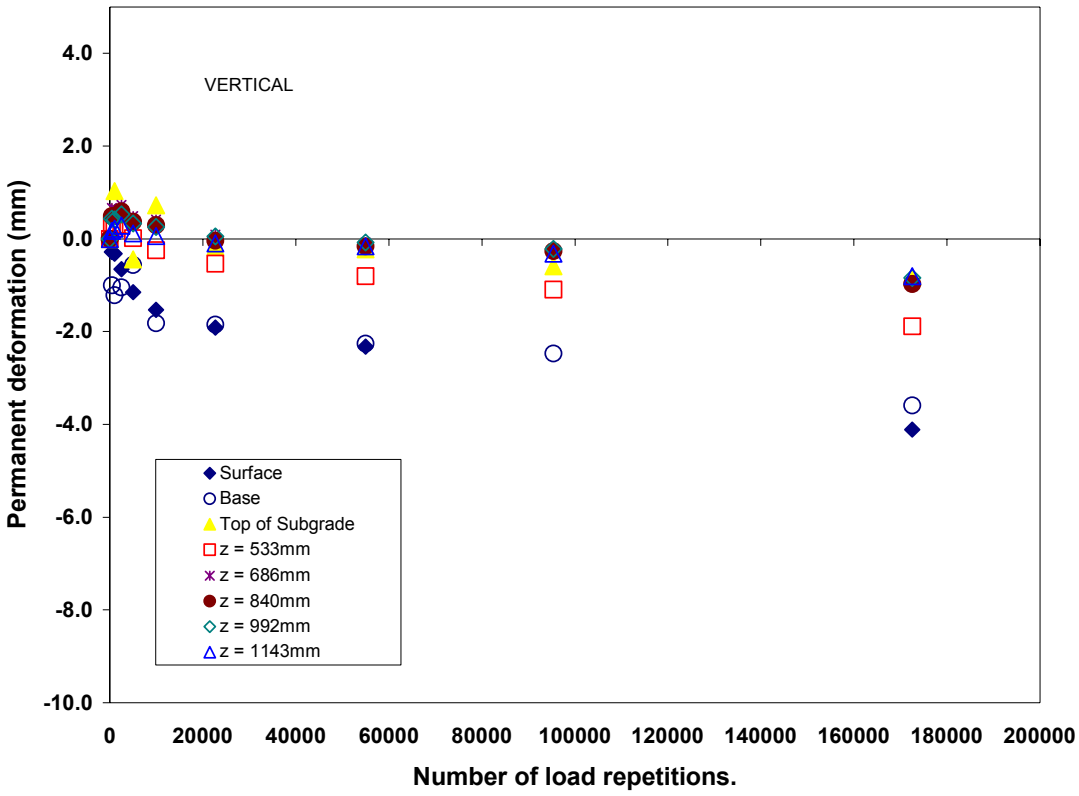

Figure 105. Development of vertical permanent deformation as a function of load repetition.

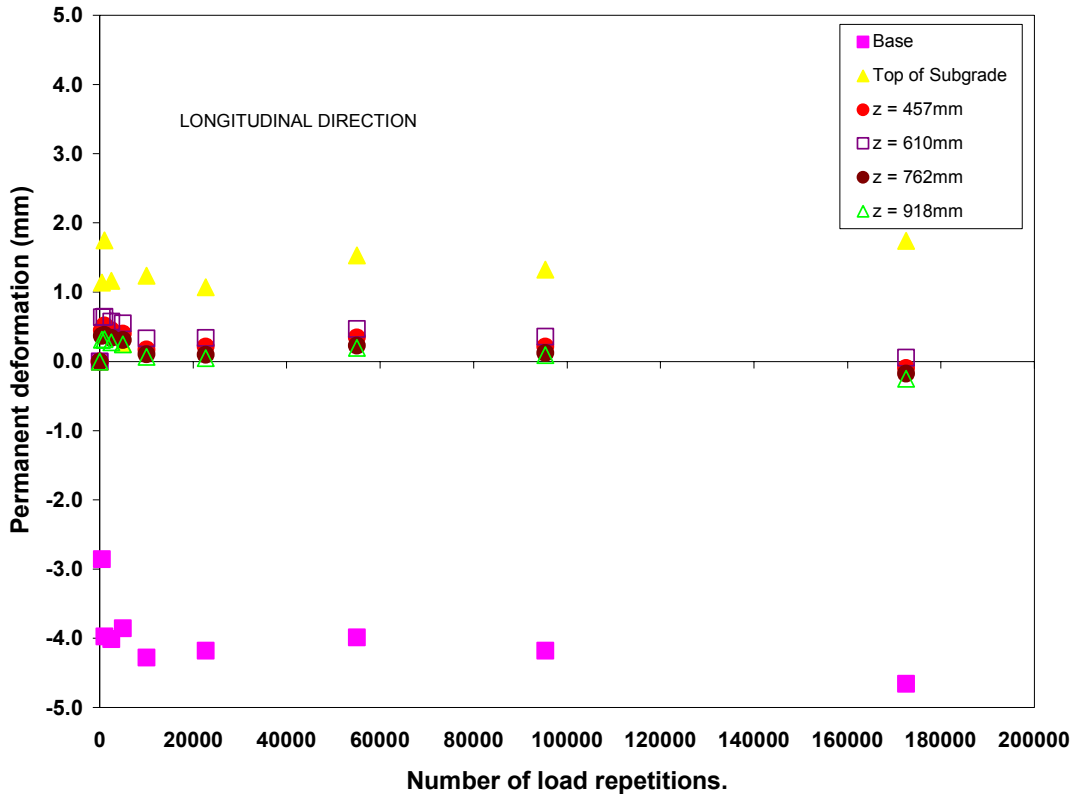

Figure 106. Development of longitudinal permanent deformation as a function of load repetition.

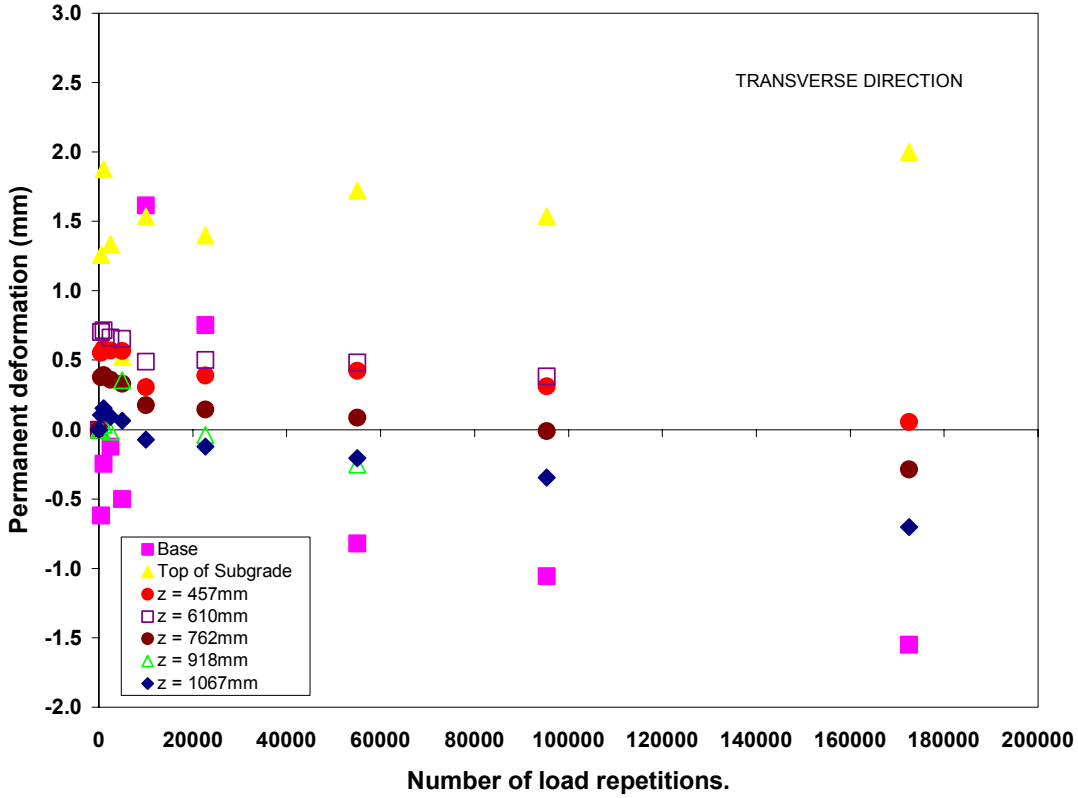

Figure 107. Development of transverse permanent deformation as a function of load repetition.

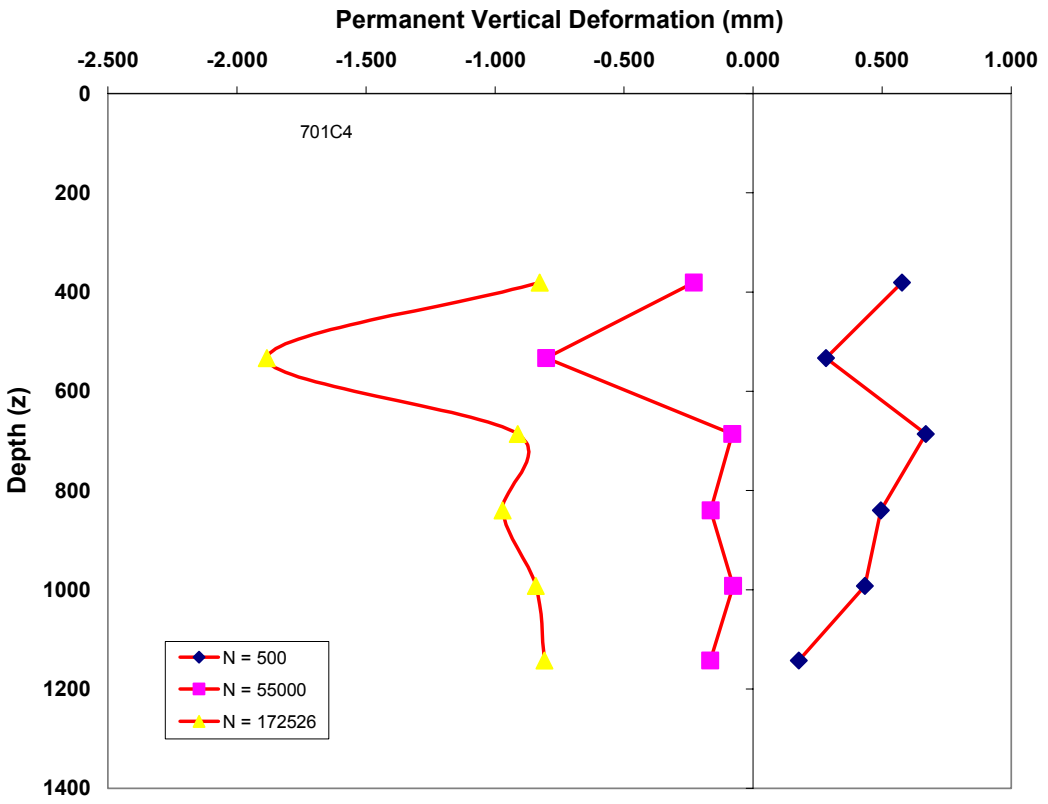

Figure 108. Progression of vertical permanent strain as a function of load repetition.

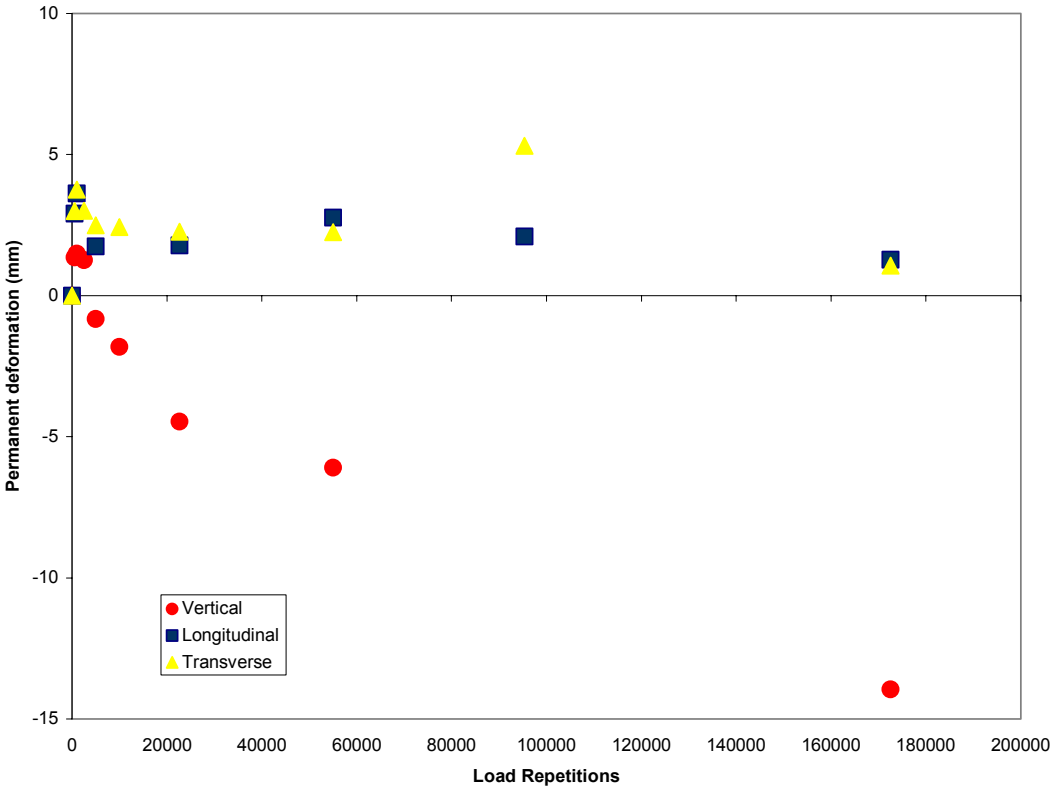

Figure 109. Development of permanent strains in the subgrade.

Surface Profile Measurements

A typical set of surface deformation as a function load repetition is shown in Figure 110. The maximum rut depths across the test section as a function of load repetition are presented in Table F-5. The variation of surface deformation or rut depth in the longitudinal direction as a function of several levels of road repetition is shown in Figure 111. The longitudinal rut depth is fairly constant along the length of the test section. Note that this section was away from the south wall, while the other three windows were close to the wall.

The sum of the subsurface permanent deformation from the coil gages are compared with the rut depths measured on the surface (Fig. 112). As seen in the figure, there is about a 4-mm difference between the two measurements. However, at failure this difference is minimal.

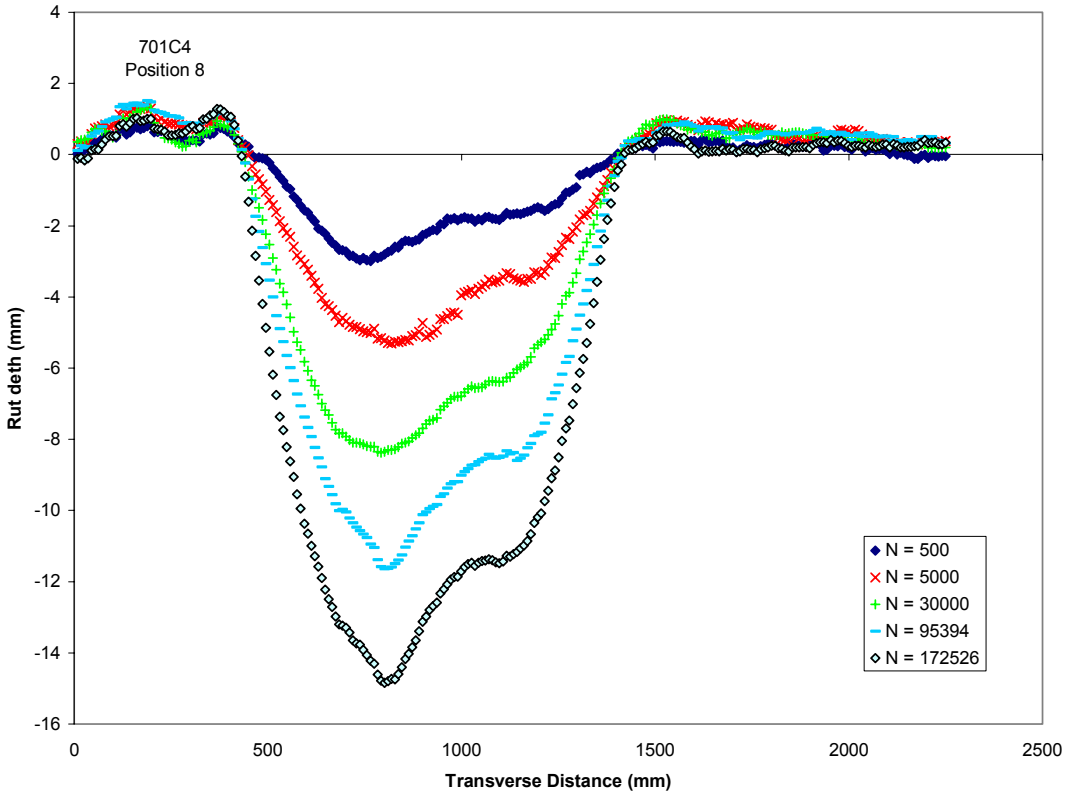

Figure 110. Typical rut depth response as a function of load repetition, position 8.

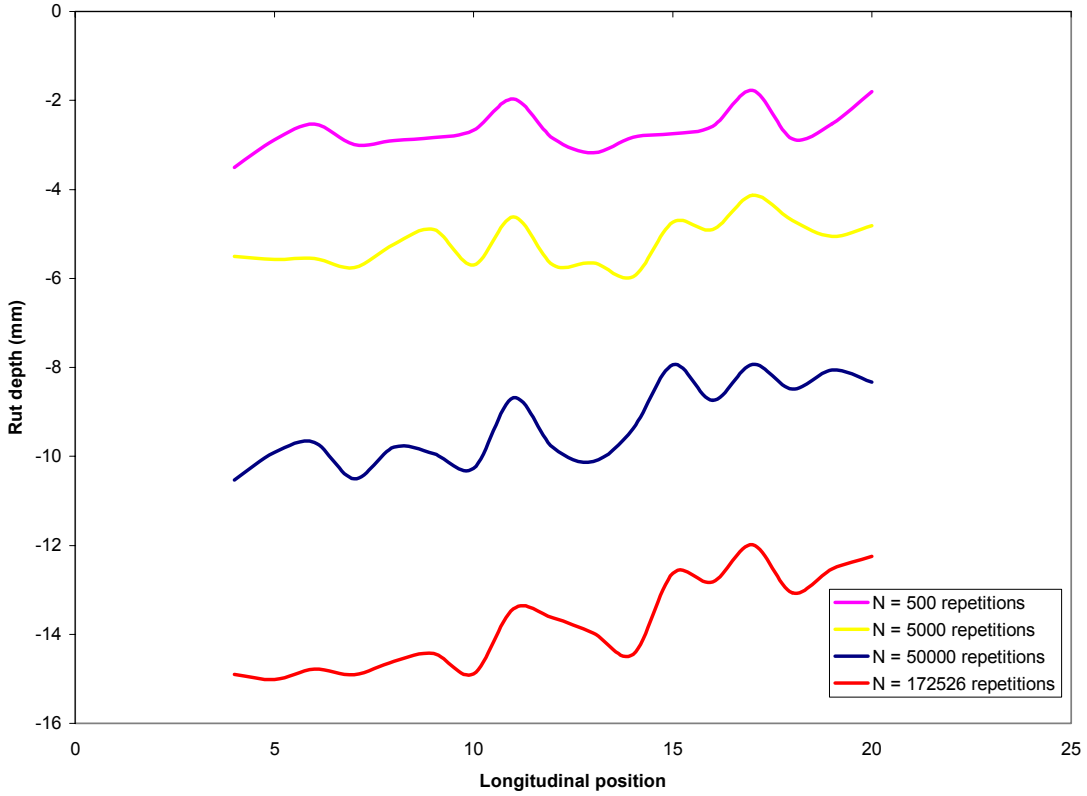

Figure 111. Longitudinal surface rutting as a function of load repetition.

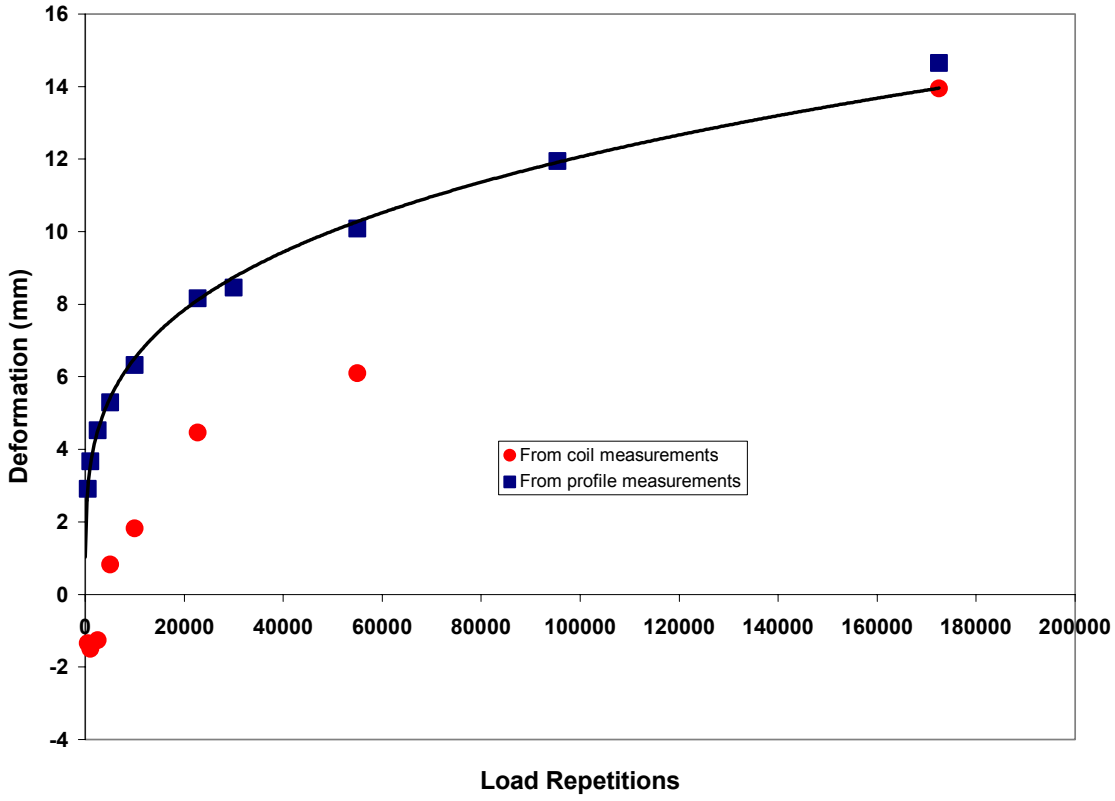

Figure112. Comparison of total pavement deformation between profilometer and coil gage systems.

SUMMARY

Accelerated pavement testing was conducted on 76 mm of asphalt concrete over a 229-mm crushed base over a 3-m, A-2-4 test subgrade soil. The test section was subdivided into six 8-m-long by 1-m-wide test windows. The subgrade was placed at an average density and moisture content of 1900 kg/m^3 and 9%, respectively. The top 1.2 m of subgrade, where most of the instrumentations were, had a dry density of 1933 kg/m^3 and moisture content of 9.5%. The dry density and moisture content of the base were 2068 kg/m^3 and 3%, respectively. In addition to density and moisture content measurements, CBR, lift thickness, and falling weight deflectometer (FWD) data were collected.

Instrumentation included temperature, moisture, stress, and strain sensors. Temperature and moisture sensors were installed outside the windows and at various depths. All test windows were instrumented with coil gages for measuring deformation in the base and subgrade. Coil gages were installed to a depth of 1.2 m at a spacing of 150 mm. The gages were used to measure both dynamic and permanent deformations. Only three of the six test windows were instrumented with pressure gages in the subgrade. Pressure cells were installed at a depth of 150 mm from the top of the subgrade. In one of the test window, an additional set of pressure cells was installed at a depth of 450 mm from the top of the subgrade. Triaxial (vertical, longitudinal, and transverse) stress and strain measurements were collected during trafficking. Permanent strains were also collected triaxially.

Traffic loading was applied through the Heavy Vehicle Simulator (HVS). The test windows were subjected to different load levels at an average tire pressure of 757 kPa. The tire was a standard dual truck tire, and the speed of load application was approximately 12 km/hr. The traffic was allowed to wander the 1-m width, and measurements were taken at three wheel positions. At the end of the dynamic stress and/or strain measurements, transverse surface rutting measurements were taken along the length of the test section. Failure was defined when the surface rut depth reached or exceeded 12.5 mm.

Accelerated pavement testing was conducted over a five-month period. The temperature in the test section varied between 15 and 20°C during the test period. According to the moisture sensors, there was a moisture gradient from the top of the subgrade to a depth of 1.2 m from the asphalt surface. In the upper 200 mm of subgrade, the moisture content ranged

between 8 and 9%. At 1.2 m from the surface, the moisture content was around 11.5%, suggesting that the material was fairly permeable. However, the variation of the moisture content at the various depths was small.

Only four of the six test windows were tested in this series. The loads were 80 (701C1), 89 (701C2), 103.5 (701C3) and 89 (701C4) kN. The tire pressure was 757 kPa. The values within the parentheses are test window identifiers. The stress measurements in all cases except one were made at these load levels. The exception was in the case of the 80-kN load tests, where the stress measurements were made at 40 kN. In general, the stresses appear to remain constant with load repetition. All measured stresses in the subgrade were compressive. The measured peak vertical stresses for the various load levels are presented in Table 12. In general, based on the limited data, the stresses were constant with load repetitions.

Table 12. Measured vertical stress as a function of applied load.

Test window	*Load (kN)*	*Vertical stress (kPa)*
701C1	40	35
701C2	89	175 (500mm from the surface) 60 (929 mm from the surface)
701C3	103.5	325
701C4	-	-

The longitudinal and transverse stresses were insignificant under the 40-kN load level. The longitudinal stress response was affected by the thickness of the pressure cells. There is a drop in the stress level as the load traverses over the thickness of the pressure cell. This drop in the stress level is significantly diminished with depth, as was seen in 701C2. The corrected longitudinal stress in 701C2 (89 kN) was around 40 kPa, and it stayed constant until near failure, when it dropped to 30 kPa. At 929 mm the longitudinal stress was around 13 kPa and in general remained constant with load repetition. In 701C3, under 103.5 kN the longitudinal stress appeared to increase with load repetition. At the beginning of the test, the stress was approximately 40 kPa. At the end of the test, the stress was around 55 kPa.

The transverse stress at 500 mm from the surface in 701C2 was around 35 kPa, which is close to the peak longitudinal stress at the same location. At 929 mm the transverse stresses were negligible. In 701C3 at 500 mm the stress was around 30 kPa. At both locations the transverse stresses were nearly constant at all load repetitions.

Base and subgrade deformations were collected periodically. The measurements were made with calibrated coaxial pairs in the vertical direction, and coplanar measurements were made in the horizontal directions. The mean vertical strains presented in this report were approximately 75 mm below the horizontal strains. The vertical strains were compressive. The longitudinal strains started out compressive as the wheel approached the coil gages. The strains turned expansive as the wheel was over the gages. As the wheel left the gages, the strains dropped, sometimes becoming slightly compressive prior to becoming zero. The value of the first compressive strain can be of the same magnitude as the expansive component. This is especially true in the base and in top 300 mm of subgrade. The transverse strains were expansive.

The dynamic strains at failure (i.e. at the 12.5-mm rut depth) were estimated from the test results (Fig. 113).

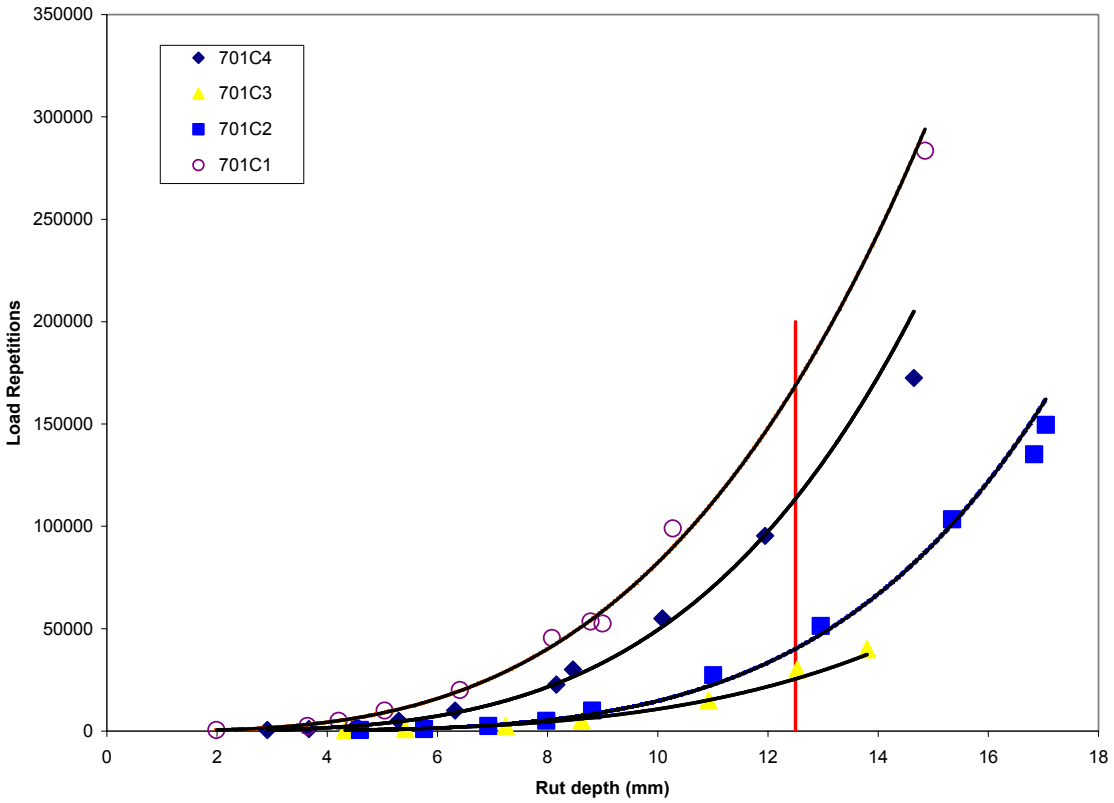

Figure 113. Number of passes and rut depth.

The corresponding number of passes at failure was then converted to an equivalent standard axle load (ESAL) of 80 kN using the fourth-power law. The number of passes to failure for the standard 80-kn load level is shown in Table 13.

Table 13. Coefficients for predicting passes to failure and ESALs.

Test window	*Load (kN)*	*A*	*n*	*R^2*	*ELAF*	*Measured passes at 12.5 mm*	*ESAL standard load*
701C1	80.0	49.516	3.2206	0.997	16	168,832	2,701,307
701C2	89.0	0.4677	4.4982	0.996	25	40,187	984,936
701C3	103.5	1.4400	3.8726	0.992	45	25,483	1,142.293
701C4	89.0	9.2725	3.7267	0.997	25	113,515	2,782,092

The vertical, longitudinal, and transverse dynamic strains at failure are shown in Table 14 and Figure 114. Only the vertical and longitudinal strains are shown in Figure 114, as there was a poor correlation between the transverse strains and load repetitions. A power curve was fitted to the data and the equations are presented below.

Table 14. Dynamic failure strains.

Test window	*Measured passes at 12.5 mm*	*ESAL standard load*	*Strains at failure*		
			Vertical	*Longitudinal*	*Transverse*
701C1	168832	2.701,307	0.001193	0.000777	0.000231
701C2	40187	984,936	0.001389	0.000853	0.000186
701C3	25483	1,142.293			
701C4	113515	2,782,092	0.001192	0.000712	0.000346

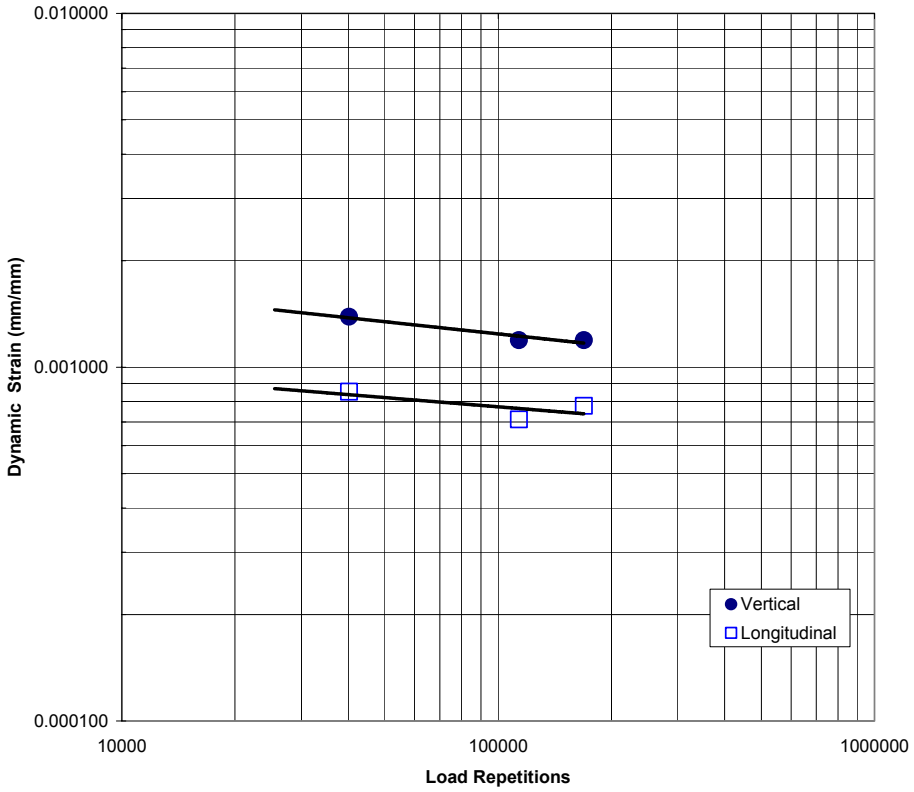

Figure 114. Dynamic failure strain as a function of load repetition.

$$\varepsilon_v = 0.0046N^{-0.1144} \quad R^2 = 0.92$$

$$\varepsilon_l = 0.0021N^{-0.0866} \quad R^2 = 0.51$$

where ε_v = vertical strain

ε_l = longitudinal strain

N = number of load repetitions.

Note that these results were measured at 12 km/hr. To be able to compare with the results from the AASHO Road tests, where the test speed was 48 km/hr, a correction factor was applied to the strain data. The correction factors were developed based on results from MnRoad (Dai and Deusen 1998). Dai and Deusen measured the stresses in the subgrade of several test sections. We used the results from a similar structure (127 mm AC, 305 mm base over subgrade). The stresses were measured at about 150 mm from the surface of the subgrade. His results and data available from this study were used to determine the effect of speed on the stress in the subgrade (Fig. 115). We have assumed that the same reduction

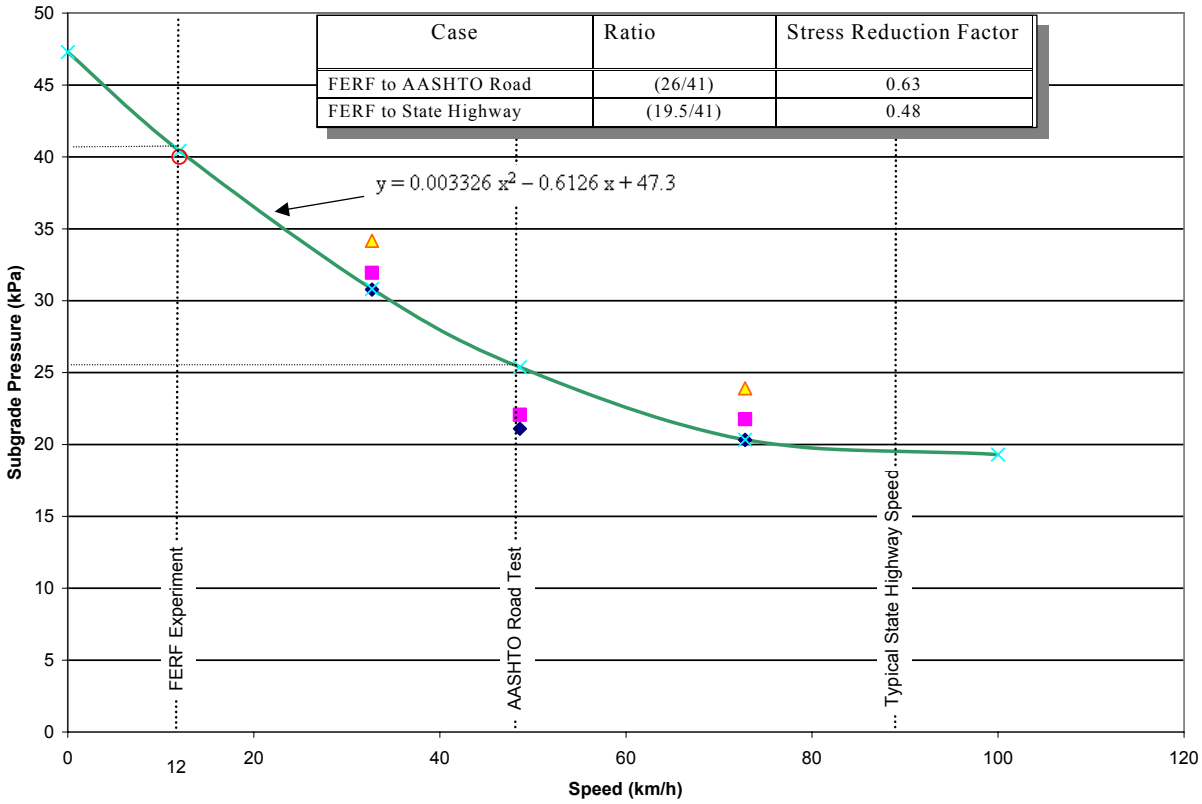

Figure 115. Effect of load repetition on the dynamic vertical strain.

factors can apply to the vertical strains. This is an area we plan to collect additional data on in the future to validate our assumption. For the longitudinal and transverse strains, additional research is needed.

From Figure 115, we estimated the reduction factors for 48 and 100 km/hr (highway speeds). The reduction factors were 37 and 52%, respectively. The comparisons are shown in Figure 116. The following equations were derived for the vertical strain as a function of load repetition:

48 km/hr $\varepsilon_v = 0.0069N^{-0.1492}$

100 km/hr $\varepsilon_v = 0.0052N^{-0.1492}$.

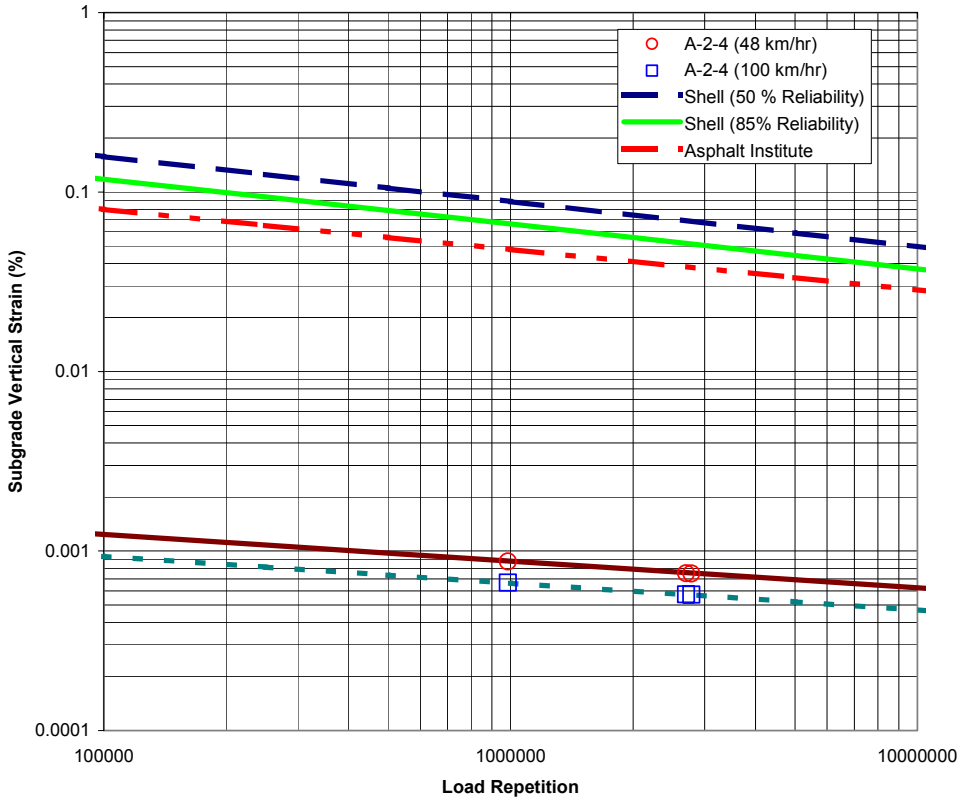

Figure 116. Comparison of test results to AASHO Road Test.

The results show that the limiting strains are about two orders of magnitude lower then that currently used in mechanistic design, suggesting that pavements constructed on this type of subgrade soils may be under designed (if the current failure criterion is used).

The permanent vertical strains at failure from the various test windows are presented in Table 15. The longitudinal and transverse permanent strains were small compared to the vertical. There was a poor correlation between the permanent strains and load repetitions.

Based on the permanent deformations measured in the base and subgrade, the proportion of the subgrade deformation to the total deformation ranged between 54 and 58%.

Table 15. Permanent failure strains.

Test window	*Measured passes at 12.5 mm*	*ESAL standard load*	*Vertical strain*
701C1	168,832	2,701,307	0.014193
701C2	40,187	984,936	0.016873
701C3	25,483	1,142.293	
701C4	113,515	2,782,092	0.012368

CONCLUSIONS

- From the results from this test section, the current subgrade failure criterion for an A-2-4 subgrade soil is inadequate. The current criterion overestimates the limiting subgrade strain at a given load level by an approximate factor of two.
- Approximately 54–58% of the total deformation was in the subgrade.
- The vertical permanent strains were significant compared to the longitudinal and transverse strains. In the vertical direction the majority of the deformation occurred in the base and the top 300 mm of subgrade. However, there was a poor correlation between the vertical strain and load repetition.

REFERENCES

Dai, S., and D.V. Deusen (1998) Field study of in situ subgrade soil response under flexible pavements. Transportation Research Board, Transportation Research Record 1639, p. 23-35.

Dawson, A. (1994) The εmu system user manual. Second Edition, University of Nottingham, United Kingdom.

Dormon, G.M., and C.T. Metcalf (1965) Design curves for flexible pavements based on layered elastic theory. Highway Research Record, No. 71.

Janoo, V., L. Irwin, and R. Eaton (1999) Pavement subgrade performance study: Project overview and design. Draft Report, Cold Regions Research and Engineering Laboratory, New Hampshire, USA.

Irwin, L.H., and Hildebrand (1994) Analysis and prediction of pavement response in the FERF. Internal Report.

Webster, S.L., R.H. Grau, and T.P. Williams (1992) Description and application of dual mass dynamic cone penetrometer. Instruction Report GL- 92-3, U.S. Army Waterways Experiment Station, Vicksburg, MS.

Zhang, W., P. Ullidtz, and R. Macdonald (1998) Pavement subgrade performance study, Part II: Modeling pavement response and predicting pavement performance. Report 87, Danish Road Institute.

APPENDIX A: CONSTRUCTION DATA

Table A-1. As constructed densities of the various layers.

	Density (kg/m^3)										
Station	*1*	*2*	*3*	*4*	*5*	*6*	*T1*	*T2*	*T3*	*T4*	*BASE*
1	1751	1820	1922	1874	1877	1829	1839	1949	1938	1842	1810
2	1914	1796	1829	1897	1906	1941	1917	1927	1945	1961	2063
3	1770	1810	1890	1903	1932	1836	1882	1860	1898	1858	2233
4	1847	1728	1869	1949	1828	1927	1874	1868	1802	1882	1972
5	1921	1877	1914	1965	1869	1914	1967	1903	1924	1981	2079
6	1874	1853	1938	1954	1932	1892	1882	1874	1961	1967	2076
7	1898	1816	1975	1916	1900	1930	1929	1945	1930	1972	2031
8	1826	1783	1881	1860	1869	1841	1965	1941	1930	1948	1889
9	1810	1857	1913	1906	1873	1868	1967	1998	1921	2010	1808
10	1833	1882	1849	1893	1889	1865	1941	1975	1961	2025	1818
11	1865	1816	1850	1893	1905	1818	1895	1906	1901	1733	1999
12	1842	1823	1866	1849	1845	1853	1895	1953	1938	1893	2183
13	1791	1736	1884	1901	1865	1852	1946	1961	1943	1895	2207
14	1837	1792	1977	1905	1877	1853	1946	1970	1954	1930	2235
15	1876	1882	1948	1929	1909	1893	1901	1954	1945	1945	2167
16	1909	1913	1999	1938	1922	1892	1908	1991	1985	1986	2031
17	1889	1808	1935	1876	1948	1930	1933	1946	1946	1964	2025
18	1857	1908	1927	1833	1909	1914	1972	1921	1999	1945	2121
19	1925	1861	1993	1895	1908	2142	1930	1922	1951	1983	2095
20	1938	1857		1873	1916	1921	1996	1986	1994	1959	2113
21	1897	1796	1871	1855	1818	1820	1850	1906	1929	1849	1970
22	1853	1889	1916	1845	1937	1839	1929	1839	1946	1858	2095
23	1807	1776	1834	1836	1889	1714	1917	1940	1938	1882	2135
24	1938	1844	1887	1849	1929	1905	1977	1897	1916	1890	2154
25	1890	1855	1845	1861	1866	1802	1924	1898	1885	1945	2044
26	1860	1874	1905	1895	1909	1882	1917	1892	1983	1961	2145
27	1852	1876	1898	1924	1893	1906	1946	2001	1961	1977	2249
28	1868	1937	1938	1949	1839	1869	1941	1941	1962	1954	2140
29	1871	1816	1930	1973	1879	1866	1970	1967	1959	1962	2097
30	1874	1887	1961	1973	1897	1877	1946	2025	1951	1956	2044

Table A-2. Moisture content in subgrade and base.

	Moisture Content (%)										
Station	*1*	*2*	*3*	*4*	*5*	*6*	*T1*	*T2*	*T3*	*T4*	*BASE*
1	9.0	9.0	8.4	7.9	8.4	8.5	6.8	8.7	10.4	11.3	2.4
2	8.3	8.3	8.1	7.7	9.1	8.6	5.6	9.8	11.6	11.1	2.7
3	8.7	7.7	8.0.	8.0	9.3	9.0	6.1	10.1	10.5	11.9	2.5
4	8.6	8.4	7.9	8.1	9.0	9.5	8.1	9.4	10.4	10.5	3.1
5	8.3	8.1	7.4	8.5	9.2	9.2	6.6	8.9	11	10.9	3.1
6	8.8	8.0	8.3	7.9	9.2	9.2	6.9	8.8	10.5	11.0	2.5
7	8.6	8.1	7.4	8.0	9.1	9.0	7.5	8.1	11.2	11.5	3.2
8	8.8	8.8	8.2	8.5	9.2	9.5	6.9	9.4	10.5	11.7	3.4
9	8.5	8.4	7.7	7.9	9.3	9.2	6.8	8.7	10.6	10.3	2.2
10	9.2	8.3	7.7	8.0	9.3	9.2	7.7	9.3	10.8	10.3	2.6
11	8.2	8.7	9.0	8.0	8.5	9.1	6.3	8.9	11.3	10.9	2.5
12	9.1	8.6	7.7	8.0	9.2	9.1	7.5	9.0	11.4	11.0	2.1
13	8.7	8.6	8.2	8.2	9.4	9.4	7.3	8.8	10.8	9.8	2.8
14	9.3	8.7	8.2	8.7	8.8	9.5	6.9	10.6	10.8	11.0	2.8
15	8.6	8.2	8.4	7.7	9.0	9.0	8.0	8.9	11.1	10.9	2.9
16	8.8	8.6	8.1	7.9	9.2	9.3	8.4	9.2	10.4	10.9	3.2
17	8.9	8.6	7.6	8.0	9.2	9.4	7.5	9.4	11.1	11.3	3
18	8.8	8.2	8.1	8.1	8.6	9.4	7.4	8.6	9.9	11.6	2.7
19	8.7	7.9	8.4	8.0	9.5	7.6	8.3	9.3	11.0	10.7	3
20	9.1	8.5		8.0	9.6	9.6	7.8	9.0	10.1	11.2	3
21	8.7	8.1	8.2	7.6	8.7	9.7	7.1	9.2	11.3	11.1	2.3
22	10.3	8.2	7.5	8.0	8.6	8.5	7.7	9.4	11.3	10.5	3.4
23	9.7	7.7	7.6	7.9	8.4	9.7	8.2	8.3	10.6	10.3	3.5
24	10.2	7.8	7.8	8.0	8.6	9.2	6.8	9.1	11.8	10.0	3.6
25	10.7	8.1	7.8	8.3	8.9	9.5	8.4	9.3	11.7	11.5	4.6
26	9.6	8.0	7.7	8.0	8.8	9.1	7.3	7.7	10.8	11.3	3.8
27	10.0	8.3	8.7	8.2	8.2	9.1	7.3	9.3	10.4	11.1	4.8
28	10.9	8.1	7.6	7.7	9.4	9.3	8.3	9.3	10.6	10.7	3.9
29	11.1	8.5	8.1	7.3	9.0	9.2	7.8	9.1	10.8	10.5	2.9
30	10.9	8.7	7.9	7.6	9.8	9.4	8.7	7.8	10.1	10.0	2.9

Table A-3. Layer CBR values from Clegg hammertests.

Stations	Lift 1	Lift 2	Lift 3	Lift 4	Lift 5	Lift 6	T1	T2	T3	T4
1							8	10	6	3
2							8	10	8	6
3							8	14	14	8
4							18	16	12	4
5							18	12	14	12
6							16	14	10	7
7							18	12	12	12
8							23	14	12	10
9							23	16	14	12
10							20	16	12	10
11							23	20	16	10
12							23	18	18	7
13	4	6	10	6	14	8	7	10	16	4
14	4	8	14	7	8	4	7	14	12	10
15	14	8	20	6	7	8	8	18	14	10
16	10	12	16	10	16	6	23	25	7	10
17	16	10	18	10	8	8	23	25	20	12
18	12	7	16	8	12	10	25	28	14	12
19	14	14	16	12	25	8	40	23	10	12
20	12	14	12	12	20	12	37	20	20	10
21	12	12	14	16	23	12	31	16	14	12
22	10	12	12	16	12	16	34	16	12	10
23	10	12	12	16	18	18	40	23	16	12
24	14	12	18	12	23	20	25	18	20	12
25	6	6	10	7	6	10	10	8	6	
26	14	10	18	12	14	4	7	8	10	
27	12	12	16	10	10	8	14	18	7	
28	12	14	20	16	12	4	20	20	8	
29	7	8	20	12	6	4	16	25	14	
30	8	7	16	7	14	4	23	23	12	
31	8	14	16	12	8	12	18	20	18	
32	12	8	10	14	10	8	25	18	23	
33	12	14	8	14	10	8	28	23	10	
34	10	16	16	18	12	14	25	23	18	14
35	8	14	10	14	12	7	28	23	18	16
36	14	14	10	25	10	4	25	23	10	14
37							8	10	6	7
38							8	18	6	10
39							12	12	18	8
40							16	10	10	12
41							14	10	10	10
42							12	8	14	10
43							23	10	16	12
44							20	16	16	14
45							20	18	16	16
46							18	20	16	14
47							25	20	14	10
48							20	20	16	10

Table A-4. CBR results from DCP measurements.

Station depth (mm)	*1*	*2*	*3*	*4*	*5*	*6*	*7*	*8*	*9*	*10*	*11*	*12*	*13*	*14*	*15*	*16*	*17*	*18*	*19*	*20*	*21*	*22*	*23*	*24*
0	6	3	8	5	5	4	6	6	5	8	12	8	5	5	6	6	4	4	6	6	5	6	5	5
40	5	5	7	6	6	10	12	10	10	12	14	12	6	6	6	10	6	5	8	10	8	8	8	5
80	5	6	6	10	9	10	12	10	10	12	17	17	5	4	8	10	6	8	10	14	6	9	8	6
140	3	10	6	6	10	9	12	12	14	10	17	16	4	3	8	8	6	5	10	10	6	6	10	8
210	3	2	7	8	19	7	10	17	14	10	17	22	2	3	6	10	5	5	6	8	8	6	5	6
250	5	8	8	8	10	8	9	19	13	14	14	16	4	12	8	12	5	5	6	8	5	6	6	6
280	6	10	9	10	19	14	9	13	12	8	17	13	5	17	10	17	6	6	8	6	5	5	5	5
310	14	10	5	10	19	26	12	12	22	10	12	19	17	14	10	22	14	14	5	14	8	12	6	14
340	14	10	4	6	19	17	22	14	31	14	14	17	6	10	14	17	14	17	5	14	22	14	14	14
385	9	8	4	5	14	19	22	17	31	12	17	11	4	10	14	14	14	17	12	14	16	19	22	14
420	5	8	12	5	10	27	26	17	22	9	26	6	3	6	14	10	14	22	14	27	22	22	27	10
455	5	6	16	5	8	19	20	19	16	8	19	6	4	10	12	9	17	13	12	5	22	14	7	22
485	6	14	13	8	12	31	19	14	13	5	16	14	22	14	9	6	17	10	9	6	16	12	10	22
510	8	17	9	7	12	16	5	14	26	5	10	14	17	14	8	6	8	14	6	8	14	12	14	22
540	6	37	5	10	14	22	9	22	37	7	9	17	19	14	12	14	10	14	10	10	14	14	14	31
580	10	26	4	9	14	19	12	26	22	14	16	14	10	17	6	16	14	16	16	9	19	17	12	6
610	6	12	7	8	22	19	10	26	31	22	19	12	10	12	14	22	22	14	22	10	27	27	12	14
640	14	10	6	7	4	22	14	26	48	22	16	14	5	14	22	22	22	10	16	8	31	37	10	14
680	10	7	5	10	6	16	10	22	7	19	12	17	8	12	14	16	22	14	22	5	22	16	14	14
668	4	5	5	10	8	16	8	22	13	22	9	5	5	8	12	22	13	8	14	6	27	14	22	22
702	6	7	5	8	10	6	7	7	10	31	8	6	6	12	12	16	9	5	10	12	14	8	23	14
742	5	8	5	10	14	8	9	11	13	16	6	10	4	22	6	5	5	8	6	19	16	6	18	10
784	4	6	4	10	10	12	17	12	11	12	9	7	3	10	6	12	8	6	6	27	8	8	12	14
820	5	4	6	16	9	22	27	9	9	12	8	8	4	8	10	10	12	8	12		14	13	27	9
882	3	3	25	16	9	12	37	8	4	14	6	14	10	8	8	10	8	6	10		12	14	37	12
915	6	4	5	13	14	17	4	8	22	31	5	12	6	6	8	10	9	6	12		14	20	35	14
954	10	5	8	26	26	20	7	6	5	28	6	19	17	6	8	6	5	9	8		14		22	14
984	14	8	8	27	22	13	6	5	8	10	5	27	16	5	5	6	5	5	8		9			14
1011	16	33	8	23	17	12	6	5	14	13	6	22	10	6	8	6	4	4	6		11			16
1042	14	5	7	24	14	10	7	6	22	13	13	39	6	17	5	17	8	10	6		19			16
1090	8	8	5	17	17	10	11	14	19	13	15	4	5	31	5	22	14	27	10		17			22
1126	5	7	4	16	19	17	13	22	19	12	20	11	5	22	17	27	17	27	12		14			14
1174	4	7	6	14	14	26	16	22	19	9	16	22	8	22	19	19	17	48	17		17			10
1228	3	6	14	11	14	31	6	31	14	8	17	27	8	17	19	14	14	26	22		17			6
1263	5	6	19	9	27	22	20	22	14	6	10	16	8	12	22	7	14	37	22		17			5
1305	10	5	24	10	22	16	32	26	14	10	7	17	14	6	19	10	14	48	16		17			5
1347	10	8	19	17	31	14	34	14	22	17	7	25	10	10	14	10	12	27	22		14			5
1407	6	11	17	18	14	10	34	27	35	23	5	11	5	10	14	6	17	4	16		17			8
1305	5	13	14	19	14	11	25	27	22	36	6	22	6	14	6	9	14	7	13		27			10
1334	7	9	17	16	5	14	26	37	6	31	17	22	4	10	17	8	12	9	8					14
1367	6	8	19	5	7	11	26	26	9	27	19	22	3	5	17	8	8	9	12					14
1406	5	8	17	8	7	5	27	6	14	28	14	27	3	8	17	7	6	9	14					14
1451	4	8	13	10	7	9		11	12	24	6	27	5	6	17	6	8	6	17					14

Table A-4 (cont.). CBR results from DCP measurements.

Station depth (mm)	1	2	3	4	5	6	7	8	9	10	11	12	13	14	15	16	17	18	19	20	21	22	23	24
1490	5	12		10	10	9		11	12		9	22	10	7	14	6	5	8	5					14
1515	8	12		7	11	8		17	11		12	22	9	6	7	7	9	12	8					17
1539	8			4	12	15		18	11		14	27	8	4	10	5	8	14	10					14
1575	11			5	12	13		10	9		13	27	5	4	10	5	6	27	11					19
1607	13			9	11	11		14	8		11		6	6	8	4	5	27	11					22
1660	7			15	15	12		12	8		13			17	6	6	5	22	14					27
1695	5			14	22	15		12	14		16			27	6	15	4	22	10					31
1729	6			12	31	14		12	25		14			16	3	20	6	22	10					
1761	6			8		26		14	24		17			14	6	27	17		14					
1787	8			8		36		27	24		22			12	9	22	24		17					

Table A-5. Thickness of subgrade, base, and asphalt concrete layer.

Station	Lift 1	Lift 2	Lift 3	Lift 4	Lift 5	Lift 6	Top 1	Top 2	Top 3	Top 4	Base	Asphalt
1	375	271	326	314	283	372	229	302	296	290	277	85
2	402	271	296	323	253	399	238	268	302	259	280	79
3	393	274	296	351	253	375	247	268	320	229	302	73
4	390	287	299	338	241	375	226	283	344	216	287	73
5	366	314	274	347	229	378	250	317	308	244	287	70
6	366	314	268	366	232	372	253	363	256	274	287	64
7	357	354	238	384	241	378	241	360	235	290	280	67
8	384	366	247	354	244	384	235	354	235	277	283	67
9	393	354	271	341	229	375	253	351	253	262	290	64
10	430	311	290	317	241	360	262	344	274	253	302	64
11	430	299	311	274	271	351	262	326	308	241	287	79
12	351	311	320	277	223	366	283	320	308	241	283	82
13	424	216	332	299	268	390	226	283	335	271	274	85
14	387	274	277	360	250	360	277	256	323	262	256	91
15	396	280	280	354	265	329	280	259	335	232	290	79
16	393	299	299	326	262	320	287	277	338	229	280	76
17	378	302	287	338	259	332	274	305	311	244	283	73
18	381	323	256	357	247	354	259	341	250	283	274	76
19	369	351	235	378	238	369	250	357	232	283	280	79
20	366	369	250	363	235	360	244	357	250	256	287	79
21	378	344	283	341	238	344	250	347	268	250	280	79

23	23	23	23	23	23	23	23	23	23	23	23	23
381	381	381	381	381	381	381	381	381	381	381	381	381
290	290	290	290	290	290	290	290	290	290	290	290	290
332	332	332	332	332	332	332	332	332	332	332	332	332
305	305	305	305	305	305	305	305	305	305	305	305	305
223	223	223	223	223	223	223	223	223	223	223	223	223
351	351	351	351	351	351	351	351	351	351	351	351	351
247	247	247	247	247	247	247	247	247	247	247	247	247
320	320	320	320	320	320	320	320	320	320	320	320	320
290	290	290	290	290	290	290	290	290	290	290	290	290
280	280	280	280	280	280	280	280	280	280	280	280	280
256	256	256	256	256	256	256	256	256	256	256	256	256
98	98	98	98	98	98	98	98	98	98	98	98	98
24	24	24	24	24	24	24	24	24	24	24	24	24
357	357	357	357	357	357	357	357	357	357	357	357	357
271	271	271	271	271	271	271	271	271	271	271	271	271
360	360	360	360	360	360	360	360	360	360	360	360	360
268	268	268	268	268	268	268	268	268	268	268	268	268
268	268	268	268	268	268	268	268	268	268	268	268	268
299	299	299	299	299	299	299	299	299	299	299	299	299
314	314	314	314	314	314	314	314	314	314	314	314	314
265	265	265	265	265	265	265	265	265	265	265	265	265
259	259	259	259	259	259	259	259	259	259	259	259	259
91	91	91	91	91	91	91	91	91	91	91	91	91
25	25	25	25	25	25	25	25	25	25	25	25	25
329	329	329	329	329	329	329	329	329	329	329	329	329
293	293	293	293	293	293	293	293	293	293	293	293	293
317	317	317	317	317	317	317	317	317	317	317	317	317
290	290	290	290	290	290	290	290	290	290	290	290	290
293	293	293	293	293	293	293	293	293	293	293	293	293
314	314	314	314	314	314	314	314	314	314	314	314	314
311	311	311	311	311	311	311	311	311	311	311	311	311
293	293	293	293	293	293	293	293	293	293	293	293	293
344	344	344	344	344	344	344	344	344	344	344	344	344
274	274	274	274	274	274	274	274	274	274	274	274	274
274	274	274	274	274	274	274	274	274	274	274	274	274
73	73	73	73	73	73	73	73	73	73	73	73	73
26	26	26	26	26	26	26	26	26	26	26	26	26
360	360	360	360	360	360	360	360	360	360	360	360	360
308	308	308	308	308	308	308	308	308	308	308	308	308
271	271	271	271	271	271	271	271	271	271	271	271	271
344	344	344	344	344	344	344	344	344	344	344	344	344
265	265	265	265	265	265	265	265	265	265	265	265	265
299	299	299	299	299	299	299	299	299	299	299	299	299
338	338	338	338	338	338	338	338	338	338	338	338	338
302	302	302	302	302	302	302	302	302	302	302	302	302
335	335	335	335	335	335	335	335	335	335	335	335	335
238	238	238	238	238	238	238	238	238	238	238	238	238
259	259	259	259	259	259	259	259	259	259	259	259	259
91	91	91	91	91	91	91	91	91	91	91	91	91

23	23	23	23	23	23	23	23	23	23	23	23	23
381	381	381	381	381	381	381	381	381	381	381	381	381
290	290	290	290	290	290	290	290	290	290	290	290	290
332	332	332	332	332	332	332	332	332	332	332	332	332
305	305	305	305	305	305	305	305	305	305	305	305	305
223	223	223	223	223	223	223	223	223	223	223	223	223
351	351	351	351	351	351	351	351	351	351	351	351	351
247	247	247	247	247	247	247	247	247	247	247	247	247
320	320	320	320	320	320	320	320	320	320	320	320	320
290	290	290	290	290	290	290	290	290	290	290	290	290
280	280	280	280	280	280	280	280	280	280	280	280	280
256	256	256	256	256	256	256	256	256	256	256	256	256
98	98	98	98	98	98	98	98	98	98	98	98	98
24	24	24	24	24	24	24	24	24	24	24	24	24
357	357	357	357	357	357	357	357	357	357	357	357	357
271	271	271	271	271	271	271	271	271	271	271	271	271
360	360	360	360	360	360	360	360	360	360	360	360	360
268	268	268	268	268	268	268	268	268	268	268	268	268
268	268	268	268	268	268	268	268	268	268	268	268	268
299	299	299	299	299	299	299	299	299	299	299	299	299
314	314	314	314	314	314	314	314	314	314	314	314	314
265	265	265	265	265	265	265	265	265	265	265	265	265
259	259	259	259	259	259	259	259	259	259	259	259	259
91	91	91	91	91	91	91	91	91	91	91	91	91
25	25	25	25	25	25	25	25	25	25	25	25	25
329	329	329	329	329	329	329	329	329	329	329	329	329
293	293	293	293	293	293	293	293	293	293	293	293	293
317	317	317	317	317	317	317	317	317	317	317	317	317
290	290	290	290	290	290	290	290	290	290	290	290	290
293	293	293	293	293	293	293	293	293	293	293	293	293
314	314	314	314	314	314	314	314	314	314	314	314	314
311	311	311	311	311	311	311	311	311	311	311	311	311
293	293	293	293	293	293	293	293	293	293	293	293	293
344	344	344	344	344	344	344	344	344	344	344	344	344
274	274	274	274	274	274	274	274	274	274	274	274	274
274	274	274	274	274	274	274	274	274	274	274	274	274
73	73	73	73	73	73	73	73	73	73	73	73	73
26	26	26	26	26	26	26	26	26	26	26	26	26
360	360	360	360	360	360	360	360	360	360	360	360	360
308	308	308	308	308	308	308	308	308	308	308	308	308
271	271	271	271	271	271	271	271	271	271	271	271	271
344	344	344	344	344	344	344	344	344	344	344	344	344
265	265	265	265	265	265	265	265	265	265	265	265	265
299	299	299	299	299	299	299	299	299	299	299	299	299
338	338	338	338	338	338	338	338	338	338	338	338	338
302	302	302	302	302	302	302	302	302	302	302	302	302
335	335	335	335	335	335	335	335	335	335	335	335	335
238	238	238	238	238	238	238	238	238	238	238	238	238
259	259	259	259	259	259	259	259	259	259	259	259	259
91	91	91	91	91	91	91	91	91	91	91	91	91

23	23	23	23	23	23	23	23	23	23	23	23	23
381	381	381	381	381	381	381	381	381	381	381	381	381
290	290	290	290	290	290	290	290	290	290	290	290	290
332	332	332	332	332	332	332	332	332	332	332	332	332
305	305	305	305	305	305	305	305	305	305	305	305	305
223	223	223	223	223	223	223	223	223	223	223	223	223
351	351	351	351	351	351	351	351	351	351	351	351	351
247	247	247	247	247	247	247	247	247	247	247	247	247
320	320	320	320	320	320	320	320	320	320	320	320	320
290	290	290	290	290	290	290	290	290	290	290	290	290
280	280	280	280	280	280	280	280	280	280	280	280	280
256	256	256	256	256	256	256	256	256	256	256	256	256
98	98	98	98	98	98	98	98	98	98	98	98	98
24	24	24	24	24	24	24	24	24	24	24	24	24
357	357	357	357	357	357	357	357	357	357	357	357	357
271	271	271	271	271	271	271	271	271	271	271	271	271
360	360	360	360	360	360	360	360	360	360	360	360	360
268	268	268	268	268	268	268	268	268	268	268	268	268
268	268	268	268	268	268	268	268	268	268	268	268	268
299	299	299	299	299	299	299	299	299	299	299	299	299
314	314	314	314	314	314	314	314	314	314	314	314	314
265	265	265	265	265	265	265	265	265	265	265	265	265
259	259	259	259	259	259	259	259	259	259	259	259	259
91	91	91	91	91	91	91	91	91	91	91	91	91
25	25	25	25	25	25	25	25	25	25	25	25	25
329	329	329	329	329	329	329	329	329	329	329	329	329
293	293	293	293	293	293	293	293	293	293	293	293	293
317	317	317	317	317	317	317	317	317	317	317	317	317
290	290	290	290	290	290	290	290	290	290	290	290	290
293	293	293	293	293	293	293	293	293	293	293	293	293
314	314	314	314	314	314	314	314	314	314	314	314	314
311	311	311	311	311	311	311	311	311	311	311	311	311
293	293	293	293	293	293	293	293	293	293	293	293	293
344	344	344	344	344	344	344	344	344	344	344	344	344
274	274	274	274	274	274	274	274	274	274	274	274	274
274	274	274	274	274	274	274	274	274	274	274	274	274
73	73	73	73	73	73	73	73	73	73	73	73	73
26	26	26	26	26	26	26	26	26	26	26	26	26
360	360	360	360	360	360	360	360	360	360	360	360	360
308	308	308	308	308	308	308	308	308	308	308	308	308
271	271	271	271	271	271	271	271	271	271	271	271	271
344	344	344	344	344	344	344	344	344	344	344	344	344
265	265	265	265	265	265	265	265	265	265	265	265	265
299	299	299	299	299	299	299	299	299	299	299	299	299
338	338	338	338	338	338	338	338	338	338	338	338	338
302	302	302	302	302	302	302	302	302	302	302	302	302
335	335	335	335	335	335	335	335	335	335	335	335	335
238	238	238	238	238	238	238	238	238	238	238	238	238
259	259	259	259	259	259	259	259	259	259	259	259	259
91	91	91	91	91	91	91	91	91	91	91	91	91

23	23	23	23	23	23	23	23	23	23	23	23	23
381	381	381	381	381	381	381	381	381	381	381	381	381
290	290	290	290	290	290	290	290	290	290	290	290	290
332	332	332	332	332	332	332	332	332	332	332	332	332
305	305	305	305	305	305	305	305	305	305	305	305	305
223	223	223	223	223	223	223	223	223	223	223	223	223
351	351	351	351	351	351	351	351	351	351	351	351	351
247	247	247	247	247	247	247	247	247	247	247	247	247
320	320	320	320	320	320	320	320	320	320	320	320	320
290	290	290	290	290	290	290	290	290	290	290	290	290
280	280	280	280	280	280	280	280	280	280	280	280	280
256	256	256	256	256	256	256	256	256	256	256	256	256
98	98	98	98	98	98	98	98	98	98	98	98	98
24	24	24	24	24	24	24	24	24	24	24	24	24
357	357	357	357	357	357	357	357	357	357	357	357	357
271	271	271	271	271	271	271	271	271	271	271	271	271
360	360	360	360	360	360	360	360	360	360	360	360	360
268	268	268	268	268	268	268	268	268	268	268	268	268
268	268	268	268	268	268	268	268	268	268	268	268	268
299	299	299	299	299	299	299	299	299	299	299	299	299
314	314	314	314	314	314	314	314	314	314	314	314	314
265	265	265	265	265	265	265	265	265	265	265	265	265
259	259	259	259	259	259	259	259	259	259	259	259	259
91	91	91	91	91	91	91	91	91	91	91	91	91
25	25	25	25	25	25	25	25	25	25	25	25	25
329	329	329	329	329	329	329	329	329	329	329	329	329
293	293	293	293	293	293	293	293	293	293	293	293	293
317	317	317	317	317	317	317	317	317	317	317	317	317
290	290	290	290	290	290	290	290	290	290	290	290	290
293	293	293	293	293	293	293	293	293	293	293	293	293
314	314	314	314	314	314	314	314	314	314	314	314	314
311	311	311	311	311	311	311	311	311	311	311	311	311
293	293	293	293	293	293	293	293	293	293	293	293	293
344	344	344	344	344	344	344	344	344	344	344	344	344
274	274	274	274	274	274	274	274	274	274	274	274	274
274	274	274	274	274	274	274	274	274	274	274	274	274
73	73	73	73	73	73	73	73	73	73	73	73	73
26	26	26	26	26	26	26	26	26	26	26	26	26
360	360	360	360	360	360	360	360	360	360	360	360	360
308	308	308	308	308	308	308	308	308	308	308	308	308
271	271	271	271	271	271	271	271	271	271	271	271	271
344	344	344	344	344	344	344	344	344	344	344	344	344
265	265	265	265	265	265	265	265	265	265	265	265	265
299	299	299	299	299	299	299	299	299	299	299	299	299
338	338	338	338	338	338	338	338	338	338	338	338	338
302	302	302	302	302	302	302	302	302	302	302	302	302
335	335	335	335	335	335	335	335	335	335	335	335	335
238	238	238	238	238	238	238	238	238	238	238	238	238
259	259	259	259	259	259	259	259	259	259	259	259	259
91	91	91	91	91	91	91	91	91	91	91	91	91

27	335	326	296	326	277	287	323	277	347	238	268	79
28	338	311	323	323	271	274	344	274	344	262	253	73
29	311	317	308	338	271	271	344	287	332	277	247	76
30	335	320	293	344	241	296	335	317	296	293	250	73
31	344	329	262	375	223	308	332	341	280	277	247	82
32	344	335	283	357	219	314	308	375	277	241	271	79
33	351	335	290	335	229	296	308	369	296	232	268	82
34	369	317	290	329	210	314	296	363	299	238	265	85
35	372	271	326	326	189	317	293	335	317	244	262	88
36	360	262	341	344	177	296	296	332	320	250	262	88
37	302	290	317	320	283	320	329	317	317	268	265	85
38	293	360	232	341	274	357	302	311	302	259	250	98
39	280	372	238	344	280	323	299	271	338	262	241	91
40	287	357	265	338	274	314	314	274	338	280	232	88
41	299	323	271	351	262	305	344	283	314	283	247	94
42	323	283	277	363	256	314	338	283	308	293	238	104
43	320	305	253	378	241	335	329	323	305	250	253	104
44	305	320	299	332	250	341	299	360	302	229	253	104
45	332	305	308	311	259	344	265	360	320	219	244	104
46	344	314	311	283	238	360	253	344	317	229	241	110
47	351	308	308	317	210	320	287	338	299	244	244	107
48	357	287	323	341	183	299	280	366	293	244	253	101

APPENDIX B: INSTRUMENTATION DATA

Table B-1. Location of coil gages in test section 701.

ID	*X (m)*	*Y (m)*	*Z (mm)*	*Window*	*Layer*
EMU383	3.05	4.42	152.40	C1	1
EMU382	3.20	4.57	152.40	C1	1
EMU381	3.05	4.57	152.40	C1	1
EMU363	3.05	4.42	304.80	C1	2
EMU362	3.20	4.57	304.80	C1	2
EMU361	3.05	4.57	304.80	C1	2
EMU343	3.05	4.42	457.20	C1	3
EMU342	3.20	4.57	457.20	C1	3
EMU341	3.05	4.57	457.20	C1	3
EMU323	3.05	4.42	609.60	C1	4
EMU322	3.20	4.57	609.60	C1	4
EMU321	3.05	4.57	609.60	C1	4
EMU303	3.05	4.42	762.00	C1	5
EMU302	3.20	4.57	762.00	C1	5
EMU301	3.05	4.57	762.00	C1	5
EMU283	3.05	4.42	917.58	C1	6
EMU282	3.20	4.57	917.58	C1	6
EMU281	3.05	4.57	917.58	C1	6
EMU263	3.05	4.42	1066.80	C1	7
EMU262	3.20	4.57	1066.80	C1	7
EMU261	3.05	4.57	1066.80	C1	7
EMU243	3.05	4.42	1219.20	C1	8
EMU242	3.20	4.57	1219.20	C1	8
EMU241	3.05	4.57	1219.20	C1	8
EMU386	3.05	3.20	152.40	C2	1
EMU385	3.20	3.35	152.40	C2	1
EMU384	3.05	3.35	152.40	C2	1
EMU366	3.05	3.20	304.80	C2	2
EMU365	3.20	3.35	304.80	C2	2
EMU364	3.05	3.35	304.80	C2	2
EMU346	3.05	3.20	457.20	C2	3
EMU345	3.20	3.35	457.20	C2	3
EMU344	3.05	3.35	457.20	C2	3
EMU326	3.05	3.20	609.60	C2	4
EMU325	3.20	3.35	609.60	C2	4
EMU324	3.05	3.35	609.60	C2	4
EMU306	3.05	3.20	762.00	C2	5
EMU305	3.20	3.35	762.00	C2	5
EMU304	3.05	3.35	762.00	C2	5
EMU286	3.05	3.20	917.58	C2	6
EMU285	3.20	3.35	917.58	C2	6
EMU284	3.05	3.35	917.58	C2	6
EMU266	3.05	3.20	1066.80	C2	7
EMU265	3.20	3.35	1066.80	C2	7
EMU264	3.05	3.35	1066.80	C2	7

EMU246	3.05	3.20	1219.20	C2	8
EMU245	3.20	3.35	1219.20	C2	8
EMU244	3.05	3.35	1219.20	C2	8
EMU389	3.05	1.98	152.40	C3	1
EMU388	3.20	2.13	152.40	C3	1
EMU387	3.05	2.13	152.40	C3	1
EMU369	3.05	1.98	304.80	C3	2
EMU368	3.20	2.13	304.80	C3	2
EMU367	3.05	2.13	304.80	C3	2
EMU349	3.05	1.98	457.20	C3	3
EMU348	3.20	2.13	457.20	C3	3
EMU347	3.05	2.13	457.20	C3	3
EMU329	3.05	1.98	609.60	C3	4
EMU328	3.20	2.13	609.60	C3	4
EMU327	3.05	2.13	609.60	C3	4
EMU309	3.05	1.98	762.00	C3	5
EMU308	3.20	2.13	762.00	C3	5
EMU307	3.05	2.13	762.00	C3	5
EMU289	3.05	1.98	914.40	C3	6
EMU288	3.20	2.13	914.40	C3	6
EMU287	3.05	2.13	914.40	C3	6
EMU269	3.05	1.98	1066.80	C3	7
EMU268	3.20	2.13	1066.80	C3	7
EMU267	3.05	2.13	1066.80	C3	7
EMU249	3.05	1.98	1219.20	C3	8
EMU248	3.20	2.13	1219.20	C3	8
EMU247	3.05	2.13	1219.20	C3	8
EMU392	18.14	4.42	152.40	C4	1
EMU391	18.29	4.57	152.40	C4	1
EMU390	18.14	4.57	152.40	C4	1
EMU372	18.14	4.42	304.80	C4	2
EMU371	18.29	4.57	304.80	C4	2
EMU370	18.14	4.57	304.80	C4	2
EMU352	18.14	4.42	457.20	C4	3
EMU351	18.29	4.57	457.20	C4	3
EMU350	18.14	4.57	457.20	C4	3
EMU332	18.14	4.42	609.60	C4	4
EMU331	18.29	4.57	609.60	C4	4
EMU330	18.14	4.57	609.60	C4	4
EMU312	18.14	4.42	762.00	C4	5
EMU311	18.29	4.57	762.00	C4	5
EMU310	18.14	4.57	762.00	C4	5
EMU292	18.14	4.42	914.40	C4	6
EMU291	18.29	4.57	914.40	C4	6
EMU290	18.14	4.57	914.40	C4	6
EMU272	18.14	4.42	1066.80	C4	7
EMU271	18.29	4.57	1066.80	C4	7
EMU270	18.14	4.57	1066.80	C4	7
EMU252	18.14	4.42	1219.20	C4	8
EMU251	18.29	4.57	1219.20	C4	8
EMU250	18.14	4.57	1219.20	C4	8

EMU395	18.14	3.20	152.40	C5	1
EMU394	18.29	3.35	152.40	C5	1
EMU393	18.14	3.35	152.40	C5	1
EMU375	18.14	3.20	304.80	C5	2
EMU374	18.29	3.35	304.80	C5	2
EMU373	18.14	3.35	304.80	C5	2
EMU355	18.14	3.20	457.20	C5	3
EMU354	18.29	3.35	457.20	C5	3
EMU353	18.14	3.35	457.20	C5	3
EMU335	18.14	3.20	609.60	C5	4
EMU334	18.29	3.35	609.60	C5	4
EMU333	18.14	3.35	609.60	C5	4
EMU315	18.14	3.20	762.00	C5	5
EMU314	18.29	3.35	762.00	C5	5
EMU313	18.14	3.35	762.00	C5	5
EMU295	18.14	3.20	914.40	C5	6
EMU294	18.29	3.35	914.40	C5	6
EMU293	18.14	3.35	914.40	C5	6
EMU275	18.14	3.20	1066.80	C5	7
EMU274	18.29	3.35	1066.80	C5	7
EMU273	18.14	3.35	1066.80	C5	7
EMU255	18.14	3.20	1219.20	C5	8
EMU254	18.29	3.35	1219.20	C5	8
EMU253	18.14	3.35	1219.20	C5	8
EMU398	18.14	1.98	152.40	C6	1
EMU397	18.29	2.13	152.40	C6	1
EMU396	18.14	2.13	152.40	C6	1
EMU378	18.14	1.98	304.80	C6	2
EMU377	18.29	2.13	304.80	C6	2
EMU376	18.14	2.13	304.80	C6	2
EMU358	18.14	1.98	457.20	C6	3
EMU357	18.29	2.13	457.20	C6	3
EMU356	18.14	2.13	457.20	C6	3
EMU338	18.14	1.98	609.60	C6	4
EMU337	18.29	2.13	609.60	C6	4
EMU336	18.14	2.13	609.60	C6	4
EMU318	18.14	1.98	762.00	C6	5
EMU317	18.29	2.13	762.00	C6	5
EMU316	18.14	2.13	762.00	C6	5
EMU298	18.14	1.98	914.40	C6	6
EMU297	18.29	2.13	914.40	C6	6
EMU296	18.14	2.13	914.40	C6	6
EMU278	18.14	1.98	1066.80	C6	7
EMU277	18.29	2.13	1066.80	C6	7
EMU276	18.14	2.13	1066.80	C6	7
EMU258	18.14	1.98	1219.20	C6	8
EMU257	18.29	2.13	1219.20	C6	8
EMU256	18.14	2.13	1219.20	C6	8

Table B-2. Calibration coefficients for coil gages.

	Vertical (Z)				Longitudinal (X)				Transverse (Y)			
	Coil ID				Coil ID				Coil ID			
701C1	Transmit	Receive	a	n	Transmit	Receive	a	n	Transmit	Receive	a	n
LAYER 1	381	361	7.965	-0.3853	381	382	6.626	-0.2893	381	383	6.8506	-0.2920
LAYER 2	361	341	7.7502	-0.3853	361	362	6.6653	-0.2910	361	363	6.8787	-0.2920
LAYER 3	341	321	8.6476	-0.3853	341	342	7.0641	-0.2947	341	342	7.2594	-0.2877
LAYER 4	321	301	7.995	-0.3806	321	322	6.6506	-0.2894	321	323	6.0566	-0.2876
LAYER 5	301	281	7.987	-0.3849	301	302	6.6625	-0.2893	301	303	6.4043	-0.2903
LAYER 6	281	261	7.9692	-0.3829	281	282	6.6494	-0.2895	281	283	6.8463	-0.2894
LAYER 7	261	241	7.9765	-0.3863	261	262	6.6744	-0.2907	261	263	6.8978	-0.2920
LAYER 8	241				241	242			241	243		
701C2			a	n			a	n			a	n
LAYER 1	384	364	7.9255	-0.3791	384	385	6.6485	-0.2919	384	386	6.8504	-0.2906
LAYER 2	364	344	7.8097	-0.3839	364	365	6.6419	-0.2905	364	366	6.8583	-0.2898
LAYER 3	344	324	7.6855	-0.2702	344	345	6.9362	-0.2906	344	346	7.1466	-0.2907
LAYER 4	324	304	7.9527	-0.3382	324	325	6.6405	-0.2901	324	326	6.8482	-0.2997
LAYER 5	304	284	8.0251	-0.3895	304	305	6.3314	-0.3071	304	306	6.4825	-0.2898
LAYER 6	284	264	7.9687	-0.3803	284	285	6.6553	-0.2907	284	286	6.862	-0.2917
LAYER 7	264	244	8.0349	-0.3872	264	265	6.6493	-0.2907	264	266	6.8631	-0.2924
LAYER 8	244				244	245			244	246		
701C3			a	n			a	n			a	n
LAYER 1	387	367	7.9255	-0.3791	387	388	6.6446	-0.2904	387	389	6.8728	-0.2906
LAYER 2	367	347	7.5133	-0.3840	367	368	6.654	-0.2890	367	369	6.8611	-0.2925
LAYER 3	347	327	9.047	-0.3848	347	348	7.3096	-0.2910	347	349	7.345	-0.2981
LAYER 4	327	307	8.0056	-0.3834	327	328	6.6538	-0.2906	327	329	6.8699	-0.2942
LAYER 5	307	287	8.012	-0.3840	307	308	6.4302	-0.2923	307	309	6.8589	-0.2898
LAYER 6	287	267	7.9277	-0.3805	287	288	6.654	-0.2889	287	289	6.8641	-0.2895
LAYER 7	267	247	7.9928	-0.3840	267	268	6.654	-0.2889	267	269	6.6841	-0.2895
LAYER 8	247				247	248			247	249		
701C4			a	n			a	n			a	n
LAYER 1	390	370	7.9974	-0.3847	390	391	6.6201	-0.2887	390	392	6.8303	-0.2887
LAYER 2	370	350	7.7374	-0.3864	370	371	6.7146	-0.3003	370	372	6.8968	-0.2946
LAYER 3	350	330	8.6408	-0.3838	350	351	7.0472	-0.2923	350	352	7.2768	-0.2871
LAYER 4	330	310	7.9571	-0.3800	330	331	6.6426	-0.2905	330	332	6.8571	-0.2926
LAYER 5	310	290	8.0131	-0.3847	310	311	6.6634	-0.2906	310	312	6.8724	-0.2900
LAYER 6	290	270	7.9685	-0.3841	290	291	6.6602	-0.2912	290	292	6.8728	-0.2897
LAYER 7	270	250	8.0119	-0.3836	270	271	6.6475	-0.2896	270	272	6.8552	-0.2879
LAYER 8	250				250	251			250	252		
701C5			a	n			a	n			a	n
LAYER 1	393	373	7.9897	-0.3859	393	394	6.6286	-0.2900	393	395	6.8358	-0.2894
LAYER 2	373	353	8.009	-0.3863	373	374	6.6715	-0.2918	373	375	6.8691	-0.2918
LAYER 3	353	333	7.9918	-0.3828	354	353	6.6512	-0.2909	353	355	6.8673	-0.2906
LAYER 4	333	313	7.9546	-0.3820	333	334	6.6528	-0.2906	333	335	6.8589	-0.2896
LAYER 5	313	293	7.9802	-0.3838	313	314	6.6479	-0.2903	313	315	6.8497	-0.2902
LAYER 6	293	273	7.986	-0.3833	293	294	6.6415	-0.2870	293	295	6.8564	-0.2875
LAYER 7	273	253	8.0421	-0.3843	273	274	6.6685	-0.2894	273	275	6.8893	-0.2884
LAYER 8	253				253	254	6.6413	-0.2892	253	255	6.8371	-0.2895
701C6			a	n			a	n			a	n
LAYER 1	396	376	7.9466	-0.3814	396	397	6.6529	-0.2928	396	398	6.8571	-0.2905
LAYER 2	376	356	7.6212	-0.3841	376	377	6.6502	-0.2902	376	378	6.8505	-0.2917
LAYER 3	356	336	8.7734	-0.3803	356	357	7.1373	-0.2917	356	358	7.3608	-0.2910
LAYER 4	336	316	7.9567	-0.3803	336	337	6.6643	-0.2920	336	338	6.8661	-0.2911
LAYER 5	316	296	7.9893	-0.3840	316	317	7.0572	-0.2904	316	318	6.8557	-0.2897
LAYER 6	296	276	7.9848	-0.3830	296	297	6.8516	-0.2597	296	298	7.0412	-0.2590
LAYER 7	276	256	8.0105	-0.3835	276	277	6.6868	-0.2908	276	278	6.8705	-0.2878

Table B-3. Locations of stress cell and calibration coefficients.

ID	*Window*	*Orientation*	*X (m)*	*Y (m)*	*Z (mm)*	*Full-scale range (kPa)*	*Gain factors (GF) mv/V/kPa*
B3.8	C1	z	5.44	2.13	482.60	800	39.4
A6.19	C1	x	5.78	2.13	495.30	200	155
A6.6	C1	y	6.15	2.13	495.30	200	161
B3.2	C2	z	5.44	3.35	482.60	800	39

A6.1	C2	x	5.77	3.35	508.00	200	159
A6.15	C2	y	6.15	3.34	495.30	200	162
B3.4	C2	z	5.45	4.57	927.10	800	40
A6.10	C2	x	5.75	4.57	933.45	200	170
A6.11	C2	y	6.15	4.57	927.10	200	164
B3.5	C3	z	5.44	3.35	508.00	800	30.4
A6.5	C3	x	5.77	3.35	495.30	200	167
A6.33	C3	y	6.15	3.35	495.30	200	166

Table B-4. Locations of Vitel Hydra moisture probes in test section 701.

ID	*X(m)*	*Y(m)*	*Z(mm)*
V410	10.9	2.7	342.9
V322	16.1	5.4	622.3
V124	4.9	1.4	965.2
V123	10.6	3.9	1238.3
V122	16.4	1.5	1524.0
V398	4.1	5.4	1778.0

Table B-5. Locations of thermocouples in test section 701.

ID	*X(m)*	*Y(m)*	*Z(mm)*
TC 1	Air		
TC 2	3.6	4.0	76.2
TC 3	3.6	4.0	152.4
TC 4	3.6	4.0	304.8
TC 5	3.6	4.0	457.2
TC 6	3.6	4.0	609.6
TC 7	3.6	4.0	762.0
TC 8	3.6	4.0	914.4
TC 9	3.6	4.0	1066.8
TC 10	3.6	4.0	1219.2

APPENDIX C: 701C1 RESULTS

Table C-1. Measured vertical stress as a function of load repetition.

Load repetitions	*Vertical stress (kPa)*		
	Position 1	*Position 2*	*Position 3*
0	-30.48	-28.49	-25.18
500	-31.62	-31.66	-24.69
1000	-30.40	-31.64	-25.18
2500	-30.12	-31.56	-28.98
5000	-31.09	-32.22	-30.83
10000	-31.63	-34.99	-30.10
20000	-34.17	-36.98	-31.68
45509	-35.84	-37.33	-34.70
52493	-33.81	-37.41	-33.22
53493	-34.93	-39.10	-34.68
63900	-37.21	-39.36	-33.40
99011	-38.51	-40.75	-36.36
200000	-41.16	-43.77	-36.36
283480		-35.99	

Table C-2. Maximum dynamic vertical subgrade strain as a function of load repetition and depth.

Mid layer depth (mm)	*0*	*500*	*1000*	*2500*	*5000*	*10000*	*20000*	*44509*	*52493*	*53493*	*63900*	*99011*	*200000*	*283480*
Position 1														
229 (Base)	-940	-1040	-1105	-1029	-1228	-1392	-1375	-1456	-1327	-1432				
381	-753	-713	-763	-825	-823	-904	-964	-972	-796	-1105	-556	-1096	-1136	
533	-462	-543	-565	-588	-605		-725		-639	-701	-542	-797	-825	
686	-427	-461	-478	-519	-544		-631	-643	-543	-603	-613	-710	-716	-716
840	-355	-369	-400	-418	-442		-535	-539	-462	-525	-556	-585	-626	-622
992	-236	-245	-279	-290	-308		-335	-371	-321	-343	-356	-405	-407	-410
1143	-209	-241	-241	-248	-275	-275	-337	-332	-305	-312	-337	-350	-371	-374
Position 2														
229 (Base)	-966	-1037	-1071	-1148	-1163	-1344		-1472	-1319	-1477			-1553	
381	-719	-824	-856	-938	-930	-988	-1024	-1033	-997	-1174	-809	-1259	-1234	-1278
533	-530	-602	-628	-673	-687	-765	-784	-811	-699	-796	-611	-909	-937	-936
686	-427	-482	-508	-548	-569		-637	-668	-583	-665	-673	-754	-779	-738
840	-344	-389	-415	-438	-459		-531	-564	-487	-548	-568	-620	-643	-623
992	-232	-263	-275	-302	-315		-372	-399	-339	-380	-394	-421	-441	-422
1143	-201	-231	-247	-256	-263	-288	-287	-342	-293	-318	-331	-359	-362	-354
Position 3														
229 (Base)	-906	-1069	-992	-1173	-1023	-1340	-1283	-1484	-1173					
381	-639	-864	-806	-959	-871	-967	-963	-926	-695	-995	-502	-1007	-1137	
533	-393	-506	-504	-573	-652	-719	-756	-766	-650	-761	-409	-847	-878	
686	-362	-438	-455	-493	-500		-577	-604	-494	-592	-537	-662	-688	-654
840	-298	-374	-384	-414	-535		-487	-520	-433	-510	-515	-558	-594	-568
992	-219	-258	-269	-289	-153		-341	-371	-307	-356	-373	-397	-416	-391
1143	-188	-212	-217	-235	-236	-249	-272	-295	-248	-291	-301	-325	-338	-323

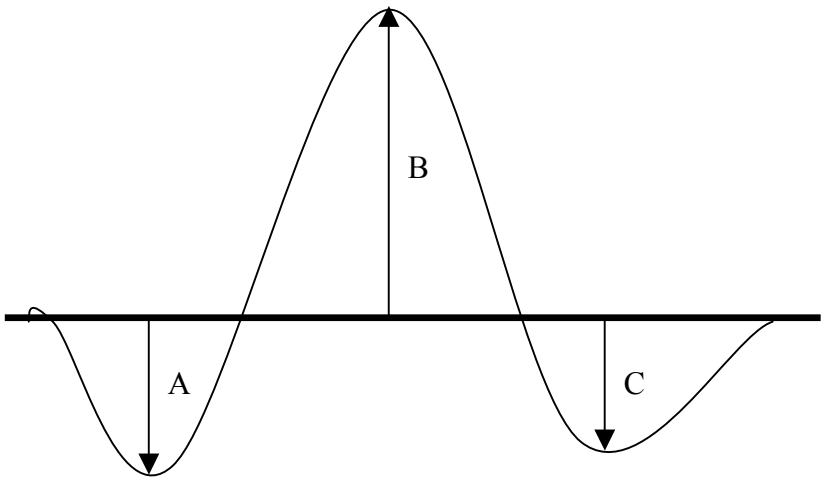

Figure C-1. Illustration of peak longitudinal strains presented in Table C-3.

Table C-3a. Maximum dynamic longitudinal subgrade strain as a function of load repetition and depth (Position 1).

Depth (mm)	*0*	*500*	*1000*	*2500*	*5000*	*10000*	*20000*	*44509*	*52493*	*53493*	*63900*	*99011*	*200000*	*283480*
(A)														
229 (Base)	-91	-101	-215	-219	-238	-304	-289	-307	-201	-243	-	-	-	-
381	-96	-154	-180	135	-182	-208	-308	-260	-227	-245	-204	-321	-358	
533	-75	-91	-91	-98	-95		-132		-134	-138	-114	-189	-215	
686	-65	-76	-86	-80	-93		-101	-115	-114	-123	-122	-149	-149	-149
840	-45	-38	-51	-47	-51		-72	-70	-71	-79	-66	-96	-91	-97
992	-30	-36	-39	-48	-37		-60	-66	-58	-57	-56	-84	-73	-74
1143	-35	-37	-37	-44	-47	-29	-39	-49	-54	-51	-40	-48		-52
(B)														
229 (Base)	254	208	377	484	335	264	369	338	451	550	-	-	-	-
381	84	121	138	-179	128	189	240	236	255	315	224	393	446	
533	161	181	179	188	191		255		256	299	227	359	443	
686	110	123	137	149	169		222	231	204	251	234	301	335	335
840	96	115	118	132	129		162	180	166	169	176	227	238	240
992	82	85	88	101	106		115	123	120	142	128	141	154	156
1143	55	66	66	73	73	100	95	99	95	91	96	114		229
(C)														
229 (Base)	-45	-34	-129	-92	-103	-164	-104	-124	-149	-177	-	-	-	-
381	-40	-41	-41	-39	-34	-33	-38	-36	-55	-56	-43	-46	-61	
533	-64	-64	-68	-56	-73		-97		-62	-72	-66	-78	-96	
686	-49	-44	-50	-57	-55		-72	-68	-76	-95	-73	-85	-90	-90
840	-54	-47	-56	-57	-67		-80	-65	-68	-64	-75	-68	-83	-99
992	-39	-52	-42	-50	-61		-58	-60	-55	-52	-48	-66	-68	-73
1143	-41	-38	-38	-41	-36	-30	-39	-44	-43	-44	-45	-48		-45

Table C-3b. Maximum dynamic longitudinal subgrade strain as a function of load repetition and depth (Position 2).

Depth (mm)	*0*	*500*	*1000*	*2500*	*5000*	*10000*	*20000*	*44509*	*52493*	*53493*	*63900*	*99011*	*200000*	*283480*
(A)														
229 (Base)	-104	-205	-260	-263	-277	-304		-363	-232	-275			-405	
381	-104	-230	-231	-241	-248	-281	-321	-304	-266	-291	-231	-364	-389	-448
533	-48	-69	-91	-107	-103	-118	-127	-151	-122	-147	-112	-190	-225	-224
686	-81	-73	-73	-69	-73		-101	-114	-94	-105	-100	-132	-153	-149
840	-16	-32	-41	-53	-50		-51	-78	-48	-63	-50	-75	-86	-65
992	-24	-17	-26	-29	-39		-44	-42	-40	-35	-38	-54	-49	-56
1143	-16	-22	-17	-17	-24	-20	-27	-33	-31	-25	-32	-38		-41
(B)														
229 (Base)	202	303	280	365	298	265		202	595	500			444	
381	66	122	116	160	153	222	250	266	289	324	229	439	483	457
533	93	179	181	200	216	283	289	361	305	354	249	450	496	534
686	110	158	171	187	208		235	277	221	267	288	334	364	357
840	62	125	132	129	146		188	210	169	203	213	241	268	275
992	54	98	100	114	112		138	149	134	135	151	154	180	162
1143	49	78	76	94	89	107	108	117	103	115	116	128		167
(C)														
229 (Base)	-25	-181	-146	-163	-137	-164		-185	-138	-179			-280	
381	-76	-77	-52	-61	-51	-69	-67	-84	-56	-67	-54	-82	-73	-113
533	-43	-46	-44	-67	-46	-59	-61	-61	-52	-69	-49	-76	-77	-77
686	-54	-42	-48	-57	-51		-60	-65	-48	-73	-63	-72	-78	-72
840	-32	-36	-41	-51	-48		-51	-64	-48	-61	-57	-75	-75	-50
992	-36	-26	-32	-30	-27		-31	-41	-34	-38	-35	-37	-38	-43
1143	-22	-17	-25	-18	-23	-21	-28	-35	-35	-52	-26	-30		-37

Table C-3c. Maximum dynamic longitudinal subgrade strain as a function of load repetition and depth (Position 3).

Depth (mm)	*0*	*500*	*1000*	*2500*	*5000*	*10000*	*20000*	*44509*	*52493*	*53493*	*63900*	*99011*	*200000*	*283480*
(A)														
229 (Base)	-106	-182	-191	-204	-232	-260	-287	-277	-219	-241				
381	-73	-158	-166	-226	-184	-238	-261	-304	-238	-257	-206	401	-339	
533	-44	-89	-86	-106	-102	-115	-143	-154	-127	-154	-95	401	-212	
686	-55	-60	-59	-74	-79		-99	-107	-89	-117	-107	293	-132	307
840	-24	-44	-46	-45	-72		-60	-69	-52	-63	-68	205	-90	235
992	-17	-34	-43	-40	-32		-38	-53	-42	-50	-51	137	-63	140
1143	-19	-27	-23	-30	-36	-38	-30	-48	-30	-38	-45	110		115
(B)														
229 (Base)	293	330	436	373	455	291	441	332	490	412				
381	207	233	243	237	230	222	257	282	244	331	223	401	545	
533	78	163	167	205	202	254	273	290	242	324	203	401	433	
686	123	150	149	159	172		225	247	184	237	232	293	325	307
840	54	113	112	120	162		160	178	149	178	182	205	236	235
992	54	83	83	90	55		115	123	97	124	126	137	155	140
1143	35	67	67	79	74	85	81	108	80	88	149	110		115
(C)														
229 (Base)	-39	-147	-138	-161	-94	-133	-103	-153	-153	-195				
381	-45	-29	-43	-47	-45	-50	-53	-23	-56	-62	-37	-61	-76	
533	-34	-43	-50	-62	-58	-58	-58	-55	-54	-81	-56	-74	-90	
686	-47	-57	-95	-91	-97		-69	-70	-53	-70	-74	-73	-83	-72
840	-38	-43	-45	-51	-80		-54	-68	-54	-67	-63	-73	-78	-71
992	-33	-32	-38	-37	-27		-43	-57	-40	-50	-52	-55	-50	-44
1143	-19	-33	-30	-31	-34	-32	-42	-47	-31	-40	-47	-42		-45

Table C-4. Maximum dynamic transverse subgrade strain as a function of load repetition and depth.

Depth (mm)	*0*	*500*	*1000*	*2500*	*5000*	*10000*	*20000*	*44509*	*52493*	*53493*	*63900*	*99011*	*200000*	*283480*
Position 1														
305	79	79	79	79	79	128	135	148	184	193	134	275	273	
457	61	61	61	61	61		77		124	144	95	190	156	
610	144	144	144	144	144		208	195	162	196	198	205	251	251
762	113	113	113	113	113		169	149	165	138	133	189	193	182
918	115	115	115	115	115		141	122	114		122	133	134	148
1067														
Position 2														
305	126	126	133	133	133	159		171	209	243	182	254	287	262
457	125	125	140	140	140	142	163	200	179	192	138	248	224	262
610		126	158	158	158		174	238	206	213	234	250	297	278
762	104	104	130	130	130		151	173	154	159	159	180	205	194
918	103	64	103	103	103		122	129	115		130	150	169	151
1067														
Position 3														
305	130	130	130	130	130	180	191	177	176	253	166	254	299	
457	135	135	135	135	135	130	183	185	162	202	62	219	208	
610	141	141	165	165	165		195	224	184	200	188	226	270	252
762	119	119	119	119	169		129	171	127	142	154	170	186	177
918	64	64	64	64	64		119	122	110		130	148	170	154
1067														

Table C-5a. Permanent vertical deformation from dynamic strain measurements (mm).

Mid-layer depth (mm)	*0*	*500*	*1000*	*2500*	*5000*	*10000*	*20000*	*44509*	*52493*	*53493*	*63900*	*99011*	*151565*	*200000*	*283480*
229	0	-0.533	-0.757	-1.028	-1.472	-1.326	-1.961	-2.243	-2.341	-2.612	-3.745			-6.930	
381	0	-0.226	-0.320	-0.120	-0.432	-0.376	-0.530	-0.079	-1.203	-1.153	-0.785	-0.587		-2.565	-3.564
533	0	-0.161	-0.153	-0.108	-0.259	-0.265	-0.610	-0.877	-1.127	-1.223	-1.172	-1.471		-2.141	-3.110
686	0	-0.098	-0.099	-0.057	-0.220		-0.479	-0.705	-0.978	-1.070	-0.984	-1.234		-1.955	-2.406
840	0	-0.091	-0.066	-0.035	-0.217		-0.367	-0.502	-0.738	-0.789	-0.737	-0.948		-1.407	-2.019
992	0	-0.054	-0.042	0.011	-0.096		-0.200	-0.297	-0.525	-0.568	-0.501	-0.651		-0.980	-1.591
1143	0	-0.108	-0.086	-0.063	-0.149	-0.122	-0.266	-0.368		-0.585		-0.658		-1.028	-1.667

Table C-5b. Permanent vertical deformation from static strain measurements (mm).

Mid-layer depth (mm)	*0*	*500*	*1000*	*2500*	*5000*	*10000*	*20000*	*44509*	*52493*	*53493*	*63900*	*99011*	*151565*	*200000*	*283480*
112	0						-1.561		-1.856			-3.077	-3.648	-4.084	-4.827
229	0	-0.205	-0.436	-0.946	-0.947	-1.057	-1.498	-2.041	-2.482	-2.564	-4.802	-5.561	-5.032	-7.090	-6.676
381	0	-0.452	-0.478	-0.411	-0.646	-0.791	-0.911	0.064	1.445	-0.524	0.666	1.378	-0.812	-1.936	-2.748
533	0	0.186	0.156	0.165	-0.027	-0.031	-0.333	-0.608	-1.452	-1.467	-1.496	-1.732	-1.979	-2.234	-2.689
686	0	0.131	0.090	0.139	-0.034		-0.284	-0.523							
840	0	0.065	0.046	0.109	-0.040		-0.220	-0.375	-0.355	-0.400	-0.373	-0.619	-0.888	-1.104	-1.610
992	0	0.053	0.043	0.111	-0.012		-0.094	-0.201	-0.036	-0.097	-0.037	-0.195	-0.453	-0.572	-1.034
1143	0	0.029	0.023	0.068	-0.050	-0.004	-0.141	-0.183	0.644	0.610	0.661	0.504	0.271	0.072	-0.399

Table C-6a. Permanent vertical strain as a function of load repetition (from dynamic strain measurements), %.

Mid-layer depth (mm)	*0*	*500*	*1000*	*2500*	*5000*	*10000*	*20000*	*44509*	*52493*	*53493*	*63900*	*99011*	*151565*	*200000*	*283480*
229	0.00	-0.29	-0.42	-0.57	-0.81	-0.73	-1.08	-1.24	-1.29	-1.44	-2.07			-3.83	
381	0.00	-0.17	-0.25	-0.09	-0.33	-0.29	-0.41	-0.06	-0.93	-0.89	-0.61	-0.45		-1.98	-2.76
533	0.00	-0.11	-0.10	-0.07	-0.17	-0.18	-0.40	-0.58	-0.75	-0.81	-0.78	-0.97		-1.42	-2.06
686	0.00	-0.07	-0.07	-0.04	-0.15		-0.32	-0.47	-0.66	-0.72	-0.66	-0.83		-1.31	-1.62
840	0.00	-0.06	-0.04	-0.02	-0.14		-0.24	-0.33	-0.48	-0.51	-0.48	-0.62		-0.91	-1.31
992	0.00	-0.04	-0.03	0.01	-0.07		-0.14	-0.21	-0.38	-0.41	-0.36	-0.47		-0.71	-1.15
1143															

Table C-6b. Permanent vertical strain as a function of load repetition (from static strain measurements), %.

Mid-layer depth (mm)	*0*	*500*	*1000*	*2500*	*5000*	*10000*	*20000*	*44509*	*52493*	*53493*	*63900*	*99011*	*151565*	*200000*	*283480*
112	0.00						-0.82		-0.98			-1.63	-1.93	-2.16	-2.55
229	0.00	-0.11	-0.24	-0.52	-0.52	-0.58	-0.83	-1.13	-1.37	-1.42	-2.65	-3.07	-2.78	-3.92	-3.69
381	0.00	-0.35	-0.37	-0.32	-0.50	-0.61	-0.70	0.05	1.12	-0.40	0.51	1.06	-0.63	-1.50	-2.12
533	0.00	0.12	0.10	0.11	-0.02	-0.02	-0.22	-0.40	-0.96	-0.97	-0.99	-1.15	-1.31	-1.48	-1.78
686	0.00	0.09	0.06	0.09	-0.02		-0.19	-0.35							
840	0.00	0.04	0.03	0.07	-0.03		-0.14	-0.24	-0.23	-0.26	-0.24	-0.40	-0.58	-0.72	-1.05
992	0.00	0.04	0.03	0.08	-0.01		-0.07	-0.15	-0.03	-0.07	-0.03	-0.14	-0.33	-0.41	-0.75
1143	0.00	0.02	0.02	0.04	-0.03	0.00	-0.09	-0.12	0.42	0.39	0.43	0.33	0.18	0.05	-0.26

Table C-7a. Permanent longitudinal deformation from dynamic strain measurements (mm).

Mid-layer depth (mm)	*0*	*500*	*1000*	*2500*	*5000*	*10000*	*20000*	*44509*	*52493*	*53493*	*63900*	*99011*	*151565*	*200000*	*283480*
150	0.000	-0.183	-0.236	-0.218	-0.350	-0.132	-0.318	-0.266	-0.280	-0.423	-0.408			-0.713	
305	0.000	-0.128	-0.148	-0.045	-0.159	-0.013	-0.303	-0.361	-0.628	-0.704	-0.316	-0.592		-1.267	-1.653
457	0.000	-0.005	-0.029	0.021	-0.072	0.022	-0.179	-0.203	-0.330	-0.383	-0.258	-0.412		-0.713	-1.140
610	0.000	-0.002	-0.030	0.040	-0.073		-0.117	-0.176	-0.336	-0.390	-0.300	-0.460		-0.962	-1.240
762	0.000	-0.020	-0.028	0.017	-0.078		-0.132	-0.157	-0.319	-0.338	-0.271	-0.396		-0.756	-1.184
918	0.000	-0.034	-0.038	-0.001	-0.081		-0.108	-0.138	-0.341	-0.349	-0.275	-0.382		-0.739	-1.205
1067	0.000	-0.048	-0.058	-0.046	-0.105	-0.059	-0.131	-0.171		-0.290		-0.312			-0.367

Table C-7b. Permanent longitudinal deformation from static strain measurements (mm).

Mid-layer depth (mm)	*0*	*500*	*1000*	*2500*	*5000*	*10000*	*20000*	*44509*	*52493*	*53493*	*63900*	*99011*	*151565*	*200000*	*283480*
150	0.000	-0.039	-0.070	-0.180	-0.062	-0.003	-0.074	-0.157	0.297	0.250	0.085	-0.012	-0.320	-0.195	-0.511
305	0.000	0.097	0.082	-0.033	0.001	-0.127	-0.073	-0.213	-1.122	-0.871	-0.866	-1.055	-1.281	-1.495	-2.087
457	0.000	0.123	0.116	0.107	0.027	0.105	-0.035	-0.091	-3.300	-3.195	-3.247	-3.326	-3.527	-3.642	-4.011
610	0.000	0.085	0.062	0.107	0.016		-0.018	-0.094	-0.548	-0.514	-0.544	-0.664	-0.951	-1.123	-1.546
762	0.000	0.019	0.005	0.044	-0.035		-0.070	-0.110	-8.750	-8.719	-8.719	-8.825	-9.075	-9.177	-9.556
918	0.000	-0.005	-0.012	0.033	-0.053		-0.068	-0.101	-0.162	-0.147	-0.132	-0.211	-0.491	-0.583	-0.967
1067	0.000	-0.013	-0.025	-0.001	-0.072	-0.030	-0.095	-0.100	-0.830	-0.805	-0.784	-0.853	-1.088		

Table C-8a. Permanent longitudinal strain as a function of load repetitions (from dynamic strain measurements), %.

Mid-layer depth (mm)	*0*	*500*	*1000*	*2500*	*5000*	*10000*	*20000*	*44509*	*52493*	*53493*	*63900*	*99011*	*151565*	*200000*	*283480*
150	0.00	-0.11	-0.15	-0.14	-0.22	-0.08	-0.20	-0.17	-0.18	-0.27	-0.26			-0.45	
305	0.00	-0.07	-0.09	-0.03	-0.09	-0.01	-0.18	-0.21	-0.37	-0.41	-0.18	-0.34		-0.74	-0.96
457	0.00	0.00	-0.02	0.01	-0.04	0.01	-0.10	-0.12	-0.19	-0.22	-0.15	-0.24		-0.41	-0.66
610	0.00	0.00	-0.02	0.02	-0.04		-0.07	-0.10	-0.20	-0.23	-0.17	-0.27		-0.56	-0.72
762	0.00	-0.01	-0.02	0.01	-0.05		-0.08	-0.10	-0.20	-0.21	-0.17	-0.24		-0.46	-0.72
918	0.00	-0.02	-0.02	0.00	-0.05		-0.07	-0.08	-0.21	-0.21	-0.17	-0.23		-0.44	-0.72
1067	0.00	-0.03	-0.04	-0.03	-0.07	-0.04	-0.08	-0.11		-0.18		-0.20			-0.23

Table C-8b. Permanent longitudinal strain as a function of load repetitions (from static strain measurements), %.

Mid-layer depth (mm)	*0*	*500*	*1000*	*2500*	*5000*	*10000*	*20000*	*44509*	*52493*	*53493*	*63900*	*99011*	*151565*	*200000*	*283480*
150	0.00	-0.02	-0.04	-0.11	-0.04	0.00	-0.05	-0.10	0.19	0.16	0.05	-0.01	-0.20	-0.12	-0.32
305	0.00	0.06	0.05	-0.02	0.00	-0.07	-0.04	-0.12	-0.65	-0.51	-0.50	-0.61	-0.75	-0.87	-1.22
457	0.00	0.07	0.07	0.06	0.02	0.06	-0.02	-0.05	-1.91	-1.84	-1.88	-1.92	-2.04	-2.10	-2.32
610	0.00	0.05	0.04	0.06	0.01		-0.01	-0.05	-0.32	-0.30	-0.32	-0.39	-0.55	-0.65	-0.90
762	0.00	0.01	0.00	0.03	-0.02		-0.04	-0.07							
918	0.00	0.00	-0.01	0.02	-0.03		-0.04	-0.06	-0.10	-0.09	-0.08	-0.13	-0.29	-0.35	-0.58
1067	0.00	-0.01	-0.02	0.00	-0.05	-0.02	-0.06	-0.06	-0.53	-0.51	-0.50	-0.54	-0.69		

Table C-9a. Permanent transverse deformation from dynamic strain measurements (mm).

Mid-layer depth (mm)	*0*	*500*	*1000*	*2500*	*5000*	*10000*	*20000*	*44509*	*52493*	*53493*	*63900*	*99011*	*151565*	*200000*	*283480*
150	0.000	0.000	0.088	0.089	-0.041	0.285	0.118	0.229	0.160	-0.029	-0.124			-0.853	
305	0.000	0.000	0.015	0.015	0.015	0.105	-0.104	-0.083	-0.317	-0.440	-0.081	-0.400		-1.234	-1.621
457	0.000	0.000	-0.012	-0.012	-0.012	0.105	-0.066	-0.044	-0.185	-0.269	-0.151	-0.285			-1.017
610	0.000	0.010	0.025	0.025	0.025		0.004	0.031	-0.147	-0.213	-0.121	-0.266		-0.599	-0.821
762	0.000	0.000	-0.009	-0.009	-0.021			-0.043	-0.266	-0.326	-0.280	-0.386		-0.734	-1.218
918	0.000	0.003	0.000	0.000	0.000		-0.044	-0.029	-0.283	-0.310	-0.229	-0.365		-0.717	-1.095
1067	0.000	0.000	-0.019	-0.018											

Table C-9b. Permanent transverse deformation from dynamic strain measurements (mm).

Mid-layer depth (mm)	*0*	*500*	*1000*	*2500*	*5000*	*10000*	*20000*	*44509*	*52493*	*53493*	*63900*	*99011*	*151565*	*200000*	*283480*
150	0.000	0.072	0.124	0.250	0.304	0.482	0.364	0.390	0.399	0.282	-0.019	-0.166	-0.407	-0.710	-1.199
305	0.000	0.067	0.223	0.043	0.121	0.004	0.091	0.097	-0.675	-0.456	-0.488	-0.714	-1.000	-1.366	-1.883
457	0.000	0.161	0.170	0.206	0.134	0.246	0.121	0.110	-2.783	-2.784	-2.780	-2.863	-2.962		-3.481
610	0.000	0.082	0.108	0.144	0.107		0.095	0.097							
762	0.000	0.031	0.012	0.090	0.006		-0.039	-0.029	1.829	1.766	1.780	1.709	1.453	1.317	0.978
918	0.000	-0.014	0.008	0.042	-0.009		-0.046	-0.039	0.093	0.086	0.110	0.002	-0.234	-0.356	-0.671
1067	0.000	-0.035	-0.023	0.001	-0.059	0.017	-0.018	-0.040							

Table C-10a. Permanent transverse strain from dynamic strain measurements (mm).

Mid-layer depth (mm)	*0*	*500*	*1000*	*2500*	*5000*	*10000*	*20000*	*44509*	*52493*	*53493*	*63900*	*99011*	*151565*	*200000*	*283480*
150	0.00	0.00	0.05	0.05	-0.02	0.17	0.07	0.13	0.09	-0.02	-0.07			-0.50	
305	0.00	0.00	0.01	0.01	0.01	0.06	-0.06	-0.05	-0.19	-0.27	-0.05	-0.24		-0.75	-0.98
457	0.00	0.00	-0.01	-0.01	-0.01	0.07	-0.04	-0.03	-0.12	-0.17	-0.09	-0.18		0.00	-0.63
610	0.00	0.01	0.02	0.02	0.02		0.00	0.02	-0.09	-0.14	-0.08	-0.17		-0.39	-0.53
762	0.00	0.00	-0.01	-0.01	-0.01		0.00	-0.03	-0.16	-0.19	-0.16	-0.23		-0.43	-0.71
918	0.00	0.00	0.00	0.00	0.00		-0.03	-0.02	-0.16	-0.18	-0.13	-0.21		-0.42	-0.64
1067	0.00	0.00	-0.01	-0.01											

Table C-10b. Permanent transverse strain from static strain measurements (mm).

Mid-layer depth (mm)	*0*	*500*	*1000*	*2500*	*5000*	*10000*	*20000*	*44509*	*52493*	*53493*	*63900*	*99011*	*151565*	*200000*	*283480*
150	0.00	0.04	0.07	0.15	0.18	0.28	0.21	0.23	0.23	0.17	-0.01	-0.10	-0.24	-0.42	-0.71
305	0.00	0.04	0.14	0.03	0.07	0.00	0.06	0.06	-0.41	-0.28	-0.30	-0.43	-0.61	-0.83	-1.14
457	0.00	0.10	0.11	0.13	0.08	0.15	0.08	0.07	-1.73	-1.73	-1.73	-1.78	-1.85		-2.17
610	0.00	0.05	0.07	0.09	0.07		0.06	0.06							
762	0.00	0.02	0.01	0.05	0.00		-0.02	-0.02							
918	0.00	-0.01	0.00	0.02	-0.01		-0.03	-0.02	0.05	0.05	0.06	0.00	-0.14	-0.21	-0.39
1067	0.00	-0.02	-0.01	0.00	-0.03	0.01	-0.01	-0.02							

Table C-11. Maximum surface rut (mm) as a function of longitudinal location and load repetition.

Location	*500*	*2500*	*5000*	*10000*	*20000*	*45509*	*52493*	*53494*	*99011*	*283480*
Pos3	2.40	4.28	5.63	6.21	7.35	9.33	10.00	10.21	11.83	18.55
Pos4	2.68	4.77	5.90	7.20	8.31	10.33	10.78	11.17	12.48	18.15
Pos5	2.79	5.75	6.71	7.97	9.45	12.10	12.42	12.74	13.84	20.32
Pos6	2.51	5.38	6.95	8.50	9.72	11.62	12.11	11.84	13.92	19.68
Pos7	2.74	4.57	5.08	5.83	7.32	9.43	10.61	10.51	12.23	16.96
Pos8	1.87	3.61	3.86	5.25	6.39	8.03	8.72	8.88	9.80	14.25
Pos9	1.36	2.74	3.67	4.04	5.52	6.77	7.67	6.95	8.79	13.34
Pos10	2.03	3.12	3.75	4.40	5.51	6.25	6.83	7.60	9.25	12.53
Pos11	1.75	2.77	3.29	4.02	4.97	6.51	6.79	7.10	7.87	12.49
Pos12	2.55	3.16	3.82	4.26	5.12	6.78	6.98	7.07	8.29	11.97
Pos13	0.93	2.36	2.86	3.70	4.38	6.27	6.34	6.70	7.39	11.40
Pos14	1.89	3.10	3.13	3.62	4.54	6.10	6.72	6.88	7.59	11.23
Pos15	1.94	3.33	3.77	4.16	5.20	6.54	7.31	7.48	8.58	11.86
Pos16	1.66	2.32	2.80	3.53	4.58	6.26	6.34	6.39	7.43	11.27
Pos17	1.49	2.81	3.28	3.74	4.70	6.47	6.64	7.13	8.18	12.22
Pos18	1.69	2.27	3.56	4.10	4.98	6.60	7.24	7.63	8.88	11.97
Pos19	1.40	2.77	3.31	4.08	5.28	6.29	6.95	7.01	7.94	11.93
Pos20	1.05	2.71	3.18	3.82	4.75	6.70	6.95	6.87	8.07	11.37
Pos21	1.61	2.49	3.02	3.88	4.33	6.07	6.78	7.04	8.21	10.84
Pos22	2.14	3.18	3.65	4.46	4.48	6.41	6.91	6.69	8.13	11.24

APPENDIX D: 701C2 RESULTS

Table D-1. Measured vertical stress as a function of load repetition.

Load repetitions	*Vertical stress (kPa)*		
	Position 1	*Position 2*	*Position 3*
Z = 500 mm			
10	-132.72	-152.81	-140.18
500	-130.66	-148.79	-137.48
1000	-134.44	-154.13	-139.73
2500	-152.71	-175.15	-161.09
5000	-140.98	-161.31	-145.09
10000	-142.40	-160.38	-140.24
27260	-138.70	-161.34	-142.79
51400	-142.62	-168.43	-145.80
103455	-142.71	-169.95	-149.30
149614	-137.64	-163.27	-135.25
Z = 929 mm			
10	-55.95	-59.98	-53.80
500	-54.77	-58.55	-52.76
1000	-56.15	-60.26	-53.85
2500	-65.13	-67.44	-61.69
5000	-58.65	-62.05	-54.10
10000	-59.96	-62.26	-52.99
27260	-59.18	-63.22	-54.31
51400	-61.36	-66.45	-55.35
103455	-62.17	-67.16	-57.51
149614	-61.55	-64.98	-53.86

Table D-2. Measured longitudinal stress as a function of load repetition.

Load repetitions	*Longitudinal stress (kPa)*		
	Position 1	*Position 2*	*Position 3*
Z = 500 mm			
10	-21.45	-26.41	-25.59
500	-20.75	-25.11	-24.80
1000	-16.63	-25.52	-25.07
2500	-24.41	-29.16	-28.90
5000	-21.75	-26.38	-25.56
10000	-21.87	-26.55	-24.69
27260	-19.36	-19.43	-22.89
51400	-17.96	-18.00	-21.58
103455	-11.39	-15.60	-15.48
149614	-11.40	-15.64	-14.43
Z = 929 mm			
10	-12.17	-13.58	-12.82
500	-12.35	-13.67	-12.74
1000	-10.23	-14.33	-13.17
2500	-15.22	-16.45	-15.01
5000	-13.84	-15.28	-13.66
10000	-14.49	-15.80	-13.54
27260	-13.96	-13.96	-14.41
51400	-15.31	-15.34	-14.78
103455	-11.34	-13.42	-12.97
149614	-10.63	-12.19	-11.65

D-3. Measured transverse stress as a function of load repetition.

Load repetitions	*Transverse stress (kPa)*		
	Position 1	*Position 2*	*Position 3*
10	-18.41	-28.83	-34.75
500	-14.99	-25.70	-34.77
1000	-12.19	-26.38	-35.21
2500	-18.45	-32.22	-40.58
5000	-16.10	-27.39	-37.51
10000	-13.98	-25.92	-36.40
27260	-10.59	-23.12	-36.56
51400	-10.56	-24.55	-39.03
103455	-5.04	-19.86	-35.65
149614	-4.13	-18.90	-30.04

Table D-4. Maximum dynamic vertical strain as a function of load repetition and depth.

Depth (mm)	*0*	*500*	*1000*	*2500*	*5000*	*10000*	*27260*	*51400*	*103455*	*149614*
Position 1										
229 (Base)	-1418	-1491	-1464	-1680	-1558	-1649	-1692	-1818	-958	-1454
381	-1124	-1209	-1191	-1352	-1233	-1285	-1306	-1390	-1388	-1275
533	-488	-811	-818	-932	-874	-935	-959	-1045	-1064	-955
686	-388	-504	-518	-605	-642	-616	-653	-629	-721	-678
840	-383	-450	-456	-536	-517	-567	-455	-640	-649	-603
992	-247	-304	-321	-372	-359	-384	-410	-447	-454	-431
1143	-143	-260	-262	-314	-293	-329	-354	-387	-397	-385
Position 2										
229 (Base)	-1519	-1559	-1584	-1753	-1719	-1728	-1874	-2307	-2928	-1556
381	-1172	-1204	-1225	-1350	-1287	-1306	-1362	-1452	-1450	-1302
533	-570	-888	-918	-1027	-1003	-1041	-1099	-1183	-1191	-1054
686	-454	-564	-583	-679	-727	-726	-737	-796	-809	-732
840	-428	-487	-501	-570	-570	-600	-652	-704	-708	-656
992	-279	-323	-336	-385	-384	-402	-430	-482	-484	-449
1143	-240	-274	-281	-331	-324	-342	-383	-414	-417	-396
Position 3										
229 (Base)	-1426	-1430	-1511	-1683	-1643	-1569	-1772	-1807	-1354	-1279
381	-949	-993	-1048	-1142	-1098	-1076	-1139	-1192	-1196	-966
533	-508	-753	-801	-893	-881	-882	-958	-1019	-1035	-867
686	-439	-483	-522	-579	-588	-593	-647	-685	-695	-594
840	-362	-410	-453	-515	-506	-527	-579	-614	-625	-540
992	-298	-322	-347	-393	-379	-386	-424	-449	-454	-345
1143	-225	-243	-262	-309	-296	-302	-340	-370	-381	-346

Table D-5a. Maximum dynamic longitudinal strain as a function of load repetition and depth (Position 1).

Depth (mm)	*0*	*500*	*1000*	*860*	*5000*	*10000*	*27260*	*51400*	*103455*	*149614*
Strain A										
150 (Base)	-276	-278	-232	-256	-239	-253	-253	-314	-398	-276
305	-209	-202	-201	-248	-232	-254	-282	-341	-382	-209
457	-114	-122	-140	-167	-154	-178	-189	-229	-251	-114
610	-67	-47	-62	-84	-62	-75	-98	-119	-132	-67
762	-44	-48	-52	-56	-53	-63	-54	-81	-103	-44
918	-26	-41	-31	-33	-33	-	-50	-48	-62	-26
1067	-	-	-	-	-	-	-	-	-	-
Strain B										
150 (Base)	489	593	686	569	693	481	692	813	1250	263
305	291	294	303	370	377	412	516	593	663	502
457	144	129	127	171	175	186	232	272	324	351
610	144	346	189	215	540	502	286	155	317	283
762	112	128	133	168	162	191	161	242	253	250
918	72	85	69	89	91	-	150	159	181	-
1067	-	-	-	-	-	-	-	-	-	-
Strain C										
150 (Base)	-575	-177	-147	-133	-125	-181	-95	-251	-524	-372
305	-46	-43	-47	-71	-66	-65	-66	-59	-68	-64
457	-35	-48	-66	-77	-64	-76	-61	-76	-82	-75
610	-39	37	-30	-45	160	42	-38	-244	-144	-95
762	-45	-37	-37	-42	-43	-36	-26	-56	-51	-67
918	-33	-42	-98	-44	-44	-	-41	-54	-43	-
1067	-	-	-	-	-	-	-	-	-	-

Table D-5b. Maximum dynamic longitudinal strains as a function of load repetition and depth (Position 2).

Depth (mm)	*0*	*500*	*1000*	*860*	*5000*	*10000*	*27260*	*51400*	*103455*	*149614*
Strain A										
150 (Base)	-344	-338	-306	-315	-255	-294	-338	-829	-160	-446
305	-208	-201	-226	-240	-248	-252	-295	-344	-401	-398
457	-112	-142	-147	-167	-174	-187	-222	-255	-271	-197
610	-73	-73	-73	-86	-120	-176	-98	-118	-133	-113
762	-37	-41	-56	-60	-57	-70	-92	-95	-111	-84
918	-47	-30	-35	-42	-35	-	-53	-57	-59	-
1067	-	-	-	-	-	-	-	-	-	-
Strain B										
150 (Base)	747	731	749	709	853	743	788	572	2234	468
305	291	298	319	382	388	451	559	662	728	488
457	143	130	137	184	191	218	270	322	365	388
610	131	191	192	218	172	187	312	374	343	297
762	126	138	154	174	179	193	219	264	262	267
918	16	90	61	66	89	-	158	180	206	-
1067	-	-	-	-	-	-	-	-	-	-
Strain C										
150 (Base)	-189	-531	-163	-169	-110	-171	-143	-501	-754	-364
305	-64	-66	-67	-94	-80	-82	-78	-78	-81	-55
457	-50	-84	-90	-92	-89	-87	-95	-100	-93	-78
610	-89	-27	-42	-56	-88	-251	-39	-14	-65	-65
762	-34	-44	-40	-46	-43	-54	-60	-49	-54	-65
918	-30	-41	-29	-47	-50	-	-48	-48	-40	-
1067	-	-	-	-	-	-	-	-	-	-

Table D-5c. Maximum dynamic longitudinal strain as a function of load repetition and depth (Position 3).

Depth (mm)	*0*	*500*	*1000*	*2500*	*5000*	*10000*	*27260*	*51400*	*103455*	*149614*
Strain A										
150 (Base)	-304	-238	-249	-268	-261	-228	-241	-217	-	-298
305	-161	-144	-164	-203	-201	-209	-244	-286	-336	-323
457	-140	-92	-95	-118	-119	-119	-158	-194	-211	-166
610	-72	-69	-64	-95	-88	-85	-101	-117	-128	-105
762	-66	-61	-64	-77	-72	-78	-83	-98	-102	-76
918	-58	-37	-52	-80	-69	-	-79	-73	-92	-71
1067	-	-	-	-	-	-	-	-	-	-
Strain B										
150 (Base)	708	735	720	664	733	628	629	689	-	423
305	230	235	252	312	338	354	476	544	607	286
457	37	146	165	195	215	230	253	307	342	280
610	116	153	218	208	171	232	236	268	276	218
762	126	133	160	182	184	185	218	240	258	196
918	34	93	68	70	64	-	139	153	163	507
1067	-	-	-	-	-	-	-	-	-	-
Strain C										
150 (Base)	-183	-154	-144	-129	-126	-120	-130	-235	-	-197
305	-79	-67	-89	-90	-75	-89	-71	-66	-60	-144
457	-98	-46	-43	-48	-47	-46	-56	-62	-59	-42
610	-32	-34	6	-14	-86	-24	-36	-30	-50	-75
762	-43	-29	-35	-41	-42	-38	-38	-50	-42	-91
918	-29	-49	-44	-60	-67	-	-60	-71	-76	42
1067	-	-	-	-	-	-	-	-	-	-

Table D-6. Maximum dynamic transverse strain as a function of load repetition and depth.

Depth (mm)	*0*	*500*	*1000*	*2500*	*5000*	*10000*	*27260*	*51400*	*103455*	*149614*
Position 1										
150	575	630	699	577	-	281	-	589	-	1450
305	-	-	96	109	112	132	181	243	245	191
457	140	111	109	152	150	170	148	241	241	226
610	188	202	203	241	315	264	278	339	340	328
762	102	112	121	138	137	152	132	196	195	175
918	93	104	105	125	119	134	135	158	173	159
1067		65	73	88	81	86	103	118	123	131
Position 2										
150	619	658	639	973	527	485	-	215	-	1257
305	-	-	96	116	130	154	194	213	231	191
457	122	96	100	128	123	149	185	222	230	225
610	175	185	197	228	194	221	265	304	318	303
762	97	105	119	129	126	146	168	191	190	180
918	88	94	95	109	113	113	122	147	154	155
1067	75	64	71	78	76	88	100	107	114	110
Position 3										
150	390	720	729	860	688	406		639		690
305			96	106	99	116	174	198	226	129
457		61	77	96	104	119	154	172	181	138
610		144	132	160	162	159	200	210	225	197
762		113	68	91	88	95	118	136	141	119
918		115	51	58	67	53	87	106	98	82
1067			57	61	64	70	69	92	95	88

Table D-7. Permanent deformation (mm) as a function of load repetition.

Depth (mm)	*10*	*500*	*1000*	*2500*	*5000*	*10000*	*27260*	*51400*	*103455*	*135000*	*135230*	*149614*
Vertical												
Surface	0.000	-1.245	-1.354	-1.618	-1.885	-2.064	-2.521	-3.562	-5.093	-4.528		-3.809
229	0.000	-1.021	-1.199	-1.438	-1.551	-1.856	-2.138	-2.887	-4.254	-3.165	-3.137	-4.012
381	0.000	-1.108	-1.383	-1.626	-1.777	-2.058	-2.456	-2.533	-3.612	-3.832	-3.788	-4.336
533	0.000	-0.402	-0.495	-0.481	-0.470	-0.236	-0.639	-0.456	-0.996	-1.384	-1.354	
686	0.000	-0.133	-0.082	0.455	-0.023	0.456	-0.200	-0.334	-1.006	-0.943	-0.911	-1.206
840	0.000	-0.166	-0.115	-0.052	0.052	0.033	-0.031	0.210	-0.717	-0.759	-0.696	-1.507
992	0.000	-0.081	-0.109	-0.075	0.019	0.007	0.006	0.226	-0.165	-0.538	-0.403	-0.867
1143	0.000	-0.208	-0.264	-0.223	-0.081	0.036	0.064	0.312	-0.097	-0.466	-0.384	
Longitudinal												
150	0.000	0.044	0.165	0.294	0.270	0.194	0.320	-0.023	-0.759	0.332	0.289	-0.564
305	0.000	-0.097	-0.092	-0.033	-0.065	-0.019	0.016	0.292	-0.183	-0.273	-0.295	
457	0.000	0.005	0.076	0.161	0.084	0.018	0.036	0.367	-0.273	-0.231	-0.270	-0.570
610	0.000	-0.455	-0.632	2.482	-0.834	2.612	0.094	0.029	0.029	-1.179	-1.309	
762	0.000	-0.155	-0.124	-0.079	-0.102	0.002	0.054	0.336	-0.202	-0.291	-0.338	0.129
918	0.000	0.668	1.539	1.950	2.000	1.645	-0.794	-0.017	-0.594			
Transverse												
150	0.000	0.851	1.145	1.285	3.934			2.863				
305	0.000	0.442	0.586	0.699	0.637	0.572	0.747	1.116	0.593	0.674	0.654	0.799
457	0.000	0.277	0.392	0.513	0.453	0.414	0.513	0.914	0.342	0.441	0.413	0.496
610	0.000	0.119	0.221	0.663	0.211	0.611	0.304	0.348	0.003	0.196	0.170	0.387
762	0.000	0.033	0.108	0.124	0.127	0.265	0.375	0.737	0.274	0.213	0.224	0.537
918	0.000	0.059	0.091	0.202	0.121	0.069	0.109	0.368	0.214	-0.066	-0.002	0.133
1067	0.000	-0.074	-0.127	-0.035	-0.071	-0.046	0.033	0.373	0.133	-0.229	-0.142	0.015

Table D-8. Permanent strain (%) as a function of load repetition.

Depth (mm)	*10*	*500*	*1000*	*2500*	*5000*	*10000*	*27260*	*51400*	*103455*	*135000*	*135230*	*149614*
Vertical												
Surface (Base)	0.00	-0.68	-0.74	-0.89	-1.03	-1.13	-1.38	-1.95	-2.79	-2.48		-2.09
229 (Base)	0.00	-0.64	-0.76	-0.91	-0.98	-1.17	-1.35	-1.82	-2.68	-2.00	-1.98	-2.53
381	0.00	-0.82	-1.02	-1.20	-1.32	-1.52	-1.82	-1.88	-2.67	-2.84	-2.80	-3.21
533	0.00	-0.30	-0.37	-0.36	-0.35	-0.18	-0.47	-0.34	-0.74	-1.03	-1.01	0.00
686	0.00	-0.09	-0.05	0.29	-0.01	0.29	-0.13	-0.21	-0.64	-0.60	-0.58	-0.77
840	0.00	-0.11	-0.08	-0.03	0.03	0.02	-0.02	0.14	-0.47	-0.50	-0.46	-0.99
992	0.00	-0.06	-0.08	-0.05	0.01	0.00	0.00	0.16	-0.12	-0.38	-0.28	-0.61
1143	0.00	-0.15	-0.19	-0.16	-0.06	0.03	0.05	0.22	-0.07	-0.33	-0.27	
Longitudinal												
150 (Base)	0.00	0.03	0.10	0.18	0.17	0.12	0.20	-0.01	-0.47	0.20	0.18	-0.35
305	0.00	-0.06	-0.06	-0.02	-0.04	-0.01	0.01	0.19	-0.12	-0.18	-0.19	0.00
457	0.00	0.00	0.05	0.10	0.05	0.01	0.02	0.23	-0.17	-0.14	-0.17	-0.35
610	0.00	-0.31	-0.43	1.69	-0.57	1.78	0.06	0.02	0.02	-0.80	-0.89	0.00
762	0.00	-0.09	-0.07	-0.05	-0.06	0.00	0.03	0.20	-0.12	-0.18	-0.20	0.08
918	0.00	0.40	0.92	1.16	1.19	0.98	-0.47	-0.01	-0.35			
Transverse												
150 (Base)	0.00	0.51	0.69	0.77	2.36	0.00	0.00	1.72	0.00	0.00	0.00	0.00
305	0.00	0.26	0.35	0.41	0.38	0.34	0.44	0.66	0.35	0.40	0.39	0.47
457	0.00	0.17	0.24	0.31	0.28	0.25	0.31	0.56	0.21	0.27	0.25	0.30
610	0.00	0.07	0.14	0.41	0.13	0.38	0.19	0.21	0.00	0.12	0.10	0.24
762	0.00	0.02	0.07	0.08	0.08	0.16	0.23	0.45	0.17	0.13	0.14	0.33
918	0.00	0.04	0.06	0.12	0.07	0.04	0.07	0.22	0.13	-0.04	0.00	0.08
1067	0.00	0.51	0.69	0.77	2.36	0.00	0.00	1.72	0.00	0.00	0.00	0.00

Table D-9. Maximum surface rut (mm) as a function of longitudinal location and load application.

Location	*0*	*500*	*1000*	*2500*	*5000*	*27260*	*51400*	*103455*	*135230*	*149614*
Pos 3	0	2.35	4.07	6.45	9.15	14.64	16.30	18.98	21.48	22.16
Pos 4	0	1.97	3.10	5.12	6.29	11.40	14.27	16.19	18.59	18.95
Pos 5	0	4.97	6.65	8.42	10.03	14.68	17.00	19.72	21.47	22.03
Pos 6	0	5.67	6.83	9.37	10.37	14.33	16.92	19.44	20.50	21.39
Pos 7	0	6.03	6.97	8.74	9.47	13.05	14.90	17.51	19.32	19.02
Pos 8	0	0.87	1.21	1.14	1.01	1.29	1.33	1.19	0.82	0.86
Pos 9	0	6.87	7.51	8.48	9.40	12.18	14.28	16.46	17.56	17.91
Pos 10	0	3.05	4.03	4.40	5.11	7.43	9.46	11.00	12.23	12.31
Pos 11	0	4.01	4.28	4.93	6.02	8.40	10.12	11.97	13.14	13.04
Pos 12	0	0.53	1.73	1.57	2.59	4.87	6.64	8.67	9.42	9.87
Pos 13	0	3.27	4.22	4.23	4.63	7.43	9.37	11.33	12.30	12.60
Pos 14	0	2.67	3.00	3.61	4.69	7.16	8.77	10.52	11.60	12.12
Pos 15	0	2.44	2.82	3.73	4.12	6.56	8.33	10.40	10.97	11.63
Pos 16	0	2.72	3.25	4.44	4.76	7.76	9.00	10.67	11.73	11.80
Pos 17	0	3.78	4.18	4.45	5.51	8.07	9.76	11.21	12.67	12.53
Pos 18	0	2.54	3.09	4.21	4.94	7.29	8.78	10.77	11.47	11.48
Pos 19	0	2.61	3.21	3.48	3.86	6.44	7.83	9.52	10.67	10.62
Pos 20	0	1.53	1.59	2.42	2.60	5.15	6.67	8.32	8.75	9.09
Pos 21	0	3.03	3.19	4.12	4.77	6.11	7.93	9.44	10.72	10.37
Pos 22	0	3.75	3.50	4.52	4.79	6.69	8.08	10.41	10.95	10.77

APPENDIX E: 701C3 RESULTS

Table E-1. Measured vertical stress as a function of load repetition.

	Vertical stress (kPa) Z = 500 mm		
Repetitions	*Position 1*	*Position 2*	*Position 3*
10			
500			
1000			
2500			
5000			
15000			
30000		-318.97	-263.25
40000		-311.34	-265.49

Table E-2. Measured longitudinal stress (uncorrected) as a function of load repetition.

	Longitudinal stress (kPa) Z = 500 mm		
Repetitions	*Position 1*	*Position 2*	*Position 3*
10			
500			
1000	-10.86	-26.40	-23.07
2500	-10.86	-27.89	-23.62
5000	-10.86	-29.08	-25.21
15000	-10.86	-30.93	
30000	-15.87	-31.66	-26.18
40000	-15.87	-32.06	-26.73

Table E-3. Measured transverse stress as a function of load repetition.

	Transverse stress (kPa) Z = 500 mm		
Repetitions	*Position 1*	*Position 2*	*Position 3*
10			
500			
1000	-11.68	-20.22	-29.48
2500	-12.23	-20.57	-28.27
5000	-13.06	-20.50	-29.05
15000	-15.70	-21.55	
30000	-16.64	-22.19	-29.93
40000	-17.08	-22.04	-30.60

Table E-4. Change in vertical dynamic strain as a function of depth and load repetition.

Depth (mm)	*500*	*1000*	*2500*	*5000*	*15000*	*30000*	*40000*
Position 1							
229(Base)	-1321	-4301	-4301	-4557	-5917	-5633	-1641
381	-1030						-1402
533		-832	-1266	-1677		-1774	-1240
686							
840	-442	-491	-525	-553	-599	-651	-720
992	-304	-344	-362	-381	-426	-455	-550
1143	-248	-269	-290	-299	-332	-365	
Position 2							
229 (Base)	-1295	-3878	-4162	-4581	-5866	-4805	-1440
381	-1138						-1284
533		-751	-1213	-1624	-1977	-1821	-1155
686							
840	-512	-548	-589	-635	-700	-740	-710
992	-264	-375	-403	-430	-480	-508	-547
1143	-271	-307	-322	-339	-422	-406	-395
Position 3							
229 (Base)	-1179	-3577	-4112	-4463	-5854	-4578	-593
381	-975						-742
533		-773	-1212	-1545	-1956	-1760	-800
686							
840	-476	-521	-545	-582	-650	-422	-570
992	-357	-384	-402	-432	-471	-395	-437
1143	-280	-285	-311	-332	-362	-374	-326

Table E-5a. Maximum dynamic longitudinal subgrade strain as a function of load repetition and depth (Position 1).

Depth (mm)	*0*	*500*	*1000*	*860*	*5000*	*10000*	*27260*	*51400*	*103455*	*149614*
Strain A										
150 (Base)	-214	-217	-226	-229	-306	-2927	-22842	-214	-217	-226
305										
457	-134	-136	-142	-152	-194	-206	-139	-134	-136	-142
610										
762	-35	-40	-40	-38	-49	-53	-6	-35	-40	-40
918	-18	-25	-28	-29	-34	-37	-9	-18	-25	-28
1067	-14	-14	-19	-19	-30	-26	-12	-14	-14	-19
Strain B										
150 (Base)	556	438	374	313	441	2282	2606	556	438	374
305										
457	484	248	279	306	1034	415	385	484	248	279
610										
762	122	169	186	204	220	244	256	122	169	186
918	122	138	135	152	162	181	182	122	138	135
1067	96	104	121	121	134	147	132	96	104	121
Strain C										
150 (Base)	-214	-217	-226	-229	-306	-2927	-22842	-214	-217	-226
305										
457	-134	-136	-142	-152	-194	-206	-139	-134	-136	-142
610										
762	-35	-40	-40	-38	-49	-53	-6	-35	-40	-40
918	-18	-25	-28	-29	-34	-37	-9	-18	-25	-28
1067	-14	-14	-19	-19	-30	-26	-12	-14	-14	-19

Table E-5b. Maximum dynamic longitudinal subgrade strain as a function of load repetition and depth (Position 2).

Depth (mm)	*0*	*500*	*1000*	*2500*	*5000*	*10000*	*27260*	*51400*	*103455*	*149614*
Strain A										
150 (Base)	-219	-217	-274	-268	-333			-219	-217	-274
305										
457	-147	-149	-150	-165	-209	-220	-18	-147	-149	-150
610										
762	-43	-38	-51	-41	-60	-62	-18	-43	-38	-51
918	-30	-30	-43	-34	-37	-41	-10	-30	-30	-43
1067										
Strain B										
150 (Base)	532	482	426	388	485			532	482	426
305										
457	257	304	333	378	443	500	450	257	304	333
610										
762	169	185	208	222	268	280	253	169	185	208
918	93	132	133	163	189	202	184	93	132	133
1067										
Strain C										
150 (Base)	-68	-136	-171	-142	-145			-68	-136	-171
305										
457	-76	-71	-73	-80	-111	-93	-72	-76	-71	-73
610										
762	-68	-71	-70	-87	-68	-80	-31	-68	-71	-70
918	-26	-27	-42	-33	-29	-29	-20	-26	-27	-42
1067										

Table E-5c. Maximum dynamic longitudinal subgrade strain as a function of load repetition and depth, (Position 3).

Depth (mm)	*0*	*500*	*1000*	*2500*	*5000*	*10000*	*27260*	*51400*	*103455*	*149614*
Strain A										
150 (Base)	-139	-128	-172	-202	-227			-139	-128	-172
305										
457	-141	-166	-145	-177	-206	-229	-27	-141	-166	-145
610										
762	-91	-68	-71	-77	-89	-50	-18	-91	-68	-71
918	-48	-63	-61	-69	-74	-66	-53	-48	-63	-61
1067	-24	-24	-30	-33	-36	-40	-10	-24	-24	-30
Strain B										
150 (Base)	399	422	476	298	387			399	422	476
305										
457	287	460	346	373	453	492	373	287	460	346
610										
762	139	175	184	212	245	193	201	139	175	184
918	114	113	118	141	152	155	123	114	113	118
1067	111	126	126	131	147	149	85	111	126	126
Strain C										
150 (Base)	-9	-76	-89	-101	-79			-9	-76	-89
305										
457	-89	-89	-67	-317	-89	-426	-22	-89	-89	-67
610										
762	-110	-86	-88	-93	-84	-85	-88	-110	-86	-88
918	-50	-45	-60	-46	-55	-56	-58	-50	-45	-60
1067	-24	-28	-33	-34	-31	-36	-36	-24	-28	-33

Table E-7. Maximum surface rut (mm) as a function of longitudinal location and load repetition.

Position	*0*	*500*	*1000*	*2500*	*5000*	*15000*	*30000*	*40000*
Pos 3	0	5.861	7.3601	9.6124	11.1821	14.0194	16.0865	17.3249
Pos 4	0	5.5451	6.7122	8.7618	10.5024	12.8178	14.9372	15.9162
Pos 5	0	5.3389	6.4818	8.441	9.6699	12.1796	13.8581	14.9312
Pos 6	0	4.591	5.8281	7.4865	9.0623	11.1651	13.0663	14.1624
Pos 7	0	4.5498	5.5445	7.6682	8.9565	11.435	12.7829	14.0257
Pos 8	0	4.2647	5.5171	7.2673	8.8899	10.9403	12.8906	14.0976
Pos 9	0	4.1574	5.1887	6.7879	8.0009	10.3834	11.9195	13.2718
Pos 10	0	3.4998	4.1122	5.9346	6.8523	9.3968	10.6263	11.6345
Pos 11	0	2.9681	4.5852	5.4084	6.7457	9.5104	11.8097	12.9807
Pos 12	0	2.5941	3.5051	5.3828	6.3885	8.5696	10.9539	12.0886
Pos 13	0	3.2887	3.9409	5.8914	7.4642	9.9952	11.5413	12.5595
Pos 14	0	2.5546	3.7535	5.161	6.6907	8.6908	10.492	11.5068
Pos 15	0	3.0903	3.803	5.2679	6.0798	8.4775	9.5593	10.7585
Pos 16	0	2.9869	3.8284	5.0389	5.9689	8.1518	9.7903	10.402
Pos 17	0	2.9557	4.0542	5.4404	6.9981	9.5652	11.1855	12.8011
Pos 18	0	2.7827	3.5924	5.443	7.0000	9.7376	11.1179	12.4476
Pos 19	0	3.0709	3.4355	5.1161	6.0762	8.6174	10.9196	11.8878
Pos 20	0	3.1094	3.3206	4.779	5.4473	7.6003	8.7801	9.9509

APPENDIX F: 701C4 RESULTS

Table F-1. Maximum dynamic vertical subgrade strain as a function of load repetition and depth.

Depth (mm)	*0*	*500*	*1000*	*2500*	*5000*	*10000*	*22700*	*55000*	*95394*	*172526*
Position 1										
229 (Base)		-1168	-1243	-1294	-1538	-1349	-1445	-1290	-1269	-1621
381		-819	-417	-850	-970	-986	-1078	-987	-949	-1107
533		-588	-645	-690	-733	-774	-819	-770	-767	-909
686		-471	-480	-549	-583	-615	-660	-633	-639	-732
840		-358	-384	-433	-460	-486	-514	-489	-499	-585
992		-253	-278	-295	-325	-339	-358	-355	-365	-414
1143		-171	-190	-206	-219	-254	-261	-248	-259	-282
Position 2										
229 (Base)		-1271	-1282	-1374	-1404	-1427	-1477	-1427	-1415	-1700
381		-909	-963	-1006	-1088	-1093	-1183	-1121	-1127	-1216
533		-672	-749	-778	-813	-847	-920	-884	-898	-1036
686		-527	-591	-614	-643	-702	-729	-712	-730	-811
840		-401	-433	-473	-491	-525	-571	-563	-574	-651
992		-275	-319	-330	-351	-372	-388	-403	-409	-459
1143		-218	-221	-548	-452	-251	-294	-281	-290	-324
Position 3										
229 (Base)		-1291	-1283	-1374	-1445	-1404	-1438	-1441	-1418	-1665
381		-915	-933	-984	-1046	-1103	-1115	-1074	-1077	-1138
533		-657	-677	-734	-769	-807	-865	-826	-848	-952
686		-498	-550	-572	-598	-644	-675	-658	-674	-733
840		-370	-407	-432	-459	-481	-511	-514	-528	-585
992		-261	-341	-299	-327	-333	-370	-441	-393	-408
1143		-186	-208	-218	-229	-223	-275	-268	-284	-302

Table F-2a. Maximum dynamic longitudinal subgrade strain as a function of load repetition and depth (Position 1).

Depth (mm)	*0*	*500*	*1000*	*2500*	*5000*	*10000*	*22700*	*55000*	*95394*	*172526*
Strain A										
150 (Base)		-459	-148	-162	-216	-173	-232	-220	-275	-278
305		-120	-63	-128	-147	-156	-179	-163	-192	-189
457		-77	-68	-91	-115	-123	-148	-136	-151	-163
610		-53	-51	-59	-76	-78	-85	-86	-100	-102
762		-38	-42	-51	-52	-66	-65	-71	-71	-83
918		-26	-25	-26	-21	-45	-39	-44	-39	-55
1067		-42	-31	-29	-28	-33	-24	-19	-28	-37
Strain B										
150 (Base)		588	381	335	420	390	458	566	848	598
305		211	132	292	259	307	400	374	369	525
457		197	207	249	271	305	355	326	320	463
610		164	160	205	231	252	297	271	270	401
762		141	122	146	169	178	202	198	201	258
918		92	90	117	123	316	136	143	142	170
1067		77	60	79	88	96	89	112	97	123
Strain C										
150 (Base)		-27	-170	-187	-141	-149	-124	-160	-125	-184
305		-68	-28	-78	-70	-73	-75	-1064	-70	-81
457		-59	-69	-73	-76	-76	-88	-83	-80	-98
610		-54	-60	-44	-62	-60	-68	-59	-59	-65
762		-35	-45	-44	-34	-48	-39	-30	-37	-47
918		-28	-29	-28	-58	-34	-41	-22	-25	-26
1067		-23	-33	-26	-21	-29	-25	-1	-15	-19

Table F-2b. Maximum dynamic longitudinal subgrade strain as a function of load repetition and depth (Position 2).

Depth (mm)	*0*	*500*	*1000*	*2500*	*5000*	*10000*	*22700*	*55000*	*95394*	*172526*
Strain A										
150 (Base)		-201	-187	-190	-305	-1020	-296	-226	-272	-221
305		-124	-146	-129	-174	-174	-207	-203	-238	-179
457		-83	-75	-87	-124	-123	-154	-154	-167	-157
610		-60	-52	-66	-73	-73	-85	-92	-105	-113
762		-48	-48	-58	-55	-64	-80	-83	-85	-88
918		-21	-26	-36	-48	-38	-35	-39	-44	-55
1067		-	-	-	-	-	-	-	-	-
Strain B										
150 (Base)		520	463	435	970	2086	2107	495	709	630
305		207	190	288	291	350	403	415	413	593
457		237	241	274	310	354	423	395	416	554
610		181	194	230	256	275	325	309	334	455
762		136	146	156	179	194	230	223	232	294
918		102	92	115	123	136	162	154	164	192
1067		-	-	-	-	-	-	-	-	-
Strain C										
150 (Base)		-190	-213	-226	-199	-821	-160	-239	-208	-231
305		-65	-110	-105	-105	-110	-106	-100	-95	-125
457		-59	-80	-85	-81	-87	-87	-91	-91	-119
610		-65	-77	-61	-63	-71	-71	-72	-68	-94
762		-40	-57	-55	-49	-56	-50	-51	-51	-58
918		-19	-46	-30	-33	-84	-28	-31	-24	-31
1067		-	-	-	-	-	-	-	-	-

Table F-2c. Maximum dynamic longitudinal subgrade strain as a function of load repetition and depth (Position 3).

Depth (mm)	*0*	*500*	*1000*	*2500*	*5000*	*10000*	*22700*	*55000*	*95394*	*172526*
Strain A										
150 (Base)		-64	-87	-148	-113	-63	-189	-156	-216	-108
305		-126	-138	-130	-158	-151	-174	-186	-204	-166
457		-79	-92	-94	-103	-111	-130	-144	-149	-131
610		-53	-52	-60	-63	-92	-89	-89	-99	-99
762		-39	-50	-52	-45	-67	-68	-74	-80	-87
918		-32	-39	-41	-40	-50	-61	-48	-60	-61
1067		-24	-51	-42	-30	-30	-62	-29	-24	-36
Strain B										
150 (Base)		664	685	361	424	673	412	511	579	605
305		204	222	236	236	281	379	373	395	504
457		217	227	252	275	302	370	367	397	504
610		174	156	225	241	237	294	282	302	386
762		142	128	165	173	184	206	209	218	260
918		77	74	95	95	102	120	108	132	173
1067		73	34	86	75	96	67	118	115	117
Strain C										
150 (Base)		-22	-56	-142	-131	-150	-109	-179	-154	-130
305		-101	-99	-107	-82	-95	-80	-85	-86	-120
457		-64	-67	-84	-81	-93	-78	-80	-82	-98
610		-61	-99	-56	-60	-80	-79	-69	-71	-83
762		-31	-64	-40	-43	-47	-51	-49	-46	-50
918		-35	-53	-39	-44	-45	-49	-59	-44	-48
1067		-29	-82	-24	-27	-19	-78	-11	-10	-19

Table F-3. Maximum dynamic transverse strain as a function of load repetition and depth.

Depth (mm)	*0*	*500*	*1000*	*2500*	*5000*	*10000*	*22700*	*55000*	*95394*	*172526*
Position 1										
150		524	359	419	337	409	403	634	813	538
305		221	165	305	249	296	350	329	312	358
457		136	118	177	187	211	234	240	252	283
610		151	134	176	200	201	237	234	238	309
762		128	117	135	158	166	188	186	189	219
918		85	83	94	268		123	120	102	
1067		71	60	77	37	80	93	97	89	99
Position 2										
150		312	272	346	807	601	268	450	613	749
305		126	97	155	141	210	226	240	252	266
457		147	119	139	172	163	235	242	260	251
610		161	151	184	198	219	241	239	220	298
762		134	125	143	161	170	181	181	176	207
918		91	84	100	266		121	118	74	
1067		70	66	74	72	83	90	101	76	87
Position 3										
150		389	478	449	438	677	543	630	725	959
305		188	219	218	231	252	290	315	326	347
457		120	114	140	148	150	194	205	206	254
610		129	110	161	172	162	211	214	225	284
762		99	110	122	123	135	169	152	155	189
918		74	48	88	137		90	67	106	
1067		52	48	76	25	64	62	79	77	88

Table F-4. Permanent deformation (mm) as a function of load repetition.

Depth (mm)	*10*	*500*	*1000*	*2500*	*5000*	*10000*	*22700*	*55000*	*95394*	*172526*
Vertical										
Surface	0.000	-0.282	-0.317	-0.657	-1.153	-1.527	-1.912	-2.324		-4.116
229	0.000	-1.004	-1.217	-1.047	-0.559	-1.817	-1.852	-2.255	-2.472	-3.587
381	0.000	0.577	1.032	0.531	-0.441	0.725	-0.174	-0.230	-0.594	-0.827
533	0.000	0.283	0.232	0.294	0.014	-0.242	-0.535	-0.801	-1.094	-1.885
686	0.000	0.669	0.642	0.732	0.493	0.414	0.088	-0.081	-0.226	-0.913
840	0.000	0.494	0.492	0.589	0.369	0.299	-0.041	-0.165	-0.261	-0.970
992	0.000	0.433	0.414	0.532	0.331	0.262	0.055	-0.077	-0.215	-0.842
1143	0.000	0.177	0.216	0.284	0.121	0.066	-0.098	-0.166	-0.322	-0.809
Longitudinal										
150	0.000	-2.858	-3.979	-4.016	-3.858	-4.278	-4.182	-3.987	-4.182	-4.657
305	0.000	1.137	1.750	1.164	0.250	1.240	1.074	1.528	1.324	1.742
457	0.000	0.449	0.521	0.450	0.399	0.173	0.215	0.345	0.212	-0.099
610	0.000	0.639	0.644	0.572	0.551	0.330	0.340	0.466	0.357	0.054
762	0.000	0.367	0.381	0.337	0.305	0.103	0.098	0.226	0.122	-0.176
918	0.000	0.311	0.323	0.278	0.244	0.067	0.049	0.198	0.088	-0.252
Transverse										
150	0.000	-0.620	-0.248	-0.124	-0.502	1.615	0.752	-0.820	-1.056	-1.549
305	0.000	1.260	1.876	1.335	0.522	1.534	1.398	1.721	1.539	2.002
457	0.000	0.554	0.581	0.570	0.567	0.307	0.390	0.423	0.313	0.053
610	0.000	0.704	0.717	0.663	0.653	0.488	0.502	0.482	0.383	7.399
762	0.000	0.378	0.394	0.357	0.331	0.175	0.143	0.085	-0.009	-0.287
918	0.000	0.000	0.035	-0.012	0.357		-0.039	-0.253	3.435	
1067	0.000	0.105	0.153	0.093	0.063	-0.074	-0.123	-0.206	-0.346	-0.702

Table F-5. Maximum surface rut (mm) as a function of longitudinal location and load repetition.

Location	*10*	*500*	*1000*	*2500*	*5000*	*10052*	*22700*	*30000*	*55000*	*95394*	*172526*
Pos 3	0	2.808	3.2647	4.1708	5.3142	6.0657	7.6005	7.9278	10.0411	11.1321	13.1473
Pos 4	0	3.5076	3.8696	4.5727	5.5077	6.4993	8.2796	8.8714	10.5314	12.368	14.8972
Pos 5	0	2.8811	3.1851	4.4081	5.578	6.3518	7.6117	8.2215	9.9092	12.226	15.0177
Pos 6	0	2.5321	3.5087	4.2681	5.5543	6.9261	7.908	8.5086	9.688	11.1007	14.7808
Pos 7	0	2.9953	3.9286	5.1315	5.7583	6.9454	8.6052	8.8748	10.5076	12.8443	14.9109
Pos 8	0	2.9047	3.4032	4.1093	5.235	6.4947	8.0227	8.2783	9.7976	11.4028	14.6041
Pos 9	0	2.8343	3.6732	4.3471	4.9003	5.5228	7.8489	8.2309	9.9439	11.5978	14.4327
Pos 10	0	2.6691	3.6313	4.7349	5.6961	6.5408	8.4364	8.8065	10.2707	11.9217	14.886
Pos 11	0	1.9656	2.9791	4.0234	4.6148	5.6714	7.8648	7.6874	8.683	10.5283	13.4281
Pos 12	0	2.8506	3.4845	5.0338	5.6984	6.6344	8.202	8.3443	9.8041	11.7018	13.6362
Pos 13	0	3.1734	3.3501	5.0202	5.6494	6.6704	8.635	8.8952	10.1154	11.7163	13.9755
Pos 14	0	2.8244	3.8988	4.671	5.9638	5.7214	7.2938	8.2649	9.3788	10.2957	14.4506
Pos 15	0	2.7472	3.2888	3.833	4.7405	5.6117	7.4437	7.799	7.9378	9.7388	12.6317
Pos 16	0	2.5826	3.1594	3.734	4.9045	5.553	7.5116	7.6848	8.7435	10.1101	12.8195
Pos 17	0	1.7756	3.2271	3.5975	4.1361	5.3214	7.1702	7.4582	7.9365	9.3837	11.9836
Pos 18	0	2.8692	2.6701	4.2864	4.6977	5.5499	7.6529	8.2176	8.4841	10.3749	13.0679
Pos 19	0	2.5274	3.6167	4.1928	5.0555	5.3802	7.0449	7.5475	8.0596	9.8425	12.5306
Pos 20	0	1.8064	2.2411	3.2615	4.8135	5.0452	6.8685	7.227	8.3281	9.5204	12.2526
Pos 21	0	2.9855	3.3448	4.5272	5.8556	6.3142	7.4466	7.7116	8.8455	10.2354	13.3467
Pos 22	0	1.1198	1.7082	3.0019	3.7515	3.6615	5.3702	5.5552	6.4984	6.6296	11.3877